



C-H Amination Catalysis from High-Spin Ferrous Complexes

Citation

Hennessy, Elisabeth Therese. 2013. C-H Amination Catalysis from High-Spin Ferrous Complexes. Doctoral dissertation, Harvard University.

Permanent link

<http://nrs.harvard.edu/urn-3:HUL.InstRepos:11169787>

Terms of Use

This article was downloaded from Harvard University's DASH repository, and is made available under the terms and conditions applicable to Other Posted Material, as set forth at <http://nrs.harvard.edu/urn-3:HUL.InstRepos:dash.current.terms-of-use#LAA>

Share Your Story

The Harvard community has made this article openly available.
Please share how this access benefits you. [Submit a story](#).

[Accessibility](#)

**C–H Amination Catalysis from High-Spin Ferrous
Complexes**

A dissertation presented

by

Elisabeth Therese Hennessy

to

The Department of Chemistry and Chemical Biology

in partial fulfillment of the requirements

for the degree of

Doctor of Philosophy

in the subject of

Chemistry

Harvard University
Cambridge, Massachusetts

August 2013

©2013 – Elisabeth Therese Hennessy

All rights reserved.

Abstract

The C–H amination and olefin aziridination chemistry of iron supported by dipyrromethene ligands (${}^R\text{L}_{\text{Ar}}$, L=1,9-R₂-5-aryldipyrromethene, R = Mes, 2,4,6-Ph₃C₆H₂, ^tBu, Ad, 10-camphoryl, Ar = Mes, 2,4,6-Cl₃C₆H₂) was explored. The weak-field, pyrrole-based dipyrinato ligand was designed to generate an electrophilic, high-spin metal center capable of accessing high valent reactive intermediates in the presence of organic azides. Isolation of the reactive intermediate in combination with a series of mechanistic experiments suggest the *N*-group transfer chemistry proceeds through a rapid, single-electron pathway and maintains an overall *S*=2 electronic configuration throughout the catalytic cycle. We have established the catalysts' strong preference for allylic amination over aziridination with olefin containing substrates. Aziridination is limited to styrenyl substrates without allylic C–H bonds, while allylic amination has been demonstrated with both cyclic and linear aliphatic alkenes. Notably, the functionalization of α -olefins to linear allylic amines occurs with outstanding regioselectivity.

We have applied the complex ${}^{\text{Ad}}\text{L}_{\text{Ar}}\text{FeCl}$ towards the generation of complex pyrrolidines using simple linear aliphatic azides via an intramolecular C–H amination reaction. A series of substrates were synthesized in order to probe the mechanism of cyclization. An intramolecular kinetic isotope effect of 5.3 suggested a stepwise mechanism for benzylic substrates, which is consistent with the intermolecular amination reaction. The stereospecificity of cyclization of an enantiopure substrate and the preservation of the cyclopropyl unit in a radical clock experiment suggest that if a stepwise mechanism is operative, the radical intermediate following H–atom abstraction is extremely short-lived. Efforts to synthesize diastereoselective and enantioselective catalysts have been taken. Exposure of ${}^{\text{Ad}}\text{L}_{\text{Ar}}\text{FeCl}$ to potassium phenoxide generates ${}^{\text{Ad}}\text{L}_{\text{Ar}}\text{FeOPh}$,

which is extremely selective for the formation of *cis*-2,5-disubstituted pyrrolidines. Incorporation of camphor substituents to the ligand platform has led to the design of a chiral, C₂-symmetric Fe-dipyrrinato complex. Application of this complex to the cyclization of 1-azido-4-phenylbutane results in the formation of 2-phenylpyrrolidine with modest levels of enantiomeric excess.

Table of Contents

Chapter 1: Transition Metal Catalyzed C–H Amination and Olefin Aziridination	1
1.1 Introduction	1
1.2 Rhodium-Catalyzed C–H Amination Chemistry	3
1.3 C–H Functionalization Chemistry of Cytochrome P450	9
1.4 Amination and Aziridination Chemistry of Synthetic Porphyrin Complexes	12
1.5 Interrogation of Reactive Intermediates in C–H Functionalization	16
1.6 C–H Amination Chemistry of High-Spin Ferrous Dipyrrinato Complexes	24
Chapter 2: Catalytic C–H Bond Amination from High-Spin Iron-Imido Complexes	29
2.1 Introduction	29
2.2 Metal Complex Synthesis	31
2.3 Intermolecular, Catalytic <i>N</i> -Group Transfer with Organic Azides	34
2.4 Proposed Mechanism	35
2.5 Conclusions	41
2.6 Experimental Methods	43
Chapter 3: Intermolecular <i>N</i>-Group Transfer Chemistry with Olefinic Substrates	74
3.1 Introduction	74
3.2 Benzylic Amination and Aziridination of Substituted Substrates with Organoazides	77
3.3 Mechanism of Benzylic Aziridination and Amination Reactions	80
3.4 Allylic Amination	84
3.5 Conclusion	89

3.6	Experimental Methods	89
-----	----------------------	----

Chapter 4: Complex *N*-Heterocycle Synthesis via Iron-Catalyzed, Direct C–H Bond

Amination **98**

4.1	Introduction	98
4.2	Stoichiometric Intramolecular C–H Bond Amination and Cyclization	101
4.3	Catalytic Pyrrolidine Formation	103
4.4	Accessing Alternate Ring Sizes	108
4.5	Proposed Mechanism	110
4.6	Conclusions	112
4.7	Experimental Methods.	113

Chapter 5: Advances in the Diastereoselectivity and Enantioselectivity of *N*-Heterocycle

Formation **157**

5.1	Introduction	157
5.2	Diastereoselective <i>N</i> -Heterocycle Formation	160
5.3	Progress towards an Enantioselective Catalyst	166
5.4	Conclusions	174
5.5	Experimental Methods	175

to my Mom and Dad

Acknowledgements

Thank you to the members of the Betley Group, past and present. To the residents of the most festive box of all: Evan, thank you for making this project what it is and for teaching me the ropes. Your ability to problem solve with such cool confidence has always inspired me. Diana, thank you for the amazing contributions you've already made to this project, just one year in. I am absolutely motivated by your dedication and precision and I can't wait to see where you take things next. Matt, thanks for being the guy who knows how to fix anything, including a GC, a calculation, this Word document, or a bad day. I really couldn't have asked for anyone better to paint the box red (or yellow or purple) with. To my classmates: Tamara, thanks for being such an amazing brainstorming partner, whether it be about chemistry, fashion, or our futures. I don't think I'll ever find a desk buddy as wonderful as you. Graham, I am always fired up after having conversations with you about science, setting you up in volleyball, or playing you in a game of 21. Thanks for being such an amazing teammate on and off the court. Austin, you have an amazing knack for keeping things in perspective and always making me laugh. Also, thank you for the Merck Index. Sarah, thank you for always being a calming voice of reason and for introducing my family to the art of homemade bread. To the next generation: Raul, thanks for being the sauest chemist on the East Coast. Your readiness to learn, to teach, and to toast is unmatched and the group is all the better for it. Benji, thanks for always asking the toughest questions and giving the most honest answers. And to Brian, thanks for keeping us all in line. To the undergrads: Thank you Polina, Ryan, Richard, and Lucy for all of your help in lab and keeping me up-to-date on what's cool. I am consistently impressed by your ability to balance so many things at once and to take pride in all of them. To the postdocs: Thank you all for being such great role-models. Alison, you've shown me that it's possible to do it all. And Dave, your enthusiasm for science and camaraderie is utterly contagious.

Thanks to Justin for getting me hooked on chemistry and being an incredible sounding board long after leaving the farm. Thanks to Nichole for teaching me everything I know about working in lab and looking cool while doing it. Thanks to Tobias for challenging me to give my project more focus and to always consider the big picture. Thanks to Eric for all of your support and encouragement and launching me into the next phase of my education. Thanks to Ted for exposing me to the world of inorganic chemistry and giving me a gift of a project. You have

taught me so much about how to be a better scientist, how to think critically and creatively, how to be more confident, and how to heckle opponents in softball. You have been such a wonderful mentor and I will really miss working for you.

Thanks to Ben. Going to work with my best friend everyday for the past five years has been pretty incredible. I've loved every lunch, dinner, and coffee break we've ever taken together and I feel stronger and happier knowing you are at my side. Thanks to my brother. I'm so lucky that we've managed to follow one another around the globe for the past twenty-seven years. I'm really going to miss being your next-door neighbor; you make every new city we conquer together feel like home. Thanks to Grandmere and Grandpere for always believing in me and celebrating in my successes. And, most of all, thanks to my mom and dad. You are the two greatest parents in the world. You have always been in my corner and knowing that I have your full love and support has given me the confidence to tackle anything that comes my way. I wish Boston were in Houston so we could meet up for some Good Company every now and again.

List of Schemes

Scheme 1.1. Nitrene C–H insertion.	1
Scheme 1.2. Dirhodium catalysts for C–H functionalization.	3
Scheme 1.3. Catalytic cycle and mechanism of functionalization.	6
Scheme 1.4. Cytochrome P450.	9
Scheme 1.5. Mechanistic probes of P450 chemistry.	11
Scheme 1.6. Catalytic reactivity of synthetic porphyrin complexes.	14
Scheme 1.7. Hypervalent iodine oxidation chemistry.	19
Scheme 2.1. Synthesis of dipyrromethene ligands.	31
Scheme 2.2. Catalytic cycle.	36
Scheme 2.3. Synthesis and reactivity of ferric-complexes.	37
Scheme 3.1. Reactivity of imido radical intermediate.	76
Scheme 3.2. Mechanisms of imide decomposition.	80
Scheme 3.3. Mechanistic probe for aziridination reaction.	81
Scheme 3.4. Mechanistic probe of allylic amination reaction.	88
Scheme 4.1. Stoichiometric C–H functionalization/cyclization reaction.	102
Scheme 4.2. Synthesis of linear azide precursors.	107
Scheme 4.3. Mechanistic possibilities.	111
Scheme 4.4. Mechanistic probes.	111
Scheme 5.1. Stereochemical models for predicting diastereoselectivity.	160
Scheme 5.2. Variations in substituent identity.	164
Scheme 5.3. Synthesis of phenoxide bound catalyst 5.4.	165
Scheme 5.4. Synthesis of Fe-complex with chiral anionic ligand.	168

Scheme 5.5. Asymmetric Friedel-Crafts alkylation.	169
Scheme 5.6. Synthesis of camphor-derived dipyrromethene Fe complexes.	171
Scheme 5.7. Enantioselectivities of C–H functionalization/cyclization reactions.	173

List of Figures

Figure 1.1. Functionalized products.	5
Figure 1.2. Challenges of dirhodium chemistry.	7
Figure 1.3. Electronic structure and reaction coordinate of P450.	9
Figure 1.4. Isolated iron imides.	16
Figure 1.5. Reactive Mn-imide.	20
Figure 1.6. Reactive bridging Cu-imide.	21
Figure 1.7. Reactive terminal nickel imide.	22
Figure 1.8. Reactive terminal Co-imide.	23
Figure 1.9. Dipyrrinato iron complexes.	25
Figure 1.10. Reactive Fe-imide.	27
Figure 2.1. X-ray structures of ferrous complexes.	32
Figure 2.2. X-ray structures of ferric complexes.	38
Figure 2.3. Spectroscopic and computational data of ferric complexes.	41
Figure 2.4. X-ray structure of 2.2 .	56
Figure 2.5. Mossbauer of 2.2 .	56
Figure 2.6 X-ray structure of 2.1 .	58
Figure 2.7. X-ray structure of 2.3 .	59
Figure 2.8. Mossbauer of 2.3 .	59
Figure 2.9. X-ray structure of 2.4 .	60
Figure 2.10. Mossbauer spectrum of 2.4 .	61
Figure 2.11. X-ray structure of 2.5 .	62
Figure 2.12. Mossbauer of 2.5 .	62

Figure 3.1. Metal-nitrenoid electronic structure and reactivity.	75
Figure 3.2. X-ray structures of imide decomposition products.	79
Figure 3.3. Single parameter Hammett analysis.	82
Figure 3.4. Dual parameter Hammett analysis.	83
Figure 3.5. Possible mechanisms of allylic amination.	87
Figure 4.1. Solid-state core structures of iron-bound pyrrolidine products.	102
Figure 4.2. Reaction time-course for 1° C–H bond functionalization.	105
Figure 4.3. Reaction time-course for 3° C–H bond functionalization.	106
Figure 4.4. Solid state core structure of Fe-bound chiral pyrrolidine.	108
Figure 4.5. Solid state core structures of iron-bound piperidine and azetidine products.	110
Figure 4.6 X-ray structure of 4.2 .	117
Figure 4.7. X-ray structure of 4.3 .	137
Figure 4.8. X-ray structure of 4.4 .	138
Figure 4.9. X-ray structure of 4.7 .	138
Figure 4.10. X-ray structure of 4.6 .	139
Figure 4.11. X-ray structure of 4.8 .	139
Figure 4.12. X-ray structure of 4.9 .	140
Figure 4.13. X-ray structures for 4.10 , 4.11 .	140
Figure 5.1. Transition state model.	163
Figure 5.2. X-ray structure of 5.4 .	165
Figure 5.3. Asymmetric dipyrromethene complexes.	166
Figure 5.4. X-ray structure of 5.5 .	167
Figure 5.5. Proposed mechanism of enantioinduction.	173

Figure 5.6. X-ray structure of **5.3**.

201

List of Tables

Table 1.1. Stoichiometric reactivity of synthetic porphyrin complexes.	13
Table 2.1. Spectral and magnetic properties of complexes 2.1 – 2.5.	33
Table 2.2. LC/MS (¹ H NMR) amination yields with 2.2.	35
Table 2.3. X-ray crystallographic experimental properties.	70
Table 3.1. Benzylic amination and aziridination of substituted toluenes and styrenes.	78
Table 3.2. Allylic amination of olefinic substrates.	84
Table 3.3. X-ray crystallographic experimental properties.	97
Table 4.1. Catalytic pyrrolidine formation.	104
Table 4.2. Product distribution for azetidine, pyrrolidine, and piperidine formation.	109
Table 4.3. X-ray crystallographic experimental properties.	156
Table 5.1. Diastereoselectivities of disubstituted pyrrolidine products.	162
Table 5.2. X-ray crystallographic experimental properties.	202

List of Chemical Abbreviations

Ad	1-adamantyl
Ar	aryl
Bn	benzyl
Boc	<i>tert</i> -butyl carbamate
CHD	cyclohexadiene
Cy	cyclohexyl
CyPhos	2-dicyclohexylphosphinobiphenyl
dba	dibenzylideneacetone
DCE	dichloroethane
DCM	dichloromethane
DDQ	2,3-dichloro-5,6-dicyano-1,4-benzoquinone
DMF	dimethylformamide
DMSO	dimethylsulfoxide
dpma	dipyrromethene
dpme	dipyrromethene or dipyrin
Et	ethyl
Et ₂ O	diethyl ether
Fc	ferrocene
HMDS	hexamethyldisilazide
ⁱ Pr	isopropyl
JohnPhos	2-di- <i>tert</i> -butylphosphinobiphenyl
L	ligand
Me	methyl
Mes	mesityl or 2,4,6-trimethylphenyl
Ns	<i>ortho</i> -nitrobenzenesulfonyl or nosyl
Oct	octanoate
OTf	trifluoromethylsulfonate or triflate
OPh	phenoxide
Pd/C	palladium on carbon
PDI	pyridyl diimine, 2,6-bis[1-(2,6-diisopropylphenylimino)ethyl]pyridine
Ph	phenyl
PPTS	pyridinium <i>para</i> -toluenesulfonate
py	pyridine
solv	solvent
TBA	tetrabutylammonium
tBu or ^t Bu	<i>tert</i> -butyl
TBS	<i>tert</i> -butyldimethylsilyl
TEA	triethylamine
TFA	trifluoroacetic acid
THF or thf	tetrahydrofuran
TMS	trimethylsilyl
Ts	<i>para</i> -toluenesulfonyl or tosyl

List of Acronyms, Symbols, and Units

•	radical
^1H	proton
^{13}C	carbon-13
Å	angstrom, 10^{-10} meters
avg	average
br	broad
CHN%	combustion or elemental analysis percentages for carbon, hydrogen, and nitrogen
cm^{-1}	wavenumbers or inverse centimeters
d	doublet in NMR
D	deuterium
d_n	deuterated (n is the number of positions where D replaces H)
d.r.	diastereomeric ratio
e	elementary charge, charge of a single proton or electron, 1.602×10^{-19} coulombs
e^-	electron
ee	enantiomeric excess
ESI ⁺	positive ion electron spray ionization
\hat{H}	Hamiltonian operator
HAA	hydrogen atom abstraction
HAT	hydrogen atom transfer
HOMO	highest occupied molecular orbital
HRMS	high-resolution mass spectrometry
IR	infrared spectroscopy
J	coupling constant
J_{HH}	proton-proton coupling constant
K	kelvin
KIE	kinetic isotope effect
LC/MS	liquid chromatography/ mass spectrometry
LUMO	lowest unoccupied molecular orbital
M	molar, moles per liter
m	multiplet in NMR
<i>m</i> -	<i>meta</i> position on an aryl ring, indicating a 1,3 relationship
<i>m/z</i>	mass to charge ratio
MHz	megahertz, 10^6 Hertz or 10^6 s^{-1}
MLMB	metal-ligand multiple bond
mmol	millimole, 10^{-3} moles
MO	molecular orbital
NOE	nuclear overhauser effect
NMR	nuclear magnetic resonance
<i>o</i> -	<i>ortho</i> position on an aryl ring, indicating a 1,2 relationship
<i>p</i> -	<i>para</i> position on an aryl ring, indicating a 1,4 relationship
ppm	parts per million
q	quartet in NMR
rt	room temperature
s	singlet in NMR or second
S	spin
\hat{S}	spin operator
sh	shoulder
SOMO	singly-occupied molecular orbital

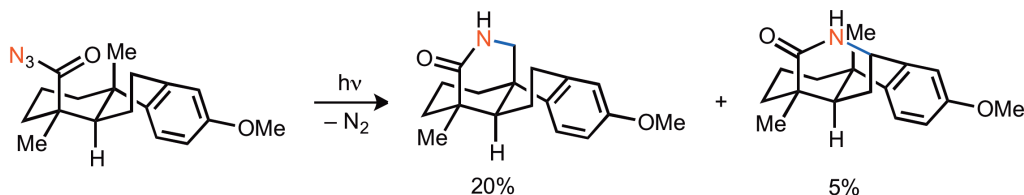
t	triplet in NMR
T	temperature
TON	turnover number
TS	transition state
UV/Vis	ultraviolet-visible absorption spectroscopy
w/w	mass fraction, or percentage weight solute per weight solution
δ	delta, chemical shift in ppm or isomer shift for ^{57}Fe Mössbauer in mm/s
ΔE_Q	quadropole splitting for ^{57}Fe Mössbauer in mm/s
α	alpha, substituent attached to same carbon as functional group of interest
ϵ	epsilon, extinction coefficient or molar absorptivity in $\text{M}^{-1} \text{cm}^{-1}$
η^n	eta, hapticity or the number, n , of contiguous atoms in a ligand bound to a metal
κ^n	kappa, denticity or the number, n , of atoms in a polydentate ligand bound to the metal
λ	lambda, wavelength in nm
μ_B	Bohn magneton, $9.274 \times 10^{-21} \text{ erg/G}$
μ_{eff}	mu effective, effective magnetic moment in Bohn magnetons
μ^n	mu, the number, n , of metal atoms to which a bridging ligand is bound
ν	frequency

Chapter 1: Transition Metal Catalyzed C–H Amination and Olefin Aziridination

1.1 Introduction

The identification of robust catalysts capable of selectively functionalizing unactivated C–H bonds has the potential to significantly impact both the construction of complex molecules as well as the elaboration of simple hydrocarbon feed stocks. Specifically, the efficient installation of amine functionalities, given their ubiquity in bioactive natural products and pharmaceuticals, is of great importance. Indeed, Edwards employed a C–H amination strategy in his synthesis of atisine in 1962, photochemically generating a reactive nitrene from an acyl azide (Scheme 1.1).¹ While this reaction exemplified a new strategy for C–N bond formation, it proceeds in poor yields and selectivities. In order to harness the reactivity of free nitrenes more efficiently, various strategies for sp^3 C–H bond amination through metal-nitrenoid intermediates have emerged over the last thirty years.

Dirhodium C–H amination catalysts have successfully been employed in the synthesis of nitrogen-rich natural products. These catalysts are well-behaved, requiring extremely low catalyst loadings and tolerating a wide-array of functional groups. Recent advances in ligand design have even demonstrated the potential for enantioselective transformations. However, the



Scheme 1.1. Nitrene C–H insertion. Unselective C–H amination through photolytic azide decomposition.

1. ApSimon, J. W.; Edwards, O. E. *Can. J. Chem.* **1962**, *40*, 896.

success of this class of catalysts is somewhat limited to intramolecular C–H amination; the scope of activatable C–H bonds is severely restricted in intermolecular reactions. Additionally, competitive aziridination is observed when oxidations are run in the presence of olefins. Finally, the reliance on an expensive 2nd-row transition metal has prompted the development of alternative C–H amination catalysts.

Inspired by the C–H functionalization chemistry of heme-based hydroxylase enzymes, a renewed interest has been placed on the use of first-row transition metals in synthetic catalysts. Unlike their second- and third-row congeners, first-row transition metal catalysts generally operate through single electron processes, which imparts them with heightened and, at times, indiscriminate levels of reactivity. For instance, the first metal-catalyzed *N*-group transfer process was reported by Kwart and Kahn using copper metal and benzenesulfonyl azide.² When heating these reagents in the presence of cyclohexene, an array of amine and aziridine products arises. However, simple modifications to the copper source, oxidant, solvent, and ligand can promote catalytic aziridination pathways over allylic amination.^{3–5}

As such, the task then becomes to design appropriate ligands for first-row transition metals that can encourage chemo- and regioselective nitrene-based chemistry without significantly diminishing their innate reactivity towards strong C–H bonds. Given their biological ubiquity, porphyrin complexes are an obvious and well-studied class of C–H amination catalysts. Recently, however, new classes of ligands are being explored with the intention of not only

2. Kwart, H.; Kahn, A. A. *J. Am. Chem. Soc.* **1967**, *89*, 1951.

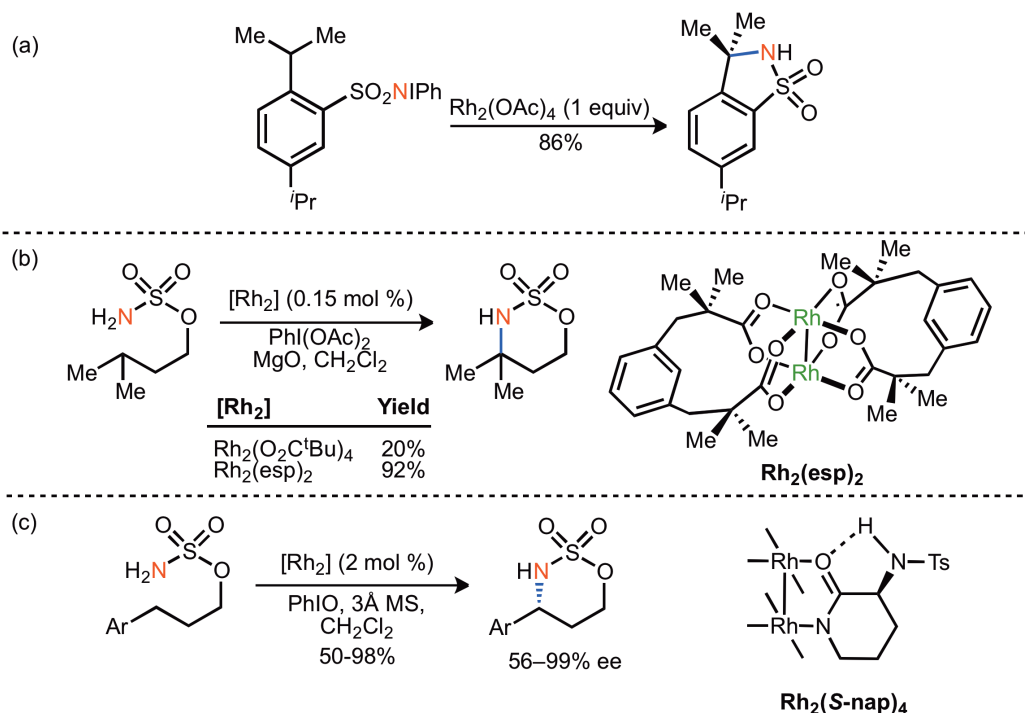
3. (a) Evans, D. A.; Faul, M. M.; Bilodeau, M. T. *J. Org. Chem.* **1991**, *56*, 6744. (b) Evans, D. A.; Faul, M. M.; Bilodeau, M. T. *J. Am. Chem. Soc.* **1994**, *116*, 2742.

4. Pérez, P. J.; Brookhart, M.; Templeton, J. L. *Organometallics* **1993**, *12*, 261.

5. Li, Z.; Conser, K. R.; Jacobsen, E. N. *J. Am. Chem. Soc.* **1993**, *115*, 5326.

improving catalysis but also isolating reactive intermediates. From these efforts, an understanding of the effects of coordination geometry, molecular oxidation state, and ligand field strength on a catalyst's reactivity is emerging.

1.2 Rhodium-Catalyzed C–H Amination Chemistry



Scheme 1.2. Dirhodium catalysts for C–H functionalization. (a) Early example of dirhodium acetate facilitating intramolecular C–H amination from an iminoiodinane intermediate. (b) An example of the improved catalytic activity of the strapped Rh₂(esp)₂ carboxylate for intramolecular C–H amination. (c) Good to excellent enantioselectivities are achieved with the chiral dirhodium carboxamidate complex Rh₂(S-nap)₄.

Dirhodium carboxylates were identified early on as promising candidates for hydrocarbon oxidation chemistry. In 1983, Breslow and Gellman employed Rh₂(OAc)₄ in an intramolecular C–H amination reaction of an (iminoiodo)benzene⁶ derivative to afford the heterocyclic insertion product in 86% yield (Scheme 1.2a).⁷ Notably, this complex significantly outcompetes the Mn- and Fe-porphyrin complexes that were the intended target catalysts of the report. Following this

6. First reports of using iminoiodinane derivatives as nitrene precursors: (a) Abramovitch, R. A.; Bailey, T. D.; Takaya, T.; Uma, V. *J. Org. Chem.* **1974**, *39*, 340. (b) Yamada, Y.; Yamamoto, T.; Okawara, M. *Chem. Lett.* **1975**, 361.

initial report, the C–H functionalization chemistry of dirhodium carboxylates was largely focused on the development of synthetically viable C–group transfer reactions using diazoalkanes.⁸ While C–N bond formation was still an intriguing target, the isolation of the iminoiodinane intermediates was troublesome in comparison to the relatively clean oxidation chemistry of diazoalkanes. Che,⁹ DuBois,¹⁰ and Dauban¹¹ recognized the limitations in isolating iminoiodinanes and found that the nitrene precursor could readily be generated *in situ* by mixing the appropriate amine with $\text{PhI}(\text{OAc})_2$. The adoption of this protocol allowed for the formation of nitrenes from a wide range of nitrogen sources and dirhodium C–H amination chemistry was rejuvenated. Highly efficient and selective dirhodium catalysts have been synthesized through the systematic variation of the carboxylate ligands. The strapped dicarboxylate catalyst $\text{Rh}_2(\text{esp})_2$ is unmatched in activity and scope (Scheme 1.2b).¹² The four-point binding motif and *gem*-dimethyl α -carbon substituents of the carboxylate ligand engender a very rigid catalyst structure that is not susceptible to ligand exchange under the conditions.¹³ Furthermore, the chiral valerolactam-derived dirhodium complex $\text{Rh}_2(S\text{-nap})_4$ was recently employed as an enantioselective catalyst for the intramolecular amination of prochiral benzylic and allylic C–H bonds (Scheme 1.2c).¹⁴

-
7. Breslow, R.; Gellman, S. H. *J. Am. Chem. Soc.* **1983**, *105*, 6728.
 8. (a) Davies, H. M.; Beckwith, R. E. *J. Chem. Rev.* **2003**, *103*, 2861. (b) Hansen, J.; Autschbach, J.; Davies, H. M. L. *J. Org. Chem.* **2009**, *74*, 6555.
 9. Yu, X. Q.; Huang, Y. S.; Zhou, X. G.; Che, C. M. *Org. Lett.* **2000**, *2*, 2233.
 10. Espino, C. G.; Du Bois, J. *Angew. Chem., Int. Ed.* **2001**, *40*, 598.
 11. Dauban, P.; Sanière, L.; Tarrade, A.; Dodd, R. H. *J. Am. Chem. Soc.* **2001**, *123*, 7707.
 12. Espino, C. G.; Williams Fiori, K.; Kim, M. Du Bois, J. *J. Am. Chem. Soc.* **2004**, *126*, 15378.
 13. Zalatan, D. N.; Du Bois, J. *J. Am. Chem. Soc.* **2009**, *131*, 7558.

The intramolecular method developed by Du Bois and Dauban has been applied towards the generation of a wide range of amination products arising from the activation of ethereal, benzylic, allylic, tertiary, and even secondary C–H bonds. Amination can be performed on a variety of sulfamate,^{15,16} sulfamide,¹⁷ carbamate,¹⁸ phosphoramidate,¹⁹ guanidine,²⁰ and urea²⁰ substrates (Figure 1.1). Moreover, efficient methods of opening the oxa- and azathiazine products have been developed in order to access synthetically appealing 1,2- and 1,3-difunctionalized amines.¹⁵⁻¹⁷

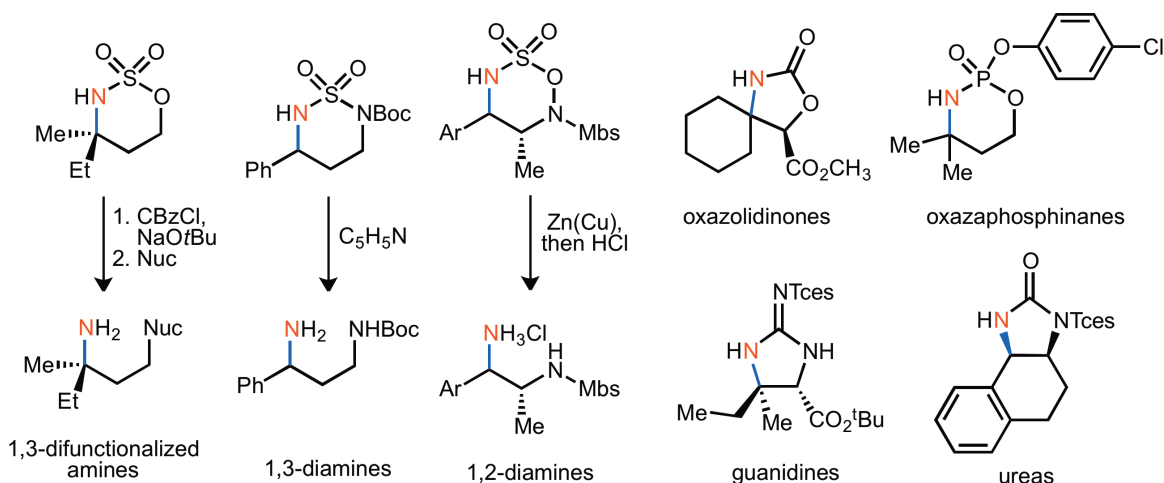
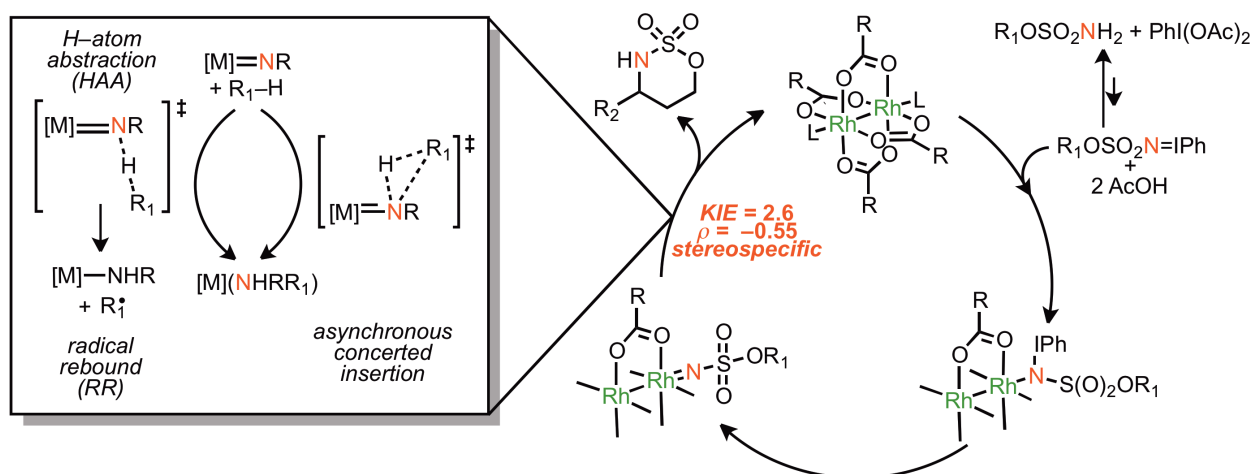


Figure 1.1. Functionalized products. Product classes accessible through intramolecular C–H amination chemistry using Rh₂(CO₂R)₄ and hypervalent iodine oxidants.

14. Zalatan, D. N.; Du Bois, J. *J. Am. Chem. Soc.* **2008**, *130*, 9220.
15. Espino, C. G.; When, P. M.; Chow, J.; Du Bois, J. *J. Am. Chem. Soc.* **2001**, *123*, 6935.
16. Olson, D. E.; Du Bois, J. *J. Am. Chem. Soc.* **2008**, *130*, 11248.
17. Kurokawa, T.; Kim, M.; Du Bois, J. *Angew. Chem., Int. Ed.* **2009**, *48*, 2777.
18. Du Bois, J. *Org. Process. Res. Dev.* **2011**, *15*, 758.
19. Roizen, J. L.; Harvey, M. E.; Du Bois, J. *Acc. Chem. Res.* **2012**, *45*, 911.
20. Kim, M.; Mulcahy, J. V.; Espino, C. G.; Du Bois, J. *Org. Lett.* **2006**, *8*, 1073.



Scheme 1.3. Catalytic cycle and mechanism of functionalization. Proposed catalytic cycle for C–H amination from dirhodium tetracarboxylates. Rate limiting step is iminoiodinane formation prior to nitrenoid formation. *Inset:* Two limiting pathways for C–H amination from metal-nitrenoid intermediates.

Given the versatility of the dirhodium C–H amination chemistry and its successful application towards the synthesis of complex natural products,²¹ substantial effort has been directed toward gaining a comprehensive understanding of the reaction mechanism. The reaction initiates with the formation of iminoiodinane $R_1SO_2N=IPh$ (Scheme 1.3) followed by rapid coordination to the dirhodium catalyst and extrusion of iodobenzene, generating the reactive rhodium nitrenoid intermediate.²² Kinetic analyses show no dependence on the initial reaction rate on the concentration of catalyst, suggesting that the rate-limiting step is formation of the iminoiodinane species. The actual C–H functionalization step likely proceeds through either a concerted insertion step or a two-step H–atom abstraction/radical rebound mechanism (inset, Scheme 1.3). A series of mechanistic experiments were undertaken in order to distinguish between the two limiting reaction pathways.²² No ring-opened amination products were observed with the use of a very fast ($k_{\text{fragment}} = 10^{11} \text{ s}^{-1}$) cyclopropyl radical clock substrate. Additionally, a

21. (a) Hinman, A.; Du Bois, J. *J. Am. Chem. Soc.* **2003**, *125*, 11510. (b) Wehn, P. M.; Du Bois, J. *J. Am. Chem. Soc.* **2002**, *124*, 12950. (c) Wehn, P. M.; Du Bois, J. *Angew. Chem., Int. Ed.* **2009**, *48*, 3802. (d) Parker, K. A.; Chang, W. A. *Org. Lett.* **2003**, *5*, 3891.

22. Williams Fiori, K.; Espino, C. G.; Brodsky, B. H.; Du Bois, J. *Tetrahedron* **2009**, *65*, 3042.

kinetic isotope effect (KIE) of 2.6 and a Hammett ρ value of -0.55 were obtained with benzylic substrates. Lastly, the amination of optically active tertiary C–H bonds results in complete stereoretention. These experiments are strongly suggestive of a mechanism that does not involve radical intermediates, but rather an amination event that operates through the insertion of a singlet nitrene into a C–H bond.

Limitations in the chemoselectivity of the catalyst can likely be attributed to the electronic structure of the rhodium-nitrenoid intermediate. Singlet nitrenoids have a high propensity to participate in olefin functionalization reactions. As such, aziridination is competitive with allylic C–H bond amination in intramolecular nitrene transfer (Figure 1.2a). Furthermore, intermolecular nitrene transfer to olefinic substrates results in selective aziridination.^{23,24} Diruthenium derivatives have recently been synthesized in attempts to address this issue and a reversal in chemoselectivity, favoring allylic amination, is observed (Figure 1.2a). Mechanistic experiments and DFT calculations implicate the involvement of a triplet nitrene intermediate, suggesting that the adjustment to an open-shell diruthenium intermediate is responsible for the shift in reactivity.²⁵

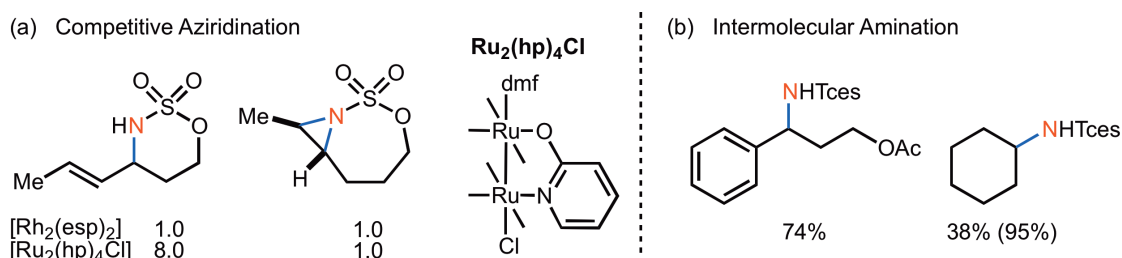


Figure 1.2. Challenges of dirhodium chemistry. (a) $\text{Rh}_2(\text{esp})_2$ catalyzes competitive intramolecular aziridination and amination, while $\text{Ru}_2(\text{hp})_4\text{Cl}$ favors allylic amination. (b) Intermolecular C–H amination with $\text{Rh}_2(\text{esp})_2$ chemistry. Yield in parentheses is based on 5 equivalents of substrate.

23. Guthikonda, K.; When, P. M.; Caliendo, B. J.; Du Bois, J. *Tetrahedron* **2006**, *62*, 11331.

24. A notable exception: Liang, C.; Collet, F.; Robert-Peillard, F.; Müller, P.; Dodd, R. H.; Dauban P. *J. Am. Chem. Soc.* **2008**, *130*, 343.

25. Harvey, M. E.; Musaev, D. G.; Du Bois, J. *J. Am. Chem. Soc.* **2011**, *133*, 17207.

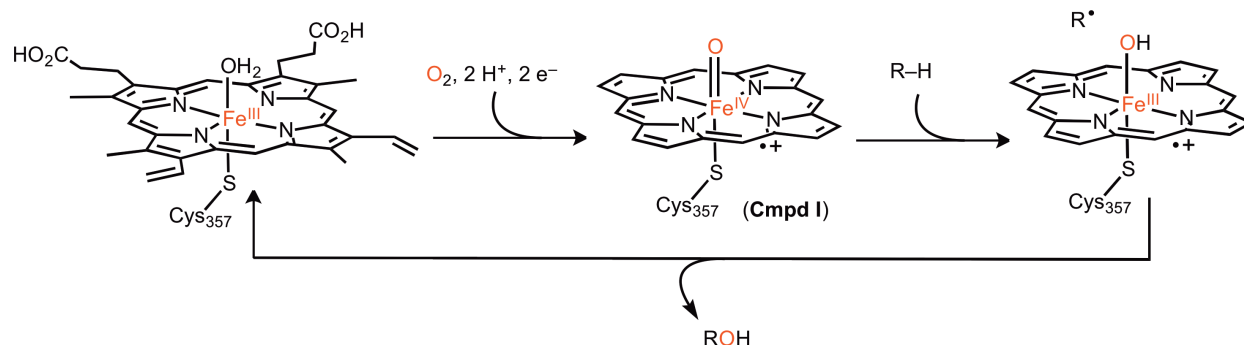
A second challenge associated with the Rh₂-catalyzed C–H amination technology is its application towards intermolecular chemistry. A method has been developed for intermolecular amination employing trichloroethylsulfamate that proceeds with high yields for limiting amounts of benzylic substrates (Figure 1.2b, 74% yield).²⁶ However, yields diminish upon introduction of more hindered or stronger C–H bond substrates. For example, the amination of cyclohexane proceeds in only 38% yield. Fiori and Du Bois attribute this behavior to a catalyst decomposition pathway²⁷ that is competitive with intermolecular amination.

Despite these challenges, dirhodium carboxylate complexes remain the state-of-the-art C–H amination catalysts. Their ability to tolerate a wide variety of functional groups and intramolecularly generate highly functionalized products in good yields is unparalleled. However, the development of new catalysts capable of readily functionalizing stronger C–H bonds with higher levels of selectivity is warranted. In order to address these challenges, the C–H functionalization chemistry mediated by late first-row transition metal-based catalysts has been explored. The compressed d-orbital manifolds of first-row metals typically generate paramagnetic complexes capable of promoting single-electron transformations. Ideally, in the presence of *N*-group transfer reagents these complexes will translate their radical character to the bound nitrene moiety to generate highly reactive intermediates.

26. Williams Fiori, K.; Du Bois, J. *J. Am. Chem. Soc.* **2007**, *129*, 562.

27. Catalyst arrest is likely due to the formation of a Rh^{II}/Rh^{III} dimer and release of *N*-sulfamoyl radical. The mixed valent species is not catalytically active, but introduction of one-electron reductants can regenerate the active Rh^{II}/Rh^{II} catalyst.

1.3 C–H Functionalization Chemistry of Cytochrome P450



Scheme 1.4. *Cytochrome P450*. Catalytic cycle of C–H hydroxylation chemistry by cytochrome P450 family of enzymes.

Inspired by the heme-based hydroxylase enzyme cytochrome P450 (Scheme 1.4),²⁸ synthetic porphyrin catalysts have dominated the literature for C–H functionalization nearly as long as dirhodium catalysts. The enzyme is purported to access a high-valent Fe(IV)–oxo intermediate (Compound I) that is responsible for the hydroxylation of alkanes, the epoxidation of alkenes, the dealkylation of amines, and many other difficult biological transformations.²⁹ Introduction of substrate to the enzyme active site displaces the bound water molecule and prompts the conversion of the low-spin ferric resting state to a high-spin electronic configuration.

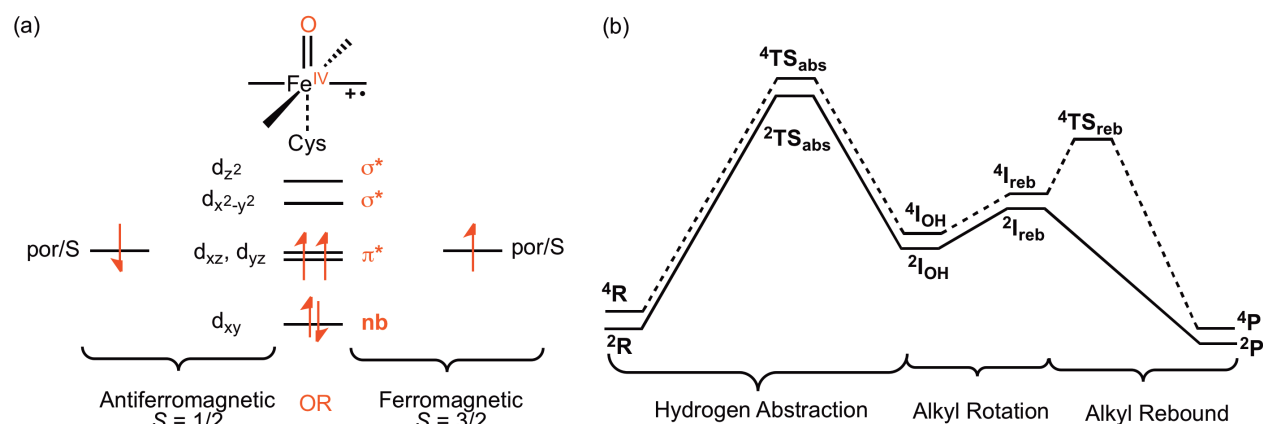


Figure 1.3. *Electronic structure and reaction coordinate of P450*. (a) Two possible electronic structures of high-valent Fe-oxo involving weakly antiferromagnetically or ferromagnetically coupled ligand cation radical. (b) Qualitative two-state transition structure of C–H hydroxylation by Compound I.

28. *Cytochrome P450: Structure, Mechanism and Biochemistry*; 4th ed.; Ortiz de Montellano, P. R., Ed.; Kluwer Academic/Plenum Publishers: New York, 2005.

29. Sono, M.; Roach, M. P.; Coulter, E. D.; Dawson, J. H. *Chem. Rev.* **1996**, *96*, 2841.

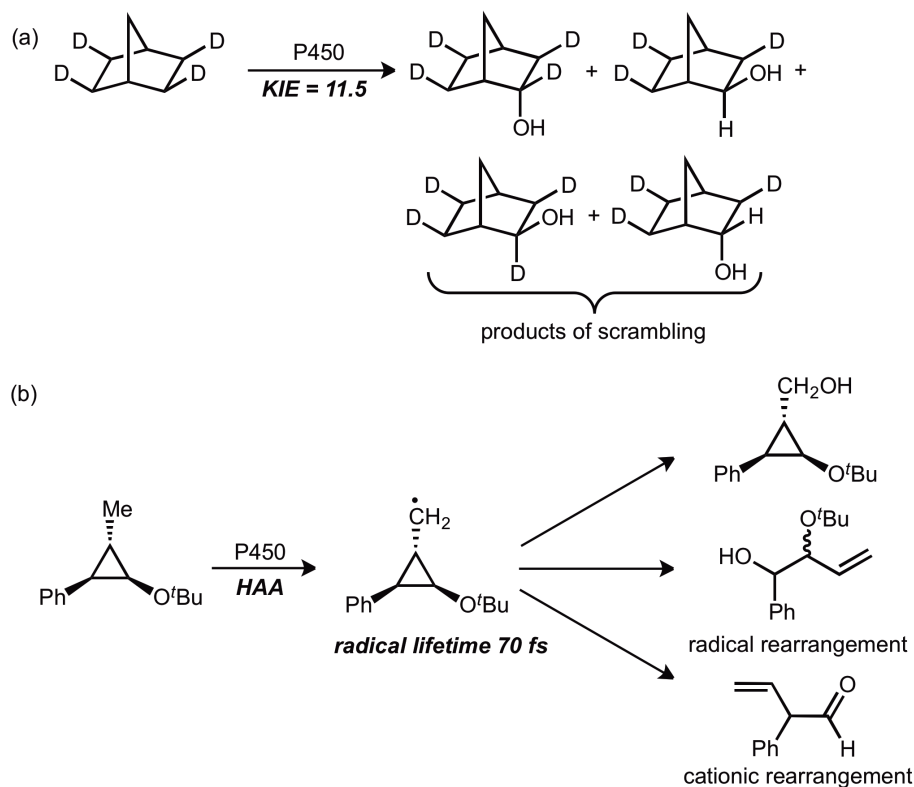
The modification to the high-spin configuration shifts the redox potential of the Fe-center such that reduction to the ferrous state by an associated reductase enzyme occurs.³⁰ Once in the ferrous state, the complex binds dioxygen and subsequently, in a series of proton and electron transfer steps, the Fe–oxo species is generated. The electronic structure of Compound I has been determined by Mössbauer and EPR studies to be an intermediate spin ($S = 1$) iron(IV) center exchange coupled with a ligand based radical ($S = 1/2$) with significant density at the axial sulfur of the cysteine ligand.³¹ The three unpaired electrons can be coupled either ferromagnetically ($S = 3/2$) in which the ligand radical is aligned with the two unpaired electrons along the Fe–O bond vector, or antiferromagnetically ($S = 1/2$) where the spin of the electron on the ligand opposes the spins on the Fe=O unit (Figure 1.3a).³² DFT calculations predict a doublet ground state, but reveal that the mechanism of C–H functionalization involves both low and high spin reaction profiles (Figure 1.3b).³³ The reaction pathway has three phases: (1) initial H–atom abstraction from the ferryl moiety, generating an alkyl radical and an iron-hydroxyl complex denoted $^{4,2}I_{OH}$; (2) alkyl rotation to achieve a favorable orientation for recombination ($^{4,2}I_{reb}$); and (3) radical recombination to form the new C–O bond and generate the ferric-alcohol complex $^{4,2}P$. The energies of the two reaction profiles remain close through the first two steps. However, once an optimal orientation for recombination is obtained, the high- and low-spin profiles diverge. The doublet state features a barrierless recombination step and is essentially concerted while the quartet state is a two-step process with a definitive alkyl radical lifetime.

30. Meunier, B.; de Visser, S. P.; Shaik, S. *Chem. Rev.* **2004**, *104*, 3947.

31. Rittle, J.; Green, M. T. *Science* **2010**, *330*, 933.

32. Shaik, S.; Filatov, M.; Schroder, D.; Schwartz, H. *Chem.–Eur. J.* **1998**, *4*, 193.

33. Kumar, D.; de Visser, S. P.; Shaik, S. *J. Am. Chem. Soc.* **2005**, *127*, 8204.



Scheme 1.5. Mechanistic probes of P450 chemistry. (a) Grove's deuterated norbornane substrate was used to determine both the non-stereospecificity of hydroxylation and the non-classical kinetic isotope effect of 11.5. (b) Newcomb's ultrasensitive radical clock substrate established that the lifetime of the carboradical is 70 fs.

Mechanistic studies by Groves and Newcomb support the possibility of a two-state reaction profile. Groves conducted a kinetic isotope experiment with tetradeuterated norborane substrate in the presence of reconstituted liver cytochrome P450 (Scheme 1.5a).³⁴ Mass spectral analysis of the product mixtures revealed a kinetic isotope effect of 11.5, suggestive of a rate-limiting C–H abstraction step. Additionally, scrambling of hydrogen atoms from *endo* to *exo* positions provided indirect evidence that radical intermediates were present. Following these results, Newcomb has designed ultra-fast radical clock substrates in attempts to quantify the rate constant for radical capture in cytochrome P450 hydroxylations (Scheme 1.5b).³⁵ The

34. Groves, J. T.; McClusky, G. A. *Biochem. Biophys. Res. Commun.* **1978**, *81*, 154.

35. (a) Newcomb, M.; Le Tadic, M.-H.; Putt, D. A.; Hollenberg, P. F. *J. Am. Chem. Soc.* **1995**, *117*, 3312. (b) Newcomb, M.; Le Tadic-Biadatti, M.-H.; Chestney, D. L.; Roberts, E. S.; Hollenberg, P. F. *J. Am. Chem. Soc.* **1995**, *117*, 12085. (c) Newcomb, M.; Toy, P. H. *Acc. Chem. Res.* **2000**, *33*, 449.

cyclopropane substrate was designed in order to distinguish between radical and cationic intermediates. Oxidation of the methyl group gave a mixture of unaltered and rearranged products; yet, the majority of the rearranged products resulted, curiously, from cationic intermediates.³⁶ The small amount of radical rearranged product indicated a 70 fs lifetime of the methyl radical. Such a short lifetime is not indicative of a true alkyl radical intermediate, but rather an insertion reaction that proceeds through an asynchronous, “side-on” transition state. The conflicting mechanistic conclusions from Groves and Newcomb highlight the sensitivity of the reaction profile to substrate probes and suggest that at least two mechanistic pathways are likely operative.

1.4 Amination and Aziridination Chemistry of Synthetic Porphyrin Complexes

Synthetic porphyrin complexes have long been a target for affecting not only C–H hydroxylation chemistry, but also C–H amination and aziridination chemistry. Much like the hydroxylation chemistry, it is proposed that the treatment of metalloporphyrins with *N*-group transfer reagents will generate a reactive, high-valent Fe(IV)-imido species capable of functionalizing alkanes and alkenes. Early reports by Mansuy^{37,38} and Breslow³⁹ highlighted the ability of both Fe- and Mn-porphyrin complexes to facilitate *N*-tosylaziridination and *N*-tosylamidation in the presence of olefin and alkane substrates using PhIN=Ts (Table 1.1). Notably, the aziridination of *cis*-stilbene

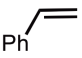
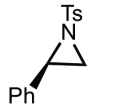
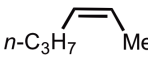
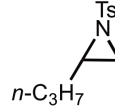

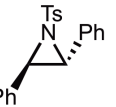
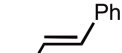
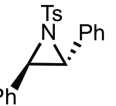
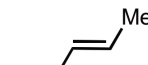
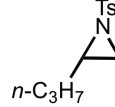
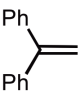
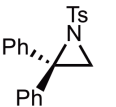
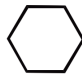

36. The presence of cationic intermediates suggests that a second type of Fe-based oxidant may also be participating in the hydroxylation chemistry. Fe-hydroperoxo species have been investigated as possible active oxidants, and will not be discussed in this text. For leading references, see: a) Wertz, D. L.; Sisemore, M. F.; Selke, M.; Driscoll, J.; Valentine, J. S. *J. Am. Chem. Soc.* **1998**, *120*, 5331. b) Toy, P. H.; Newcomb, M.; Coon, M. J.; Vaz, A. D. *J. Am. Chem. Soc.* **1998**, *120*, 9718.

37. Mansuy, D.; Mahy, J.-P.; Dureault, A.; Bedi, G.; Battioni, P. *J. Chem. Soc., Chem. Commun.* **1984**, 1161.

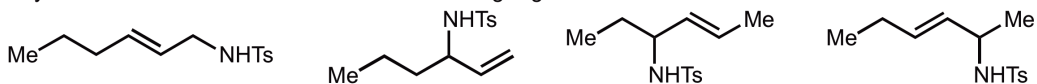
38. Mahy, J.-P.; Bedi, G.; Battioni, P.; Mansuy, D. *Tetrahedron Lett.* **1988**, *29*, 1927.

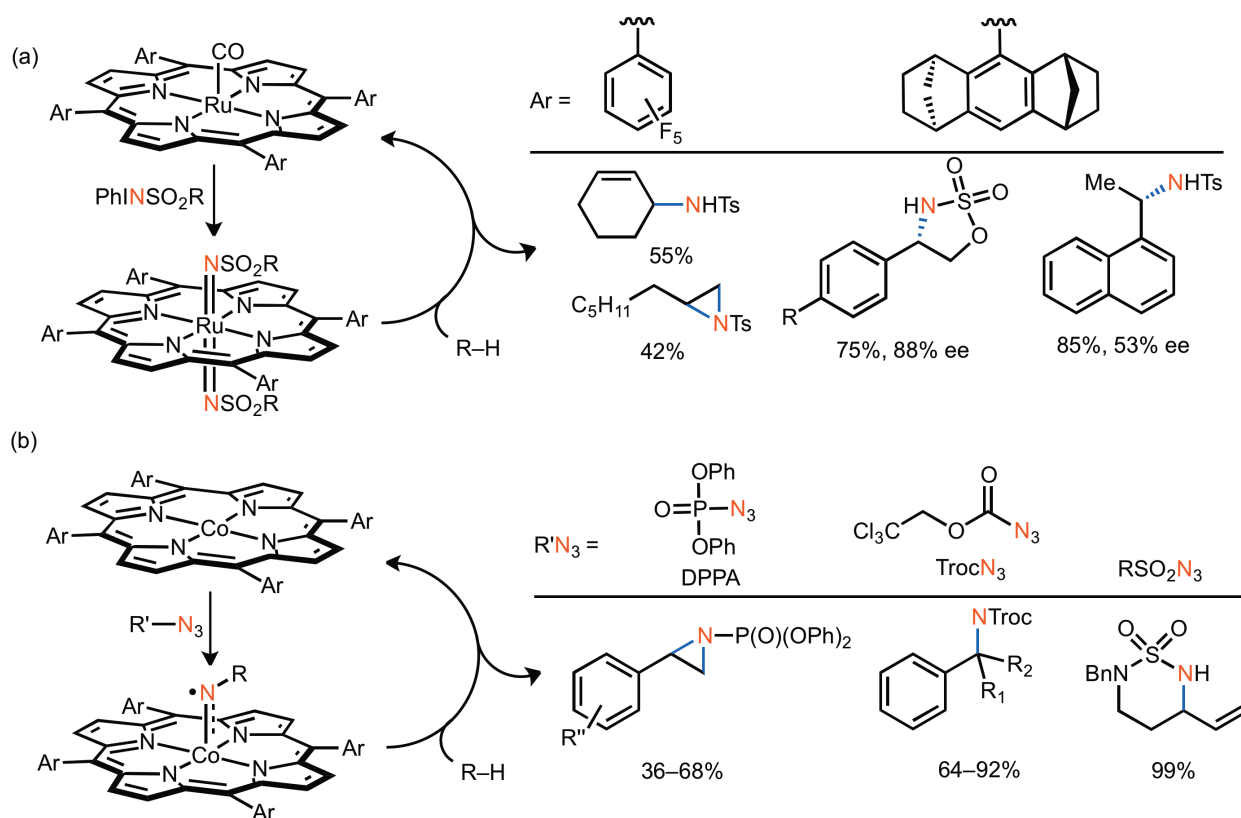
with both complexes resulted in the isomerized *trans*-substituted aziridine product.³⁷ Fe-catalyzed oxidation of substrates containing allylic C–H bonds typically resulted in a mixture of both aziridine and allylic amine products, while reactions with Mn(TPP)Cl show a strong preference for amination over aziridination.³⁸ However, allylic amines are formed as a mixture of several isomers in low yields. Lastly, the amidation of the secondary C–H bond of cyclohexane is possible, albeit in very poor yields.³⁹ In each of these reactions, a significant amount of tosylamine is generated.

Table 1.1. Stoichiometric reactivity of synthetic porphyrin complexes.^{37–39}

Alkene	Products	Yield %		Alkene	Products	Yield %	
		Aziridine (TsNH ₂) Fe(TPP)Cl	Mn(TPP)Cl			Fe(TPP)Cl	Mn(TPP)Cl
		55 (40)	80 (20)			12	<2
		37 (63)	20 (80)		allylic amines ^a	20	37
		32 (65)	16 (80)			27	<2
		21 (75)	56 (40)			3	7

^a Allylic amines formed as a mixture of the following regioisomers:





Scheme 1.6. Catalytic reactivity of synthetic porphyrin complexes. (a) Ruthenium-porphyrinato complexes competent for C–H amination and aziridination catalysts. (b) Exposure of cobalt-porphyrinato complexes to a variety of organic azides results in the formation of benzylaziridines and benzylamines through a proposed imido radical intermediate.

While these initial reports highlight the innate reactivity of porphyrin complexes for nitrene transfer, the low yields and selectivities have inspired the development of new porphyrin catalysts and nitrene precursors. Over the past twenty years, Che and co-workers have worked with ruthenium porphyrin complexes and explored their potential for inter- and intramolecular nitrene transfer (Scheme 1.6a). Mechanistic studies on the stoichiometric aziridination of styrene and toluene derivatives are consistent with rate-determining formation of a carboradical from a bis(tosylimido)ruthenium(VI) intermediate.⁴⁰ Cenini and co-workers have recently isolated and crystallographically characterized the purported bis-imido intermediate using aryl azides and

39. Au, S.-M.; Huang, J.-S.; Yu, W.-Y.; Fung, W.-H.; Che, C.-M. *J. Am. Chem. Soc.* **1999**, *121*, 9120.

shown that it is competent for nitrene transfer.⁴¹ The perfluorophenyl-substituted ruthenium porphyrin complex can be employed in very low catalyst loadings (1.33 mol%) with only a slight excess of olefinic substrate to encourage intermolecular nitrene transfer with hypervalent iodine oxidants.⁴² Despite improvements in the yields and reaction conditions, the catalyst's chemoselectivity is still unpredictable. For instance, an allylic amine forms upon exposure to cyclohexene and an aziridine forms upon exposure to 1-octene. The fact that a minor perturbation in substrate could promote such different reactivity suggests that multiple reaction pathways are energetically accessible using this catalyst. Asymmetric porphyrins have also been synthesized and implemented in intra- and intermolecular amidation chemistry with varying levels of enantioselectivity.⁴³

Zhang and co-workers have exploited the paramagnetic nature of cobalt(II) porphyrins and explored their reaction chemistry with organic and inorganic azides. Reaction with phosphoryl azides,⁴⁴ trichloroethoxycarbonyl azide (TrocN₃),⁴⁵ and sulfonyl azides⁴⁶ can generate a variety of benzylaziridine and benzylamine products in good yield through a purported Co(III)-bound nitrene radical intermediate (Scheme 1.6b),⁴⁷ through could result from the Co-templated

-
40. Fantauzzi, S.; Gallo, E.; Caselli, A.; Ragaini, F.; Casati, N.; Macchi, P.; Cenini, S. *Chem. Commun.* **2009**, 3952.
 41. Yu, X.-Q.; Huang, J.-S.; Zhou, X.-G.; Che, C.-M. *Org. Lett.* **2000**, *2*, 2233.
 42. Liang, J.-L.; Yuan, S.-X.; Huang, J.-S.; Yu, W.-Y.; Che, C.-M. *Angew. Chem., Int. Ed.* **2002**, *41*, 3465.
 43. (a) Gao, G.-Y.; Jones, J. E.; Vyas, R.; Harden, J. D.; Zhang, X. P. *J. Org. Chem.* **2006**, *71*, 6655. (b) Lu, H.; Tao, J.; Jones, J. E.; Wojtas, L.; Zhang, X. P. *Org. Lett.* **2010**, *12*, 1248.
 44. Lu, H.; Subbarayan, V.; Tao, J.; Zhang, X. P. *Organometallics* **2010**, *29*, 389.
 45. (a) Ruppel, J. V.; Kamble, R. M.; Zhang, X. P. *Org. Lett.* **2007**, *9*, 4889. (b) Ruppel, J. V.; Jones, J. E.; Huff, C. A.; Kamble, R. M.; Chen, Y.; Zhang, X. P. *Org. Lett.* **2008**, *10*, 1995. (c) Subbarayan, V.; Ruppel, J. V.; Zhu, S.; Perman, J. A.; Zhang, X. P. *Chem. Comm.* **2009**, 4266. (d) Lu, H.; Jiang, H.; Hu, Y.; Wojtas, L.; Zhang, X. P. *Chem. Sci.* **2011**, *2*, 2361.

N_2 release and concomitant nitrene expulsion from the azide precursor.⁴⁸ The *N*-based radical encourages single electron chemistry and exclusively favors amination over aziridination with alkene substrates. The authors rationalize this striking preference for allylic C–H amination based on the combination of a weak homolytic bond dissociation energy and the greater stability of the ensuing allylic versus alkyl radical that would result from a radical aziridination pathway.^{46d} Zhang’s chemistry alludes to the important relationship between molecular electronic structure and reactivity. However, the bonding formulation for the reactive intermediate is largely based on DFT calculations and literature precedent from our lab.⁴⁹ In order to truly distinguish between the various bonding formulations accessible for transition metals interacting with nitrene moieties, the isolation and full characterization of the reactive intermediates is desirable.

1.5 Interrogation of Reactive Intermediates in C–H Functionalization

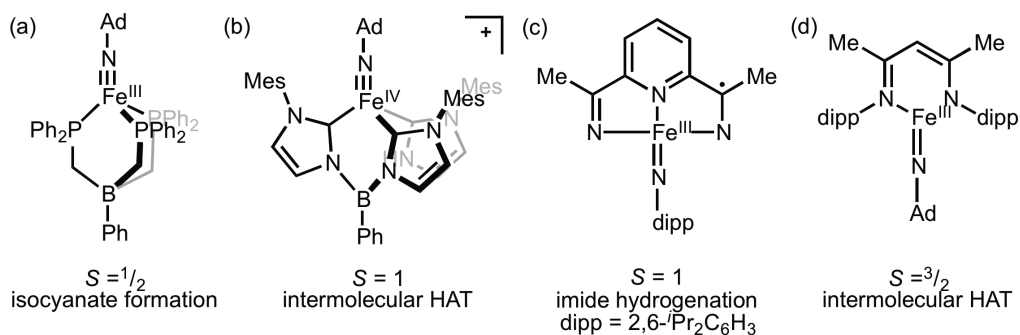


Figure 1.4. Isolated iron imides. Selected examples of crystallographically characterized iron imides; spin state and reactivity are designated below each structure.

The field of C–H functionalization via group transfer has operated on the belief that

-
46. Lyaskovskyy, V.; Olivos Suarez, A. I.; Lu, H.; Jiang, H.; Zhang, X. P.; de Bruin, B. *J. Am. Chem. Soc.* **2011**, *133*, 12264.
47. Mankad, N. P.; Antholine, W. E.; Szilagy, R. K.; Peters, J. C. *J. Am. Chem. Soc.* **2009**, *131*, 3878.
48. King, E. R.; Hennessy, E. T.; Betley, T. A. *J. Am. Chem. Soc.* **2011**, *133*, 4917.

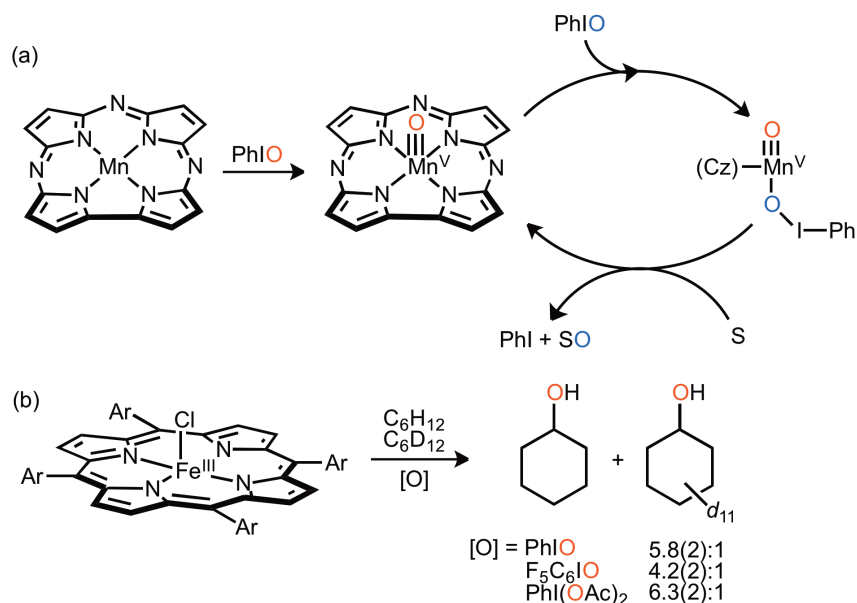
metal-ligand multiply-bonded intermediates at high-valent metal centers are necessary and responsible for the polarization and ultimate functionalization of C–H bonds.⁵⁰ Given this, a significant amount of inorganic chemistry has been devoted to the synthesis of metal-oxo, -imido, -alkylidene, -nitride, and -carbide products. Specifically, the synthesis and isolation of Fe-oxos and, by extension, Fe-imidos has been a primary focus, considering their purported role in enzymatic hydroxylase chemistry. In 2000, Lee crystallographically characterized the first terminal iron imide within a tetranuclear iron cubane.⁵¹ Mössbauer spectroscopy was used to assign the oxidation state of the unique terminal Fe-imide as Fe(IV). Peters and co-workers synthesized the first mononuclear example using a tris(phosphino)borate platform (Figure 1.4a).⁵² Since this initial report, a series of mononuclear terminal imides have been isolated in a variety of oxidation (Fe^{II}, Fe^{III}, Fe^{IV}) and spin states ($S = 0, 1/2, 1$) using modified tripodal ligand platforms (Figure 1.4b).^{53,54} Chirik has employed the bis(imino)pyridine ligand platform to isolate Fe-imides in a square planar geometry from organic azides (Figure 1.4c).⁵⁵ The two-electron oxidation upon azide decomposition can be distributed between both the Fe-center and the redox-active ligand, dependent upon the imide substituent. Holland has isolated a series of

-
49. Nugent, W. A.; Mayer, J. M. *Metal-Ligand Multiple Bonds: The Chemistry of Transition Metal Complexes Containing Oxo, Nitrido, Imido, Alkylidene, or Alkylidyne Ligands*; Wiley-Interscience: Georgetown, 1988.
50. Verma, A. K.; Nazif, T. N.; Achim, C.; Lee, S. C. *J. Am. Chem. Soc.* **2000**, *122*, 11013.
51. Brown, S. D.; Betley, T. A.; Peters, J. C. *J. Am. Chem. Soc.* **2003**, *125*, 322.
52. Selected examples: (a) Betley, T. A.; Peters, J. C. *J. Am. Chem. Soc.* **2003**, *125*, 10782. (b) Thomas, C. M.; Mankad, N. P.; Peters, J. C. *J. Am. Chem. Soc.* **2006**, *128*, 4956. (c) Lu, C. C.; Saouma, C. T.; Day, M. W.; Peters, J. C. *J. Am. Chem. Soc.* **2007**, *129*, 4.
53. (a) Nieto, I.; Ding, F.; Bontchev, R. P.; Wang, H. B.; Smith, J. M. *J. Am. Chem. Soc.* **2008**, *130*, 2716. (b) Scepianiak, J. J.; Young, J. A.; Bontchev, R. P.; Smith, J. M. *Angew. Chem., Int. Ed.* **2009**, *48*, 3158.
54. (a) Bart, S. C.; Lobkovsky, E.; Bill, E.; Chirik, P. J. *J. Am. Chem. Soc.* **2006**, *128*, 5302. (b) Bowman, A. C.; Milsman, C.; Bill, E.; Turner, Z. R.; Lobkovsky, E.; DeBeer, S.; Wieghardt, K.; Chirik, P. J. *J. Am. Chem. Soc.* **2011**, *133*, 17353.

stable intermediate spin ($S = 3/2$) Fe^{III}-imides using β -diketiminato ligands (Figure 1.4d).⁵⁶ After isolation and electronic structure determination, the reactivity of each of the isolated imides was explored. In most cases, group transfer to carbon monoxide or isocyanides is observed and select examples have proven competent for the abstraction of weak C–H bonds.^{54a,56c} Curiously, however, none of the isolated Fe-imidos are competent for C–H functionalization. Such findings suggest that the generation of strongly bound metal-imido complexes is not sufficient, but perhaps even deleterious for *N*-group transfer to C–H bonds.

Moreover, investigations into the active oxidant in *O*-group transfer chemistry have suggested that the analogous metal-oxos are not solely responsible for C–H hydroxylation. Through a series of *O*-atom labeling studies, Goldberg *et al.* have determined that high-valent manganese–oxo porphyrinoid complexes act simply as Lewis acid catalysts for the activation of PhIO, where the *O*-atom of the bound PhIO is preferentially transferred to substrate (Scheme 1.7a).⁵⁷ Similar conclusions have been drawn in the analogous *N*-group transfer chemistry with Mn-corroles.⁵⁸ In fact, a high-valent metal oxidation state is not even necessary, as M^{III}-porphyrinoid–oxidant intermediates have also been implicated as oxidizing agents. For instance, Collman and co-workers established that kinetic isotope values from competitive

-
55. (a) Eckert, N. A.; Vaddadi, S.; Stoian, S.; Lachicotte, R. J.; Cundari, T. R.; Holland, P. L. *Angew. Chem., Int. Ed.* **2006**, *45*, 6868. (b) Cowley, R. E.; DeYonker, N. J.; Eckert, N. A.; Cundari, T. R.; DeBeer, S.; Bill, E.; Ottenwaelder, X.; Flaschenriem, C.; Holland, P. L. *Inorg. Chem.* **2010**, *49*, 6172. (c) Cowley, R. E.; Eckert, N. A.; Vaddadi, S.; Figg, T. M.; Cundari, T. R.; Holland, P. L. *J. Am. Chem. Soc.* **2011**, *133*, 9796.
56. Wang, S. H.; Mandimutsira, B. S.; Todd, R.; Ramdhanie, B.; Fox, J. P.; Goldberg, D. P. *J. Am. Chem. Soc.* **2004**, *126*, 18.
57. (a) Eikey, R. A.; Khan, S. I.; Abu-Omar, M. M. *Angew. Chem., Int. Ed.* **2002**, *41*, 3591. (b) Zdilla, M. J.; Dexheimer, J. L.; Abu-Omar, M. M. *J. Am. Chem. Soc.* **2007**, *129*, 11505.



Scheme 1.7. Hypervalent iodine oxidation chemistry. (a) ^{18}O -labelling studies with manganese corrolazine (Cz) demonstrate that Mn(V)-oxo may not be responsible for *O*-atom transfer. (b) Oxidant-dependent variation in product ratios in the Fe-catalyzed hydroxylation of cyclohexane and d_6 -cyclohexane suggests that iodine reagent involved in the C–H functionalization step.

functionalization of *proteo*- and *deutero*-cyclohexane are oxidant dependent (Scheme 1.7b).⁵⁹ If the hypervalent iodine oxidants were simply responsible for the generation of a reactive Fe-oxo intermediate, the small, but significant, differences in KIE would be inexplicable. Therefore, they conclude that the active oxidizing species generated from the reaction of (por)FeCl with PhIO, F_5 -PhIO, and $PhI(OAc)_2$ are different from each other and are likely the respective catalyst–oxidant complexes. Each of these experiments suggests that the emphasis placed on metal-ligand multiply bonded intermediates is misguided.

58. Collman, J. P.; Chien, A. S.; Eberspacher, T. A.; Brauman, J. I. *J. Am. Chem. Soc.* **2000**, *122*, 11098.

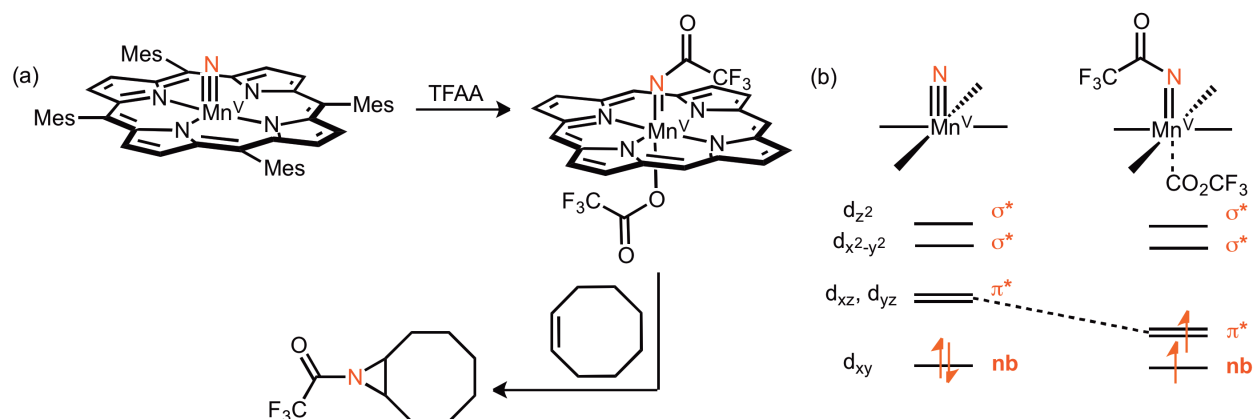


Figure 1.5. Reactive Mn-imide. (a) Isolated Mn(V)-nitride is unreactive towards substrates until addition of trifluoroacetic anhydride (TFAA), which forms the Mn(V)-imido. (b) Molecular orbital depiction of nitride and imido. Installation of electron-withdrawing substituent on *N*-atom weakens the π -bonding with the Mn d_{xz} and d_{yz} orbitals and allows for high-spin electronic configuration.

For instance, Groves synthesized a nitridomanganese(V) porphyrin complex via photolysis of the manganese–azide adduct to affect alkene aziridination chemistry.⁶⁰ However, this diamagnetic, Mn–N triply bonded species is unreactive towards alkene substrates until trifluoroacetic anhydride is introduced to the reaction (Figure 1.5a). The installation of an electron-withdrawing substituent on the *N*-atom weakens the π -interaction with the Mn d_{xz} and d_{yz} orbitals, lowers their energy and encourages a high-spin electronic configuration (Figure 1.5b). Population of the π^* -orbital decreases the Mn–N bond order and increases the propensity for *N*-transfer to substrate.⁶¹

An optimal application of this concept would involve the design of a catalyst with a greater number of d-electrons, encouraging the maximum population of d-orbitals with metal-ligand antibonding character. Warren and co-workers have applied this strategy towards the design of a copper diketimate C–H amination catalyst (Figure 1.6a).⁶² The catalyst can

59. Groves, J. T.; Takahashi, T. *J. Am. Chem. Soc.* **1983**, *105*, 2074.

60. For a more synthetically useful stoichiometric aziridination protocol that does not require azide photolysis to generate the Mn-nitride, see: Du Bois, J.; Tomooka, C. S.; Hong, J.; Carreira, E. M. *Acc. Chem. Res.* **1997**, *30*, 364.

competently activate benzylic, tertiary, secondary, and aldehydic C–H bonds when exposed to organic azides at 110 °C. Additionally, amination experiments with a benzyl radical clock and *cis*-dimethylcyclohexane are highly suggestive of an H-atom abstraction/radical rebound pathway.⁶³ An isolated bridging dicopper imido species is competent for nitrene transfer when exposed to substrate. However, the bridging imido is a “masked” reactive intermediate; kinetic studies demonstrate that the dissociation of the bridging imido to the terminal copper imido is required to affect C–H amination.⁶³ DFT calculations on the purported terminal copper-imide suggest a singlet biradical electronic structure that places a significant amount of electron density

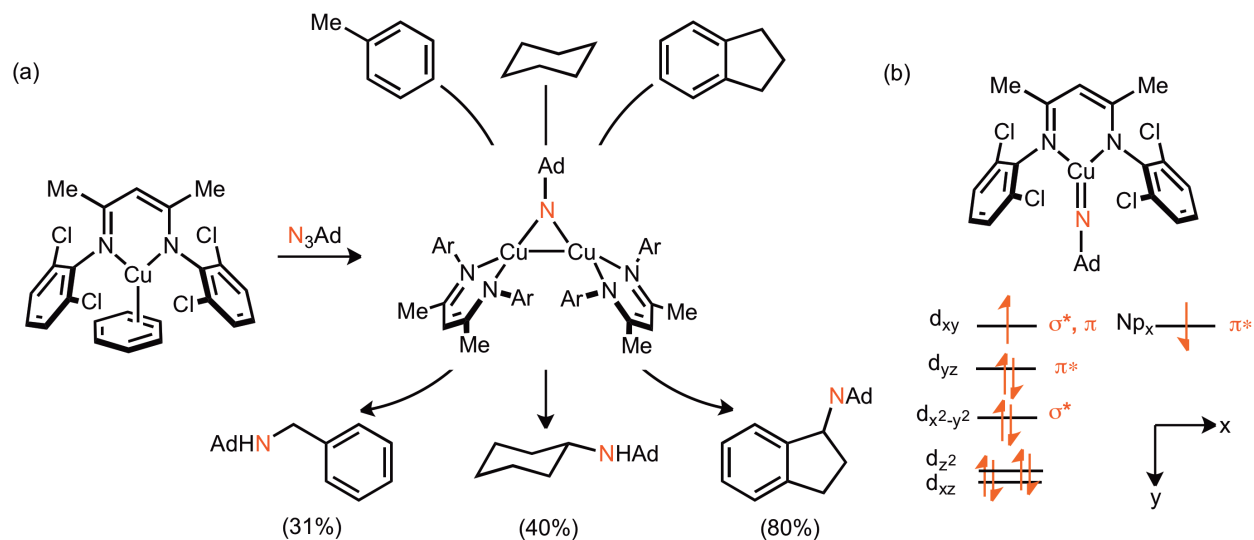


Figure 1.6. Reactive bridging Cu-imide. (a) Isolated bridging dicopper imido capable of stoichiometric (depicted) and catalytic N-group transfer to a variety of C–H bond substrates. (b) Molecular orbital depiction of proposed terminal imido intermediate.

61. Badiei, Y. M.; Dinescu, A.; Dai, X.; Palomino, R. M.; Heinemann, F. W.; Cundari, T. R.; Warren, T. H. *Angew. Chem., Int. Ed.* **2008**, *47*, 9961.

62. Aguila, M. J. B.; Badiei, Y. M.; Warren, T. H. *J. Am. Chem. Soc.* **2013**, *135*, 9399.

on the *N*-atom (Figure 1.6b).⁶⁴ A similar electronic structure is invoked for an isolated Ni^{III}-imide supported by the same ligand scaffold, although its C–H functionalization chemistry is less straightforward.⁶⁵

Hillhouse successfully isolated and characterized a unique two-coordinate Ni^{II}-imido using a bulky *N*-heterocyclic carbene ligand (Figure 1.7a).⁶⁶ Interestingly, the imido can insert into the C–H bond of ethene to form the vinylamine via a proposed azanickelacyclobutane intermediate. X-ray studies of the nickel-imide revealed a very short Ni–N bond of 1.663(3) Å. Variable temperature magnetometry indicated that the imide has a high-spin triplet ground state (Figure 1.7b). The unpaired electrons reside in π^* orbitals, as orbital mixing between the Ni 4s and 3d_{z²} orbital significantly stabilizes the σ^* orbital; DFT calculations corroborate this bonding depiction. The unusual high-spin electronic configuration of this d⁸ Ni^{II}-imido is likely responsible for its increased reactivity. Previously synthesized three coordinate Ni^{II}-imides have

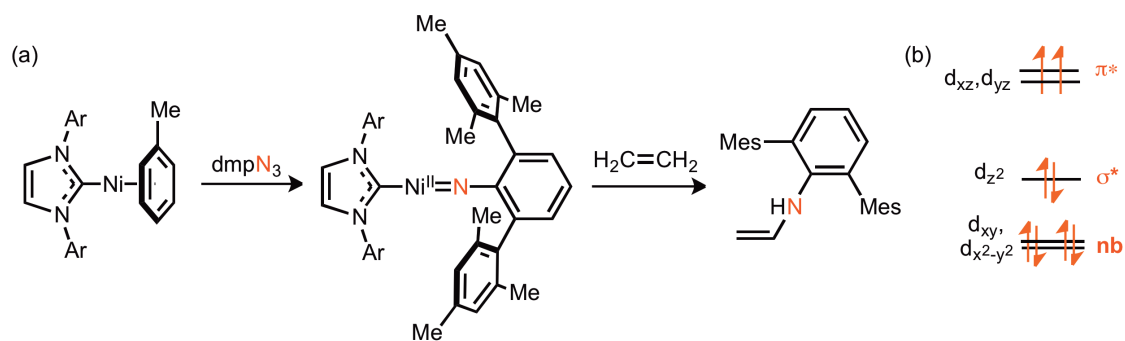


Figure 1.7. Reactive terminal nickel imide. (a) Isolated nickel imido capable of *N*-group transfer to ethylene. (b) Molecular orbital depiction of imido intermediate.

63. Cundari, T. R.; Dinescu, A.; Kazi, A. B. *Inorg. Chem.* **2008**, *47*, 10067.

64. Wiese, S.; McAfee, J. L.; Pahls, D. R.; McMullin, C. L.; Cundari, T. R.; Warren, T. H. *J. Am. Chem. Soc.* **2012**, *134*, 10114.

65. Laskowski, C. A.; Miller, A. J. M.; Hillhouse, G. L.; Cundari, T. R. *J. Am. Chem. Soc.* **2011**, *133*, 771.

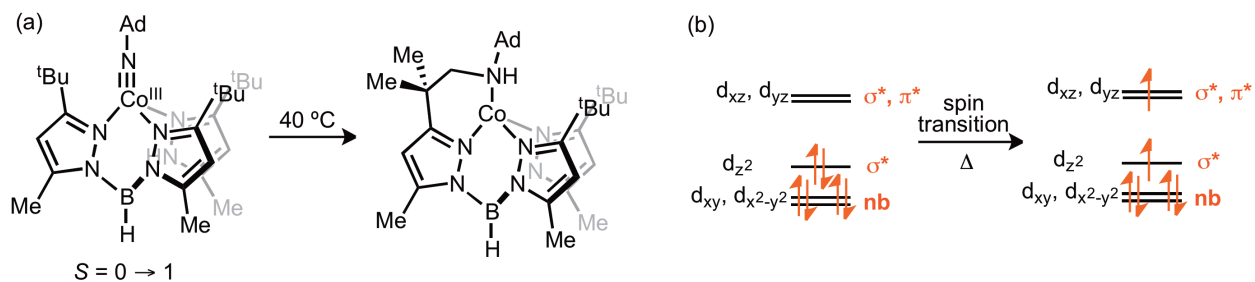


Figure 1.8. Reactive terminal Co-imide. (a) Isolated cobalt imido capable of intramolecular *N*-group transfer, predicted to go through a thermally induced $S=1$ excited state. (b) Molecular orbital depiction of ground and excited state electronic configurations of imido intermediate.

singlet ground states and are known to be unreactive towards C–H functionalization.⁶⁷

Using a tris(pyrazolyl)borate ligand platform, Theopold isolated a cobalt(III)-imide which undergoes intramolecular C–H amination of the ligand with slight heating (Figure 1.8a).⁶⁸ Both the solution magnetic moment and NMR spectroscopic data suggest the presence of a thermally accessible triplet ground state that is responsible for the C–H amination chemistry (Figure 1.8b).

Each of the examples from Warren, Hillhouse, and Theopold feature an isolated, crystallographically characterized, late transition-metal imido intermediate capable of C–H functionalization. Notably, the electronic ground (or low-lying excited) states of these reactive intermediates bear unpaired electron density in molecular orbitals with significant σ^* or π^* character along the metal-imido bond vector. Similarly, our work has focused on the development of a ferrous C–H amination catalyst surrounded by weak-field ligands to encourage a maximally high-spin electronic structure of an iron-imide. Such an electronic structure serves not only to weaken the metal-bound nitrene fragment so that it is poised for facile transfer to substrates, but also strongly favors radical reaction pathways that will have important implications in reaction selectivity and the scope of activatable C–H bonds.

66. (a) Mindiola, D. J.; Hillhouse, G. L. *J. Am. Chem. Soc.* **2001**, *123*, 4623. (b) Waterman, R.; Hillhouse, G. L. *J. Am. Chem. Soc.* **2008**, *130*, 12628. (c) Iluc, V. M.; Hillhouse, G. L. *J. Am. Chem. Soc.* **2010**, *132*, 15148.

1.6 C–H Amination Chemistry of High-Spin Ferrous Dipyrrinato Complexes

Weak field ancillary ligands are primarily featured in metalloproteins and, as such, typically engender intermediate- and high-spin electronic configurations in the reactive metal center. For instance, carboxylates and imidazoles of amino acid side chains bind Fe in soluble methane monooxygenase (*s*MMO)⁶⁹ and taurine α -ketoglutarate dioxygenase (TauD).⁷⁰ The tetrachelating porphyrin ligand found in cytochrome P450 is also considered a weak-field ligand. The pyrrole subunit of the porphyrin makes for a weak σ donor and its aromatic properties dramatically diminish its propensity to act as a π -base. In fact, a recent study assessing ligand donor properties through computational and experimental methods determined that the donicity of pyrrolide ligands is most similar to that of fluorinated alkoxides and halides.⁷¹

As discussed above, porphyrin ligands have been utilized extensively in synthetic C–H functionalization reactions.⁷² However, the macrocyclic ligand is both difficult to synthesize and offers a fairly restrictive tetragonal coordination geometry and ligand field. As such, dipyrrens⁷³ (or dipyrromethenes), composed of two pyrrole subunits in conjugation with one another, are an appealing ligand for the exploration of oxidative group transfer chemistry (Figure 1.9A). The

-
67. Shay, D. T.; Yap, G. P. A.; Zakharov, L. N.; Rheingold, A. L.; Theopold, K. H. *Angew. Chem., Int. Ed.* **2005**, *44*, 1508.
68. Ragsdale, S. W. *Chem. Rev.* **2006**, *106*, 3317.
69. Krebs, C.; Price, J. C.; Baldwin, J.; Saleh, L.; Green, M. T.; Bollinger J. M. *Inorg. Chem.* **2005**, *44*, 742.
70. DiFranco, S. A.; Maciulis, N. A.; Staples, R. J.; Batrice, R. J.; Odom, A. L. *Inorg. Chem.* **2012**, *51*, 1187.
71. Liu, H.; Zhang, X. P. *Chem. Soc. Rev.* **2011**, *40*, 1899.
72. (a) In *Die Chemie des Pyrrols*; Fischer, H.; Orth, H., Eds.; Akademische Verlagsgesellschaft: Leipzig, 1940; Vol. IX, pp 1-151. (b) Falk, H. *The Chemistry of Linear Oligopyrroles and Bile Pigments*; Springer-Verlag: Vienna, 1989. (c) Wagner, R. W.; Lindsey, J. S. *Pure Appl. Chem.* **1996**, *68*, 1373.

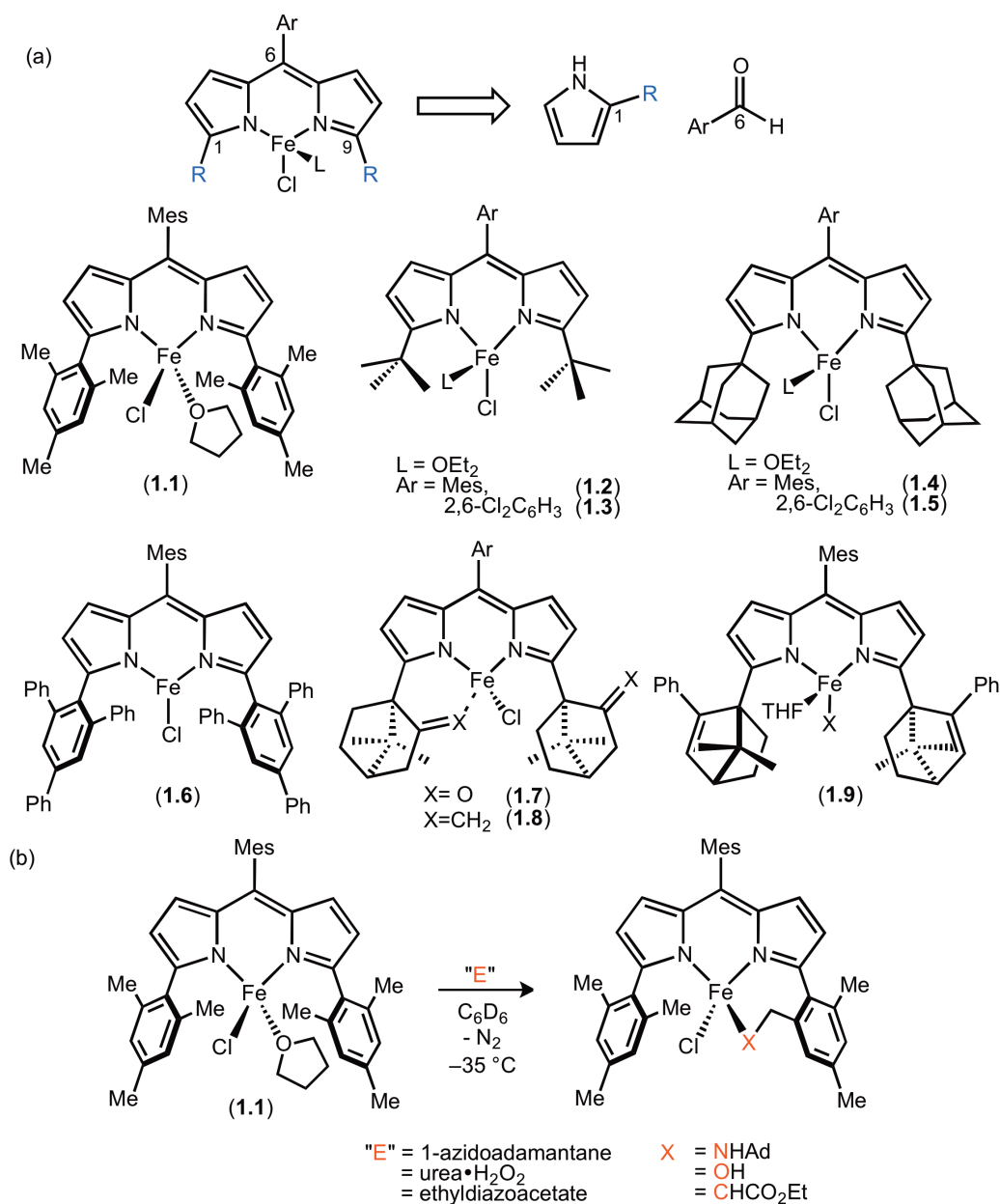


Figure 1.9. Dipyrinato iron complexes. (a) Dipyrinato ferrous chloride complexes referred to throughout this thesis. (b) Intramolecular group transfer chemistry to form C–N, C–O, and C–C bonds using the ferrous dipyrinato complex.

bidentate ligand binds transition metals in various coordination geometries and exhibits many of the interesting electronic properties of porphyrin ligands.⁷⁴ Bulky R-groups can readily be

73. (a) Loudet, A.; Burgess, K. *Chem. Rev.* **2007**, *107*, 4891. (b) Dolphin, D.; Harris, R. L. N.; Huppatz, J. L.; Johnson, A. W.; Kay, I. T.; Leng, J. *J. Chem. Soc. C* **1966**, 98. (c) Chierici, L.; Gardini, G. P. *Tetrahedron* **1966**, *22*, 53. (d) Ferguson, J.; West, B. O. *J. Chem. Soc. A* **1966**, 1565. (e) Murakami, Y.; Matusda, Y.; Sakata, K. *Inorg. Chem.* **1971**, *10*, 1728. (f) Bruckner, C.; Karunaratne, V.; Rettig, S. J.; Dolphin, D. *Can. J. Chem.* **1996**, *74*, 2182. (g) Bruckner, C.; Zhang, Y. J.; Rettig, S. J.; Dolphin, D. *Inorg. Chim. Acta* **1997**, *263*, 279.

installed at the 1 and 9 positions of the dipyrin via a straightforward two-step procedure starting from the corresponding pyrrole and aldehyde or acetal (Figure 1.9a). Such a substitution pattern encourages a low-coordinate metal environment with tunable levels of steric protection. We have employed this “semi-porphyrin” ligand platform in concert with various first-row transition metals to explore oxidative group transfer chemistry in an as of yet unexplored coordination geometry.

During the investigation of the mesityl substituted dipyrinato-iron complex **1.1**, it was observed that exposure to organic azides led to facile intramolecular delivery of the nitrene functional group into the benzylic C–H bond of the ligand (Figure 1.9b). While no intermediate buildup was detected, the reaction was postulated to proceed via a high-valent Fe^{IV}(NAd) species, akin to the Fe^{IV}-oxo species found in the hydroxylation pathway of cytochrome P450.⁷⁵ Similarly, exposure of **1.1** to urea hydrogen peroxide and ethyldiazoacetate resulted in intramolecular C–O and C–C bond formation.

The intermolecular variant of this reaction required removal of reactive C–H bonds from the ligand platform. Thus, dipyrromethene platforms featuring sterically encumbered alkyl and aryl substituents that lack weak C–H bonds were targeted. As will be discussed in **Chapter 2**, the alkyl-substituted dipyrinato-iron complexes **1.2** and **1.4** are competent for catalytic C–H amination of toluene and aziridination of styrene. In order to isolate the reactive intermediate, the aryl-substituted complex **1.6** was used in combination with 4-*t*Bu-C₆H₄N₃ (Figure 1.10a). Crystallographic and spectroscopic data suggest that the Fe-imide is best described as an Fe^{III}-

74. King, E. R.; Betley, T. A. *Inorg. Chem.* **2009**, 58, 2361.

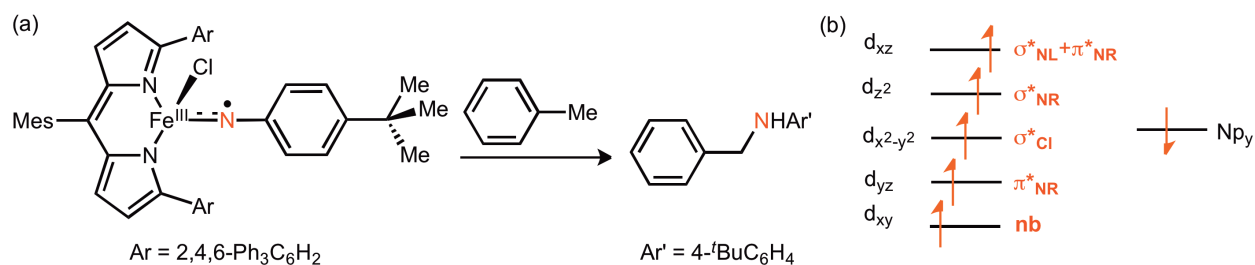


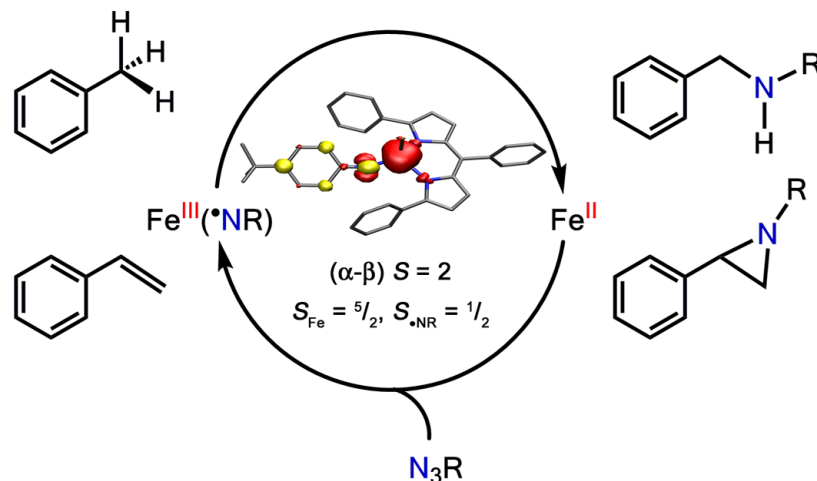
Figure 1.10. Reactive Fe-imide. (a) Isolated imido radical intermediate derived from **1.6** is competent for group transfer to benzylic C–H bond substrates. (b) Molecular orbital depiction of imido radical intermediate.

center ($S = 5/2$) antiferromagnetically coupled to an imido-based radical ($S = -1/2$) (Scheme 1.10b). The Fe–NAr bond distance (1.768(2) Å) is elongated relative to previously reported terminal Fe-imido complexes^{52,55,56} and the overall $S = 2$ complex is competent for stoichiometric group transfer to benzylic C–H bonds. The enhanced reactivity of this Fe-imide in comparison to those discussed above truly highlights the importance of electronic structure considerations when designing complexes for C–H functionalization chemistry.

In **Chapter 3**, the discussion will focus on the selectivity of intermolecular nitrene transfer with **1.3** and **1.5** in the presence of olefinic substrates. Selective intermolecular allylic C–H amination is notoriously difficult (*vide supra*); competitive aziridination and alkene isomerization pathways often result in a mixture of products. However, complexes **1.3** and **1.5** promote regio- and chemoselective intermolecular amination of both terminal and cyclic olefins. In **Chapter 4**, a new synthetic protocol for the construction of *N*-heterocycles from linear aliphatic azide precursors using catalyst **1.5** is discussed.⁷⁶ Facile intramolecular amination of benzylic, allylic, tertiary, secondary, and primary C–H bonds in combination with an *in situ* protection strategy provides access to a wide variety of highly substituted pyrrolidine and piperidine products. A series of mechanistic experiments were conducted in order to distinguish between a direct insertion or H-atom abstraction/radical rebound pathway. In **Chapter 5**, ligand modifications to catalyst **1.4** are explored in order to promote diastereo- and enantioselective

cyclization reactions. The diastereoselective synthesis of *cis*-2,5-disubstituted pyrrolidines is achieved via replacement of the ancillary chloride ligand with a phenoxide anion. A transition state model is developed in order to rationalize the heightened selectivity. The incorporation of optically active camphor-derived substituents to the dipyrin ligand generates complexes **1.7-9**, one of which is competent for low-levels of enantioinduction at room temperature.

75. Hennessy, E. T.; Betley, T. A. *Science* **2013**, *340*, 591.



Chapter 2: Catalytic C–H Bond Amination from High-Spin Iron- Imido Complexes⁷⁷

2.1 Introduction

Introducing functionality into unactivated C–H bonds remains a significant challenge both in the realm of complex molecule synthesis as well as in the elaboration of simple hydrocarbon feed stocks into value-added commodity chemicals.^{78,79} C–H amination in particular has been the focus of much recent synthetic progress, although many mechanistic details and their interplay in effecting chemo- and regioselectivity remain poorly understood.⁸⁰ Biological C–H bond functionalization is primarily performed by iron-containing enzymes that utilize dioxygen as the terminal oxidant.²⁸ A key structural element of the putative hydroxylation catalyst in both heme

76. This chapter was adapted with permission from King, E. R.; Hennessy, E. T.; Betley, T. A. *J. Am. Chem. Soc.* **2011**, *133*, 4917. Copyright 2011 American Chemical Society.

77. Bergman, R. G. *Nature* **2007**, *446*, 391.

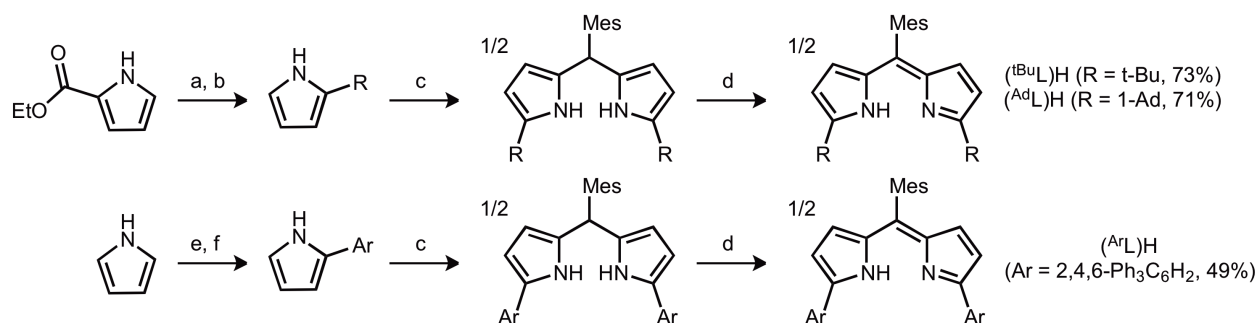
78. Labinger, J. A.; Bercaw, J. E. *Nature* **2002**, *417*, 507.

79. For a review of catalytic C–H amination systems, see: Collet, F.; Dodd, R. H.; Dauban, P. *Chem. Commun.* **2009**, 5061.

(where iron is embedded in a porphyrin) and non-heme systems is a transiently-formed terminal iron oxo, typically thought to involve multiple bond character.^{28,81} Furthermore, the reactivity of this intermediate is believed to be dictated by its electronic structure.^{82,83,84} In non-heme enzymes four such Fe^{IV}(oxo) complexes have been characterized, and their reactivity has been linked to a common electronic feature, namely a high-spin ground state ($S = 2$).⁸¹ However, an isolable, high-spin synthetic analogue has not been reported that mimics the catalytic transfer of the metal-ligand multiply-bonded functionality found in the biological systems.⁸⁵⁻⁹⁰ Herein we report room temperature, catalytic C–H bond and olefin functionalization from a transiently formed, high-spin iron-imido complex.

-
80. Krebs, C.; Fujimori, D. G.; Walsh, C. T.; Bollinger, M. J., Jr. *Acc. Chem. Res.* **2007**, *40*, 484.
 81. Decker, A.; Rhode, J.-U.; Klinker, E. J.; Wong, S. D.; Que, L., Jr.; Solomon, E. I. *J. Am. Chem. Soc.* **2007**, *129*, 15938.
 82. Bernasconi, L.; Louwse, M. J.; Baerends, E. J. *Eur. J. Inorg. Chem.* **2007**, 3023.
 83. Ye, S.; Neese, F. *Curr. Opin. Chem. Biol.* **2009**, *13*, 89.
 84. Pestovsky, O.; Stoian, S.; Bominaar, E. M.; Shan, X.; Munck, E.; Que, L., Jr.; Bakac, A. *Angew. Chem., Int. Ed.* **2009**, *48*, 3622.
 85. Kaizer, J.; Klinker, E. J.; Oh, N. Y.; Rhode, J.-U.; Song, W. J.; Stubna, A.; Kim, J.; Munck, E.; Nam, W.; Que, L., Jr. *J. Am. Chem. Soc.* **2004**, *126*, 472.
 86. Kumar, D.; Hirao, H.; Que, L., Jr.; Shaik, S. *J. Am. Chem. Soc.* **2005**, *127*, 8026.
 87. England, J.; Martinho, M.; Farquhar, E. R.; Frisch, J. R.; Bominaar, E. L.; Munck, E.; Que, L., Jr. *Angew. Chem., Int. Ed.* **2009**, *48*, 3622.
 88. England, J.; Guo, Y.; Farquhar, E. R.; Young, V. G., Jr.; Munck, E.; Que, L., Jr. *J. Am. Chem. Soc.* **2010**, *132*, 8635.
 89. Lacy, D. C.; Gupta, R.; Stone, K. L.; Greaves, J.; Ziller, J. W.; Hendrich, M.; Borovik, A. S. *J. Am. Chem. Soc.* **2010**, *132*, 12188.

2.2 Metal Complex Synthesis



Scheme 2.1. *Synthesis of dipyrromethene ligands.* Depicted yields are for last two steps. Reagents and conditions: (a) *tert*-butyl chloride or 1-adamantyl chloride, 2 equiv. AlCl_3 , DCM, 1 h; (b) 5 equiv. NaOH, ethylene glycol, reflux, 12 h; (c) 0.5 equiv $\text{MesCH}(\text{OMe})_2$, 0.1 equiv PPTS, DCM, 3 h; (d) DDQ, DCM, 12h; (e) 2 equiv. 60% NaH, THF, 4 h; (f) 0.33 equiv. 1-bromo-2,4,6-triphenylbenzene, ZnCl_2 , 1.33% *S*-Phos, 0.67% $\text{Pd}_2(\text{dba})_3$, THF, 90 °C, 24 h; (g) 0.5 equiv. $\text{MesCH}(\text{OMe})_2$, 0.1 equiv PPTS, DCM, 80 °C, 24 h

During our investigations of dipyrromethene-iron complexes as heme surrogates, we observed that reaction of an Fe^{II} complex with organic azides led to facile intramolecular delivery of the nitrene functional group into a ligand C–H bond.⁷⁵ The reaction was postulated to proceed via a high-valent $\text{Fe}^{\text{IV}}(\text{NR})$ species, akin to the hydroxylation pathway of cytochrome P450 and its functional analogues.^{91,92} Extending this reactivity to an intermolecular reaction required removal of reactive C–H bonds from the ligand platform. Thus, dipyrromethene platforms were targeted featuring sterically encumbered aryl or alkyl substituents that lack weak C–H bonds to circumvent intramolecular C–H bond activation pathways. Pyrroles substituted in the 2-position were afforded using modified Negishi coupling for 2-aryl pyrroles, and directed Friedel-Crafts alkylations for 2-alkyl pyrroles. For example, 2,4,6- $\text{Ph}_3\text{-C}_6\text{H}_2\text{Br}$ was cleanly coupled to sodium pyrrolide to afford 2-Ar(pyrrole) using conditions outlined by Sadighi and coworkers (3 eq. sodium pyrrolide, 3 eq. ZnCl_2 , $\text{Pd}_2(\text{dba})_3$ (2%)/*S*-Phos (4%); THF, 90°C, 24 h, 84%; Ar = 2,4,6- $\text{Ph}_3\text{C}_6\text{H}_2$).⁹³ Alkyl-substituted pyrroles were synthesized in good yields by

90. Groves, J. T. *J. Chem. Ed.* **1985**, 62, 928.

91. Sono, M.; Roach, M. P.; Coulter, E. D.; Dawson, J. H. *Chem. Rev.* **1996**, 96, 2841.

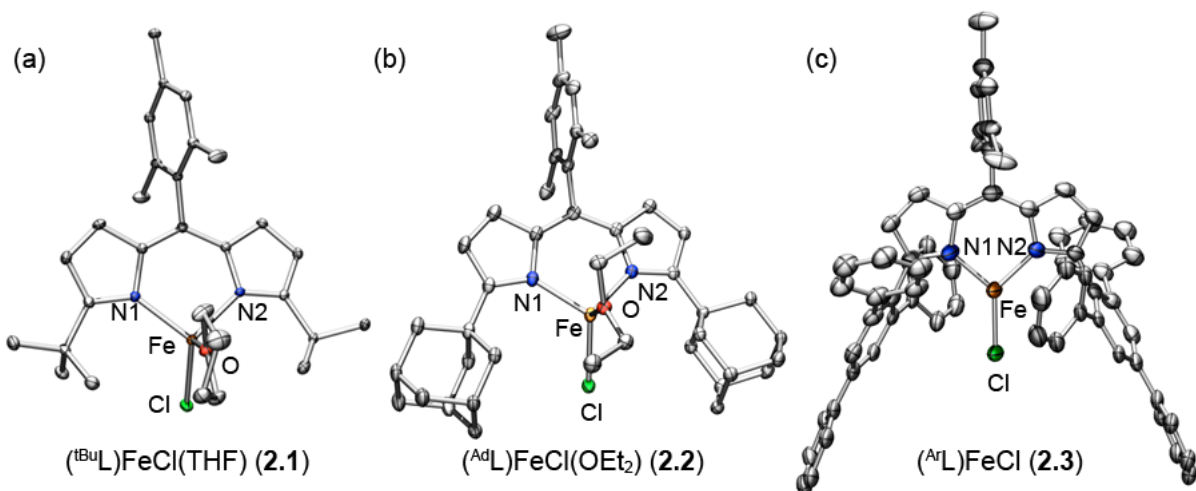


Figure 2.1. X-ray structures of ferrous complexes. Solid-state molecular structures for (a) $({}^{\text{tBu}}\text{L})\text{FeCl}(\text{thf})$ (**2.1**), (b) $({}^{\text{Ad}}\text{L})\text{FeCl}(\text{OEt}_2)$ (**2.2**), and (c) $({}^{\text{Ar}}\text{L})\text{FeCl}$ (**2.3**) with thermal ellipsoids at 50% probability level for (a) and (b) and (c) 30% probability level (Fe orange, Cl green, C black, N blue; hydrogens, solvent molecules, and aryl ring disorder in **2.3** are omitted for clarity). Bond lengths (\AA) for $({}^{\text{tBu}}\text{L})\text{FeCl}(\text{thf})$ (**2.1**): Fe-N1, 2.026(2); Fe-N2, 2.028(2); Fe-Cl, 2.255(1); Fe-O, 2.077(2); $({}^{\text{Ad}}\text{L})\text{FeCl}(\text{OEt}_2)$ (**2.2**): Fe-N1, 2.028(3); Fe-N2, 2.042(3); Fe-Cl, 2.250(2); Fe-O, 2.090(2); $({}^{\text{Ar}}\text{L})\text{FeCl}$ (**2.3**): Fe-N1, 1.966(5); Fe-N2, 1.966(5); Fe-Cl, 2.154(2).

reaction of the corresponding alkyl-chloride (R-Cl), AlCl_3 , and ethyl pyrrole-2-carboxylate following decarboxylation (KOH, glycol, 200°C , 12 h, R = adamantyl 88%, ${}^{\text{tBu}}$ 65%).⁹⁴ As outlined in Scheme 2.1, disubstituted dipyrromethene ligands (${}^{\text{X}}\text{L}$, X = 1,9-substituent) were prepared using literature procedures to produce the novel ligands in good overall yields ($({}^{\text{Ar}}\text{L})\text{H}$, 49%; $({}^{\text{tBu}}\text{L})\text{H}$, 73%; $({}^{\text{Ad}}\text{L})\text{H}$, 71%).⁷⁵ Dipyrromethene deprotonation with phenyl lithium in thawing benzene afforded the lithium salts $({}^{\text{Ar}}\text{L})\text{Li}$, $({}^{\text{tBu}}\text{L})\text{Li}$, and $({}^{\text{Ad}}\text{L})\text{Li}$ as brightly colored powders in nearly quantitative yields (88-92%) for subsequent transmetalation to iron.

Formation of the iron-dipyrromethene complexes proceeds cleanly from reaction of the lithio dipyrromethene species with a thawing slurry of FeCl_2 in an ethereal solvent. For example, reaction of $({}^{\text{Ad}}\text{L})\text{Li}$ with FeCl_2 in thawing diethyl ether cleanly affords the solvated complex $({}^{\text{Ad}}\text{L})\text{FeCl}(\text{OEt}_2)$ (**2.2**) as a luminescent green-brown solid following precipitation (yield: 58%). Utilizing the aryl-substituted ligand $({}^{\text{Ar}}\text{L})\text{Li}$ under similar reaction conditions afforded the three-

92. Rieth, R. D.; Mankad, N. P.; Calimano, E.; Sadighi, J. P. *Org. Lett.* **2004**, *6*, 3981.

coordinate species ($^A\text{T}\text{L}$)FeCl (**2.3**) as a bright purple solid following crystallization (46%). The compositions and purity of **2.2** and **2.3** were established by ^1H NMR, UV-visible spectroscopy, ^{57}Fe Mössbauer spectroscopy, and combustion analysis, the data of which are compiled in Table 2.1. The respective geometries of four-coordinate **2.2** and three-coordinate **2.3** were verified by X-ray diffraction studies on a single crystal of each (Figure 2.1). The solid-state molecular structure of **2.2** shows a trigonal-monopyramidal geometry with a diethyl ether molecule capping the pyramid. Complex **2.3** has a trigonal-planar geometry about iron, wherein the large 2,4,6- $\text{Ph}_3\text{C}_6\text{H}_2$ ligand substituents flank iron above and below the $[\text{N}_2\text{FeCl}]$ plane. The average bond lengths of the four-coordinate complex (Fe– N_L 2.035(4) Å, Fe–Cl 2.249(1) Å) is expanded relative to three-coordinate species (Fe– N_L 1.966(7) Å, Fe–Cl 2.154(2) Å). The shorter bond lengths in the three-coordinate species are likely a result of both decreased steric repulsion and the iron being extremely electron deficient in the absence of a fourth donor. The room temperature solution magnetic moments determined using the method of Evans are 5.2(2) μ_B for **2.2** and 5.1(2) μ_B for **2.3**, both consistent with high spin ($S = 2$) iron(II).⁹⁵

Table 2.1. Spectral and magnetic properties of complexes 2.1 – 2.5.

complex	$\mu_{\text{eff}} (\mu_B)$	S	$\lambda / \text{nm} (\epsilon / \text{M}^{-1}\cdot\text{cm}^{-1})$	$\delta (\text{mm}/s)^b$	$ \Delta E_0 (\text{mm}/s)^b$
($^{\text{tBu}}\text{L}$)FeCl(thf) (2.1)	5.2(2)	2	497 (40000) ^a	--	--
($^{\text{Ad}}\text{L}$)FeCl(OEt ₂) (2.2)	5.1(1)	2	494 (59000) ^a	0.98	3.70
($^{\text{Ar}}\text{L}$)FeCl (2.3)	5.1(2)	2	554 (26000)	0.68	0.68
[($^{\text{Ar}}\text{L}$)FeCl] ₂ (μ -N(Ph)(C ₆ H ₅)N) (2.4)	7.8(2)	2	551 (27000)	0.33	2.15
($^{\text{Ar}}\text{L}$)FeCl(NC ₆ H ₄ - <i>p</i> - ^t Bu) (2.5)	5.3(1)	2	553 (26000)	0.29	2.29

93. Bailey, D. M.; Johnson, R. E.; Albertson, N. F. *Organic Syntheses* **1988**, Coll. Vol. 6, 618.

94. Evans, D. F. *J. Am. Chem. Soc.* **1959**, 81, 2003.

2.3 Intermolecular, Catalytic N-Group Transfer with Organic Azides

As the reaction of organic azides with (^{Mes}L)FeCl(THF) gives rise to intramolecular amination of a ligand C–H bond,⁷⁵ we canvassed the reactivity of complex **2.2** with organic azides. When alkyl azides (e.g., (H₃C)₃CN₃, 1-azidoadamantane) are added to **2.2** in toluene, rapid azide consumption is evident and the product of intermolecular, nitrene-insertion into a benzylic C–H bond of toluene (PhCH₂NHR) is observed. Catalytic turnover is observed at room temperature when multiple equivalents of azide are used. Reactions of 1-azidoadamantane (N₃Ad) with **2.2** in toluene at room temperature yielded a mixture of benzyladamantylamine (95% of converted azide), benzyladamantylimine (2.8%), and adamantylamine (1.8%) for a total of 6.7 turnovers (TON) (see Table 2.2). Turnover is maximized by running the reaction at 60 °C (TON = 10-12), but decreases substantially at elevated temperatures (TON: 8.7 at 90 °C; 6 at 120 °C). The ratios of the amination products changes at elevated temperatures as well (at 120 °C: benzyladamantylamine (75% of converted azide), benzyladamantylimine (4%), and adamantylamine (21%)). At elevated temperatures (120 °C) the presence of 1,2-diphenylethane (product of coupling two PhCH₂) becomes significant. While elevated temperatures may facilitate amine dissociation from the iron catalyst, it does so at the expense of thermal stability of the iron catalyst. Complex **2.2** is also effective for nitrene delivery to olefinic substrates. Near quantitative nitrene transfer was observed when **2.2** is reacted with N₃Ad in styrene at room temperature, giving 85% of the corresponding aziridine (17 TON based on 20 equivalents of azide).

Catalysis screens for the amination of toluene showed complex **2.2** to be the most active, whereas the *tert*-butyl analogue **2.1** only showed evidence for 5.6 turnovers at 60°C, and complex **2.3** showed only trace amounts of aminated product by mass spectrometry. While THF

Table 2.2. LC/MS (¹H NMR) amination yields with **2.2**.

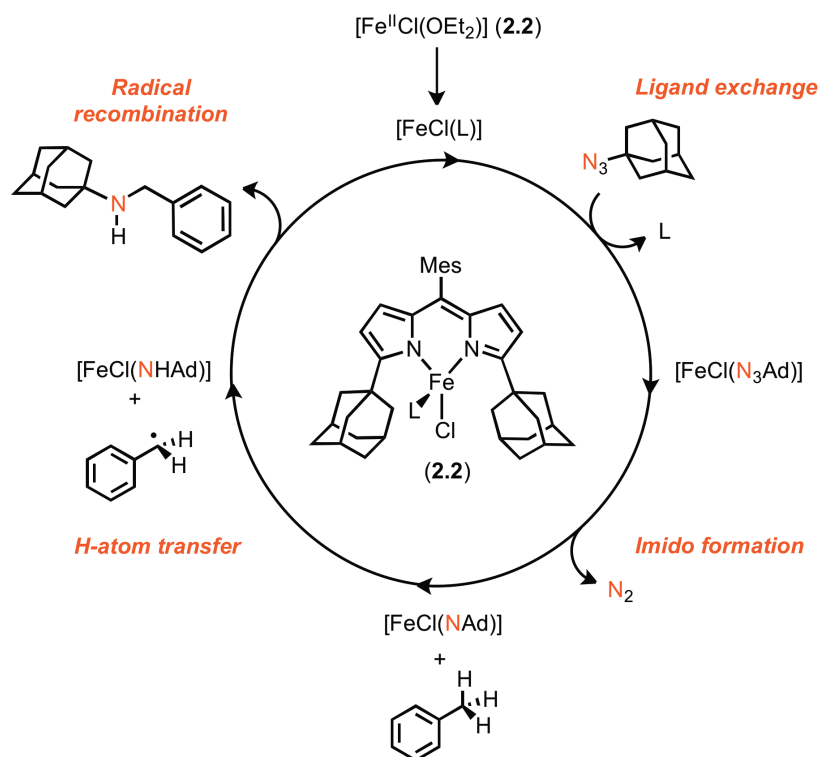
Temperature	BnAdNH(%)	PhC(H)NAd(%)	AdNH ₂ (%)	(PhCH ₂) ₂ (%)	TON
25 °C	34 (25)	1 (1)	3	(–)	6.7 (5.0)
60 °C	50 (56)	1 (1)	2	(1)	10 (11)
90 °C	41 (41)	3 (4)	11	(4)	8.7 (8.8)
120 °C	29 (29)	1.4 (1)	8	(9)	6.0 (5.7)

found in the precatalyst (e.g. (^{Ad}L)FeCl(THF)) is tolerated during catalysis, added THF (10 equivalents) to the reaction completely suppresses amination as THF presumably outcompetes azide association. Addition of a Lewis-acid promoter (1 equivalent of B(C₆F₅)₃) to scavenge THF from the precatalyst did not increase the turnover observed for any of the pre-catalysts screened. Furthermore, the reaction is impeded by product inhibition. Addition of 10 equivalents of adamantylamine or 15 equivalents of benzyladamantylamine to **2.2** under typical catalytic conditions (5% **2.2**, toluene 60°C) suppresses the catalytic amination to an undetectable amount.

2.4 Proposed Mechanism

2.4.1 Kinetic Isotope Experiment

The detection of 1,2-diphenylethane during the formation of benzyl-adamantylamine strongly suggests an H-atom abstraction pathway is operative. As a probe for direct H-atom transfer, a competition experiment employing a 1:1 ratio of toluene to its perdeutero analogue provides a kinetic isotope effect, k_H/k_D , of 12.8(5) for precatalyst **2.2**. The k_H/k_D ratio is consistent with a C–H bond breaking event as the rate determining step and the reaction proceeding by a hydrogen atom abstraction/rebound mechanism as illustrated in Scheme 2.2. The observed KIE exceeds the values Che and coworkers reported for stoichiometric C–H amination from isolated



Scheme 2.2. Catalytic cycle. Proposed catalytic cycle for the amination of C–H bonds by reaction of **2.2** with organic azides.

Ru^{VI} bis-imido complexes (KIE: 4.8-11)^{40,96} and those reported by Warren and coworkers for nitrene delivery from a putative $[\text{Cu}]_2(\text{imido})$ complex (KIE: 5-6),⁶² though the isotope effect reported for ethylbenzene amination by a Cu(amido) is substantially higher (KIE: 70).⁹⁷ The large KIE value also suggests H-tunneling is operative, akin to that observed in TauD monooxygenases (KIE: 37)⁸¹ and several Fe^{IV} -oxo model complexes reported by Que and Nam (KIE: 18-50).^{88,98,99} The larger kinetic isotope effect values are common to reactive species

95. Leung, S. K. Y.; Tsui, W. M.; Huang, J. S.; Che, C. M.; Liang, J. L.; Zhu, N. Y. *J. Am. Chem. Soc.* **2005**, *127*, 16629.

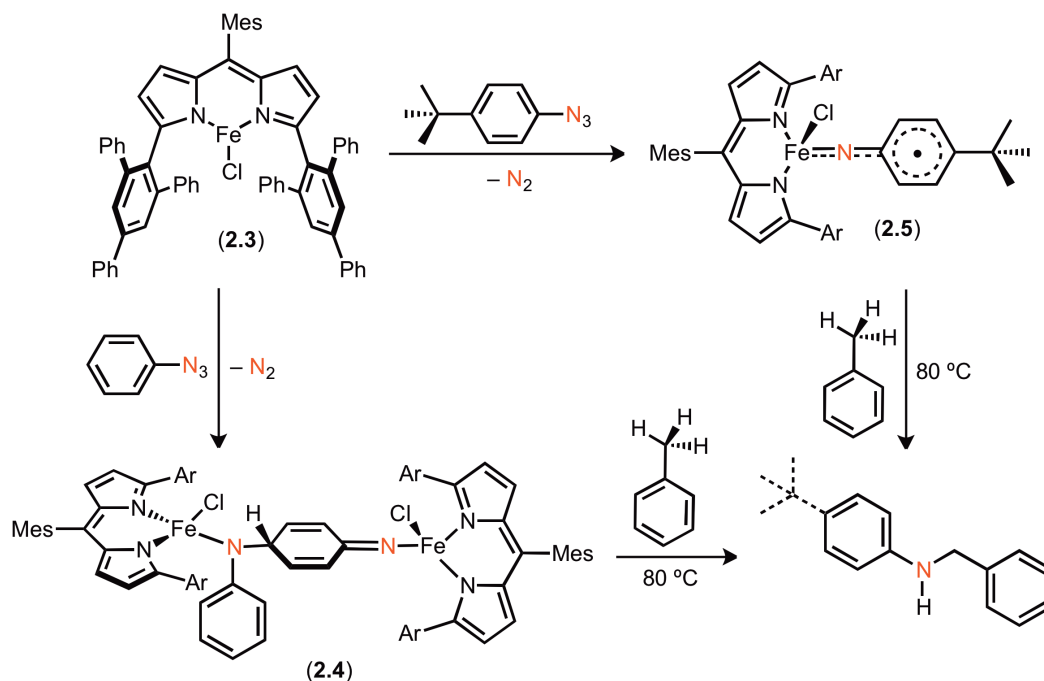
96. Wiese, S.; Badiel, Y. M.; Gephart, R. T.; Mossin, S.; Varonka, M. S.; Melzer, M. M.; Meyer, K.; Cundari, T. R.; Warren, T. H. *Angew. Chem., Int. Ed.* **2010**, *49*, 8850.

97. Que, L., Jr. *Acc. Chem. Res.* **2007**, *40*, 493.

98. Nam, W. *Acc. Chem. Res.* **2007**, *40*, 522.

featuring high-spin ground states, or high-spin states thermally accessible under the reaction conditions.¹⁰⁰

2.4.2 Isolation of Reactive Intermediate



Scheme 2.3. *Synthesis and reactivity of ferric-complexes.* Synthesis of the bimolecularly-coupled Fe^{III} imido-precursor **3** and the terminal imido complex **4** with a delocalized imido-based radical, Fe^{III}(NAr), and their subsequent reactivity with C–H bonds.

While our proposed mechanism suggests the intermediacy of an Fe^{IV} imido complex prior to the rate-determining step of H atom abstraction, we sought to validate this hypothesis via isolation or characterization of the putative intermediate. Reacting a thawing solution of **2.3** in benzene with a stoichiometric amount of phenylazide quantitatively produces an ¹H NMR silent

99. Klinker, E. J.; Shaik, S.; Hirao, H.; Que, L., Jr. *Angew. Chem., Int. Ed.* **2009**, *48*, 1291.

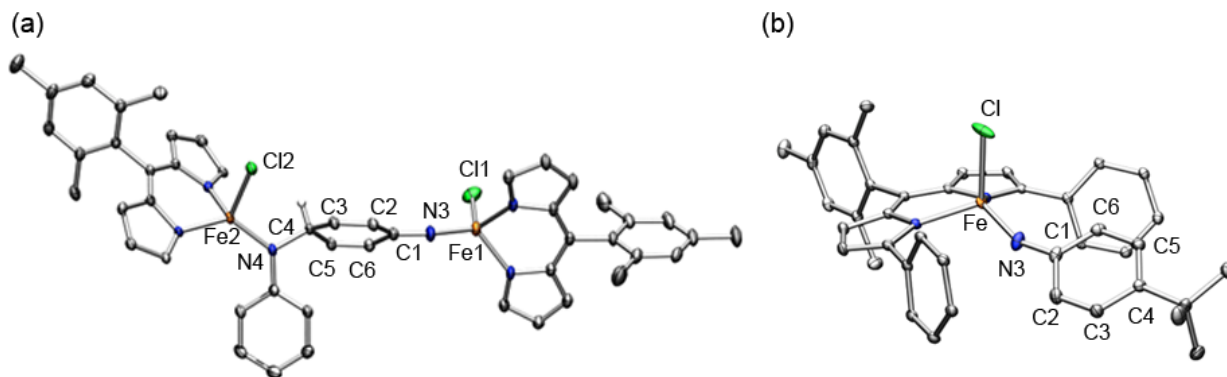


Figure 2.2. X-ray structures of ferric complexes. Solid-state core molecular structures for (a) **2.4** and (b) **2.5** (ligand aryl substituents, hydrogen atoms and solvent molecules are omitted for clarity). Bond lengths (Å) for **2.4**: Fe1-N3, 1.810(2); Fe1-Cl1, 2.202(1); C1-N3, 1.276(3); C1-C2, 1.462(4); C2-C3, 1.328(3); C3-C4, 1.490(4); C4-C5, 1.489(4); C5-C6, 1.331(3); C6-C1, 1.462(4); N4-C4, 1.484(3); Fe2-Cl2, 2.228(1); Fe2-N4, 1.886(2); for **2.5**: Fe-Cl, 2.210(1); Fe-N3, 1.768(2); N3-Cl, 1.331(2); C1-C2, 1.423(3); C2-C3, 1.372(3); C3-C4, 1.406(3); C4-C5, 1.405(3); C5-C6, 1.378(3); C6-C1, 1.414(3).

complex following consumption of the azide as ascertained by the disappearance of the azide stretch (ν_{N_3}) by infrared spectroscopy. An X-ray diffraction study on crystals grown from the reaction revealed the product to be the bimolecularly-coupled species $[(^{\text{Ar}}\text{L})\text{FeCl}]_2(\mu\text{-N}(\text{Ph})(\text{C}_6\text{H}_5)\text{N})$ (**2.4**) shown in Scheme 2.3, the solid-state molecular structure of which is shown in Figure 2.2a. The coupled product **2.4** presumably arises from radical coupling of two monomeric $(^{\text{Ar}}\text{L})\text{FeCl}(\text{NPh})$ moieties to intermolecularly form a new N–C bond. Complex **2.4** features chemically distinct N(Ph)R ligation to one iron center (Fe1) and ketimide ligation to the second (Fe2). The (NPh) ketimide formulation is supported by the dearomatization of the C1-C6 ring, featuring localized double bonds (C2-C3 1.328(3) Å, C5-C6 1.331(3) Å, C1-N6 1.276(3) Å). The room temperature magnetic moment for **2.4** is 7.8(2) μ_B , slightly lower than the calculated value of 8.3 μ_B for two non-interacting high-spin Fe^{III} centers ($S = 5/2$). The Fe^{III} formulation is corroborated by zero-field ^{57}Fe Mössbauer analysis of **2.4** at 100 K which reveals that both iron centers in **2.4** have isomer shifts and quadrupole splitting parameters consistent with high-spin Fe^{III} (δ , $|AE_Q|$ ($^{\text{mm}}/\text{s}$) 0.33, 2.15). The parameters are significantly distinct from both the Fe^{II} precursor **2.3** (δ , $|AE_Q|$ ($^{\text{mm}}/\text{s}$) 0.68, 0.68) and the four-coordinate Fe^{II} species **2.2** (δ ,

$|\Delta E_Q|$ ($^{\text{mm}}/\text{s}$) 0.98, 3.70) (Table 1). The three-coordinate chloride **2.3**, had a lower isomer shift than all of the other dipyrromethene Fe^{II} complexes and a particularly small quadrupole splitting, similarly unique parameters have been reported for planar three-coordinate β -diketimate complexes.¹⁰¹

In an effort to obtain a monomeric imido complex, **2.3** was reacted with $p\text{-}^t\text{BuC}_6\text{H}_4\text{N}_3$ where the aryl *para*-substitution was selected to sterically prevent the radical coupling pathway observed in the formation of **2.4**. Peters and co-workers reported a Cu di-*para*-tolyl aminyl radical, in which the tolyl methyl groups prevented radical coupling to form aryl-aryl linked dimers if methyl was replaced with hydrogen by using a diphenyl amido unit.⁴⁸ Analogously, in contrast to the dimerization observed in the reaction of **2.3** with phenylazide, a new product from reaction of **2.3** with $p\text{-}^t\text{BuC}_6\text{H}_4\text{N}_3$ is easily discernible by ^1H NMR as a C_2 -symmetric species distinct from the starting material. The room temperature magnetic moment for this species is $5.3(1) \mu_B$, consistent with an $S = 2$ complex. Zero-field, ^{57}Fe Mössbauer analysis of the crude reaction product at 100 K reveals a single iron-containing species (δ , $|\Delta E_Q|$ ($^{\text{mm}}/\text{s}$) 0.29, 2.29) that is nearly super-imposable with the spectrum obtained for **2.4**, suggesting the new product also contains Fe^{III} (Figure 2.3a).

An X-ray diffraction study on single crystals grown from the reaction of **2.3** with $p\text{-}^t\text{BuC}_6\text{H}_4\text{N}_3$ revealed the product to be a monomeric species bearing a terminally bound imido ligand ($^{\text{Ar}}\text{L})\text{FeCl}(\text{NC}_6\text{H}_4\text{-}p\text{-}^t\text{Bu})$ (**2.5**) (Figure 2.2b). The Fe–Cl (2.210(1) Å) and Fe–N_L (2.005(2) Å) bond lengths are consistent with those found in the bimolecularly coupled Fe^{III} dimer **2.4**. The Fe–N_{Ar} bond length in **2.5** (1.768(2) Å) is elongated relative to previously reported terminal imido complexes (e.g. $[\text{PhBP}_3]\text{Fe}(\text{N-tol})$ 1.658(2) Å, $S = 1/2$;⁵² $(^{\text{Me}}\text{nacnac})\text{Fe}(\text{NAd})$ 1.662(2) Å, S

100. Andres, H.; Bominaar, E. L.; Smith, J. M.; Eckert, N. A.; Holland, P. L.; Munck, E. *J. Am. Chem. Soc.* **2002**,

$= {}^3/2$; ^{56b} (^{IPr}PDI)Fe(NAr) 1.705-1.717 Å, $S = 1$; ^{55a} [(N4Py)Fe(NTs)]²⁺ 1.73 Å, $S = 1$ ¹⁰²), suggesting the iron-imido multiple bond character is severely attenuated. To account for the anomalously long Fe–NAr bond length in **2.5**, the similar Mössbauer parameters for **2.4** and **2.5**, and the observed magnetic moment of monomeric **2.5**, we propose **2.5** is comprised of a high-spin Fe^{III} (d^5 , $S = 5/2$) center antiferromagnetically coupled to an imido-based radical ($S = 1/2$). The presence of an aryl- delocalized radical can be gleaned from the C–C bond distances within the nitrene aryl ring (N3-C1, 1.331(2); C1-C2, 1.423(3); C2-C3, 1.372(3); C3-C4, 1.406(3); C4-C5, 1.405(3); C5-C6, 1.378(3); C6-C1, 1.414(3)). In comparison for a true Fe^{III} imido (*para*-substituted), without radical character the average bond distances are C-N, 1.383 Å, C_{ipso}-C_{ortho}, 1.401 Å, C_{ortho}-C_{meta}, 1.378 Å, and C_{meta}-C_{para}, 1.387 Å.⁵² Probing the electronic structure by DFT corroborates the proposed electronic structure. Broken-symmetry calculations estimate the antiferromagnetic magnetic exchange coupling (J)¹⁰³ to be -673 cm⁻¹ and the calculated Mössbauer parameters match well with those observed for **2.5** (calculated δ , $|AE_Q|$ (mm/s) 0.34, -2.00).^{104,105} The calculated spin density plot ($\alpha - \beta$) for **2.5**, shown in Figure 2.3b, illustrates this exchange interaction.

124, 3012.

101. Klinker, E. J.; Jackson, T. A.; Jensen, M. P.; Stubna, A.; Juhasz, G.; Bominaar, E. L.; Munck, E.; Que, L., Jr. *Angew. Chem., Int. Ed.* **2006**, *45*, 7394.
102. With spin-Hamiltonian, $H = -2\vec{J}_{Fe} \cdot \vec{S}_{NR}$, and coupling constant, $J = -(E_{HS} - E_{BS}) / (\langle S^2 \rangle_{HS} - \langle S^2 \rangle_{BS})$.
103. Ye, S.; Tuttle, T.; Bill, E.; Simkhovich, L.; Gross, Z.; Thiel, W.; Neese, F. *Chem.–Eur. J.* **2008**, *14*, 10839.
104. Neese, F. ORCA-An *ab initio*, Density Functional and Semi-empirical Electronic Structure Package Version 2.7-00 ed., Universitat Bonn, Bonn (Germany), **2009**.

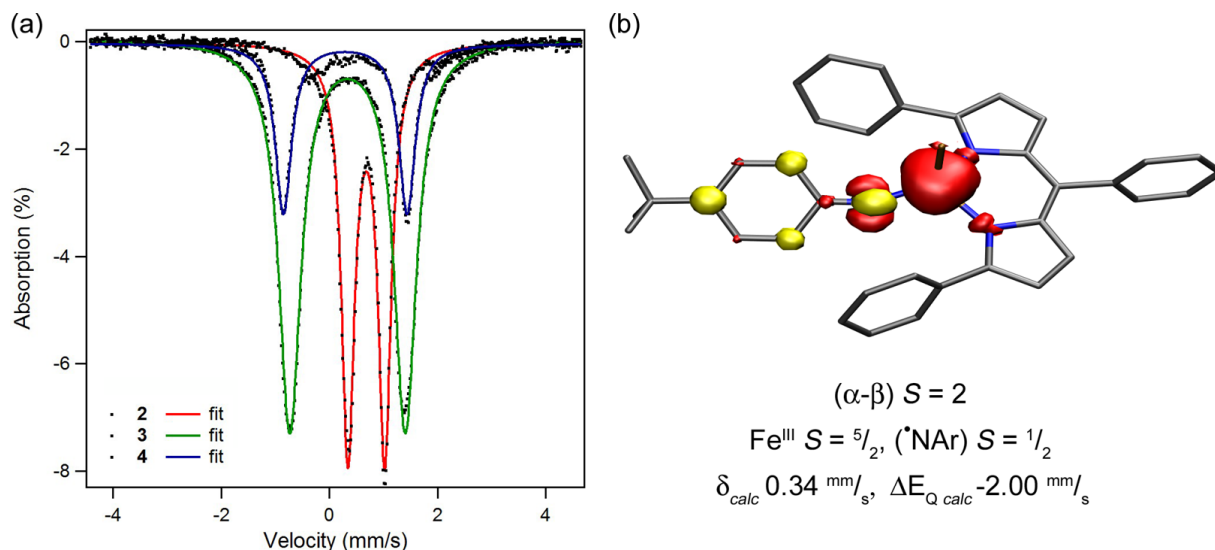


Figure 2.3. Spectroscopic and computational data of ferric complexes. The terminal imido radical complex **2.5** exhibits nearly identical Mössbauer metrical parameters to the bimolecularly-coupled di-ferric **2.4**, illustrated in (a) by the the zero-field, 100 K ^{57}Fe Mössbauer spectra data presented as black dots with spectral fits as solid lines (δ , $|\Delta E_{\text{Q}}|$ (mm/s): Fe^{II} **2.3** (red) 0.68, 0.68; $(\text{Fe}^{\text{III}})_2$ **2.4** (green) 0.33, 2.15; and $\text{Fe}^{\text{III}}(\text{NAr})$ **2.5** (blue) 0.29, 2.29. The antiferromagnetic coupling between the high-spin Fe^{III} ion with the terminal imido radical in **2.5** is illustrated in (b) by the calculated spin density population ($\alpha - \beta$) for the **2.5** ($S = 2$) by DFT (B3LYP/TZVP, SV(P); ORCA 2.7¹⁰⁵).

Gratifyingly, monomeric **2.5** is a reactive source of aryl-nitrene. Complex **2.5** reacts rapidly with 1,4-cyclohexadiene to produce $\text{H}_2\text{NC}_6\text{H}_4\text{-}p\text{-}^t\text{Bu}$ and benzene, in addition to reacting with PMe_2Ph to produce the phosphinimide $\text{Me}_2\text{PhP}=\text{NC}_6\text{H}_4\text{-}p\text{-}^t\text{Bu}$ and **2.3**. Heating **2.5** in toluene to 80 °C produces PhCH_2NHAr (product of "NAr" insertion into the benzylic C–H bond of toluene) and free $\text{H}_2\text{NC}_6\text{H}_4\text{-}p\text{-}^t\text{Bu}$ (observed by HR-MS). Traces of diazene ($\text{ArN}=\text{NAr}$) are also observed by HR-MS. Furthermore, dimeric **2.4** is also a reactive source of phenyl-nitrene, affording PhCH_2NHPh upon heating **2.4** in toluene to 80 °C (observed by HR-MS). Thus, dimeric **2.4** must be in equilibrium with its monomeric precursor, $(^{\text{Ar}}\text{L})\text{FeCl}(\text{NPh})$, which reacts analogously to **2.5** to effect intermolecular C–H bond amination (Figure 2.2).

2.5 Conclusions

We have concluded that an imido radical strongly coupled to a high-spin Fe^{III} ion, $(\text{L})\text{Fe}^{\text{III}}\text{Cl}(\cdot\text{NR})$, is the putative group-transfer reagent in both the amination and aziridination

processes. The reactive species reported herein is a departure from the typical Fe^{IV} assignment invoked in Fe-mediated group transfer catalysis.^{79,91} The isolation of the stable terminal imido radical **2.5** and the imido precursor **2.4** lend support to this assignment. Reaction with alkyl azides in the catalytic reaction should localize the radical character on the imido N, giving rise to the observed enhanced reactivity towards C–H bond or olefinic substrates. We attribute the observed group transfer catalysis to the electronic structure, more specifically the localized radical character on the imido N, as the reactivity reported here is distinct from other Fe^{III} and Fe^{IV}(imido) complexes.^{52,53b,54a,55b,56a,106} Metal imido complexes which bear radical character have been invoked in other transition metal complexes.^{62,68,107} Warren and coworkers have shown that a putative terminal Cu^{III}(imido)⁶² and a terminal Cu^{II}(amido),⁹⁷ both bearing radical character at N, are key intermediates in their C–H bond amination chemistry. A cobalt(III) imido, published by Theopold, which aminates an intramolecular C-H bond is also believed to have nitrogen radical character at room temperature despite a diamagnetic ground state.⁶⁸

The terminal imido radical bound to a ferric center (**2.5**) is the first example of an isolated complex featuring this type of high-spin electronic configuration, but the electronic structure may arise in other synthetic and biochemical catalytic cycles.^{81,108,109,110,111} Ye and Neese proposed that prior to oxo-transfer in TauD, the high-valent, non-heme iron(oxo) complex undergoes a preparatory change en route to H-atom abstraction where the iron-oxo bond lengthens, leading to

105. Mankad, N. P.; Müller, P.; Peters, J. C. *J. Am. Chem. Soc.* **2010**, *132*, 4083.

106. Kogut, E.; Wiencko, H. L. Zhang, L.; Cordeau, D. E.; Warren, T. H. *J. Am. Chem. Soc.* **2005**, *127*, 11248.

107. Groves, J. T.; Van Der Puy, M. *J. Am. Chem. Soc.* **1974**, *96*, 5274.

108. Groves, J. T.; McClusky, G. A. *J. Am. Chem. Soc.* **1976**, *98*, 859.

109. Chen, M. S.; White, M. C. *Science* **2007**, *318*, 783.

a ferric oxyl radical ($\text{Fe}^{\text{III}}(\text{O}\cdot)$) state akin to the electronic structure observed in **2.5**.⁸⁴ While this preparatory step is predicted to be only 9.4 kcal/mol higher in energy than the ground state, the strong covalent interaction between the iron and the oxo is diminished, resulting in a more reactive oxyl radical. Interestingly, reactive non-heme, high-spin $\text{Fe}^{\text{IV}}(\text{oxo})$ intermediates exhibit isomer shifts (δ 0.30-0.31 mm/s) very much like the ferric imido radical **2.5** (δ 0.29 mm/s), but shifted significantly from the two isolated high-spin $\text{Fe}^{\text{IV}}(\text{oxo})$ complexes which exhibit more classic Fe^{IV} Mössbauer metrical parameters (δ 0.02 and 0.09 mm/s).⁸⁸⁻⁹⁰ Taken together, the similarities in Mössbauer metrical parameters between the reactive biological intermediates and **2.5** might suggest the ferric oxyl radical formulation should be favored over an $\text{Fe}^{\text{IV}}(\text{oxo})$ formulation. This observation highlights the important implications for the *electronic* structure-function relationships not only in generating reactive functional analogues, but also in gaining a full understanding of these important biological intermediates.

2.6 Experimental Methods

2.6.1 General Considerations.

All manipulations of metal complexes were carried out in the absence of water and dioxygen using standard Schlenk techniques, or in an MBraun inert atmosphere drybox under a dinitrogen atmosphere. Ligand and ligand precursor syntheses were carried out in air, except where noted. All glassware was oven dried for a minimum of 1 h and cooled in an evacuated antechamber prior to use in the drybox. Benzene, diethyl ether, dichloromethane, *n*-hexane, tetrahydrofuran, and toluene were dried and deoxygenated on a Glass Contour System (SG Water USA, Nashua, NH) and stored over 4 Å molecular sieves (Strem) prior to use. Anhydrous

110. Chen, M. S.; White, M. C. *Science* **2010**, 327, 566.

n-pentane, hexamethyldisiloxane, styrene, and trifluoromethylbenzene were purchased from Aldrich, degassed if necessary, and stored over 4 Å molecular sieves prior to use. Chloroform-*d* was purchased from Cambridge Isotope Labs and used as received. Benzene-*d*₆, dichloromethane-*d*₂ and toluene-*d*₈ were purchased from Cambridge Isotope Labs and were degassed and stored over 4 Å molecular sieves prior to use. Pyridinium *p*-toluenesulfonate, DDQ, 1,4-cyclohexadiene, 1-azidoadamantane, 1-chloroadamantane, *tert*-butyl chloride, aluminum trichloride, 1-aminoadamantane and *tert*-butylisocyanide were purchased from Aldrich and used as received. Anhydrous iron(II) chloride, 2-dicyclohexylphosphino-2',6'-dimethoxy-1,1'-biphenyl (S-Phos), dipalladium tris(dibenzylideneacetone), dimethylphenylphosphine, tris(pentafluorophenyl)borane and zinc chloride were purchased from Strem and used as received. Ethyl 1*H*-pyrrole-2-carboxylate,⁹⁴ 2-*tert*-butyl-1*H*-pyrrole,¹¹² mesitaldehyde dimethyl acetal,¹¹³ azidobenzene,¹¹⁴ and 1-azido-4-*tert*-butylbenzene,¹¹⁴ 2-bromo-1,3,5-triphenylbenzene,¹¹⁵ and sodium pyrrolide,¹¹⁶ were synthesized according to literature procedures. Celite® 545 (J. T. Baker) and silica gel 32-63 μ (Dynamic Adsorbents, Atlanta, GA), were dried in a Schlenk flask for 24 h under dynamic vacuum while heating to at least 150 °C prior to use in a drybox.

2.6.2 Characterization and Physical Measurements.

UV/Visible spectra were recorded on a Varian Cary 50 UV/Visible spectra using quartz cuvettes and a scan rate of 300 or 600 nm/min. Extinction coefficients were determined from a

111. Harman, W. H.; Harris, T. D.; Freedman, D. E.; Fong, H.; Chang, A.; Rinehart, J. K.; Ozarowski, A.; Sougrati, M. T.; Grandjean, F.; Long, G. J.; Long, J. R.; Chang, C. J. *J. Am. Chem. Soc.* **2010**, *132*, 18115.

112. Ji, N.; O'Dowd, H.; Rosen, B. M.; Myers, A. G. *J. Am. Chem. Soc.* **2006**, *128*, 14825.

113. Smith, P. A.; Hall, J. H. *J. Am. Chem. Soc.* **1962**, *184*, 480.

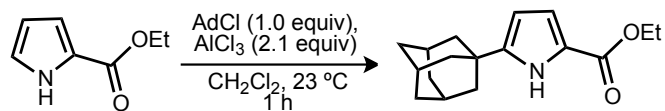
114. Lawson Daku, L. M.; Pécaut, J.; Lenormand-Foucaut, A.; Vieux-Melchior, B.; Iveson, P.; Jordanov, J. *Inorg. Chem.* **2003**, *42*, 6824.

minimum of three concentrations per sample, and were calculated by a linear regression fit of the absorbance vs. concentration data. ^1H , ^{13}C , ^{19}F , and ^{31}P NMR spectra were recorded on Varian Mercury 400 MHz or Varian Unity/Inova 500 MHz spectrometers. ^1H and $^{13}\text{C}\{^1\text{H}\}$ NMR chemical shifts are reported relative to SiMe_4 using the chemical shift of residual solvent peaks as reference. Solution magnetic susceptibilities were determined by the Evans method^{95,117} using hexamethyldisiloxane or trifluoromethylbenzene as an internal reference. Mass spectrometry was performed at the Harvard University FAS Center for Systems Biology Mass Spectrometry and Proteomics Resource Laboratory on an Agilent 6210 TOF LC/MS with a dual nebulizer ESI source for HRMS and on a Waters Q-ToF Micro LC/MS/MS with a ESI source for yield determination. Elemental analyses were carried out by Complete Analysis Laboratories, Inc. (Parsippany, NJ). ^{57}Fe Mössbauer spectra were measured on liquid nitrogen cooled samples at zero magnetic field with a constant acceleration spectrometer (SEE Co., Edina, MN). Solid or crystalline samples were prepared as Paratone-N mulls in a drybox and frozen in liquid nitrogen prior to handling in air. Isomer shifts are quoted relative to Fe foil at room temperature. Data was processed, simulated, and analyzed using an in-house package written by E.R.K. for IGOR Pro 6 (Wavemetrics, Lake Oswego, OR).

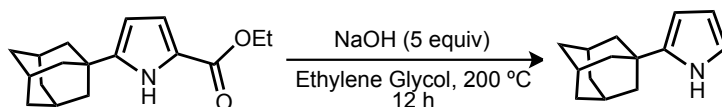
115. Rieth, R. D.; Mankad, N. P.; Calimano, E.; Sadighi, J. P. *Org. Lett.* **2004**, *6*, 3981.

116. Sur, S. K. *J. Magn. Reson.* **1989**, *82*, 169.

2.6.3 Ligand Syntheses.



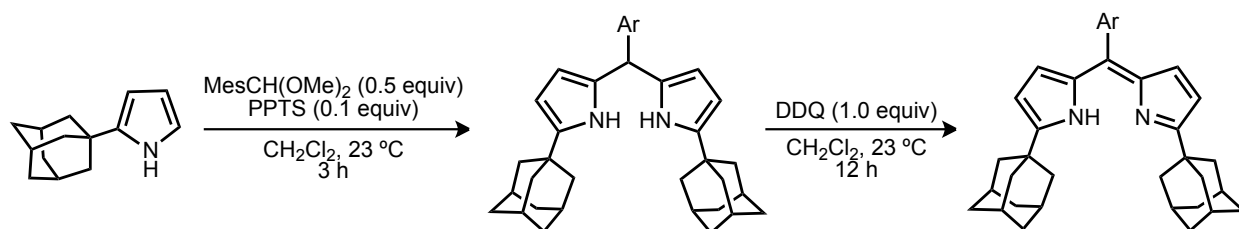
Ethyl 5-(1-adamantyl)-1H-pyrrole-2-carboxylate:¹¹⁸ A dry, 3-L round-bottomed flask was charged with ethyl 1H-pyrrole-2-carboxylate (20.40 g, 146.7 mmol) and 1.5 L of dry dichloromethane. The flask was purged with nitrogen and AlCl₃ (41.15g, 308.7 mmol, 2.1 equiv.) was added in one portion, followed by the *immediate* addition of 1-chloroadamantane (25.00 g, 146.7 mmol, 1 equiv.), The resulting mixture was stirred under nitrogen for 1 h. The reaction mixture was then quenched by careful addition to a saturated solution of aqueous NaHCO₃ (750 mL). Diethyl ether was added and the organic layer separated. The aqueous layer was further extracted with ether (2 x 200 mL) and the combined organics dried over anhydrous MgSO₄ and concentrated by rotary evaporation to yield off-white solid ethyl 5-(1-adamantyl)-1H-pyrrole-2-carboxylate (26.9 g, 67%), which was used without further purification. ¹H NMR (500 MHz, CDCl₃) δ: 8.80 (br s, 1H, N-H), 6.83 (m, 1H, pyrrole C-H), 5.99 (m, 1H, pyrrole C-H), 4.31 (m, 2H, OCH₂CH₃), 2.08 (br s, 3H, adamantyl 3° C-H), 1.90 (s, 6H), 1.80-1.73 (m, 6H), 1.34 (m, 3H, OCH₂CH₃). ¹³C{¹H} NMR (100 MHz, C₆D₆) δ: 161.4, 148.0, 120.8, 115.5, 104.9, 60.0, 42.3, 36.52, 33.5, 28.3, 14.5. HRMS (ESI⁺) *m/z* Calc. 274.18070 [C₃₈H₄₆N₂+H]⁺, Found 274.18016 [M+H]⁺.



2-(1-adamantyl)-1H-pyrrole:¹¹⁸ A slurry of ethyl 5-(1-adamantyl)-1H-pyrrole-2-carboxylate (26.90 g, 98.46 mmol) and powdered NaOH (19.70 g, 492.5 mmol, 5 equiv.) in ethylene glycol

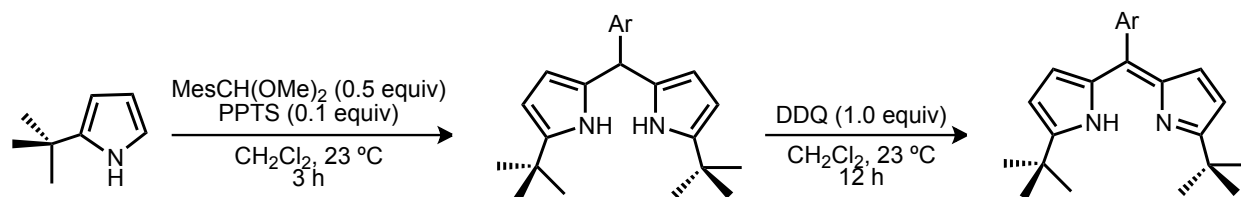
117. Modified from the prep for 2-*tert*-butylpyrrole from Ref 112.

(200 mL) was brought to reflux with the aid of a heating mantle. After 12 h, the reaction mixture was allowed to cool to room temperature, diluted with water (300 mL) and extracted with CH₂Cl₂ (5 x 100 mL). The organic portions were dried over anhydrous Na₂SO₄ and concentrated by rotary evaporation to yield a light brown solid which was recrystallized from hexanes, affording 2-(1-adamantyl)-1*H*-pyrrole (17.4 g, 88%) as a tan powdery solid. **¹H NMR** (500 MHz, CDCl₃) δ: 8.0 (br s, 1H, N-*H*), 6.67 (m, 1H), 6.14 (m, 1H), 5.92 (m, 1H), 2.06 (br s, 3H), 1.90 (s, 6H), 1.8-1.73 (m, 6H), 1.35 (t, 3H). **¹³C{¹H}** NMR (100 MHz, C₆D₆) δ: 141.7, 115.9, 108.2, 102.5, 43.1, 37.1, 33.3, 29.0. **HRMS** (ESI⁺) *m/z* Calc. 202.15957 [C₃₈H₄₆N₂+H]⁺, Found 202.15903 [M+H]⁺.



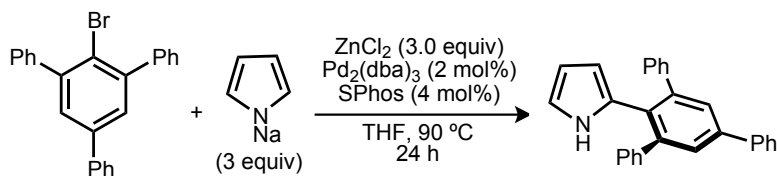
1,9-di(1-adamantyl)-5-mesityldipyrromethene (^{Ad}L)H****: Under an inert atmosphere a 500 mL round-bottomed flask was charged with 2-(1-adamantyl)-1*H*-pyrrole (10.00 g, 49.71 mmol), mesitaldehyde dimethyl acetal (4.830 g, 24.86 mmol, 0.5 equiv.), and 250 mL of dry CH₂Cl₂. After stirring until all materials were dissolved, pyridinium *p*-toluenesulfonate (1.249 g, 4.971 mmol, 0.1 equiv.) was added resulting in a color change from colorless to emerald green. The reaction was stirred at room temperature for 3 h. The solution was concentrated *in vacuo* and filtered through a plug of silica gel in a medium porosity frit (30 mL) with CH₂Cl₂ to give a pale yellow filtrate. Solvent was removed *in vacuo* and the solid was triturated twice with 50 mL hexanes, followed by removal of the hexanes *in vacuo*, affording 1,9-di(1-adamantyl)-5-mesityldipyrromethene (13.0 g, 97%) as a pale pink powder. **¹H NMR** (500 MHz, C₆D₆) δ: 7.68

(br s, 2H, pyrrole N-*H*), 6.78 (s, 2H, aryl C-*H*), 6.05 (m, 2H, pyrrole C-*H*), 6.02 (t, *J* = 3 Hz, 2H, pyrrole C-*H*), 5.89 (s, 1H, MesCH(C₄H₂AdNH)₂), 2.16 (s, 6H, *ortho*-C₆H₂(CH₃)₃), 2.11 (s, 3H, *para*-C₆H₂(CH₃)₃), 1.81 (s, 6H, adamantyl 3° C-*H*), 1.73 (s, 12H, adamantyl 2° C-*H*), 1.58-1.50 (m, 12H, adamantyl 2° C-*H*). ¹³C{**1H**} NMR (100 MHz, CD₂Cl₂) δ: 141.79, 137.60, 136.25, 135.40, 130.29, 130.04, 105.83, 101.72, 43.16, 38.87, 36.95, 33.32, 28.97, 20.72, 20.43. The product (8.00 g, 15.01 mmol) was dissolved in 300 mL CH₂Cl₂. The oxidant, 2,3-dichloro-5,6-dicyanoquinone (DDQ) (3.392 g, 15.01 mmol, 1 equiv.), was added to immediately give a dark brown solution. After stirring for 12 h, the solution was concentrated *in vacuo* and filtered through a plug of silica gel in a medium porosity frit (30 mL) with benzene to give a dark brownish yellow filtrate. Solvent was removed *in vacuo* and the dark brown solid was washed with diethyl ether (2 x 50 mL) to give (^{Ad}L)H (5.57 g, 71%) as a mustard yellow powder. ¹H NMR (500 MHz, C₆D₆) δ: 6.76 (s, 2H, aryl C-*H*), 6.54 (d, *J* = 4 Hz, 2H, pyrrole C-*H*), 6.23 (d, *J* = 4 Hz, 2H, pyrrole C-*H*), 2.15 (s, 3H, *para*-C₆H₂(CH₃)₃), 2.14 (s, 6H, *ortho*-C₆H₂(CH₃)₃), 2.06 (d, *J* = 3 Hz, 12H, adamantyl 2° C-*H*), 1.95 (br s, 6H, adamantyl 3° C-*H*), 1.67 (br s, 12H, adamantyl 2° C-*H*). ¹³C{**1H**} NMR (100 MHz, CD₂Cl₂) δ: 166.6, 138.7, 137.6, 137.1, 134.0, 128.7, 128.3, 128.0, 113.6, 42.3, 37.2, 35.8, 29.0, 21.2, 20.1. HRMS (ESI⁺) *m/z* Calc. 531.3739 [C₃₈H₄₆N₂+H]⁺, Found 531.3763 [M+H]⁺.



1,9-di-*tert*-butyl-5-mesityldipyrromethene (^{tBu}L)H: Under an inert atmosphere a 200 mL round-bottomed flask was charged with 2-*tert*-butylpyrrole (2.130 g, 17.30 mmol), mesitaldehyde dimethyl acetal (1.680 g, 8.652 mmol, 0.5 equiv.), and 85 mL of dry CH₂Cl₂.

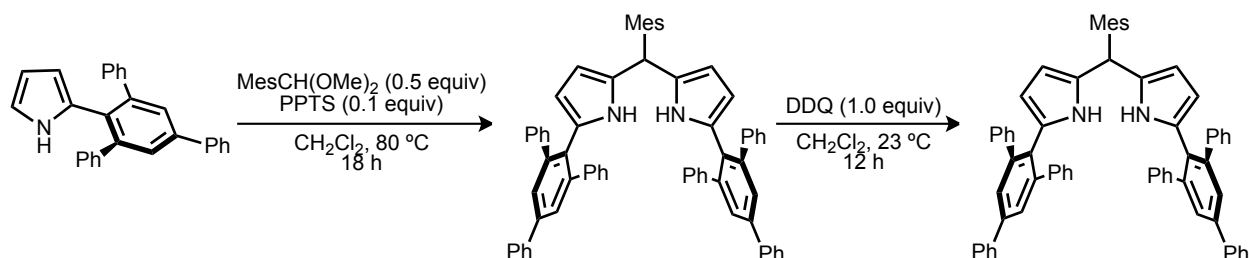
After stirring until all materials were dissolved, pyridinium *p*-toluenesulfonate (0.435 g, 1.730 mmol, 0.1 equiv.) was added resulting in a color change from colorless to bright yellow. The reaction was stirred at room temperature for 3 h. The solution was concentrated *in vacuo* and filtered through a plug of silica gel (30 mL) in CH₂Cl₂ to give a pale yellow filtrate. Solvent was removed *in vacuo* and the solid was triturated twice with 50 mL hexanes, followed by removal of the hexanes *in vacuo*, affording 1,9-di-*tert*-butyl-1-5-mesityldipyrromethane (3.25 g, 99%) as a pale yellow oil. ¹H NMR (500 MHz, CD₂Cl₂) δ: 7.78 (br s, 2H, pyrrole N-*H*), 6.86 (s, 2H, aryl C-*H*), 5.81 (s, 1H, MesCH(C₄H₂^{*t*}BuNH)₂), 5.79 (m, 2H, pyrrole C-*H*), 5.62 (s, 2H, pyrrole C-*H*), 2.27 (s, 3H, *para*-C₆H₂(CH₃)₃), 2.08 (s, 6H, *ortho*-C₆H₂(CH₃)₃), 1.24 (s, 18H, C(CH₃)₃). ¹³C{¹H} NMR (125 MHz, CD₂Cl₂) δ: 141.15, 137.74, 136.48, 135.54, 130.51, 106.04, 102.60, 39.04, 34.54, 31.54, 30.74, 22.75, 20.61. The product (3.252 g, 8.642 mmol) was dissolved in 175 mL hexanes. The oxidant, 2,3-dichloro-5,6-dicyanoquinone (DDQ) (1.962 g, 8.642 mmol, 1 equiv.), was added to give a mustard yellow solution. After stirring for 6 h, the solution was concentrated *in vacuo* and filtered through Celite in hexanes, followed by a plug of silica gel (30 mL) in hexanes to give an orange-yellow filtrate. Solvent was removed *in vacuo* to give (^{*t*}BuL)H (2.36 g, 73%) as an orange-yellow crystalline solid. ¹H NMR (400 MHz, CDCl₃) δ: 13.57 (1H, s), 6.79 (s, 2H, aryl C-*H*), 6.55 (d, *J* = 4.4 Hz, 2H, pyrrole C-*H*), 6.23 (d, *J* = 4.4 Hz, 2H, pyrrole C-*H*), 2.19 (s, 9H, *para*, *ortho*-C₆H₂(CH₃)₃), 1.35 (s, 18H, C₄H₉). ¹³C{¹H} NMR (100 MHz, CD₂Cl₂) δ: 166.3, 139.4, 137.7, 137.5, 137.1, 133.9, 128.0, 126.9, 114.3, 33.7, 30.0, 21.2, 20.1. HRMS (ESI⁺) *m/z* Calc. 375.2800 [C₂₆H₃₅N₂+H]⁺, Found 375.2794 [M+H]⁺.



2-(2,4,6-triphenylphenyl)-1H-pyrrole¹¹⁹: In the glovebox a 1 L air-free storage flask with a Teflon valve was charged with a stir bar, sodium pyrrolide (31.2 g, 351 mmol, 3 equiv.), and 400 mL anhydrous THF. While stirring zinc chloride (47.8 g, 351 mmol, 3 equiv.) was slowly added over the course of 20 min, evolving heat and causing the solvent to reflux. In a 20 mL scintillation vial, SPhos (1.92 g, 4.68 mmol, 0.04 equiv.) and dipalladium tris(dibenzylideneacetone) (2.14 g, 2.34 mmol, 0.02 equiv.) were stirred in 15 mL THF. The catalyst mixture was then added to the reaction mixture, followed by the addition of 2-bromo-1,3,5-triphenylbenzene (45.0 g, 117 mmol, 1 equiv.). The flask was placed under partial vacuum and the valve sealed. The reaction was heated in an oil bath at 90 °C for 24 h. After cooling to room temperature the reaction mixture was extracted with water and Et₂O. The organic fractions were combined, dried over MgSO₄, and the solvent was removed by rotary evaporation. The dark brown solids were then dissolved in dichloromethane, flashed through a 15 in × 1 in silica column, dried over MgSO₄, and the solvent was removed by rotary evaporation. The light tan solid was washed on a frit with 250 mL pentane. The solid was dried in vacuo to yield 31.8 g (73.2%) of 2-(2,4,6-triphenylphenyl)-1H-pyrrole. ¹H NMR (500 MHz, CDCl₃) δ: 5.56 (m, 1H, pyrrole C-H), 5.94 (m, 1H, pyrrole C-H), 6.46 (m, 1H, pyrrole C-H), 7.25 (m, 4H, aryl C-H), 7.28-7.32 (m, 6H, aryl C-H), 7.38 (t, *J* = 7.3 Hz, 1H, aryl C-H), 7.46 (t, *J* = 7.3 Hz, 2H, aryl C-H), 7.66 (s, 2H), 7.69 (d, *J* = 7.3 Hz, 2H aryl C-H), 7.80 (br s, 1H, N-H) ¹³C{¹H} NMR (125

118. Modification of the 2-arylpyrrole syntheses from Rieth, R. D.; Mankad, N. P.; Calimano, E.; Sadighi, J. P. *Org. Lett.* **2004**, *6*, 3981.

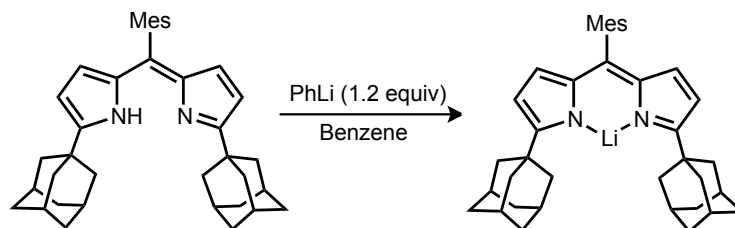
MHz, CDCl₃) δ : 108.3, 111.8, 117.2, 126.7, 127.1, 127.5, 127.9, 128.4, 128.8, 129.1, 129.6, 129.7, 140.1, 140.3, 142.0, 142.6. **HRMS** (ESI⁺) m/z Calc. 372.1747 [C₂₈H₂₁N+H]⁺, Found 372.1762 [M+H]⁺.



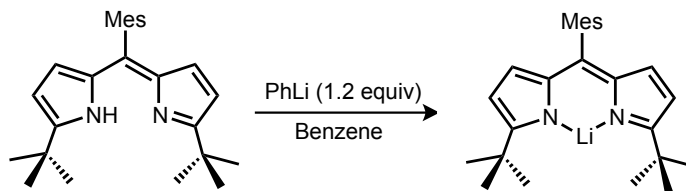
5-mesityl-1,9-di(2,4,6-triphenylphenyl)dipyrromethene, (^{Ar}L)H: In the glovebox a 1 L air-free storage flask with a Teflon valve was charged with a stir bar, 2-(2,4,6-triphenylphenyl)-1H-pyrrole (31.18 g, 84 mmol, 2 equiv.), mesitaldehyde dimethyl acetal (8.15 g, 42 mmol, 1 equiv.), and 300 mL anhydrous dichloromethane. Pyridinium *p*-toluenesulfonate (1.055, 4.2 mmol, 0.1 equiv.) was added resulting in immediate color change from light orange to dark brown. The bomb was placed under partial vacuum, sealed with a Teflon screw-cap, and heated to 80 °C for 18 h in an oil bath. After cooling to room temperature the dichloromethane solution was filtered through a silica plug, dried over MgSO₄, and the solvent was removed via rotary evaporation yielding 5-mesityl-1,9-(2,4,6-triphenylphenyl)dipyrromethane as a light orange powder (31.75 g, 87%). **¹H NMR** (500 MHz, CD₂Cl₂) δ : 1.75 (br s, 6H, *ortho*-C₆H₂(CH₃)₃), 2.21 (s, 3H, *para*-C₆H₂(CH₃)₃), 5.20 (t, $J = 3.2$ Hz, 2H, pyrrole C-H), 5.35 (s, 1H, methine C-H), 5.39 (t, $J = 3.2$ Hz, 2H, pyrrole C-H), 6.70 (s, 2H, N-H), 6.95 (s, 2H, C₆H₂(CH₃)₃), 7.14 (m, 8H, aryl C-H), 7.17-7.21 (m, 12H, aryl C-H), 7.35 (t, $J = 8.3$ Hz, 2H, aryl C-H), 7.44 (t, $J = 7.8$ Hz, 4H, aryl C-H), 7.61 (s, 4H), 7.68 (d, $J = 8.3$ Hz, 4H, aryl C-H). **¹³C{¹H} NMR** (125 MHz, CD₂Cl₂) δ : 20.74, 20.82, 38.19, 106.71, 112.50, 126.42, 127.07, 127.35, 127.94, 128.19, 128.48, 129.22, 129.50, 129.67, 130.10, 130.44, 130.80, 134.50, 136.35, 140.34, 140.63, 142.49, 143.23. In a 500 mL

round-bottomed flask equipped with a stir bar the product (31.75 g, 36.4 mmol, 1 equiv.) was dissolved in 300 mL anhydrous dichloromethane. 2,3-Dichloro-5,6-dicyano-1,4-benzoquinone (8.5 g, 37.4 mmol, 1.03 equiv.) was added resulting in an immediate color change from light orange to dark purple. The reaction was stirred for 3 h and then solvent was removed via rotary evaporation. The resulting solids were dissolved in benzene and filtered through a silica plug to give a red solution, which was dried over MgSO_4 , and dried by rotary evaporation to give a red solid. The product was refluxed in 200 mL hexanes for 2 h, then stirred for an additional 12 h, before filtering to collect 5-mesityl-1,9-(2,4,6-triphenylphenyl)dipyrromethene as a red powder (18.14 g, 50%). Crystals suitable for X-ray diffraction were grown from a 2:1 benzene/*n*-hexane solution at $-35\text{ }^\circ\text{C}$. **^1H NMR** (500 MHz, CD_2Cl_2) δ : 2.03 (s, 6H, *ortho*- $\text{C}_6\text{H}_2(\text{CH}_3)_3$), 2.34 (s, 3H, *para*- $\text{C}_6\text{H}_2(\text{CH}_3)_3$), 5.56 (d, $J = 4.1$ Hz, 2H, pyrrole C-H), 5.89 (d, $J = 4.1$ Hz, 2H, pyrrole C-H), 6.90 (s, 2H, $\text{C}_6\text{H}_2(\text{CH}_3)_3$), 7.13 (t, $J = 7.3$ Hz, 8H, aryl C-H), 7.21-7.28 (m, 12H, aryl C-H), 7.45 (t, $J = 8.2$ Hz, 2H, aryl C-H), 7.55 (t, $J = 7.8$ Hz, 4H, aryl C-H), 7.84 (s, 4H, $\text{C}_6\text{H}_2\text{Ph}_3$), 7.87 (d, $J = 7.8$ Hz, 4H, aryl C-H), 11.50 (br s, 1H, N-H). **$^{13}\text{C}\{^1\text{H}\}$ NMR** (125 MHz, CD_2Cl_2) δ : 19.5, 21.3, 120.9, 125.1, 127.1, 127.6, 127.9, 128.0, 128.1, 128.3, 129.3, 129.8, 131.9, 133.9, 136.8, 137.5, 138.0, 140.6, 140.8, 141.3, 142.1, 143.1, 152.4. **HRMS** (ESI⁺) m/z Calc. 871.4052 [$\text{C}_{28}\text{H}_{21}\text{N}+\text{H}$]⁺, Found 871.4048 [$\text{M}+\text{H}$]⁺. **UV/vis** (THF) $\lambda_{\text{max}}/\text{nm}$ ($\epsilon/\text{M}^{-1}\text{cm}^{-1}$) 245 (65,000), 321 (27,000), 510 (31,000).

2.6.4 Metal Complex Syntheses.

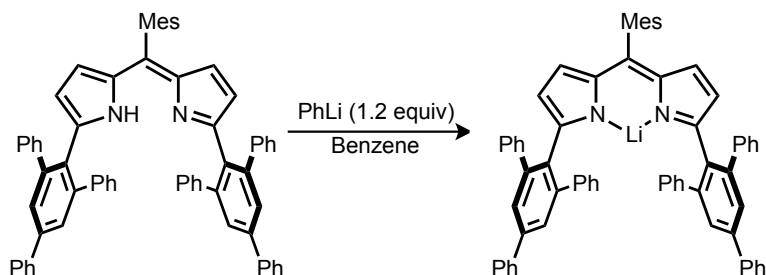


[^{Ad}L][Li]: In a 200 mL round-bottomed flask (^{Ad}L)H (2.000 g, 3.771 mmol) was dissolved in 100 mL benzene and placed in a liquid nitrogen cooled cold well until partially frozen. Phenyl lithium (380.6 mg, 4.525 mmol, 1.2 equiv.) was added as a solid. The solution was allowed to stir overnight and became dark yellow-orange. The mixture was filtered through a medium porosity glass frit with celite to remove a small amount of insoluble material and afford an orange solution. The benzene was removed *in vacuo* to give [^{Ad}L][Li] as a bright orange powder (1.86 g, 92%). ¹H NMR (500 MHz, C₆D₆): δ/ppm 6.87 (s, 2H, aryl C-H), 6.86 (d, *J* = 4 Hz, 2H, pyrrole C-H), 6.43 (d, *J* = 4 Hz, 2H, pyrrole C-H), 2.39 (s, 6H, *ortho*-C₆H₂(CH₃)₃), 2.23 (s, 3H, *para*-C₆H₂(CH₃)₃), 1.90 (br s, 6H, adamantyl 3° C-H), 1.87 (s, 12H, adamantyl 2° C-H), 1.62 (m, 12H, adamantyl 2° C-H). ¹³C{¹H} NMR (CD₂Cl₂) δ: 171.19, 138.57, 138.00, 136.83, 136.52, 130.37, 128.67, 127.57, 112.66, 42.93, 37.17, 36.66, 29.16, 21.17, 20.07.

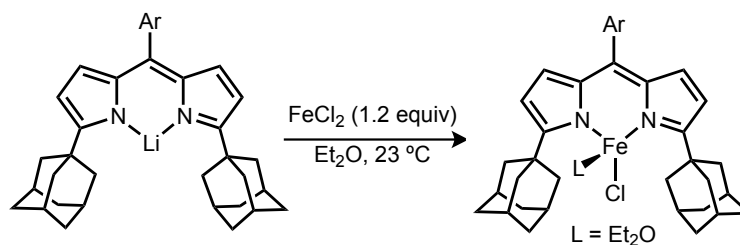


[^{tBu}L][Li]: In a 250 mL round-bottomed flask (^{tBu}L)H (2.357 g, 6.297 mmol) was dissolved in 150 mL diethyl ether and placed in a liquid nitrogen cooled cold well until partially frozen. Phenyl lithium (529.6 mg, 6.297 mmol, 1.0 equiv.) was added as a solid. The solution was allowed to stir overnight and became red-orange. The mixture was filtered through a medium porosity glass frit with celite to remove a small amount of insoluble material and afford an

orange solution. The benzene was removed *in vacuo* to give [¹⁸BuL][Li] as a bright orange powder (2.38 g, 87%). ¹H NMR (500 MHz, CD₂Cl₂) δ: 6.91 (s, 2H, aryl C-H), 6.28 (d, *J* = 4 Hz, 2H, pyrrole C-H), 6.23 (d, *J* = 4 Hz, 2H, pyrrole C-H), 2.36 (s, 3H, *para*-C₆H₂(CH₃)₃), 2.08 (s, 6H, *ortho*-C₆H₂(CH₃)₃), 1.40 (s, 18H, C(CH₃)₃). ¹³C{¹H} NMR (125 MHz, CD₂Cl₂) δ: 170.9, 145.7, 138.4, 137.8, 136.8, 136.6, 130.8, 128.7, 127.6, 113.3, 34.6, 30.4, 21.2, 20.1.



[^AL][Li]: A 100 mL round-bottomed flask was charged with a stir bar, (^AL)H (3.00 g, 3.44 mmol, 1 equiv.), and 50 mL anhydrous benzene. The reaction mixture was frozen prior to addition of phenyl lithium (0.318 g, 3.79 mmol, 1.1 equiv) as a solid. The reaction was allowed to thaw and was stirred for 16 h. Conversion was monitored by ¹H NMR on reaction aliquants, additional phenyllithium was added as necessary to consume remaining protonated ligand. Removal of the solvent *in vacuo* gave (^AL)Li (3.02 g, 88%) as a dark purple powder. ¹H NMR (400 MHz, C₆D₆) δ: 2.25 (s, 3H, *para*-C₆H₂(CH₃)₃), 2.26 (s, 6H, *ortho*-C₆H₂(CH₃)₃), 5.84 (d, *J* = 4.9 Hz, 2H, pyrrole C-H), 6.32 (d, *J* = 4.9 Hz, 2H, pyrrole C-H), 6.84 (s, 2H, C₆H₂(CH₃)₃), 7.03 (t, *J* = 7.7 Hz, 8H), 7.09 (t, *J* = 7.0 Hz, 4H, aryl C-H), 7.22 (t, *J* = 7.7 Hz, 2H, aryl C-H) 7.25 (d, *J* = 7.7 Hz, 8H, aryl C-H), 7.30 (t, *J* = 7.7 Hz, 4H, aryl C-H), 7.62 (d, *J* = 7.7 Hz, 4H, aryl C-H), 7.76 (s, 4H, C₆H₂Ph₃). ¹³C{¹H} NMR (100 MHz, C₆D₆) δ: 19.8, 21.2, 120.5, 127.4, 127.5, 127.8, 127.9, 128.4, 128.7, 129.2, 129.2, 129.4, 135.5, 136.2, 136.6, 138.1, 140.6, 140.8, 141.3, 142.1, 142.6, 146.4, 155.7. UV/vis (CH₂Cl₂) λ_{max}/nm (ε/M⁻¹cm⁻¹) 253 (75,000), 331 (29,000), 565 (57,000). **Anal.** Calc. for C₆₆H₄₉LiN₂: C 90.38, H 5.63, N 3.19; Found: C 90.36, H 5.65, N 3.16.



(^{Ad}L)FeCl(L): A 100 mL oven-dried, round-bottomed flask was charged with [^{Ad}L][Li] (2.000 g, 3.730 mmol) and 40 mL of diethyl ether. The flask was placed in a liquid nitrogen cooled cold well until frozen. FeCl₂ (0.5635 g, 4.476 mmol, 1.2 equiv.) was added to the thawing slurry of [^{Ad}L][Li]. After stirring for 3 hours, the dark brown reaction mixture was concentrated and filtered through a medium porosity glass frit with celite to remove excess FeCl₂ and LiCl in benzene. Removal of the solvent *in vacuo* gave a dark brown solid. (^{Ad}L)FeCl(OEt₂), **2.2**: The solid was washed with Et₂O and collected on a medium porosity glass frit to give (^{Ad}L)FeCl(OEt₂) as a luminescent green brown solid (1.50 g, 58%). Crystals suitable for x-ray diffraction were grown from an Et₂O solution of (^{Ad}L)FeCl(OEt₂). **¹H NMR** (500 MHz, C₆D₆) δ: 62.47 (s), 16.21 (s), 9.56 (s), 2.50 (s), 1.36 (s), -0.20 (br s), -4.29 (br s). μ_{eff} (296 K) 5.2(2) μ_{B} .

(^{Ad}L)FeCl(THF): The solid was redissolved in THF and reconcentrated to give (^{Ad}L)FeCl(THF) as a brown powder (1.89 g, 73%). **¹H NMR** (500 MHz, C₆D₆) δ: 52.8 (s), 19.0 (br, s), 17.5 (s), 10.7 (s), 7.35 (s), 5.91 (s), 3.63 (s), 2.77 (s), 1.14 (s), -3.28 (br, s). **Anal.** Calc. for C₄₂H₅₂N₂ClFeO: C 72.88, H 7.57, N 4.05; Found: C 72.93, H 7.46, N 3.98.

(^{Ad}L)FeCl(C₅H₅N): Several drops of pyridine were added to a stirring solution of (^{Ad}L)FeCl(OEt₂) (20.0 mg, 0.0288 mmol) in 2 mL benzene in a 5 mL scintillation vial. The dark red solution was stirred for 2 hours. Solvent was removed *in vacuo* to yield (^{Ad}L)FeCl(C₅H₅N) as a brown powder (20.0 mg, 99%). **¹H NMR** (500 MHz, C₆D₆): δ/ppm 50.7 (s), 41.7 (br s), 19.3 (s), 8.5 (s), 3.3 (s), 2.1 (s), 1.3 (s), -3.16 (br. s). Due to instability of THF and Et₂O adducts at high dilutions, the pyridine

complex was synthesized to obtain UV/Vis data. UV/vis (THF) $\lambda_{\text{max}}/\text{nm}$ ($\epsilon/M^{-1}\text{cm}^{-1}$) 497 (40,000).

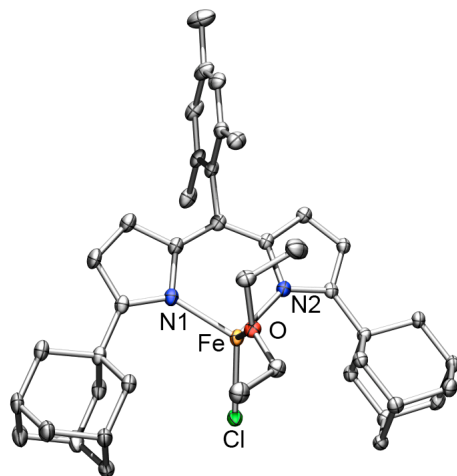


Figure 2.4. X-ray structure of 2.2. Thermal ellipsoids at 50% probability level. Hydrogens and an ether solvent molecule omitted for clarity.

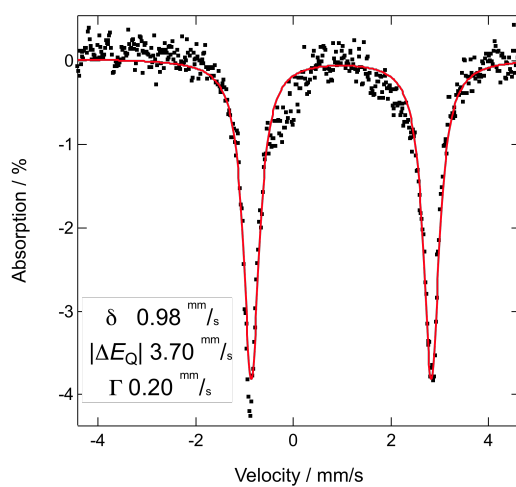
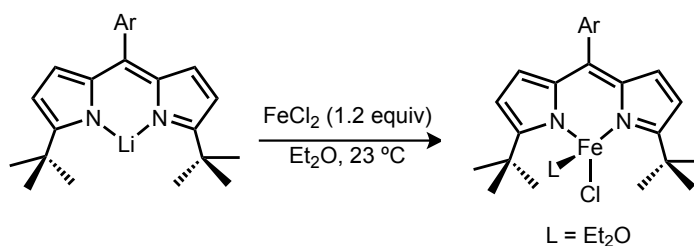


Figure 2.5. Mössbauer of 2.2. 100 K data (black) and fit (red) using listed parameters.



(^tBuL)FeCl(L): A 100 mL oven-dried, round-bottomed flask was charged with [^tBuL][Li] (2.00 g, 5.259 mmol) and 40 mL of diethyl ether. The flask was placed in a liquid nitrogen cooled cold

well until frozen. FeCl₂ (0.9270 g, 7.363 mmol, 1.4 equiv.) was added to the thawing slurry of [A^dL][Li]. After stirring for 3 hours, the dark brown reaction mixture was concentrated and filtered through a medium porosity glass frit with Celite to remove excess FeCl₂ and LiCl in benzene. Removal of the solvent *in vacuo* gave a dark brown solid. The solid was washed with TMS₂O and collected on a medium porosity glass frit. (^{tBu}L)FeCl(OEt₂): The solid was redissolved in Et₂O and reconcentrated to give (^{tBu}L)FeCl(THF) (1.750 g, 62%) as a reddish-brown solid. ¹H NMR (500 MHz, C₆D₆) δ: 65.0 (s), 7.83 (s), 5.75 (s), 2.15 (s), 1.75 (s), 1.32 (s), 1.26 (s), -9.39 (br s). μ_{eff} (296 K) 5.3(1) μ_B. (^{tBu}L)FeCl(THF), **2.1**: The solid was redissolved in THF and reconcentrated to give (^{tBu}L)FeCl(THF) (1.265 g, 55%) as a dark brown solid. Crystals suitable for x-ray diffraction were grown from a hexanes/THF solution of (^{tBu}L)FeCl(THF). ¹H NMR (500 MHz, C₆D₆) δ: 53.3 (s), 19.5 (s), 9.93 (br s), 7.77 (s), 5.16 (s), 4.58 (s), 2.95 (s), 1.92 (br s). μ_{eff} (296 K) 5.1(1) μ_B. **Anal.** Calc. for C₃₀H₄₀N₂ClFeO: C 67.23, H 7.52, N 5.23; Found: C 67.18, H 7.39, N 5.18. (^{tBu}L)FeCl(C₅H₅N): Several drops of pyridine were added to a stirring solution of (^{tBu}L)FeCl(OEt₂) (19.8 mg, 0.0374 mmol) in 2 mL benzene in a 5 mL scintillation vial. The dark red solution was stirred for 2 hours. Solvent was removed *in vacuo* to yield (^{tBu}L)FeCl(C₅H₅N) as a brown powder (19.3 mg, 98%). ¹H NMR (500 MHz, C₆D₆) δ: 50.7 (s), 42.0 (br s), 19.4 (s), 8.50 (s), 3.32 (s), 2.14 (s), 1.30 (s), -3.18 (br s). Due to instability of THF and Et₂O adducts at high dilutions, the pyridine complex was synthesized to obtain UV/Vis data. **UV/vis** (THF) λ_{max}/nm (ε/M⁻¹cm⁻¹) 494 (59,000).

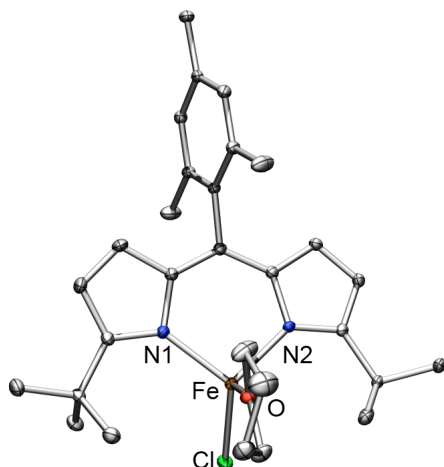
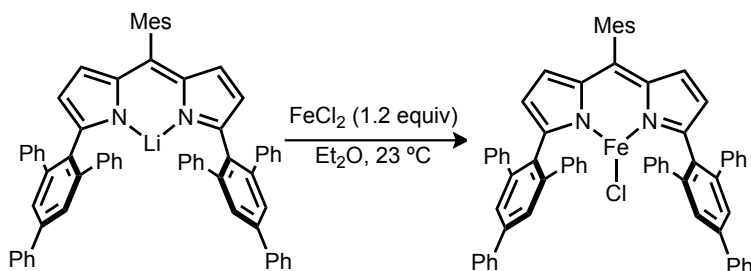


Figure 2.6. X-ray structure of **2.1**. Thermal ellipsoids at 50% probability level. One of 2 molecules present in the asymmetric unit shown. Hydrogens and THF disorder omitted for clarity.



(^{Ar}L)FeCl, 2.3: In a 20 mL vial (^{Ar}L)Li (500.0 mg, 0.570 mmol, 1 equiv.) was dissolved in 15 mL of diethyl ether. In another 20 mL vial FeCl₂ (0.108 g, 0.855 mmol, 1.5 equiv.) was slurried in 5 mL of THF. Both vials were placed in a liquid nitrogen cooled cold well until frozen. The solution of [^{Ar}L][Li] was thawed and added to the thawing slurry of FeCl₂. The reaction was stirred at room temperature for 16 h, changing from an orange and pink slurry to a dark violet solution. The mixture was filtered through a medium porosity glass frit with celite and washed with 15 mL diethyl ether and 30 mL benzene until the celite was nearly colorless. Solvent was removed *in vacuo* to give a dark purple powder which was redissolved in 6 mL benzene, followed by addition of 12 mL *n*-hexane. The solution was left in the freezer (-35 °C) to recrystallize overnight. Short dark purple needles were collected, by decanting the benzene/hexane mixture and washing the crystals with hexane. Drying *in vacuo* gave (^{Ar}L)FeCl

(252 mg, 46%) as a bright purple crystalline solid. $^1\text{H NMR}$ (400 MHz, C_6D_6) δ : -34.00, -20.93, -15.98, 10.42, 10.61, 10.78, 11.79, 13.99, 20.29, 25.16, 61.44, 65.56. **UV/vis** (CH_2Cl_2) $\lambda_{\text{max}}/\text{nm}$ ($\epsilon/\text{M}^{-1}\text{cm}^{-1}$) 244 (58,000), 321 (14,000), 554 (26,000). μ_{eff} (295 K) 5.1(2) μ_{B} . **Anal.** Calc. for $\text{C}_{66}\text{H}_{49}\text{ClFeN}_2$: C 82.45, H 5.14, N 2.91; Found: C 82.38, H 5.29, N 2.75.

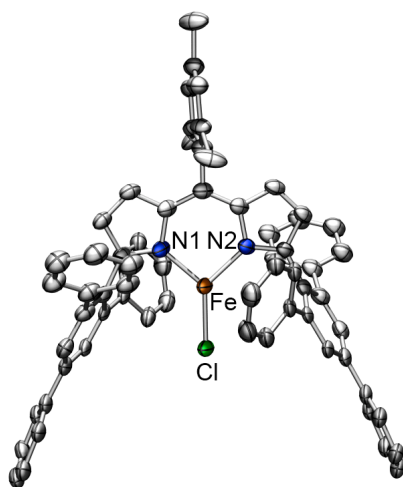


Figure 2.7. X-ray structure of 2.3. Thermal ellipsoids at 50% probability level. Half of the molecule is a symmetry equivalent. Aryl ring disorder and benzene solvent molecules omitted for clarity.

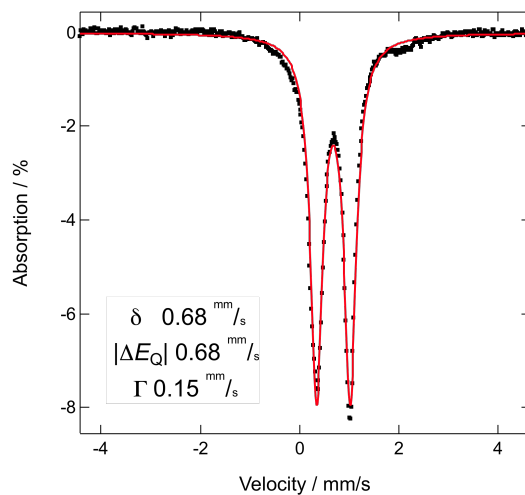
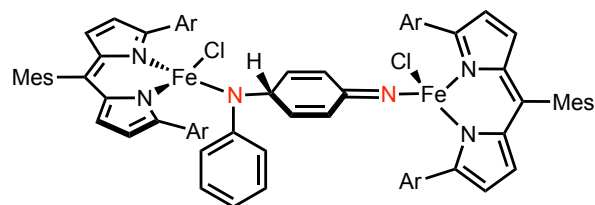


Figure 2.8. Mössbauer of 2.3. 100 K data (black) and fit (red) using listed parameters



[^{Ar}L]FeCl₂(μ -NPh(C₆H₅)N), 2.4: In a 20 mL vial (^{Ar}L)FeCl (110.0 mg, 0.114 mmol, 1 equiv.) was dissolved in 4 mL of benzene. In a 5 mL vial azidobenzene (13.6 mg, 0.114 mmol, 1 equiv.) was dissolved in 2 mL of benzene and was then added to the iron complex. The reaction was stirred for 1 h, turning from dark violet to dark purple. Addition of 12 mL *n*-hexane followed by crystallization overnight at -35 °C afforded the product as black crystals (106 mg, 88%). **UV/vis** (CH₂Cl₂) λ_{max} /nm (ϵ /M⁻¹cm⁻¹) 247 (88,000), 314 (21,000), 528 (27,000, sh), 551 (30,000). μ_{eff} (295 K) 7.8(2) μ_{B} . **Anal.** Calc. for C₁₄₄H₁₀₈Cl₂Fe₂N₆: C 82.16, H 5.17, N 3.99; Found: C 82.22, H 5.26, N 3.86.

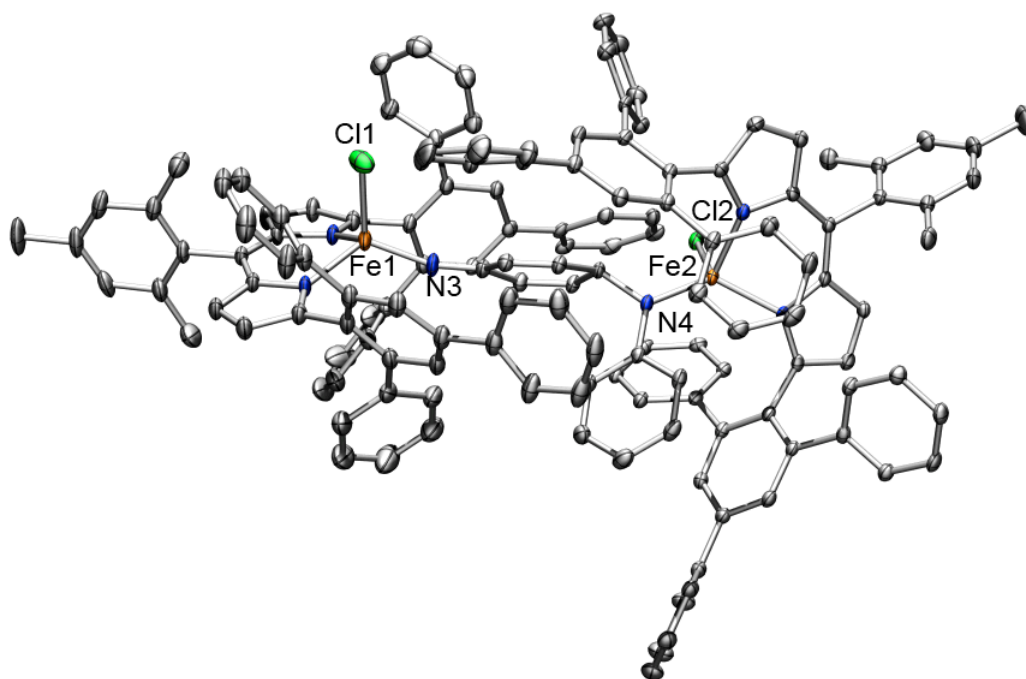


Figure 2.9. X-ray structure of 2.4. Thermal ellipsoids at 50% probability level. Hydrogens and benzene solvent molecules omitted for clarity.

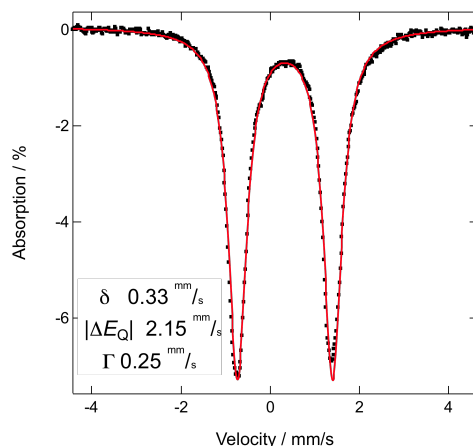
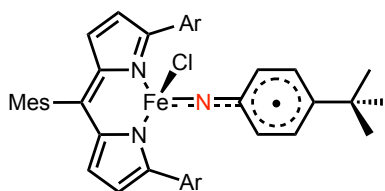


Figure 2.10. Mössbauer spectrum of **2.4**. 100 K data (black) and fit (red) using listed parameters.



(^{A^r}L)FeCl(NC₆H₄-*p*-^tBu), **2.5**: In a 20 mL vial (^{A^r}L)FeCl (100.0 mg, 0.104 mmol, 1 equiv.) was dissolved in 4 mL of benzene. In a 5 mL vial 1-azido-4-*tert*-butylbenzene (18.3 mg, 0.104 mmol, 1 equiv.) was dissolved in 2 mL of benzene and was then added to the iron complex. The reaction was stirred for 1 h, turning from dark violet to dark red. The solution was frozen and benzene was removed by sublimation *in vacuo* affording (^{A^r}L)FeCl(NC₆H₄-*p*-^tBu) (105.6 mg, 95%) as a dark purple powder. Crystals suitable for X-ray diffraction were grown from a concentrated *n*-pentane solution at -35 °C. ¹H NMR (400 MHz, C₆D₆) δ: -17.14, 0.46, 1.97, 5.73, 5.86, 6.20, 7.10, 7.42, 7.67, 10.27, 10.83, 27.48, 38.19, 60.17. UV/Vis (CH₂Cl₂) λ_{max}/nm (ε/M⁻¹cm⁻¹) 247 (73,000), 323 (17,000), 377 (15,000), 553 (26,000). μ_{eff} (295 K) 5.3(1) μ_B. **Anal.** Calc. for C₇₆H₆₂Cl₂FeN₃: C 82.34, H 5.64, N 3.79; Found: C 82.32, H 5.58, N 3.73.

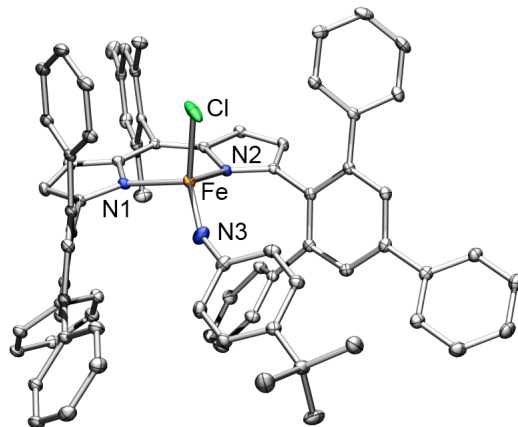


Figure 2.11. X-ray structure of **2.5**. Thermal ellipsoids at 50% probability level. Hydrogens and a pentane solvent molecule omitted for clarity.

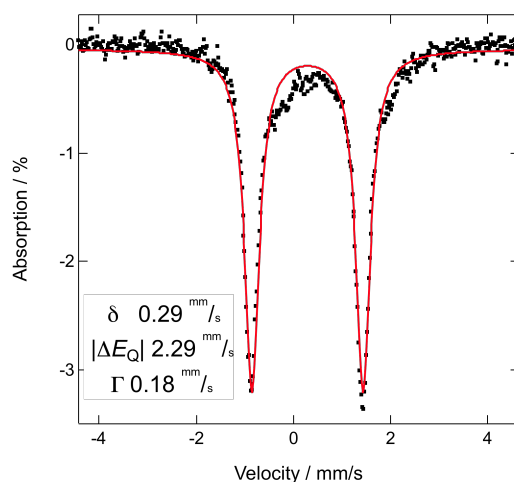


Figure 2.12. Mössbauer of **2.5**. 100 K data (black) and fit (red) using listed parameters.

2.6.5 Reactivity and Catalysis Experiments

Determination of Intermolecular Primary Kinetic Isotope Effect for C–H Insertion

Reactions via Competition Experiments. Under an inert N₂ atmosphere, 1-azidoadamantane (51.0 mg, 0.29 mmol, 10 equiv.) was added to a stirring solution of (^{Ad}L)FeCl(OEt₂) (**2.2**) (20.0 mg, 0.029 mmol) in an equimolar mixture of toluene (540 mg, 5.43 mmol) and toluene-*d*₈ (500 mg, 5.43 mmol) in a pressure vessel. After heating for 12 hours at 60 °C, an aliquot of the solution (0.05 mL) was diluted with 20 mL MeOH and analyzed by LC/MS. Comparison of the area of the selected ion recording (SIR) of the formed proteo/deutero amine products (A_H/A_D)

were equated to k_H/k_D to give a value of 12.8(5). Three runs were performed to obtain the reported value and the calculated standard deviation.

Yield Determination of Catalytic Amination Reactions with 1-Azidoadamantane using LC/MS. Under an inert N₂ atmosphere, 1-azidoadamantane (35.4 mg, 0.2 mmol, 20 equiv.) was added to a stirring solution of (^{Ad}L)FeCl(OEt₂) (**2.2**) (6.9 mg, 0.01 mmol) in 1 mL of toluene in a sealed pressure vessel. The resultant inky, dark red solution reacted for 12 hours at the specified temperature. The pressure vessel was then cooled and an LC/MS sample of this solution was prepared for yield determination. The solution was diluted to 10 mL with MeOH. An aliquot (0.1 mL) of this solution was diluted to 10 mL with MeOH and analyzed by LC/MS. A series of standard samples composed of a 1:1:1 molar ratio of PhCH₂NHAd:PhCHNAd:AdNH₂ with concentrations ranging from 3x10⁻⁸ to 1x10⁻⁴ M were run prior to each set of experiments to establish a calibration curve. Peak areas of the formed products were compared to the calibration curve and gave the turnover numbers and product distributions.

Yield Determination of Catalytic Amination Reactions with 1-Azidoadamantane using ¹H NMR. Under an inert N₂ atmosphere, 1-azidoadamantane (35.4 mg, 0.2 mmol, 20 equiv.) was added to a stirring solution of (^{Ad}L)FeCl(OEt₂) (**2.2**) (6.9 mg, 0.01 mmol) and ferrocene (1.9 mg, 0.01 mmol, 1 equiv.) in 1 mL of toluene in a sealed pressure vessel. The resultant inky, dark red solution reacted for 12 hours at the specified temperature. The pressure vessel was then cooled and the solvent was removed *in vacuo*. The resulting dark brown oil was dissolved in a 20:1 mixture of CH₂Cl₂ and MeOH and flash chromatographed through a short pipette of deactivated silica gel to give a clear bright orange solution. ¹H NMR yields were determined via integration against ferrocene.

Yield Determination of Catalytic Aziridination Reactions with 1-Azidoadamantane using ^1H NMR. Under an inert N_2 atmosphere, 1-azidoadamantane (51.0 mg, 0.288 mmol, 20 equiv.) was added to a stirring solution of $(^{\text{Ad}}\text{L})\text{FeCl}(\text{OEt}_2)$ (**2.2**) (10.0 mg, 0.0144 mmol) and the internal standard ferrocene (2.7 mg, 0.0144 mmol, 1 equiv.) in 1 mL of styrene in a 20 mL scintillation vial. The resultant inky, dark red solution was stirred for 12 hours at 25 °C. The solvent was removed *in vacuo*. The resulting dark brown oil was dissolved in a 20:1 mixture of CH_2Cl_2 and MeOH and flash chromatographed through a short pipette of silica gel to give a clear bright orange solution. The crude ^1H NMR yields were determined via integration against ferrocene to be 85% (based on azide, averaged over two runs).

Yield Determination of Catalytic Amination Reactions with 1-Azidoadamantane and $(^{\text{tBu}}\text{L})\text{FeCl}(\text{THF})$ using ^1H NMR. Under an inert N_2 atmosphere, 1-azidoadamantane (35.4 mg, 0.2 mmol, 20 equiv.) was added to a stirring solution of $(^{\text{tBu}}\text{L})\text{FeCl}(\text{THF})$ (**2.1**) (5.4 mg, 0.01 mmol) and ferrocene (1.9 mg, 0.01 mmol, 1 equiv.) in 1 mL of toluene in a sealed pressure vessel. The resultant inky, dark red solution reacted for 12 hours at 60 °C. The pressure vessel was then cooled and the solvent was removed *in vacuo*. The resulting dark brown oil was dissolved in a 20:1 mixture of CH_2Cl_2 and MeOH and flash chromatographed through a short pipette of deactivated silica gel to give a clear bright orange solution. ^1H NMR yields were determined via integration against ferrocene and a TON of 5.6 was established.

Catalytic Amination Reactions with 1-Azidoadamantane in the Presence of THF Scavenger. Under an inert N_2 atmosphere, 1-azidoadamantane (35.4 mg, 0.2 mmol, 20 equiv.) was added to a stirring solution of $(^{\text{tBu}}\text{L})\text{FeCl}(\text{THF})$ (**2.1**) (10 mg, 0.019 mmol), ferrocene (3.45 mg, 0.019 mmol, 1 equiv.) and the Lewis acid $\text{B}(\text{C}_6\text{F}_5)_3$ (9.7 mg, 0.019 mmol, 1 equiv.) in 1 mL of toluene in a sealed pressure vessel. The resultant inky, dark red solution reacted for 12 hours

at the specified temperature. The pressure vessel was then cooled and the solvent was removed *in vacuo*. The resulting dark brown oil was dissolved in a 20:1 mixture of CH₂Cl₂ and MeOH and flash chromatographed through a short pipette of deactivated silica gel to give a clear bright orange solution. ¹H NMR yields were determined via integration against ferrocene and a TON of 4.6 was established.

Product Inhibition in Catalytic Amination Reactions. Under an inert N₂ atmosphere, 1-azidoadamantane (35.4 mg, 0.2 mmol, 20 equiv.) was added to a stirring solution of (^{Ad}L)FeCl(OEt₂) (**2.2**) (6.9 mg, 0.01 mmol), ferrocene (1.9 mg, 0.01 mmol, 1 equiv.), and benzyl adamantylamine (36.3 mg, 0.15 mmol, 15 equiv.) in 1 mL of toluene in a sealed pressure vessel. The resultant inky, dark red solution reacted for 12 hours at the specified temperature. The pressure vessel was then cooled and the solvent was removed *in vacuo*. The resulting dark brown oil was dissolved in a 20:1 mixture of CH₂Cl₂ and MeOH and flash chromatographed through a short pipette of deactivated silica gel to give a clear bright orange solution. No additional benzyl adamantylamine was formed as determined by ¹H NMR.

Adamantyl Amine Inhibition in Catalytic Amination Reactions. Under an inert N₂ atmosphere, 1-azidoadamantane (35.4 mg, 0.2 mmol, 20 equiv.) was added to a stirring solution of (^{Ad}L)FeCl(OEt₂) (**2.2**) (6.9 mg, 0.01 mmol), ferrocene (1.9 mg, 0.01 mmol, 1 equiv.), and adamantylamine (15.1 mg, 0.15 mmol, 10 equiv.) in 1 mL of toluene in a sealed pressure vessel. The resultant inky, dark red solution reacted for 12 hours at the specified temperature. The pressure vessel was then cooled and the solvent was removed *in vacuo*. The resulting dark brown oil was dissolved in a 20:1 mixture of CH₂Cl₂ and MeOH and flash chromatographed through a short pipette of deactivated silica gel to give a clear bright orange solution. No benzyl adamantylamine was formed as determined by ¹H NMR.

Addition of 1,4-Cyclohexadiene. A J. Young tube was charged with either (^AL)FeCl(NC₆H₄-*p*-¹Bu) or [(^AL)FeCl]₂(*μ*-NPh(C₆H₅)N) (**2.4**) (10.0 mg) and 1 mL dichloromethane-*d*₂. 1,4-Cyclohexadiene (~5 equiv.) was dissolved in 0.5 mL dichloromethane-*d*₂ and then transferred to the J. Young tube, which was closed and mixed. ¹H NMR (400 MHz, CD₂Cl₂) after 5 min showed resonances for both benzene (δ: 7.36 ppm) and 1,4-cyclohexadiene (δ/ppm 2.66, 5.69).

Addition of Dimethylphenylphosphine. A J. Young tube was charged with (^AL)FeCl(NC₆H₄-*p*-¹Bu) (**2.5**) (10.0 mg) and 1 mL benzene-*d*₆. Two equivalents Me₂PhP were added as a 1% *w/w* stock solution in benzene-*d*₆. The tube was sealed and mixed. Formation of the phosphinidene, Me₂PhP=N(C₆H₄-*p*-¹Bu) was confirmed by ³¹P NMR (160 MHz, C₆D₆) which showed a single peak at 2.79 ppm and disappearance of phosphine at -45.46 ppm. The chemical shift of the phosphinidene product was confirmed by independent synthesis directly from the reaction of Me₂PhP and N₃(C₆H₄-*p*-¹Bu) in benzene-*d*₆.

General Procedure for C-H Insertion from (^AL)FeCl. A 5 mL vial was charged with a stir-bar, (^AL)FeCl (**2.3**) (10.0 mg), and 1 mL toluene-*d*₈. 1-Azido-4-*tert*-butylbenzene or 1-azidobenzene (1 equiv.) was added as a 1% *w/w* solution in toluene-*d*₈. The mixture stirred for 1 h and was then transferred to a J. Young tube. Conversion of (^AL)FeCl (**2.3**) to (^AL)FeCl(NC₆H₄-*p*-¹Bu) (**2.5**) or [(^AL)FeCl]₂(*μ*-NPh(C₆H₅)N) (**2.4**) was confirmed by ¹H NMR. The tube was heated to 85 °C in an oil bath for 2 h. Consumption of (^AL)FeCl(NC₆H₄-*p*-¹Bu) (**2.5**) or [(^AL)FeCl]₂(*μ*-NPh(C₆H₅)N) (**2.4**) was confirmed by ¹H NMR, and formation of the C-H insertion products was confirmed by HRMS: LCMS (ESI⁺) *m/z* (C₆D₅)CD₂NH(C₆H₄-*p*-¹Bu) Calc. [C₁₇H₁₄D₇N+H]⁺ 247.2184, Found 247.2180 [M+H]⁺; (C₆D₅)CD₂NH(C₆H₅) Calc. [C₁₃H₆D₇N+H]⁺ 191.1558, Found 191.1560 [M+H]⁺.

Yield Determination of Stoichiometric Amination and Aziridination by (^{Ar}L)FeCl(NC₆H₄-*p*-^tBu) using ¹H NMR. Under an inert N₂ atmosphere, (^{Ar}L)FeCl(NC₆H₄-*p*-^tBu), **2.5**, (15.0 mg) and ferrocene (1 equiv.) were dissolved in 2 mL of toluene or styrene. The resultant dark red solution was heated for 12 hours at 80 °C in a J. Young tube. The tube was then cooled and the solvent was removed *in vacuo*. The resulting residue was dissolved in a 20:1 mixture of CH₂Cl₂ and MeOH and flash chromatographed through a short pipette of deactivated silica gel to give a clear bright orange solution. ¹H NMR yields were determined via integration against ferrocene. The average yield for the amination of toluene was 34% (based on **2.5**, two runs), and for the aziridination of styrene 20% (based on **2.5** two runs).

2.6.6 X-Ray Diffraction Techniques.

All structures were collected on a Bruker three-circle platform goniometer equipped with an Apex II CCD and an Oxford cryostream cooling device. Radiation was from a graphite fine focus sealed tube Mo K α (0.71073 Å) source. Crystals were mounted on a cryoloop or glass fiber pin using Paratone N oil. Structures were collected at 100 K. Data was collected as a series of ϕ and/or ω scans. Data was integrated using SAINT¹²⁰ and scaled with either a numerical or multi-scan absorption correction using SADABS.¹²⁰ The structures were solved by direct methods or Patterson maps using SHELXS-97¹²¹ and refined against F^2 on all data by full matrix least squares with SHELXL-97.¹²¹ All non-hydrogen atoms were refined anisotropically. Hydrogen atoms were placed at idealized positions and refined using a riding model. The isotropic displacement parameters of all hydrogen atoms were fixed to 1.2 times the atoms they

119. Bruker AXS (2009). Apex II. Bruker AXS, Madison, Wisconsin.

120. Sheldrick, G. M. *Acta Cryst.* **2008**, A64, 112.

are linked to (1.5 times for methyl groups). Further details on particular structures are noted below.

(^tBuL)FeCl(THF), 2.1. The structure was solved in the triclinic space group $P\bar{1}$ with 4 molecules per unit cell. There were 2 equivalent molecules in the asymmetric unit. One of the bound THF molecules exhibited minor disorder.

(^AdL)FeCl(OEt₂), 2.2. The structure was solved in the monoclinic space group $P2_1/n$ with 4 molecules per unit cell. There was an additional molecule of uncoordinated diethyl ether present in the asymmetric unit.

(^ArL)H. The structure was solved in the triclinic space group $P\bar{1}$ with 2 molecules per unit cell. There was a single molecule of benzene present in the asymmetric unit. The acidic N-H hydrogen was picked from the Fourier map and refined semi-freely by restraining the N-H distance to 0.88 Å (the average effective distance for sp² N-H bonds at -173 °C), and by setting the isotropic displacement parameter to 1.2 times that of the nitrogen atom.

(^ArL)FeCl, 2.3. The structure was solved in the monoclinic space group $C2/c$ with 4 molecules per unit cell, and half of the molecule in the asymmetric unit. The Fe and Cl, atoms lie on a crystallographic mirror plane. Two of the phenyl rings exhibited disorder which was modeled by addition of a second position for each ring. The mesityl ring lies about a mirror plane and was modeled with all atoms at half-occupancy, with the second position being generated by symmetry. There were 2 benzene sites in the structure, one on a mirror plane, and the second exhibiting significant disorder, which could not be modeled as multiple positions but was improved by allowing partial occupancy (0.775). The difficulty of accurately modeling the disordered solvent molecules is the reason for the higher than usual R values but does not seriously affect the chemically significant features of the structure.

$[(^A\text{rL})\text{FeCl}]_2(\mu\text{-NPh}(\text{C}_6\text{H}_5)\text{N})$, **2.4**. The structure was solved in the triclinic space group $P\bar{1}$ with 2 molecules per unit cell. There were four molecules of benzene present in the asymmetric unit. There were also residual density peaks corresponding to 2 molecules of *n*-hexane. Due to apparent low occupancy and high disorder of the hexane, an acceptable model could not be refined. Instead the hexanes were treated as diffuse contributors to the scattering using the SQUEEZE option in the PLATON¹²² package. Similarity and rigid bond restraints of the anisotropic displacement parameters were placed on all atoms.

$(^A\text{rL})\text{FeCl}(\text{NC}_6\text{H}_4\text{-}p\text{-Bu})$, **2.5**. The structure was solved in the monoclinic space group $P2_1/c$ with 4 molecules per unit cell. There was a single molecule of *n*-pentane present in the asymmetric unit.

121. Spek, A. L. *Acta Cryst.* **2009**, *D65*, 148.

Table 2.3. X-ray crystallographic experimental properties.^{a,b}

	2.1	2.2	(^AL)H	2.3	2.4	2.5
CCDC Deposit Number	791228	791229	792018	792019	792020	792021
Moiety Formula	C ₃₀ H ₄₁ ClFeN ₂ O	C ₄₂ H ₅₅ ClFeN ₂ O; C ₄ H ₁₀ O	C ₆₆ H ₅₀ N ₂ ; 3•(C ₆ H ₆)	C ₆₆ H ₄₉ ClFeN; 2.55•(C ₆ H ₆)	C ₁₄₄ H ₁₀₈ Cl ₂ Fe ₂ N ₆ ; 4•(C ₆ H ₆)	C ₇₆ H ₆₂ ClFeN ₃ ; C ₃ H ₁₂
FW	536.95	769.3	1105.4	1160.64	2417.4	1180.73
Crystal System	triclinic	monoclinic	triclinic	monoclinic	triclinic	monoclinic
Space Group (Z)	<i>P</i> $\bar{1}$ (4)	<i>P</i> 2 ₁ /n (4)	<i>P</i> $\bar{1}$ (2)	<i>C</i> 2/c (4)	<i>P</i> $\bar{1}$ (2)	<i>P</i> 2 ₁ /c (4)
a (Å)	14.2661(5)	14.497(3)	12.5350(5)	15.840(5)	14.4691(12)	21.0117(10)
b (Å)	15.0088(5)	16.196(3)	13.6512(6)	21.273(7)	21.4975(18)	12.2392(6)
c (Å)	15.1843(5)	18.331(3)	20.4250(8)	19.136(9)	23.560(2)	25.0442(12)
α (°)	91.591(2)	90	75.509(2)	90	94.3420(10)	90
β (°)	99.021(2)	106.605(3)	85.664(2)	108.066(5)	93.7780(10)	91.1800(10)
γ (°)	115.438(2)	90	65.022(2)	90	102.9270(10)	90
Volume (Å³)	2883.16(17)	4124.4(13)	3065.6(2)	6130(4)	7096.1(10)	6439.2(5)
Calc. ρ (mg/m³)	1.237	1.239	1.198	1.258	1.131	1.218
μ (mm⁻¹)	0.640	0.470	0.068	0.338	0.295	0.323
Crystal Size (mm)	0.24×0.18 ×0.12	0.42×0.31 ×0.22	0.82×0.43 ×0.39	0.7×0.17 ×0.07	0.32×0.32 ×0.06	0.4×0.3 ×0.16
Reflections	20840	62277	41971	30219	120338	135338
Completeness (to 2θ)	99.7% 27.52°	99.6% 25.79°	99.9% 26.37°	100.0% 27.10°	99.9% 26.79°	100.0% 27.48°
GOF on F²	1.018	1.008	1.022	1.000	0.878	1.041
R1, wR2^c [I>2σ(I)]	0.0425, 0.1029	0.0525, 0.1202	0.0426, 0.1042	0.0859, 0.2152	0.0563, 0.1267	0.0423, 0.0954

^a λ = 0.71073 Å; ^b T = 100(2) K; ^c R1 = $\sum ||F_o| - |F_c|| / \sum |F_o|$, wR2 = $\{\sum [w(F_o^2 - F_c^2)^2] / \sum [w(F_o^2)^2]\}^{1/2}$

2.6.7 Computational Methods.

Computations were carried out utilizing the ORCA 2.7¹⁰⁵ program package. The B3LYP¹²³ functional was used with the def2-TZVP (Fe, N, Cl) and def2-SV(P) (C, H) basis sets.¹²⁴ For single point calculations and property calculations the def2-TZVP/J (Fe, N, Cl) and def2-SVP/J (C, H) auxiliary basis sets¹²⁵ were employed to utilize the RIJCOSX¹²⁶ approximation for accelerating the calculation. For the calculation of Mössbauer parameters the basis set at Fe was expanded to the CP(PPP) basis.¹²⁷ The ^AL ligand was approximated as 1,5,9-triphenyldipyrromethene, ^{Ph}L'. Geometries were taken from x-ray structures and truncated by replacing -Ph or -Me with -H where appropriate.

Mössbauer. Mössbauer parameters were obtained from additional single-point calculations, following methods described by F. Neese.^{128,129} Quadrupole splittings (ΔE_Q) were calculated from the electric field gradient, Eq. 2.1.

$$\Delta E_Q = \frac{1}{2} eQV_{zz} \sqrt{1 + \frac{1}{3} \eta^2} \quad (2.1)$$

The nuclear quadrupole moment $Q(^{57}\text{Fe})$ was taken to be 0.16 barn.¹²⁹ The principal tensor components of the EFG are V_{xx} , V_{yy} , and V_{zz} , from which the asymmetry parameter $\eta = (V_{xx} - V_{yy})/V_{zz}$ can be defined.

$$\delta = a(\rho_0 - C) + b \quad (2.2)$$

-
122. (a) Becke, A. D. *J. Chem. Phys.* **1993**, 98, 5648. (b) Lee, C. T.; Yang, W. T.; Parr, R. G. *Phys Rev. B* **1988**, 33, 785.
123. (a) Schäfer, A.; Horn, H.; Ahlrichs, R. *J. Chem. Phys.* **1992**, 97, 2571. (b) Schäfer, A.; Huber, C.; Ahlrichs, R. *J. Chem. Phys.* **1994**, 100, 5829. (c) Weigand, F.; Ahlrichs, R. *Phys. Chem. Chem. Phys.* **2005**, 7, 3297.
124. Weigand, F. *Phys. Chem. Chem. Phys.* **2006**, 8, 1057.
125. Neese, F.; Wennmohs, F.; Hansen, A.; Becker, U. *Chem. Phys.* **2009**, 356, 98.
126. Neese, F. *Inorg. Chim. Acta* **2002**, 337, 181.
127. Ye, S.; Tuttle, T.; Bill, E.; Simkhovich, L.; Gross, Z.; Thiel, W.; Neese, F. *Chem.–Eur. J.* **2008**, 14, 10839.
128. Sinnecker, S.; Slep, L. P.; Bill, E.; Neese, F. *Inorg. Chem.* **2005**, 44, 2245.

Isomer shifts (δ) were calculated from the electron density at the nucleus ρ_0 , using a linear equation, Eq. 2.2,¹²⁹ with constants determined by fitting the calculated densities to experimental isomer shifts for a series of dipyrromethane, dipyrromethene, and tripyrroethane complexes synthesized in our lab.¹³⁰ The basis sets and functional described above were used for all structures. X-ray coordinates were used, and spin-states were assigned based on magnetic measurements and experimental Mössbauer data. For this series of compounds the parameters were determined to be $C = 11797.145 \text{ au}^{-3}$, $a = -0.402 \text{ au}^3 \text{ mm s}^{-1}$, and $b = 8.605 \text{ mm}$. The maximum disagreement between calculated and experimental isomer shift was 0.05 mm s^{-1} .

Broken Symmetry Model of 2.5. A broken symmetry solution was used to model the antiferromagnetically coupled Fe^{III} imido radical. The broken symmetry notation $\text{BS}(m,n)$ ¹³¹ refers to a system with $(m+n)$ unpaired electrons, and a net spin of $(m-n)/2$ (if antiferromagnetically coupled). One fragment will bear m α spin electrons, and the other fragment n β spin electrons. For the Fe^{III} imido radical, $(^{\text{Ph}}\text{L}')\text{FeCl}(\text{NC}_6\text{H}_5\text{-}p\text{-Bu})$ (the truncated analog of **2.5**), $\text{BS}(5,1)$ was the appropriate description for a high-spin Fe^{III} ($S = 5/2$) coupled to a imido radical ($S = 1/2$). The corresponding orbital transformation,¹³¹ and the resultant corresponding orbital overlap were used as an indicator of a spin-coupled system. One pair of corresponding orbitals had overlap of 0.59, which is significantly less than 1, and suggests a broken symmetry solution. The broken symmetry solution ($\text{BS}(5,1)$, $E_{\text{BS}} = -3315.28806 E_{\text{h}}$) was found to have the same energy as the unrestricted quintet ($S = 2$, $E = -3315.28800 E_{\text{h}}$). The exchange coupling constant J was determined from the energy difference between the high-spin

129. Compounds used for the calibration of δ to ρ_0 : $(^{\text{Mes}}\text{L})\text{FeCl}(\text{THF})$ (King, E. R.; Betley, T. A. *Inorg. Chem.* **2009**, *48*, 2361), $(\text{dpma})\text{Fe}(\text{py})_2$, $(\text{dpma})\text{Fe}(\text{bpy})$ (King, E. R.; Betley, T. A. *J. Am. Chem. Soc.* **2009**, *131*, 14374.); $(\text{tpe})\text{Fe}(\text{py})^-$ (Sazama, G. T.; Betley, T. A. *Inorg. Chem.* **2010**, *49*, 2512.); $(^{\text{Bu}}\text{L})\text{FeCl}(\text{THF})$, $(^{\text{Ad}}\text{L})\text{FeCl}(\text{Et}_2\text{O})$, $(^{\text{Ar}}\text{L})\text{FeCl}$ (this work). (dpma = 1,9-dimesityl-5,5-dimethyl-dipyrromethane, tpe = tris(2-mesitylpyrrolyl)ethane)

($S = 3$, $E_{HS} = -3315.27162 E_h$) and broken-symmetry states, using the spin-Hamiltonian in Eq. 2.3, and the formula¹³² in Eq. 2.4.

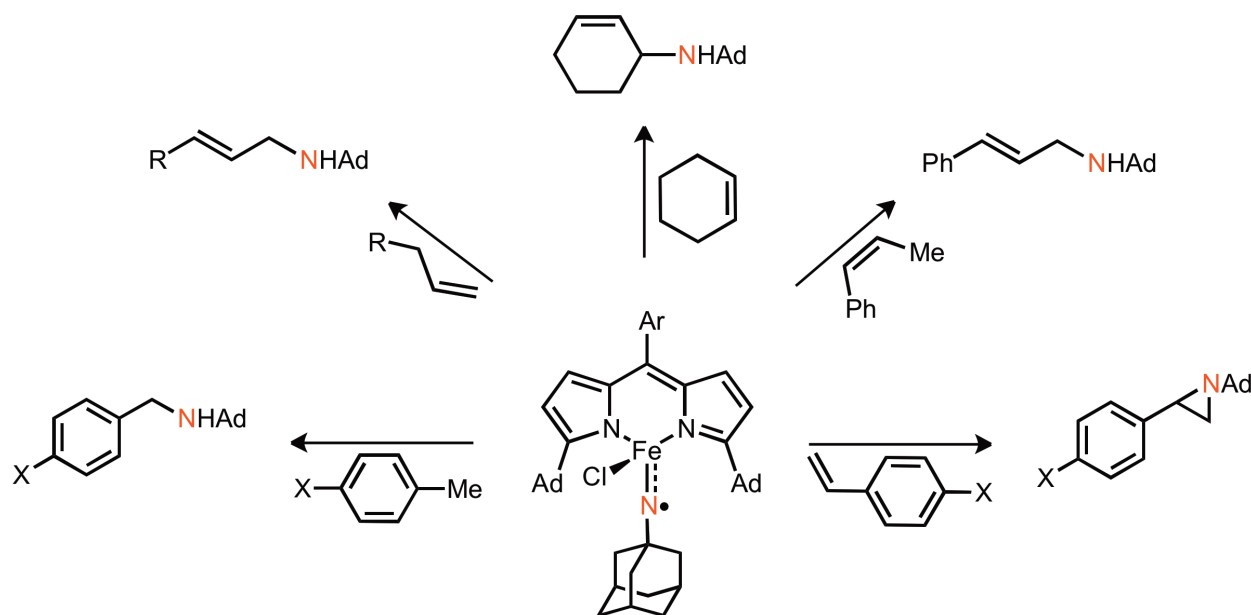
$$H = -2J\vec{S}_{Fe} \cdot \vec{S}_{NR} \quad (2.3)$$

$$J = -\frac{E_{HS} - E_{BS}}{\langle S^2 \rangle_{HS} - \langle S^2 \rangle_{BS}} \quad (2.4)$$

Based on the energy difference of $E_{HS} - E_{BS} = 3610 \text{ cm}^{-1}$, the antiferromagnetic coupling constant is estimated to be $J = -673 \text{ cm}^{-1}$.

130. Kirchner, B.; Wenmohs, F.; Ye, S.; Neese, F. *Curr. Opin. Chem. Biol.* **2007**, *11*, 134.

131. (a) K. Yamaguchi, Y. Takahara, T. Feuono in *Applied Quantum Chemistry* (Eds.: V. H. Smith), Reidel, Dordrecht, **1986**, 586. (b) Soda, T.; Kitigawa, Y.; Onishi, T.; Takano, Y.; Shigeta, Y.; Nagao, H.; Yoshioka, Y.; Yamaguchi, K. *Chem. Phys. Lett.* **2000**, *319*, 223.



Chapter 3: Intermolecular *N*-Group Transfer Chemistry with Olefinic Substrates

3.1 Introduction

The prevalence of nitrogen functionalities in bioactive molecules and materials has inspired the development of numerous techniques for direct C–H bond amination. In particular, metal stabilized nitrene transfer using noble metal catalysts, specifically dirhodium,^{18,19} have been successfully applied in the context of complex molecule synthesis. These well-behaved catalysts have been extensively studied and are believed to transfer functionality via a singlet nitrenoid intermediate in a concerted asynchronous mechanism.²² In contrast, a renewed interest in late, first-row transition metal nitrenoid catalysts has emerged, composed of copper,^{3–5,62} cobalt,^{46,133} manganese,^{37–39,58,61} nickel,^{65,66} and iron^{134,135} where radical intermediates have been invoked or fully characterized. Their high *d*-electron count and compressed ligand fields create a

132. Caselli, A.; Gallo, E.; Ragaini, F.; Oppezzo, A.; Cenini, S. *J. Organomet. Chem.* **2005**, 690, 2142.

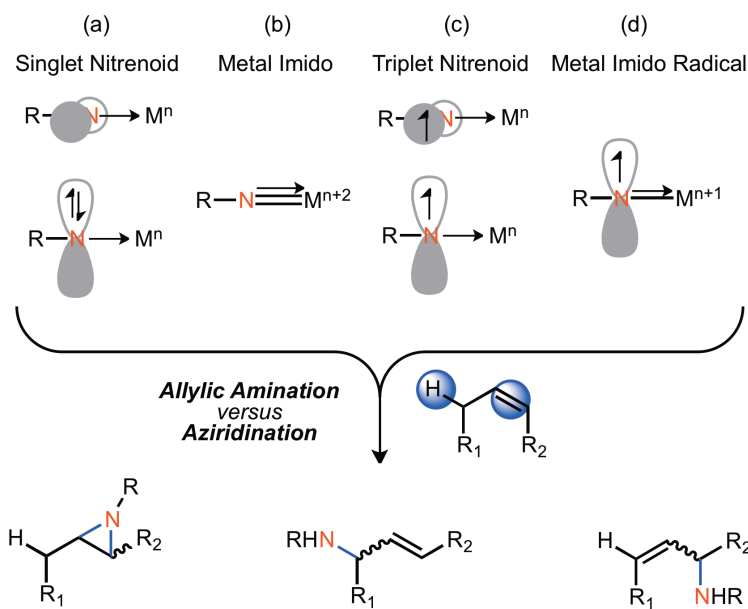


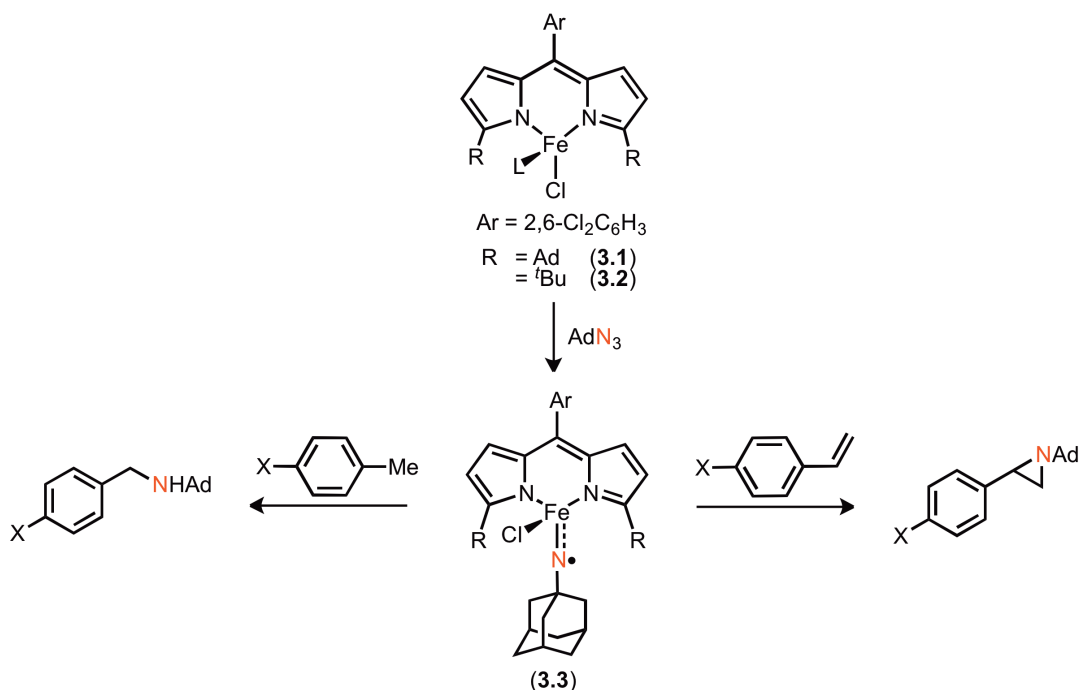
Figure 3.1. Metal-nitrenoid electronic structure and reactivity. Possible electronic configurations of reactive intermediates for *N*-group transfer to olefins.

unique opportunity for ancillary ligands to strongly influence the bonding interactions between the nitrene moiety and the metal center (Figure 3.1). For instance, the binding of strong field ligands destabilizes metal-ligand antibonding orbitals and encourages low-spin electronic configurations. Similar to their second- and third-row congeners, closed-shell first-row transition metals will interact with nitrene precursors to generate either a metal-bound singlet nitrenoid (Figure 3.1a) or a covalently-bound metal imido (Figure 3.1b). Alternatively, weak field ligand environments favor population of metal-ligand antibonding orbitals and high-spin electronic configurations. Communication between highly paramagnetic metal centers and *N*-group transfer reagents has the potential to translate radical character directly to the *N*-atom or along the metal-nitrogen bond vector (Figure 3.1c and d).

Given the range of accessible metal-nitrenoid electronic configurations, it is not surprising that the established catalysts exhibit dramatically different reactivity, particularly when considering the functionalization of olefinic substrates (Figure 3.1). For instance, exposure of a

macrocyclic tetracarbene-ligated Fe-complex exclusively catalyzes the aziridination of aliphatic olefins,¹³⁵ while a phthalocyaninato Fe-complex facilitates preferential intramolecular allylic C–H amination,¹³⁴ and an Fe-porphyrin complex generates mixtures of both aziridine and allylic amine products.³⁸ While each of these complexes is confined to a tetragonal field by tetra-chelating macrocyclic ligands, the ligand field strength, metal oxidation state, and nitrene source vary and are likely responsible for the changes in chemoselectivity. However, in each of these examples, the structure and electronic configuration of the reactive intermediate are only posited, as is the case for nearly all C–H amination catalysts.

Ideally, one would like to probe the influence a given metal, ligand, and nitrene unit bears on reactivity and selectivity through the isolation of the reactive metal-nitrenoid intermediate. We previously reported⁴⁹ intermolecular amination and aziridination with aryl and alkyl azides



Scheme 3.1. Reactivity of imido radical intermediate. Formation of proposed reactive intermediate for benzylic amination and aziridination

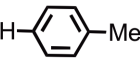
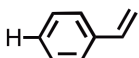
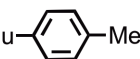


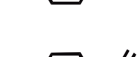
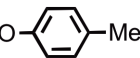

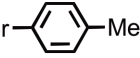
134. Cramer, S. A.; Jenkins, D. M. *J. Am. Chem. Soc.* **2011**, *133*, 19342.

using ferrous dipyrinato complexes (^RL)FeCl(Et₂O) [R = 2,4,6-Ph₃C₆H₂, 1-adamantyl (**3.1**), ^tBu (**3.2**)] (Scheme 3.1). Isolation and characterization of a reactive intermediate elucidated the electronic structure of the high-spin iron-bound imido radical **3.3**, wherein a high-spin Fe(III) ($S = 5/2$) is antiferromagnetically coupled to the imido radical ($S = -1/2$) to give an overall high-spin ground state ($S = 2$). This electronic structure places significant radical character on both the Fe–N σ and π bond vectors, facilitating both H-atom abstraction and radical recombination pathways. In this report, we have explored the implications of the reactive intermediate's unique electronic structure on both the reaction mechanism and chemoselectivity of intermolecular *N*-group transfer. We have established the catalyst's strong preference for allylic amination over aziridination with aliphatic olefin substrates. Additionally, we report on the functionalization of α -olefins to linear allylic amines with outstanding regioselectivity.

3.2 Benzylic Amination and Aziridination of Substituted Substrates with Organoazides

We previously discovered that **3.1** catalyzes nitrogen group transfer to styrene and toluene with 1-azidoadamantane, resulting in the formation of 1-adamantyl-2-phenylaziridine (85% yield) and benzyladamantylamine (60% yield) respectively. In attempts to expand the substrate scope, a series of *para*-substituted toluenes and styrenes were subjected to **3.1** (5-10 mol%) and 1-azidoadamantane (Table 3.1). All substrates successfully underwent the desired intermolecular nitrogen group transfer, demonstrating that catalysis is amenable to substrates with both electron withdrawing and donating groups and ethereal C–H bonds (Table 3.1, entry 4 and 8). The yields for aziridination at room temperature are overall higher than that for amination (75-85% vs. 46-60%), this trend correlates with the lower propensity for the aziridine product to bind to the catalyst and retard the rate of catalysis. Amination yields can be improved

Table 3.1. Benzylic amination and aziridination of substituted toluenes and styrenes.

Amination				Aziridination						
Entry	Substrate	Yield (%) ^a	k_X/k_H ^b	Entry	Substrate	Yield (%) ^a	k_X/k_H ^b	Entry	Azide	Yield (%) ^e
1		60 ^c	1.00	6		85 ^d	1.00	10	^t BuN ₃	86
2		46	1.10	7		80	1.11	11	ⁿ BuN ₃	53
3		52	1.14	8		75	1.20	12	PhN ₃	17
4		47	1.08	9		80	1.09	13	<i>p</i> - ^t BuPhN ₃	64
5		47	1.18					14	<i>p</i> -NO ₂ PhSO ₂ N ₃	0
								15	TMSN ₃	0

^a Reaction with specified substrate and **3.1** (10 mol%) and AdN₃ at room temperature for 12 h. Yields determined by ¹H NMR, using ferrocene as an internal standard. ^b Ratio determined by ¹H NMR from single turnover competition experiment run with **3.1** and AdN₃ (1 equiv) in 1:1 substituted:parent toluene or styrene. ^c Reaction run at 60 °C. ^d Reaction run with 5 mol% **3.1**. ^e Reaction with styrene and **3.1** (20 mol%) and specified azide at room temperature for 12 h. Yields determined by ¹H NMR, using ferrocene as an internal standard.

upon heating to 60 °C (entry 1) to encourage product dissociation from the electrophilic Fe center.

Styrene aziridination is amenable to a variety of organoazides. Exposure of **3.1** and styrene to 5 equivalents of *tert*-butyl azide (Table 3.1, entry 10) resulted in the corresponding aziridine in good yield (86%). The yield for 1-azidobutane drops significantly (entry 11, 53%), likely due to imide decomposition pathways. In general, primary and secondary alkyl azides rapidly react with **3.1** to generate the imide intermediate, but are then prone to undergo either intramolecular C–H amination to yield *N*-heterocycles or α -hydrogen abstraction to yield linear imines (see Chapter 4 for more details) rather than intermolecular group transfer chemistry. Aryl azides are also compatible with the aziridination reaction. *Para*-substitution of the aryl ring eliminates a bimolecular imido decomposition pathway,⁴⁹ and noticeably improves the yield of aziridination (entry 12 vs. entry 13).

Ultimately, we were interested in generating the parent N–H aziridines and thus explored the *N*-group transfer chemistry of azides with cleavable groups attached to the γ *N*-atom.

Exposure of **3.2** to 2-nitrobenzenesulfonyl (nosyl) azide (entry 14) in the presence of styrene did not yield the desired nosyl-protected aziridine. ^1H NMR and Mössbauer spectroscopic analyses ($\delta=0.31$ mm/s; $\Delta E_Q=0.3$ mm/s) of the crude reaction mixture support the formation of the Fe^{III} -containing product **3.4** that is catalytically inactive. Low-quality crystals were obtained from a concentrated dichloromethane solution of the reaction mixture in order to decipher the atom connectivity in the product (Figure 3.2a). The short N–S bond distance (1.502(11) Å) and elongated S–O bond distances (1.414(12) and 1.406(12) Å) suggest an H–atom abstraction event that occurs at a sulfur-bound *O*-atom. In general, sulfonyl azides and hypervalent iodine reagents (*eg.* PhINTs) are incompatible with **3.2**. Sulfonyl-derived nitrenes likely suffer from resonance delocalization of the *N*-based radical onto the sulfonyl *O*-atoms in the imido intermediate (Scheme 3.2a). Next, *O*-mediated H-atom abstraction stalls the catalyst at an $\text{Fe}(\text{III})$ oxidation state and precludes productive amination chemistry.

Exposure of **3.1** to azidotrimethylsilane and styrene did not result in productive intermolecular nitrene transfer (Table 3.1, entry 15), but rather the isolation of a clean, new

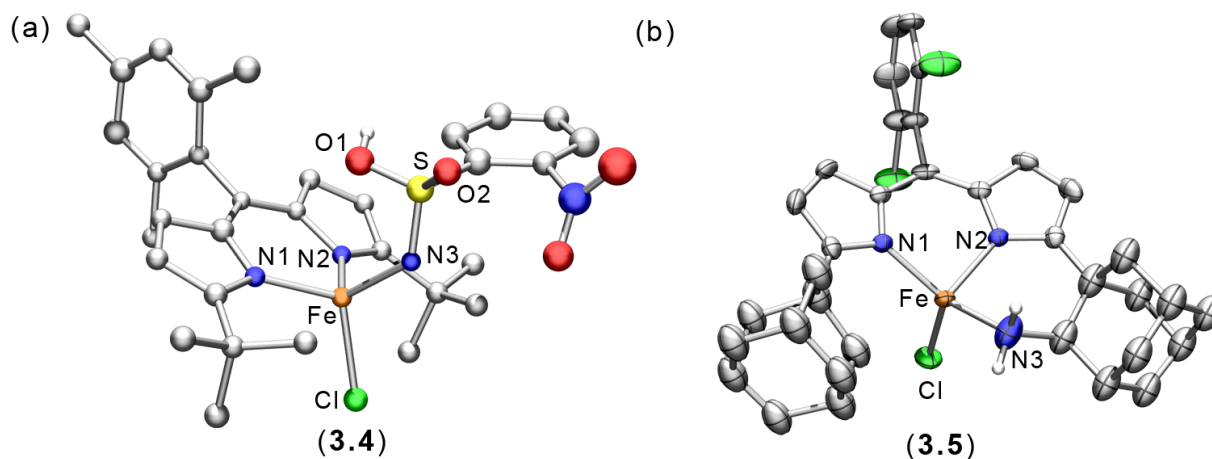
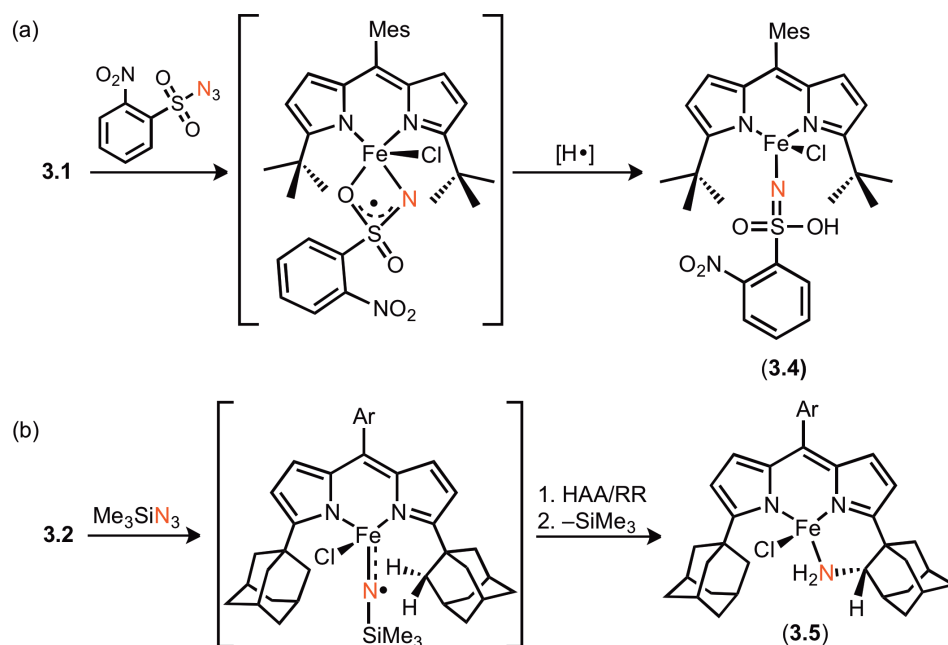


Figure 3.2. X-ray structures of imide decomposition products. (a) Solid-state structure of **3.4**. Due to poor crystal quality, anisotropic atom refinement was not possible (Fe, orange; C, gray; H, white; N, blue; Cl, green). Bond lengths (Å): Fe–N1, 1.946(12); Fe–N2, 1.932(12); Fe–N3, 1.955(12); Fe–Cl, 2.157(4); N3–S, 1.502(11); S–O1, 1.414(12), S–O2, 1.406(12). (b) Solid-state structure of **3.5**. Thermal ellipsoids set at the 50% probability level (Fe, orange; C, gray; H, white; N, blue; Cl, green). Bond lengths (Å): Fe–N1,2, 2.019(5); Fe–N3, 2.103(13); Fe–Cl 2.263(3).

paramagnetic species. An X-ray diffraction study on single crystals grown from a concentrated hexanes solution revealed the product to be the pseudo-tetrahedral Fe complex **3.5** (Figure 3.2b).¹³⁶ The structure confirms that azidotrimethylsilane is competent for *intramolecular* nitrene insertion. A secondary C–H bond on each adamantyl ligand substituent has undergone C–H amination and subsequently ligated to the Fe-center (Scheme 3.2b). Curiously, during the course of the reaction protodesilylation of the nitrene moiety occurs through an unknown mechanism. We are interested in developing this chemistry with more stable azidosilanes and exploring their potential for intermolecular nitrene transfer.

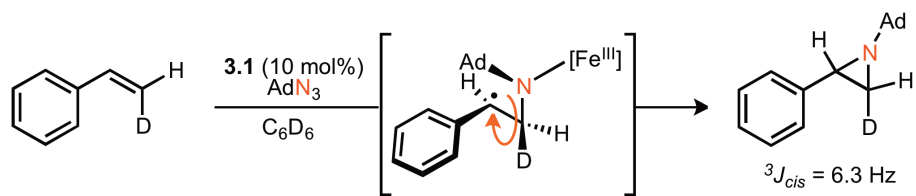


Scheme 3.2. Mechanisms of imide decomposition. (a) Exposure of **3.2** to 2-nitrobenzenesulfonyl azide results in the formation of the ferric product **3.4** after HAA at the sulfonyl oxygen. (b) Exposure of **3.1** to 1-azidotrimethylsilane results in the ligand aminated product **3.5** after HAA and RR, followed by protodesilylation.

3.3 Mechanism of Benzylic Aziridination and Amination Reactions

In Chapter Two, we proposed that the mechanism of catalytic toluene amination and styrene aziridination proceeds via one-electron pathways, largely based on the non-classical KIE

135. X-Ray structure obtained by Benjamin Lin.



Scheme 3.3. Mechanistic probe for aziridination reaction. Aziridination of *cis*-deutero-styrene occurs without any deuterium scrambling, generating only *cis*-1-adamantyl-2-deutero-3-phenylaziridine. The coupling constant (6.3 Hz) between the vicinal hydrogens is indicative of a *cis* orientation. If aziridination is occurring through a stepwise mechanism, the radical recombination step must be faster than C–C bond rotation (red arrow), preventing isomerization to the *trans*-aziridine

values (12.8) for toluene amination and the high-spin electronic structure of the isolated intermediate **3.3**. Following this initial report, we have conducted a series of labeling and Hammett studies to further corroborate a mechanistic proposal in which short-lived carboradical intermediates are formed en route to the functionalized products.

Exposure of **3.1** and 1-azidoadamantane to excess *cis*- β -deuterostyrene resulted in the isolation of *cis*-1-adamantyl-2-deutero-3-phenylaziridine, with no evidence of the *trans* isomer (Scheme 3.3). While isomerization of the *cis*-olefin to a mixture of *cis*- and *trans*-aziridines is suggestive of a stepwise mechanism, lack of isomerization is less definitive. Either the reaction is occurring via a concerted mechanism or a two-step mechanism with radical recombination out-competing C–C bond rotation. The adamantyl units on both the dipyrin and imido generate a very narrow cleft in which the substrate can orient itself. The crowded environment likely impedes C–C bond rotation and renders radical recombination more facile. However, we cannot rule out a concerted aziridination mechanism with this experiment alone.

The electronic nature of the transition state was further studied by conducting a Hammett analysis of both the aziridination and amination reactions. The relative rates of catalytic aziridination and amination of a series of *para*-substituted styrenes and toluenes using **3.1** with one equivalent of 1-azidoadamantane were determined through pairwise competition experiments. Equimolar mixtures of styrene or toluene and a *para*-substituted styrene or toluene

derivative were treated with 1-azidoadamantane in the presence of a catalytic amount of the Fe complex **3.1**. The ratios of the resulting aziridines and benzylamines were determined by ^1H NMR integration of the spectra taken on unpurified material and by GC/MS analysis. The results are summarized in Table 3.1.

In all cases, k_R (k_X/k_H) is only slightly greater than one, suggesting that the rate of amination and aziridination is marginally enhanced with substitution by both electron donating and electron withdrawing groups. Plotting these values against σ^+ parameters (Figure 3.3) results in a non-linear correlation between reaction rate and electron-donating ability of the *para*-substituent. Linear correlations are consistent with cationic charge stabilization in the transition

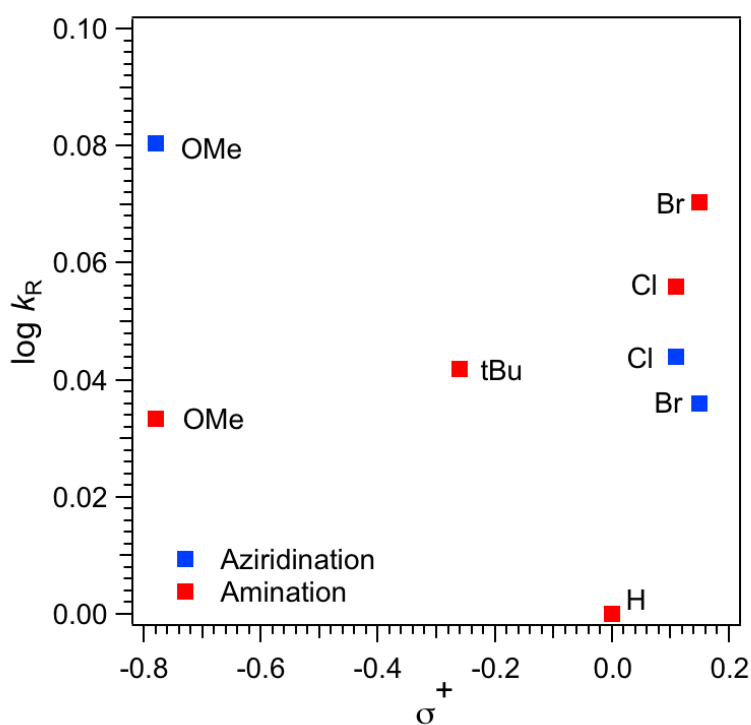


Figure 3.3. Single parameter Hammett analysis. Linear-free-energy correlation of $\log k_R$ vs σ^+ for the reactions of **3.1** with AdN_3 (1 equivalent) and a series of *para*-substituted toluenes (red) and styrenes (blue).

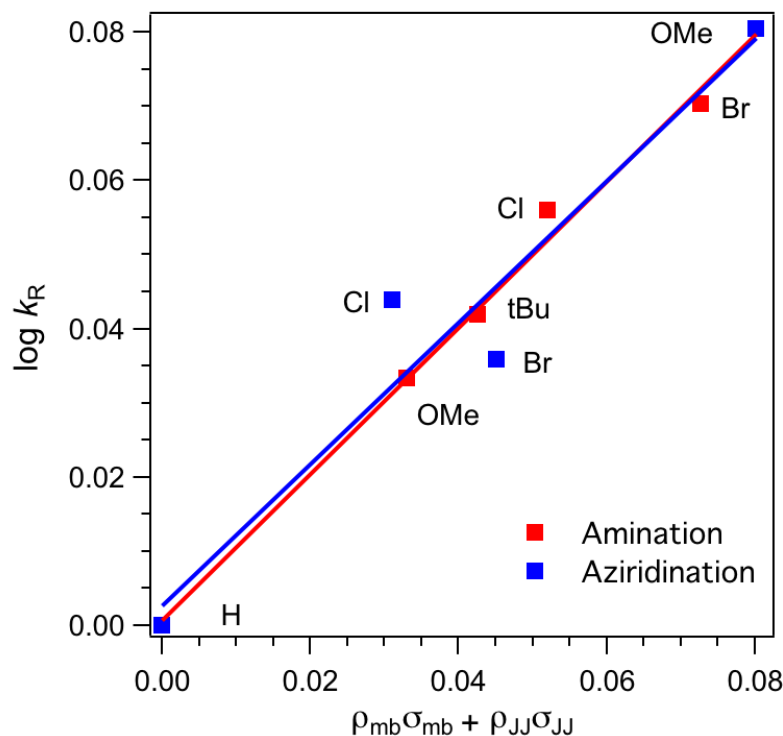


Figure 3.4. Dual parameter Hammett analysis. Linear-free-energy correlation of $\log k_R$ vs $(\sigma_{mb}, \sigma_{JJ}^{\bullet})$ for the reactions of **3.1** with AdN_3 (1 equivalent) and a series of para-substituted toluenes (red) and styrenes (blue). For the amination reaction, $\rho_{mb}, \rho_{JJ} = 0.086, 0.24$. For the aziridination reaction, $\rho_{mb}, \rho_{JJ} = -0.0073, 0.18$.

state and typically observed in concerted amination chemistry with Rh_2 -carboxylate catalysts.¹³⁷

The lack of correlation with our catalyst led us to consider the incorporation of a spin delocalization parameter, σ_{JJ}^{\bullet} , developed by Jiang and co-workers.¹³⁸ The $\log k_R$ vs $(\sigma_{mb}, \sigma_{JJ}^{\bullet})$ plot (Figure 3.4) gave rise to an appreciably more linear relationship ($R^2 = 0.99, 0.93$ for amination and aziridination respectively). Multiple coefficient linear regression for the dual-parameter equation

$$\log k_R = \rho_{mb}\sigma_{mb} + \rho_{JJ}^{\bullet}\sigma_{JJ}^{\bullet} \quad (\text{Eq. 3.1})$$

provided $\rho_{mb} = 0.086$ and $\rho_{JJ}^{\bullet} = 0.24$ for amination and $\rho_{mb} = -0.0073$ and $\rho_{JJ}^{\bullet} = 0.18$ for aziridination. The positive ρ_{JJ}^{\bullet} values reveal that the para-substituents delocalize spin in the

136. See reference 22 for a detailed Hammett analysis of $\text{Rh}_2(\text{oct})_4$ -catalyzed C–H amination of competition substrates. A ρ value of -0.55 was observed when fitting the data against σ^+ parameters. Such a value is described as consistent with an asynchronous, concerted transition structure.

transition state. In addition, the large $|Q_{JJ}/Q_{mb}|$ values indicate that the spin delocalization effect is dominant in the N-group transfer reactions. Ru-⁴⁰ and Cu-based¹³⁹ aziridination and amination catalysts behave similarly; the relative reaction rates were relatively insensitive to substituent effects. Such behavior is indicative of a two-step reaction mechanism involving radical intermediates.

3.4 Allylic Amination

Table 3.2. Allylic amination of olefinic substrates.

Entry	Substrate	Product	Yield (%) ^a
1			38 ^d (1:0 E:Z)
2			12 ^b 7(9) ^c 17(19) ^d
3			77 ^b 29 ^c 43 ^d
4			52 ^b 15(15) ^c (38) ^d
5			(17) ^d
6		---	0 ^d

^a Yields were determined by GC/MS (¹H NMR). Isomeric ratio determined by integration of peaks in GC trace. ^b Reaction with specified substrate and **3.2** (100 mol%) and AdN₃ at 23°C for 12 h. ^c Reaction with specified substrate and **3.2** (20 mol%) and AdN₃ at 23°C for 12 h. ^d Reaction with specified substrate and **3.2** (20 mol%) and AdN₃ at 60°C for 12 h.

Next, the reactivity of a series of olefins with **3.2** and 1-azidoadamantane was investigated (Table 3.2) in order to determine the preference for aziridination over allylic C–H bond amination. Reaction of **3.2** with *cis*-β-methylstyrene (Table 3.2, entry 1) resulted in the

exclusive formation of *N*-cinnamyladamantan-1-amine with complete isomerization to the *trans* olefin. Cyclic alkenes similarly resulted in allylic amination products in comparatively poorer yields (entry 2, 7% at 23 °C, 17% at 60 °C). In fact, the stoichiometric reaction of **3.2** with 1 equivalent of 1-azidoadamantane in cyclohexene resulted in only 12% of the allylic amine. While some azide remained unconsumed, a significant amount of radically coupled bicyclohexenyl product was formed (as determined by GC/MS).

Interestingly, exposure of **3.2** and 1-azidoadamantane to linear, non-styrenyl terminal olefins resulted in exclusive formation of the linear allylic amine products (Table 3.2, entry 3, 4, and 6) as a mixture of *cis* and *trans* isomers. Stoichiometric application of catalyst **3.2** to 1-azidoadamantane at room temperature in excess 1-hexene resulted in the formation of the allylic amine *N*-adamantyl-*N*-hex-2-enylamine in 77% yield, with the remaining mass balance belonging to 1-aminoadamantane and 1,2-diadamantyldiazene. Lowering the catalyst loading (20 mol%) and extending the reaction time to 24 hours resulted in only a slight increase in product formation (29%) and a significant portion of unreacted azide remains (64%). As the reaction temperature is increased, product dissociation from the Fe center is encouraged, allowing for catalyst turnover and increased yields (29% at 25 °C versus 43% at 60 °C) but without reaching full conversion. At elevated temperatures (100 °C), the azide is completely consumed, yet the yield of the desired *N*-adamantyl-*N*-hex-2-enylamine is diminished. We suspect that free nitrene forms via thermal decomposition of 1-azidoadamantane under these conditions, generating significant amounts of diazene and 1-aminoadamantane. Additionally, several new products corresponding to *N*-group transfer to 1-hexene appear in the GC/MS trace at this temperature.

138. Díaz-Requejo, M. M.; Pérez, P. J.; Brookhart, M.; Templeton, J. *Organometallics* **1997**, *16*, 4399.

Importantly, the linear allylic amine is not formed to any extent in the absence of catalyst **3.2**, regardless of the reaction temperature.

Recently developed C–H amination protocols^{26,140,141} have highlighted the ability to run intermolecular reactions with limiting amounts of the C–H bond substrate. As such, we were interested in determining the effect of diluting the olefin substrate with a chemically inert solvent. As expected, the highest TON (2.3) occurred when the reaction was conducted in 1-hexene without dilution. Addition of benzene to the reaction mixture (aryl C–H bonds are inactive) significantly hampered catalysis [1.3 TON (50% v/v 1-hexene/benzene); 0.9 TON (25% v/v); 0.6 TON (10% v/v); 0.3 TON (5% v/v)]. This trend can be attributed to competitive amination of the secondary C–H bonds of the adamantyl groups of **3.2** upon dilution of the substrate with benzene (see Scheme 3.2 above).

Under optimized conditions, we explored the reactivity of a terminal, linear diene (entry 4). Again, primary amination products were obtained in moderate yield favoring the *trans* olefin isomer. Diamine formation was not observed due to the large excess of diene substrate. Exposure of **3.2** and 1-azidoadamantane to 2,3-dimethylbutene (entry 5), a substrate with two chemically distinct allylic C–H bonds, gave exclusive C–N bond formation of the less hindered primary carbon. No reaction is observed with substrates lacking allylic C–H bonds (entry 6).

While the method has synthetic limitations, the interesting chemo- and regioselectivity of linear allylic amination inspired us to investigate the mechanism of this transformation. Typically, intermolecular transition metal-catalyzed allylic amination does not proceed with

139. Reed, S.; White, M. C. *J. Am. Chem. Soc.* **2008**, *130*, 3316.

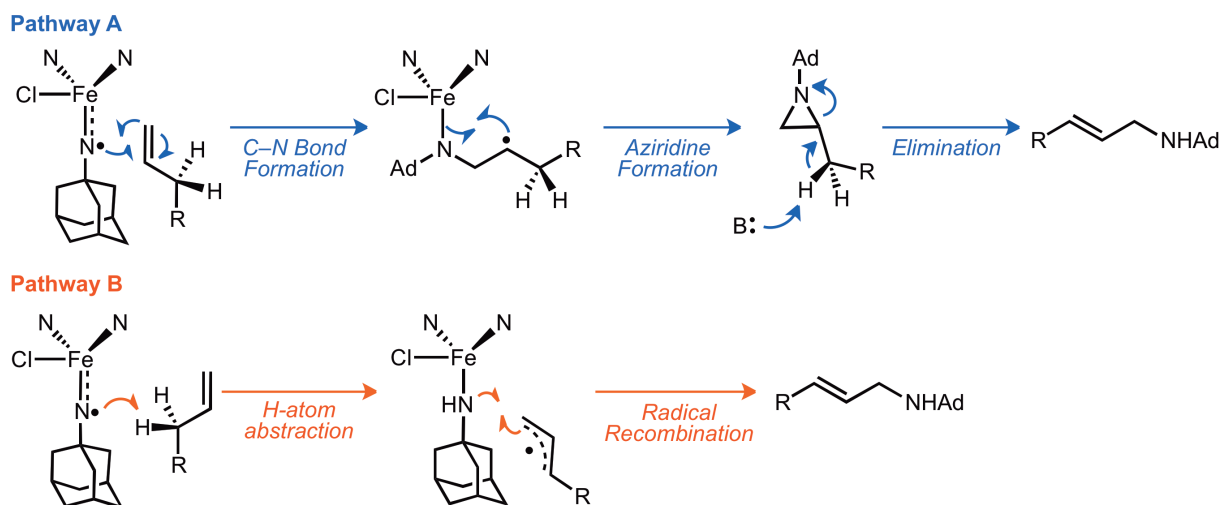


Figure 3.5 Possible mechanisms of allylic amination.

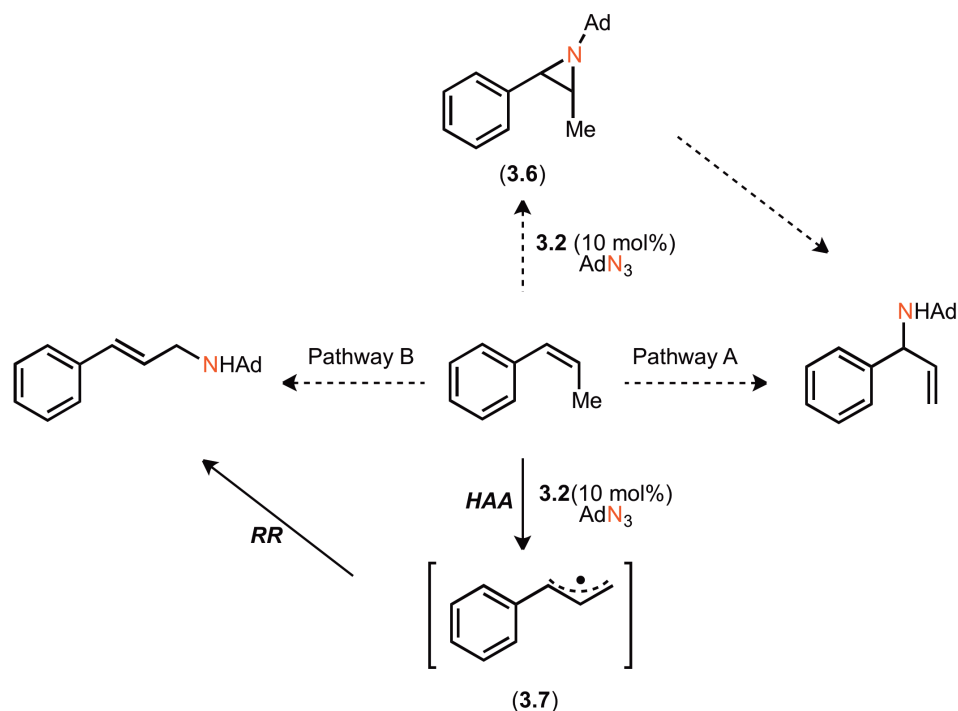
exclusive olefin transposition.^{9, 141} However, precedence for this transformation has been demonstrated previously using simple Fe^{II} and Fe^{III} halide salts¹⁴² and Fe phthalocyanine complexes¹⁴³ in the presence of phenylhydroxylamine. Recently, a hetero-bimetallic Pd and Cr catalytic protocol has also been developed to affect a similar amination reaction.¹⁴⁰

We have proposed two possible mechanistic pathways (Figure 3.5). Both mechanisms begin with formation of the reactive imido radical intermediate, consisting of three bulky adamantyl units (two on the dipyrrinato ligand, one on the imido *N*). The olefin then approaches the sterically crowded reaction center. As such, heightened reactivity is observed with the least bulky, mono-substituted olefin substrates (Table 3.2, entries 3 and 4). The bulkier 1,1- and 1,2-disubstituted olefins undergo allylic amination in reduced yields. In pathway A (Figure 3.5), approach of the olefin induces C–N bond formation at the primary carbon and homolytic cleavage of the π -bond. Next, the carbon radical rapidly recombines with the Fe-bound amide to

140. (a) Liang, C.; Robert-Peillard, F.; Fruit, C.; Müller, P.; Dodd, R. H.; Dauban, P. *Angew. Chem., Int. Ed.* **2006**, *45*, 4641. (b) Liang, C.; Collet, F.; Robert-Peillard, F.; Müller, P.; Dodd, R. H.; Dauban, P. *J. Am. Chem. Soc.* **2008**, *130*, 343.

141. Srivastava, R. S.; Nicholas, K. M. *Tetrahedron Lett.* **1994**, *35*, 8739.

generate an aziridine product. Finally, under the reaction conditions, the aziridine is ring opened to the primary allylamine through either a heterolytic (as drawn) or homolytic pathway. In pathway B, the Fe-imido intermediate abstracts an H-atom from the olefin substrate to generate an allylic radical, followed by radical recombination at the terminal carbon.



Scheme 3.4. Mechanistic probe of allylic amination reaction. Product analysis of reaction with *cis*- β -methylstyrene elucidates reaction mechanism proceeding through H-atom abstraction (HAA)/radical rebound (RR).

Analysis of the reaction with *cis*- β -methylstyrene was used to distinguish between pathways A and B. If pathway A were operative, initial aziridination would generate 1-adamantyl-2-methyl-3-phenylaziridine **3.6** (Scheme 3.4). *In situ* aziridine ring opening would then install the amino group at the benzylic carbon. If pathway B were operative, radical recombination would occur regioselectively at the less-hindered terminal position of the unsymmetrical allylic radical **3.7** (Scheme 3.4) to generate *N*-cinnamyladamantan-1-amine. As discussed earlier, the linear allylic amine is the only product of the reaction, suggesting that

pathway B is operative. This is an appealing mechanistic possibility, as it correlates well with our proposed mechanism for the benzylic amination of toluenes.

3.5 Conclusion

In line with previous studies of this system, we have determined that one-electron reaction pathways dominate intermolecular *N*-group transfer chemistry when mediated by the dipyrinato ferrous complexes. As such, an innate preference for amination over aziridination has been established for a range of allylic C–H bond containing substrates. We attribute the extremely high levels of chemoselectivity to the high-spin electronic configuration of the reactive imido radical intermediate **3.3**. Further, the steric demands of our ligand coupled with the bulky adamantyl imido fragment enforce regioselective amination at the terminal position of linear α -olefins. The preservation of unsaturation following imido transfer furnishes products that are amenable to subsequent functionalization. In this manner, the iron dipyrinato platform could ultimately provide access to value-enhanced, 1,2,3-functionalized products from cheap, readily-available olefinic feedstocks.

3.6 Experimental Methods

3.6.1 General Considerations

All manipulations of metal complexes were carried out in the absence of water and dioxygen using standard Schlenk techniques, or in an MBraun inert atmosphere drybox under a dinitrogen atmosphere. Ligand, ligand precursor syntheses, and substrate syntheses were carried out in air, except where noted. All glassware was oven dried for a minimum of 1 h and cooled in an evacuated antechamber prior to use in the drybox. Benzene, diethyl ether, *n*-hexane, and tetrahydrofuran were dried and deoxygenated on a Glass Contour System (SG Water USA,

Nashua, NH) and stored over 4 Å molecular sieves (Strem) prior to use. Chloroform-*d* was purchased from Cambridge Isotope Labs and used as received. Benzene-*d*₆ was purchased from Cambridge Isotope Labs and was degassed and stored over 4Å molecular sieves prior to use. All reagents, unless otherwise specified, were purchased from Aldrich and used as received. Substrates from Table 3.2 were distilled from CaH₂ and deoxygenated prior to use in the amination reactions. Celite® 545 (J. T. Baker) was dried in a Schlenk flask for 24 h under dynamic vacuum while heating to at least 150 °C prior to use in a drybox. Silica gel 32-63 μ (AIC, Framingham, MA) was used as received.

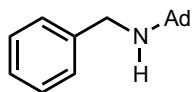
3.6.2 Characterization and Physical Measurements

¹H, ¹³C, and were recorded on Varian Mercury 400 MHz or Varian Unity/Inova 500 MHz spectrometers. ¹H and ¹³C{¹H} NMR chemical shifts are reported relative to SiMe₄ using the chemical shift of residual solvent peaks as reference. Infrared (FTIR) spectra were recorded on a Varian 1000 Scimitar FT-IR spectrophotometer referenced to a polystyrene standard. Gas chromatography/mass spectrometry (GC/MS) was performed on a Shimadzu GCMS–QP2010S. Elemental analyses were carried out by Complete Analysis Laboratories, Inc. (Parsippany, NJ).

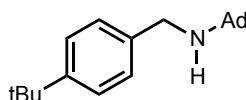
3.6.3 Catalysis Experiments and Characterization Data

General Procedure for Catalytic Amination and Aziridination Reactions. Under an inert N₂ atmosphere, 1-azidoadamantane (60.9 mg, 0.28 mmol, 10 equiv.) was added to a stirring solution of (^{Ad}L_{Cl₂)FeCl(OEt₂) (**3.1**) (20 mg, 0.028 mmol, 1 equiv.) or (^{tBu}L_{Cl₂)FeCl(OEt₂) (**3.2**) (16 mg, 0.028 mmol, 1 equiv.) in 1 mL of substrate in a 20 mL scintillation vial. The resultant inky, dark red solution was stirred for 12 hours at 25 °C. The dark mixture was flash chromatographed through a short pipette of triethylamine-treated silica gel (10:1 hexanes:EtOAc) to yield a}}

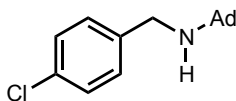
brightly colored solution. The solvent was removed *in vacuo* to yield pure amine or aziridine product. The yields were determined by ^1H NMR *via* integration against ferrocene, averaging over three runs for each substrate. GC/MS yields for allylic amination reactions were also obtained after obtaining a calibration curve for the desired allylic amine products.



***N*-benzyladamantan-1-amine**¹⁴⁴

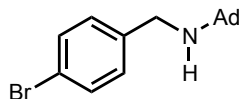


***N*-(4-(*tert*-butyl)benzyl)adamantan-1-amine:** ^1H NMR (500 MHz, CDCl_3) δ /ppm 7.34 (d, $J = 8.3$ Hz, 2H), 7.29 (d, $J = 8.3$ Hz, 2H), 3.73 (s, 3H), 2.10 (m, 3H), 1.77–1.59 (m, 12H), 1.30 (m, 9H). $^{13}\text{C}\{^1\text{H}\}$ NMR (100 MHz, CDCl_3) δ : 149.6, 138.3, 128.0, 125.3, 51.1, 44.7, 42.7, 36.7, 34.4, 31.4, 29.6. **IR** (thin film) $n_{\text{max}} = 2966, 2908, 2852, 1718, 1516, 1454, 1362, 1311, 1265, 1136, 1097$ cm^{-1} . **HRMS** (ESI⁺) m/z . Calc. 298.2564 [$\text{C}_{21}\text{H}_{31}\text{N}+\text{H}$]⁺, Found 298.2571 [$\text{M}+\text{H}$]⁺.

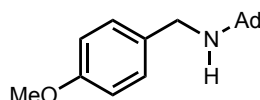


***N*-(4-chlorobenzyl)adamantan-1-amine:** ^1H NMR (500 MHz, CDCl_3) δ : 7.32–7.21 (m, 4H), 3.72 (s, 3H), 2.11–2.05 (m, 3H), 1.71–1.56 (m, 12H). $^{13}\text{C}\{^1\text{H}\}$ NMR (125 MHz, CDCl_3) δ : 140.0, 132.3, 129.6, 128.4, 51.0, 44.4, 42.7, 36.6, 31.4, 29.7. **IR** (thin film) $n_{\text{max}} = 2931, 2852, 1723, 1493, 1451, 1359, 1312, 1265, 1137, 1097$. **HRMS** (ESI⁺) m/z . Calc. 276.1549 [$\text{C}_{17}\text{H}_{22}\text{ClN}+\text{H}$]⁺, Found 276.1544 [$\text{M}+\text{H}$]⁺.

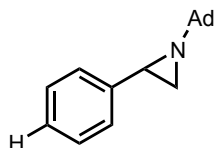
143. For physical and spectroscopic characterization data, see: Calet, S.; Urso, F.; Alper, H. *J. Am. Chem. Soc.* **1989**, *111*, 931.



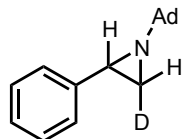
N-(4-bromobenzyl)adamantan-1-amine: $^1\text{H NMR}$ (500 MHz, CDCl_3) δ : 7.30 (d, $J = 8.6$ Hz, 2H), 6.84 (d, $J = 8.6$ Hz, 2H), 3.76 (s, 3H), 3.71 (s, 3H), 2.08 (m, 3H), 1.75 (m, 6H), 1.65 (q, $J = 12.1$ Hz, 6H). $^{13}\text{C}\{^1\text{H}\}$ NMR (100 MHz, CDCl_3) δ : 158.7, 131.8, 130.0, 113.8, 55.2, 53.4, 44.3, 42.0, 36.5, 31.6, 29.5. **IR** (thin film) $n_{\text{max}} = 2960, 2932, 2912, 1720, 1613, 1513, 1458, 1252, 1248, 1137, 1037$ cm^{-1} . **HRMS** (ESI $^+$) m/z Calc. 272.2014 $[\text{C}_{18}\text{H}_{25}\text{NO}+\text{H}]^+$, Found 272.2005 $[\text{M}+\text{H}]^+$.



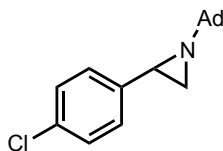
N-(4-methoxybenzyl)adamantan-1-amine: $^1\text{H NMR}$ (400 MHz, CDCl_3) δ : 7.42 (d, $J = 8.4$ Hz, 2H), 7.23 (d, $J = 8.4$ Hz, 2H), 3.71 (s, 2H), 2.09 (m, 3H), 1.73–1.63 (m, 12H). $^{13}\text{C}\{^1\text{H}\}$ NMR (100 MHz, CDCl_3) δ/ppm 140.8, 131.6, 130.2, 120.7, 53.7, 44.7, 43.0, 36.8, 29.9. **IR** (thin film) $n_{\text{max}} = 2911, 2851, 1702, 1591, 1488, 1450, 1358, 1098, 1070$ cm^{-1} . **HRMS** (ESI $^+$) m/z Calc. 320.0954 $[\text{C}_{16}\text{H}_{22}\text{NBr}+\text{H}]^+$, Found 320.0968 $[\text{M}+\text{H}]^+$.



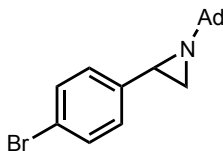
1-(adamantan-1-yl)-2-phenylaziridine: $^1\text{H NMR}$ (600 MHz, CDCl_3) δ/ppm 7.34–7.30 (m, 2 H), 7.28 (t, $J = 7.6$ Hz, 2 H), 7.22 - 7.18 (m, 1 H), 2.81 (dd, $J = 3.2, 6.2$ Hz, 1 H), 2.10 (br. s., 3 H), 2.07 (d, $J = 6.2$ Hz, 1 H), 1.72–1.66 (m, 3 H), 1.64 (m, 6 H), 1.62 (d, $J = 3.2$ Hz, 1 H). $^{13}\text{C}\{^1\text{H}\}$ NMR (125 MHz, CDCl_3) δ/ppm 141.5, 128.1, 126.7, 126.5, 52.8, 40.4, 39.8, 31.7, 29.5, 28.4. **HRMS** (ESI $^+$) m/z Calc. 254.1909 $[\text{C}_{18}\text{H}_{23}\text{N}+\text{H}]^+$, Found 254.1940 $[\text{M}+\text{H}]^+$.



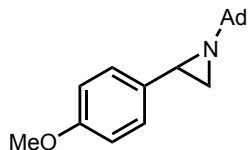
1-(adamantan-1-yl)-3-deutero-2-phenylaziridine: ^1H NMR (500 MHz, CDCl_3) δ : 7.33–7.25 (m, 4 H), 7.23 - 7.17 (m, 1 H), 2.81 (d, $J = 6.4$ Hz, 1 H), 2.09 (br. s., 3 H), 2.06 (d, $J = 6.4$ Hz, 1 H), 1.72–1.66 (m, 3 H), 1.62 (br. s., 6 H).



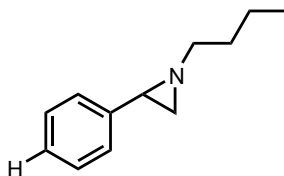
1-(adamantan-1-yl)-2-(4-chlorophenyl)aziridine: ^1H NMR (500 MHz, CDCl_3) δ /ppm 7.24 (m, 4H), 2.76 (dd, $J = 6.3, 3.0$ Hz, 1H), 2.12–2.01 (m, 5H), 1.79–1.47 (m, 12H). $^{13}\text{C}\{^1\text{H}\}$ NMR (125 MHz, CDCl_3) δ /ppm 140.4, 132.3, 128.4, 128.2, 53.1, 40.6, 37.0, 34.9, 31.8, 29.7. IR (thin film) $\nu_{\text{max}} = 2955, 2852, 1722, 1492, 1456, 1356, 1311, 1265, 1136, 1076$ cm^{-1} . HRMS (ESI $^+$) m/z Calc. 288.1514 [$\text{C}_{18}\text{H}_{22}\text{NCl}+\text{H}$] $^+$, Found 288.1508 [$\text{M}+\text{H}$] $^+$.



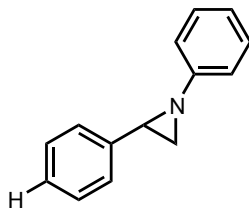
1-(adamantan-1-yl)-2-(4-bromophenyl)aziridine: ^1H NMR (500 MHz, CDCl_3) δ /ppm 7.38 (d, $J = 8.4$ Hz, 2H), 7.18 (d, $J = 8.5$ Hz, 2H), 2.74 (dd, $J = 6.4, 3.0$ Hz, 1H), 2.11–2.02 (m, 5H), 1.76–1.37 (m, 12H). $^{13}\text{C}\{^1\text{H}\}$ NMR (125 MHz, CDCl_3) δ /ppm 144.7, 140.9, 131.4, 128.6, 53.1, 45.7, 40.6, 37.0, 31.8, 29.7. IR (thin film) $\nu_{\text{max}} = 2910, 2899, 1488, 1450, 1358, 1289, 1136, 1012$ cm^{-1} . HRMS (ESI $^+$) m/z Calc. 332.1008 [$\text{C}_{18}\text{H}_{22}\text{NBr}+\text{H}$] $^+$, Found 332.1000 [$\text{M}+\text{H}$] $^+$.



1-(adamantan-1-yl)-2-(4-methoxyphenyl)aziridine: $^1\text{H NMR}$ (600 MHz, CDCl_3) δ 7.29 (d, $J = 8.6$ Hz, 2H), 6.89 (d, $J = 8.6$ Hz, 2H), 3.84 (s, 3H), 2.17–2.13 (m, 5H), 1.71–1.30 (m, 12H). $^{13}\text{C}\{^1\text{H}\}$ NMR (100 MHz, CDCl_3) δ /ppm 164.3, 131.4, 127.8, 113.7, 55.4, 52.8, 40.5, 37.0, 31.8, 29.9. IR (thin film) = 2959, 2913, 2855, 1613, 1513, 1300, 1248, 1036 cm^{-1} . HRMS (ESI $^+$) m/z Calc. 284.2009 [$\text{C}_{19}\text{H}_{25}\text{NO}+\text{H}$] $^+$, Found 284.2012 [$\text{M}+\text{H}$] $^+$.



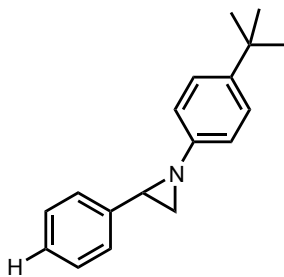
1-butyl-2-phenylaziridine¹⁴⁵



1,2-diphenylaziridine¹⁴⁶

144. For physical and spectroscopic characterization, see: Fantauzzi, S.; Gallo, E.; Caselli, A.; Piangiolino, C.; Ragaini, F.; Cenini, S. *Eur. J. Org. Chem.* **2007**, 36, 6053.

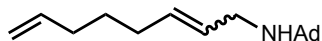
145. For physical and spectroscopic characterization, see: Chamchaang, W.; Pinhas, A. R. *J. Org. Chem.* **1990**, 55, 2943.



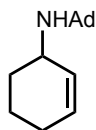
1-(4-(*tert*-butyl)phenyl)-2-phenylaziridine¹⁴⁵



***N*-(hex-2-en-1-yl)adamantan-1-amine:** ¹H NMR (600 MHz, C₆D₆) δ (mixture of *E* and *Z* isomers): 6.26–6.34 (m, 0.3 H), 6.12–6.21 (m, 0.7 H), 5.58–5.72 (m, 2 H), 3.46 (d, *J* = 7.0 Hz, 0.6 H), 3.30 (d, *J* = 7.0 Hz, 1.4 H), 2.07–2.14 (m, 6 H), 1.97–2.05 (m, 2 H), 1.84–1.90 (m, 3 H), 1.34–1.49 (m, 8 H), 0.87 - 0.93 (m, 3 H). ¹³C{**1H**} NMR (125 MHz, C₆D₆) δ (*Z*-olefin in parentheses): 137.7(135.2), 122.8(122.5), 57.3, 42.4, 36.7(37.2), 35.8, 34.7, 29.5, 22.4(22.7), 13.9. **HRMS** (ESI⁺) *m/z* Calc. 234.4017 [C₁₆H₂₇N+H]⁺, Found 234.4012 [M+H]⁺.

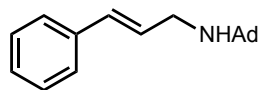


***N*-(octa-2,7-dien-1-yl)adamantan-1-amine:** ¹H NMR (600 MHz, C₆D₆) δ: 5.72 (ddt, *J* = 16.7, 9.9, 6.7 Hz, 2 H), 5.61–5.49 (m, 1 H), 5.03–4.90 (m, 2 H), 3.26 (d, *J* = 6.8 Hz, 0.3 H), 3.17 (d, *J* = 6.8 Hz, 1.7 H), 1.99–1.85 (m, 7 H), 1.62 (br. s, 6 H), 1.55–1.43 (m, 6 H), 1.38 (p, *J* = 7.5 Hz, 2 H). ¹³C{**1H**} NMR (125 MHz, C₆D₆) δ: 138.9, 131.5, 130.2, 114.8, 51.3, 43.1, 42.7, 36.9, 33.6, 32.2, 30.0, 29.0. **HRMS** (ESI⁺) *m/z* Calc. 260.4392 [C₁₈H₂₉N+H]⁺, Found 260.4388 [M+H]⁺.



***N*-(cyclohex-2-en-1-yl)adamantan-1-amine:** ¹H NMR (600 MHz, C₆D₆) δ: 6.21 (d, *J* = 10.0 Hz, 1 H), 5.81–5.87 (m, 1 H), 3.48–3.56 (m, 1 H), 2.32–2.45 (m, 2 H), 2.13 (br. s., 6 H), 1.90 (br. s., 5 H), 1.79–1.87 (m, 1 H), 1.68–1.77 (m, 1 H), 1.31–1.56 (m, 6 H). ¹³C{**1H**} NMR (125

MHz, C₆D₆) δ : 132.1, 126.8, 59.1, 49.2, 39.1, 36.2, 30.0, 29.3, 24.9, 21.1. **HRMS** (ESI⁺) m/z Calc. 234.4017 [C₁₅H₂₃N+H]⁺, Found 234.4018 [M+H]⁺.



N-cinnamyladamantan-1-amine: ¹H NMR (500 MHz, CDCl₃) δ /ppm 7.23–7.15 (m, 3H), 7.12 (d, J = 7.2 Hz, 2H), 6.48–6.41 (m, 1H), 6.29 (d, J = 13.0 Hz, 1H), 3.35 (d, J = 6.3 Hz, 1H), 1.97 (m, 3H), 1.64 (m, 6H), 1.55 (m, 6H). ¹³C{¹H} NMR (126 MHz, CDCl₃) δ /ppm 137.3, 128.7, 127.6, 126.6, 52.0, 43.2, 42.5, 36.8, 29.9. **HRMS** (ESI⁺) m/z Calc. 268.2065 [C₁₉H₂₅N+H]⁺, Found 268.2069 [M+H]⁺.

3.6.4 X-Ray Crystallographic Data

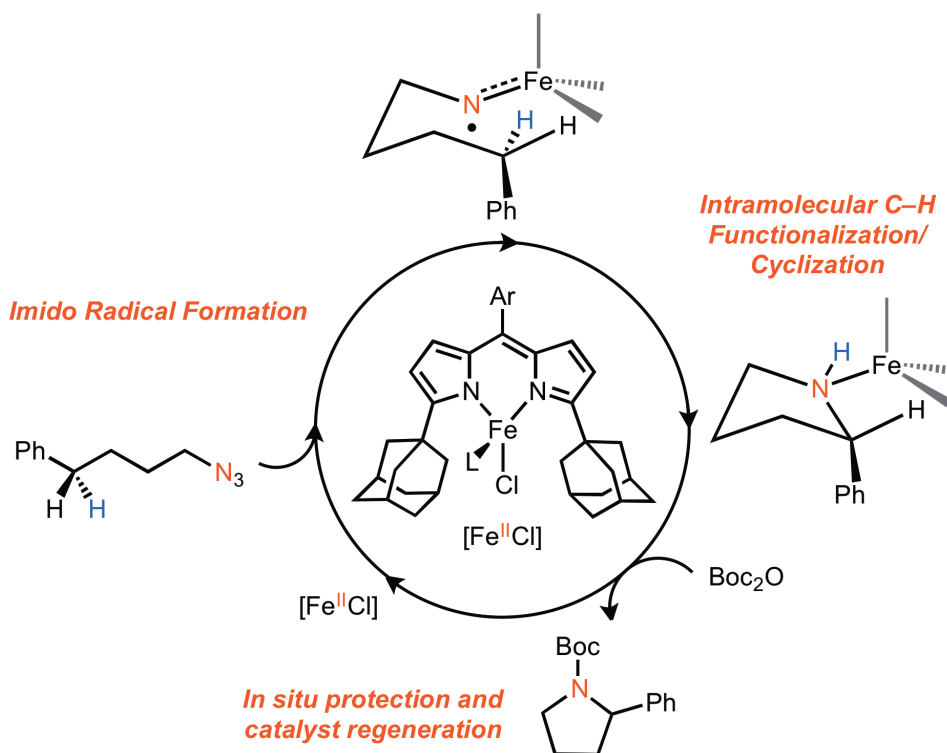
See section for 2.6.6 for equipment and software details.

(^tBu₃L)FeCl(NSO₂(H)(2-NO₂)-C₆H₄) (**3.4**). The structure was solved in the monoclinic space group $P2_1/c$ with 4 molecules per unit cell. There was one molecule of dichloromethane in the asymmetric unit. The incompleteness of the data set did not allow for anisotropic or refinement.

(^{Ad}L(NH₂))FeCl (**3.5**). The structure was solved in the orthorhombic space group $Pnma$ with 4 molecules per unit cell. There is half a molecule of toluene in the asymmetric unit. The adamantyl unit exhibited disorder which was modeled by addition of a second position for each ring.

Table 3.3. X-ray crystallographic experimental properties.

	(3.4)	(3.5)
Moiety Formula	C ₃₂ H ₃₈ ClFeN ₄ SO ₄ · CH ₂ Cl ₂	C ₃₆ H ₃₈ Cl ₃ FeN ₃ · C ₇ H ₈
FW	711.67	753.21
Crystal System	monoclinic	orthorhombic
Space Group (Z)	<i>P</i> 2 ₁ / <i>c</i> (4)	<i>P</i> nma (4)
a (Å)	10.6350(12)	13.3421(10)
b (Å)	19.827(2)	17.4976(13)
c (Å)	15.8327(19)	15.7561(11)
α (°)	90	90
β (°)	95.962(8)	90
γ (°)	90	90
Volume (Å ³)	3320.4(6)	3678.3(5)
Calc. ρ (mg/m ³)	1.4235	1.3705
μ (mm ⁻¹)	0.800	0.663
Crystal Size (mm)	0.24×0.18 ×0.12	0.42×0.31 ×0.22
Reflections	7026	33269
Completeness (to 2θ)		99.9% 26.27°
GOF on F ²	1.1164	0.969
R1, wR2 ^c	0.1481,	0.1264,
[I>2σ(I)]	0.4146	0.3445



Chapter 4: Complex *N*-Heterocycle Synthesis via Iron-Catalyzed, Direct C–H Bond Amination¹⁴⁷

4.1 Introduction

Saturated, cyclic amines (*N*-heterocycles) are important building blocks for the synthesis of biologically active natural products, pharmaceutical agents, and materials. Current strategies for constructing saturated *N*-heterocycles are heavily dependent on functional group exchange, leading to inefficient synthetic protocols with poor atom economy and waste generation. A streamlined synthetic approach to this product class would rely on a catalyst capable of the direct amination of aliphatic C–H bonds. An advantage of this method is its potential to harness saturated hydrocarbon feedstocks. Unfortunately, current C–H bond functionalization protocols

often require substrate preoxidation, directing groups, or strong chemical oxidants, which contribute to a lack of generality for this bond construction.^{79,148–150} Herein, we report an iron catalyst capable of functionalizing a broad range of aliphatic C–H bonds to form saturated, cyclic amine products.

A challenge to the development of a general and mild aliphatic C–H bond functionalization strategy is the unreactive nature of the substrates themselves. Saturated hydrocarbons are chemically inert due to the large C–H bond dissociation energy (93 to 105 kcal/mol) coupled with the energetic and spatial inaccessibility of the C–H bonding and antibonding orbitals. Nature provides a blueprint to overcome these obstacles. The reaction of dioxygen with heme iron in cytochrome P450 produces a strong oxidant consisting of an iron-oxygen multiple bond (iron-oxo).²⁸ The iron-oxo bond contains two electrons residing in Fe–O π^* orbitals [Fe(dxz,dyz)–O(px,py)], which result in a weakened Fe–O bond vector possessing radical character, thus rendering the entire unit a reactive functionality. As a consequence of this electronic configuration, the iron-oxo bond can activate substrate aliphatic C–H bonds via an H-atom abstraction mechanism and thereby circumvent the orbital spatial restrictions that hinder oxidative addition pathways. Subsequent substrate functionalization results from recombination of the organic radical generated in the activation step with the open-shell iron-hydroxyl to produce an alcohol product with concomitant reduction of the iron. Despite this 30-year-old

146. This chapter was adapted with permission from Hennessy, E. T.; Betley, T. A. *Science* **2013**, *340*, 591. Copyright 2013 AAAS.

147. Zalatan, D. N.; Du Bois, J. *Top. Curr. Chem.* **2010**, *292*, 347.

148. Ryabov, A. D. *Chem. Rev.* **1990**, *90*, 403.

149. Dick, A. R.; Sanford, M. S. *Tetrahedron* **2006**, *62*, 2439.

mechanistic precedent,³⁴ viable catalysts fashioned with these design principles are only now being discovered.

The direct functionalization of C–H bonds based on a strategy exemplified by cytochrome P450 would be transformative in converting ubiquitous C–H bonds into functional group handles and would circumvent the traditional synthetic requirement for functional group exchange.¹⁵¹ The electronic structure of the cytochrome P450 reactive iron-oxo intermediate can, in principle, be replicated with any metal-ligand multiple bond⁵⁰ and would constitute a general strategy for the conversion of unactivated C–H bonds into a variety of C–heteroatom bond products. Indeed, metal stabilized carbene and nitrene transfer has garnered considerable interest through the use of noble metal catalysts.^{22,40,141,152–154} Specifically, Fiori *et al.*²² and Liang *et al.*¹⁴¹ have developed a class of C–H amination Rh₂-dicarboxylate catalysts capable of generating cyclic carbamate, guanidine, and sulfamide products. Recently, this methodology has been extended to include aryl azides to produce indolines via an intramolecular sp³ C–H amination, as reported by Nguyen *et al.*¹⁵⁴ In contrast, late, first-row transition metal complexes are potentially ideal catalyst candidates but have been less explored. Their high d-electron count and compressed ligand fields (compared with their second- and third-row analogs) favor population of metal-ligand antibonding orbitals leading to destabilization and reactivity akin to the cytochrome P450 iron-oxo intermediate.^{47,49,62,66,98,110,134,155,156} With these design principles in mind,

150. King, A. O.; Yasuda, N. *Top. Organomet. Chem.* **2004**, *6*, 205.

151. Davies, H. M. L.; Manning, J. R. *Nature* **2008**, *451*, 417.

152. Driver, T. G. *Org. Biomol. Chem.* **2010**, *8*, 3831.

153. Nguyen, Q.; Sun, K.; Driver, T. G. *J. Am. Chem. Soc.* **2012**, *134*, 7262.

154. Groves, J. T. *J. Inorg. Biochem.* **2006**, *100*, 434.

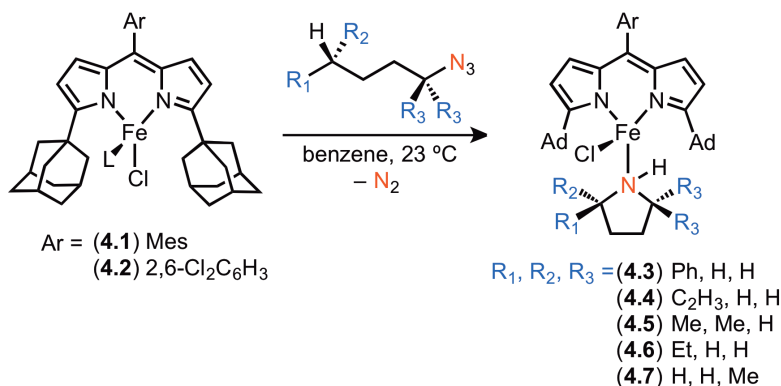
we describe an iron- dipyrinato catalyst that can selectively aminate sp^3 C–H bonds. Herein, we present the application of this catalyst toward the production of complex cyclic amine structures from simple linear aliphatic substrates requiring a single functionality, an azide.

In Chapter 2 we reported intermolecular amination of benzylic C–H bonds with aryl and alkyl azides using the ferrous dipyrinato complex (^RL)FeCl(solv) (R = 2,4,6-Ph₃C₆H₂, Ad with meso-Ar = mesityl (**4.1**), 2,6-Cl₂C₆H₃ (**4.2**); solv = Et₂O, THF). Isolation and characterization of the reactive intermediate elucidated the electronic structure of the high-spin, iron-bound imido radical, wherein a high-spin Fe(III) ($S = 5/2$) is antiferromagnetically coupled to the imido radical ($S = -1/2$) to give a high-spin ground state. This electronic structure places substantial radical character on both the Fe–N σ and π bond vectors, facilitating both radical H-atom abstraction and radical recombination pathways to proceed. Furthermore, the amination catalytic cycle remains in the quintet spin state ($S = 2$), making each step of the catalytic cycle spin-allowed. We envisioned that the intramolecular extension of this reactivity profile to linear, aliphatic azide substrates would generate cyclic amine products in a single operation.

4.2 Stoichiometric Intramolecular C–H Bond Amination and Cyclization

To test the viability of catalyst 1 for intramolecular C–H amination, we subjected a variety of substituted aliphatic azides to complex 1 (Scheme 4.1). Exposure of 1-azido-4-phenylbutane to 1 at room temperature in benzene resulted in consumption of the azide, as ascertained by the disappearance of the azide stretch in the infrared spectrum, and afforded a new paramagnetically shifted ^1H NMR spectrum. Crystallization occurred from a concentrated hexanes solution of the product at 23°C to yield crystals in which 2-phenylpyrrolidine was bound to the ($^{\text{Ad}}\text{L}$)FeCl complex (**4.3**, Figure 4.1a). Similarly, treatment of 1-azido-5-hexene with **4.1**

155. Nguyen, Q.; Nguyen, T.; Driver, T. G. *J. Am. Chem. Soc.* **2013**, *135*, 620.



Scheme 4.1. Stoichiometric C–H functionalization/cyclization reaction. Reaction of complexes **4.1** and **4.2** with linear alkyl azides to generate Fe-bound pyrrolidine products.

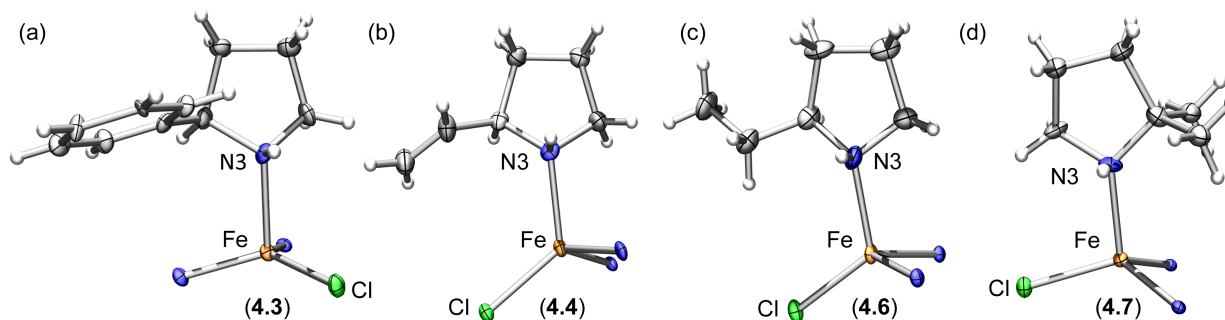


Figure 4.1. Solid-state core structures of iron-bound pyrrolidine products. (a) Fe-bound 2-phenylpyrrolidine **4.3** from reaction of **4.1** with 1-azido-4-phenylbutane; (b) Fe-bound 2-vinylpyrrolidine **4.4** from reaction of **4.1** with 1-azido-5-hexene; (c) Fe-bound 2-ethylpyrrolidine **4.6** from reaction of **4.1** with 1-azido-hexane. (d) Fe-bound 2,2-dimethylpyrrolidine **4.7** from reaction of **4.2** with 2-azido-2-methylpentane. Thermal ellipsoids set at the 50% probability level (Fe, orange; C, gray; H, white; N, blue; Cl, green).

afforded the cyclized product 2-vinylpyrrolidine as an iron-bound adduct (**4.4**, Figure 4.1b). In addition to allylic and benzylic C–H bonds, less reactive tertiary C–H bonds could be similarly functionalized. The reaction of 1-azido-5-methylpentane and **1** under standard conditions gave the 2,2-dimethylpyrrolidine iron-bound product (**4.5**). Gratifyingly, even secondary aliphatic C–H bonds could be functionalized through this method. Addition of 1-azidohexane to **1** resulted in the rapid consumption of the azide to afford the 2-ethylpyrrolidine complex (**4.6**, Figure 4.1c). In an attempt to activate the primary C–H bond of an aliphatic azide substrate, 1-azidobutane was exposed to **1**. However, the only products observed in this transformation were linear *n*-butylamine and *n*-butylimine. To eliminate the potential for imine formation, through a process involving intermolecular C–H bond activation or β -hydride elimination, the gem-dimethyl

substrate 2-azido-2-methylpentane was prepared and subjected to 1 at room temperature for 6 hours to afford the cyclized 2,2-dimethylpyrrolidine complex (**4.7**, Figure 4.1d) in quantitative yield. The presence of the two α -Me substituents may facilitate the C–H bond functionalization and cyclization process through the Thorpe-Ingold effect.¹⁵⁷

4.3 Catalytic Pyrrolidine Formation

With a reliable protocol for the stoichiometric C–H functionalization of aliphatic azides in hand, we attempted to render the reaction catalytic (5 to 10 equiv. of azide per 1 equiv. of **4.1** or **4.2**). Unfortunately, examination of the cyclization reaction under catalytic conditions did not markedly increase the yield of the resultant free heterocyclic product. We attribute the lack of catalyst turnover to product inhibition, in which a tight Lewis acid/base pair between the dipyrinato iron and the heterocyclic nitrogen atom is formed (Figure 4.1). To overcome product inhibition, we performed the cyclization reaction in the presence of an *in situ* protection reagent, which would reduce the nucleophilicity of the product *N*-heterocycle while avoiding the generation of by-products that might retard or prevent catalysis. Accordingly, treatment of a solution of 1-azido-4-phenylbutane and 9-fluorenylmethyl *N*-succinimidyl carbonate (Fmoc-OSuc; a base-cleavable protecting group) in benzene at room temperature with a stoichiometric amount of **4.2** for 12 hours afforded the Fmoc-protected 2-phenylpyrrolidine in 98% yield (Table 4.1, entry 1). Similarly, addition of an equivalent of 2 to a solution of 1-azido-4-phenylbutane and di-*tert*-butyl dicarbonate (Boc₂O; an acid-cleavable protecting group) under similar reaction conditions afforded the *tert*-butyloxycarbonyl (Boc)-protected product 1-Boc-2-phenylpyrrolidine in 93% yield. As catalyst loading was decreased, the *N*-hydroxysuccinimide

156. Beesley, R. M.; Ingold, C. K.; Thorpe, J. F. *J. Chem. Soc. Trans.* **1915**, 107, 1080.

Table 4.1. Catalytic pyrrolidine formation.

Entry	Azide	Pyrrolidine	Yield (%) ^a	Entry	Azide	Pyrrolidine	Yield (%) ^a
1			98 ^b (PG = Fmoc) 93 ^b 57 ^{cd} (PG = Boc)	10			66
2			72 ^{cd}	11			70
3			60 ^d 49 ^{cd}	12			98
4			19 ^{cd}	13			75 ^c 93% ee
5			17 ^{cd}	14			84
6			11	15			67
7			47	16			73
8			68 ^c	17			58
9			60	18			14 (PG = Boc) 78 ^b (PG = Fmoc)

^a ¹H NMR yield using ferrocene or trimethoxybenzene as an internal standard unless otherwise noted. ^b Stoichiometric reaction with one equivalent of catalyst **4.2** at 23 °C. ^c Isolated yield. ^d 10 mol% catalyst **4.2**.

by-product of Fmoc-protection led to catalyst decomposition through ligand protonation and limited the reaction to a single turnover. Fortunately, the by-products of protection with Boc₂O (tBuOH, CO₂) did not inhibit catalyst turnover, permitting the heterocycle to be synthesized with

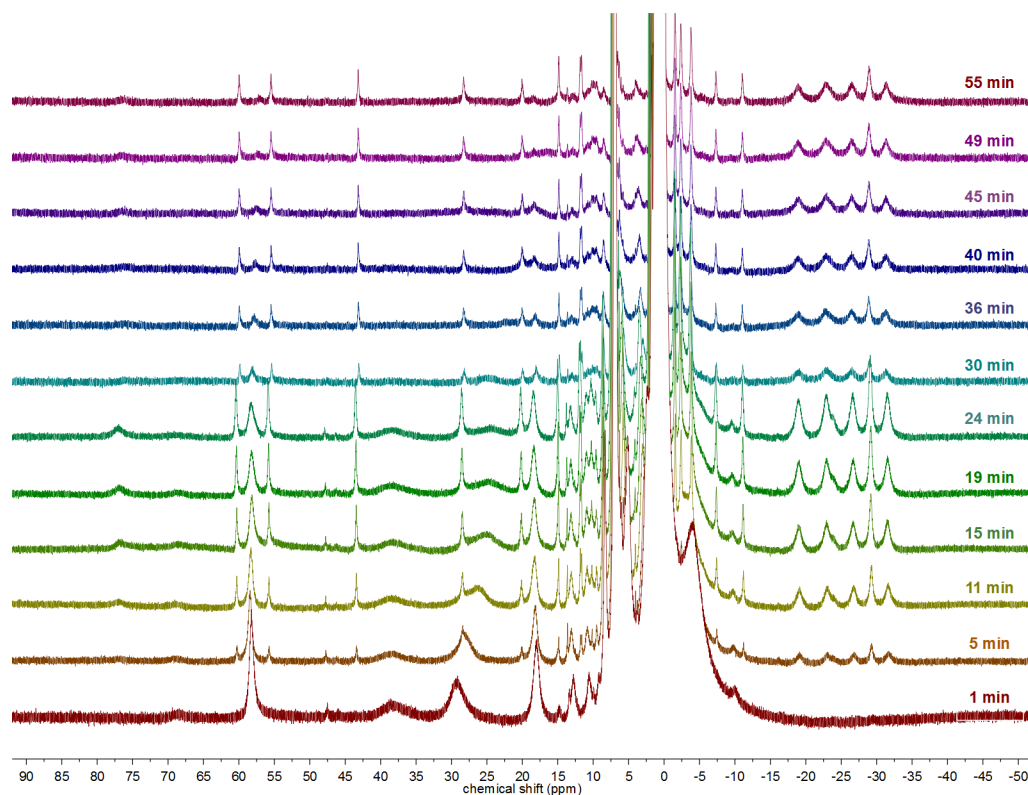


Figure 4.2. Reaction time-course for 1° C–H bond functionalization. ^1H NMRs at various time points of stoichiometric reaction of **4.1** with 2-azido-2-methylpentane going to Fe-bound 2,2-dimethylpyrrolidine. catalytic amounts of **4.2** (chosen to eliminate benzylic C–H bonds from catalyst meso-aryl substituent).

We investigated application of catalytic quantities of **4.2** (Table 4.1) to the established *in situ* protection protocol for C–H functionalization and cyclization. Exposure of substrates containing allylic, benzylic, or tertiary C–H bonds to **4.2** (10 mol%) provided the corresponding Boc-protected pyrrolidine in good isolated yield (49 to 72%, entries 1 to 3). Catalytic functionalization of a secondary C–H bond was also possible, affording 1-Boc-2-ethylpyrrolidine in a lower isolated yield (19%, entry 4). The formation of undesired linear side products is competitive with cyclization at the strong secondary C–H bond and contributes to the low yield. Even a primary C–H bond in 2-azido-2-methylpentane could be functionalized to give 1-Boc-2,2-dimethylpyrrolidine in 17% isolated yield (entry 5), with a mass balance of unreacted azide. Unlike the previous example, we hypothesize that the diminished yield reflects the ability of the

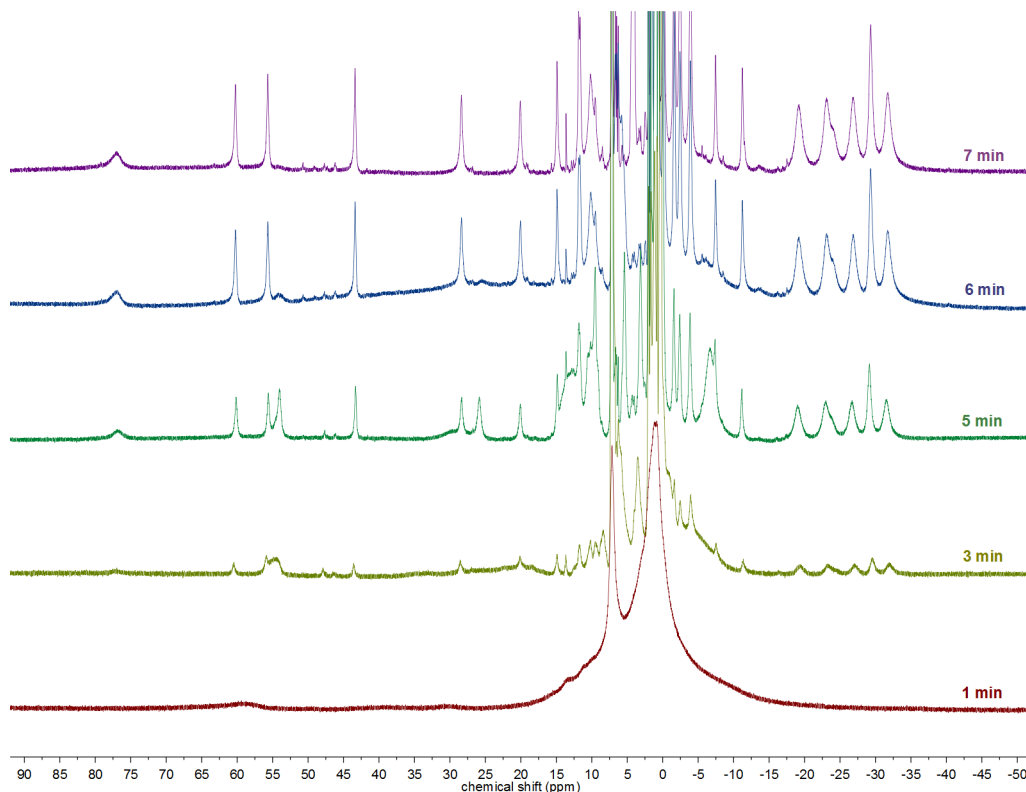
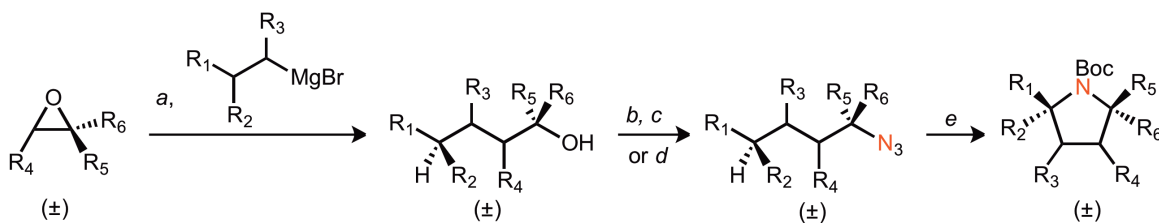


Figure 4.3. Reaction time-course for 3° C–H bond functionalization. ^1H NMRs at various time points of stoichiometric reaction of **4.1** with 1-azido-5-methylpentane going to Fe-bound 2,2-dimethylpyrrolidine.

tertiary azide to access the iron catalyst. In situ ^1H NMR monitoring of the stoichiometric reaction between **4.1** and 2-azido-2-methylpentane to generate the 2,2-dimethylpyrrolidine iron adduct requires 55 min at room temperature (with no detectable buildup of an intermediate), whereas conversion of 1-azido-5-methylpentane to the same product is complete in 5 min (Figures 4.2 and 4.3). The long reaction time to aminate the primary C–H bond likely has an adverse effect on the overall catalysis, as competitive catalyst inactivation occurs on a similar time scale. We then expanded the substrate scope to include heteroatom-containing functional groups. Exposure of ethyl-5-azidopentanoate to **4.2** under standard the α -position of the azide with gem-dimethyl substituents led to productive catalytic conditions resulted in only linear primary amine and imine products. Again, blocking the α position of the azide with gem-



Scheme 4.2. Synthesis of linear azide precursors. Highly substituted pyrrolidines generated from simple, three-step reaction sequence. Reagents and conditions: (a) Lithium chloride, 0.1 equiv., copper(II) chloride, 0.1 equiv., THF, $-40\text{ }^{\circ}\text{C}$, 3 h; (b) Tosyl chloride, 2.0 equiv., pyridine, 1.9 equiv., DCM, $0\text{ }^{\circ}\text{C}$, 12 h; (c) Sodium azide, 5.0 equiv., DMSO, $23\text{ }^{\circ}\text{C}$, 48 h; (d) Azidotrimethylsilyane, 1.5 equiv., $\text{BF}_3\cdot\text{OEt}_2$, 1.5 equiv., benzene, $23\text{ }^{\circ}\text{C}$, 12 h; (e) 5, 20 mol%, Boc_2O , 1 equiv., benzene, $60\text{ }^{\circ}\text{C}$, 12 h. See experimental methods for reaction yields.

dimethyl substituents led to productive cyclization (entry 6), albeit in the low yield characteristic of tertiary azide substrates. Introduction of heteroatoms between the reactive functionalities allowed for the formation of 1-Boc-2-phenyloxazolidine in 47% yield (entry 7). The reaction is also tolerant of siloxy groups, as shown in the formation of 1-Boc-2-vinyl-4-trimethylsiloxypyrrolidine in 68% isolated yield (entry 8).

Next, we explored the synthesis of highly substituted pyrrolidine products using substrates accessible via cuprate-assisted epoxide opening¹⁵⁸ followed by azide formation (Scheme 4.2). The use of commercially available epoxide and alkyl halide building blocks permits virtually any substitution pattern to be programmed into the ensuing heterocyclic product. After $\text{Li}_2[\text{CuCl}_4]$ promoted epoxide opening, the resultant primary or secondary alcohols were tosylated and displaced with sodium azide to provide the desired cyclization precursor. Alternatively, tertiary and benzylic alcohols were directly converted to the corresponding azide by exposure to trimethylsilylazide and boron trifluoride diethyl etherate.¹⁵⁹ Allylic, tertiary, and secondary C–H bond substrates available through either reaction sequence underwent facile C–H functionalization and cyclization (Table 4.1, entries 9 to 17, 58 to 98% yield). Notably, this

157. Drouin, J.; Leyendecker, F.; Conia, J. M. *Tetrahedron* **1980**, *36*, 1195.

158. Mukaiyama, T.; Kuroda, K.; Maruyama, Y. *Heterocycles* **2010**, *80*, 63.

method provides access to an all-carbon spiro-center (entry 15, 67%). Functionalization of primary C–H bonds required stoichiometric catalyst loading (entry 18, 78% yield), for reasons stated above. Use of (*R*)-2-phenyl-5-azidopentane (95% ee) in the catalytic transformation resulted in (*S*)-2-methyl-2-phenylpyrrolidine with retention of configuration (entry 13, 75%, 93% ee). Application of stoichiometric quantities of catalyst **4.1** to the reaction gave the corresponding (*S*)-2-methyl-2-phenylpyrrolidine iron-bound adduct **4.8** whose absolute stereochemistry was verified by x-ray diffraction (Figure 4.4).

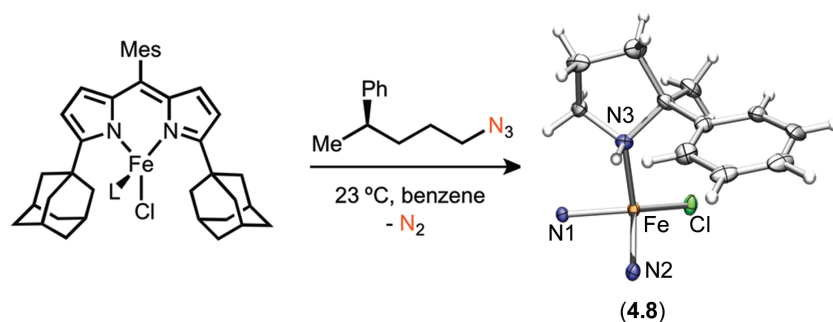


Figure 4.4. Solid state core structure of Fe-bound chiral pyrrolidine. Stereoretention upon cyclization was verified by single crystal X-ray analysis of **4.8**.

4.4 Accessing Alternate Ring Sizes

Last, we investigated the potential of this method to generate *N*-heterocycles of various ring sizes. We anticipated that a vinyl directing group could be employed to encourage the site-selective functionalization of the allylic C–H bond within the acyclic precursor. Gratifyingly, treatment of 1-azido-6-heptene and Boc₂O (1 equiv.) with **4.2** (1 equiv.) at room temperature generated the six-membered 1-Boc-2-vinylpiperidine (Table 4.2, entry 1) as the exclusive product. As with the pyrrolidine products, the reaction product could be crystallized from a concentrated hexane solution to permit structure elucidation of the piperidine-iron adduct **4.9**

Table 4.2. Product distribution for azetidine, pyrrolidine, and piperidine formation.

Entry	Azide	Product(s)	Conv. (%) ^{ab}
1			45
2			82
3			52 (1.0:0.9)
4			47 (1.0:1.5)
5			47 (1.0:1.5)

^a Yields determined by ¹H NMR using ferrocene or trimethoxybenzene as internal standards. ^b Ratios determined by integration of GC/MS peaks.

shown in Figure 4.5a. Use of the vinyl activating group to target seven-membered azepane products, however, led to exclusive formation of the corresponding pyrrolidine (entry 2). In contrast, a phenyl activating group was not effective in favoring the formation of a six-membered-ring product. Addition of 2 to 1-azido-5-phenylpentane under standard conditions resulted in a 1:0.85 mixture of both 1-Boc-2-phenylpiperidine and 1-Boc-2-benzylpyrrolidine (entry 3). Similarly, the use of a tertiary C–H bond to favor six-membered-ring formation in the case of 1-azido-5-methylhexane resulted in a mixture of piperidine and pyrrolidine products (entry 4). An attempt was made to block the potential for pyrrolidine formation; exposure of 2-azido-2,5,5-trimethylhexane and Boc₂O to 2 resulted in both the anticipated 1-Boc-2,2,5,5-tetramethylpiperidine and the unexpected 1-Boc-2,2-dimethyl-4-tert-butylazetidine (entry 5). Alternatively, use of catalyst 1 and omission of Boc₂O allowed for the characterization of the

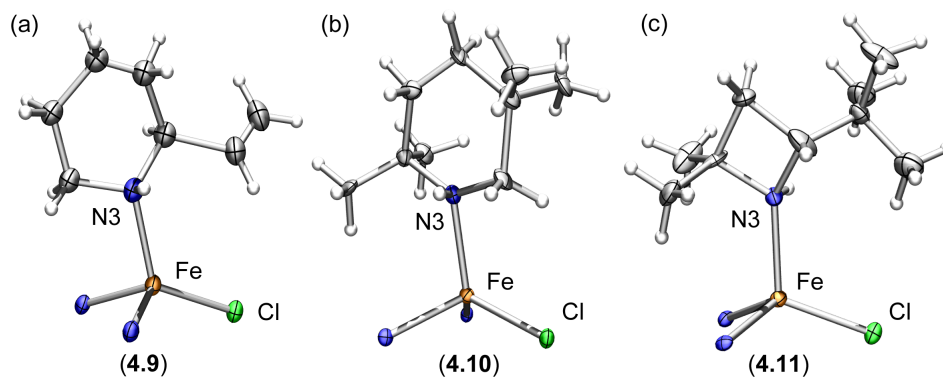


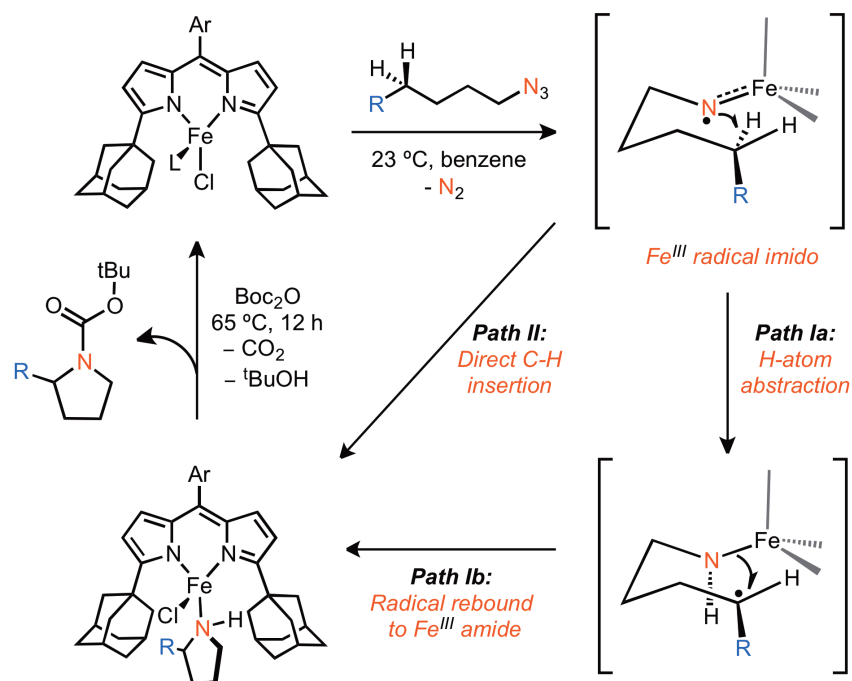
Figure 4.5. Solid state core structures of iron-bound piperidine and azetidine products. (a) Fe-bound 2-vinylpiperidine **4.9** from reaction of **4.1** with heptenylazide; (b) Fe-bound 2,2,5,5-tetramethylpiperidine **4.10** from reaction of **4.1** with 2-azido-2,5,5-trimethylhexane; (c) Fe-bound 2,2-dimethyl-4-*tert*-butylazetidine **4.11** from reaction of **4.1** with 2-azido-2,5,5-trimethylhexane. Thermal ellipsoids set at the 50% probability level (Fe, orange; Cl, gray; H, white; N, blue; Cl, green).

corresponding iron-bound piperidine (**4.10**) and azetidine (**4.11**) adducts by X-ray analysis (Figure 4.5b and c).

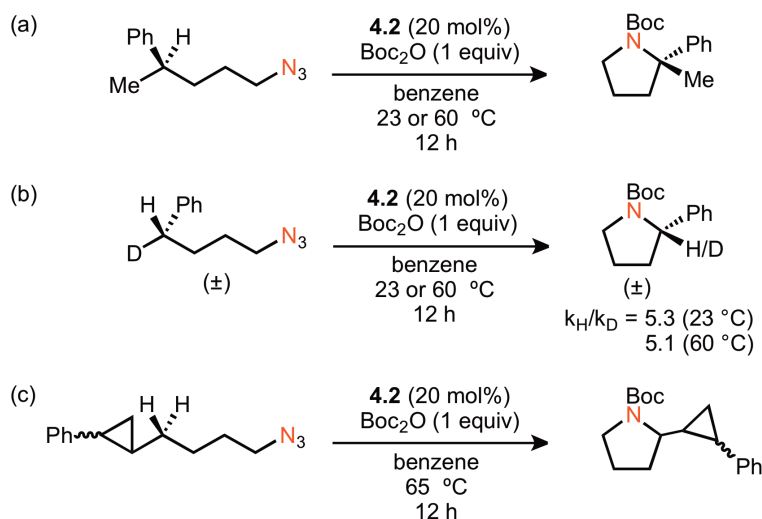
4.5 Proposed Mechanism

As illustrated in Scheme 4.3, we hypothesize that the C–H bond functionalization reaction occurs via a three-step process involving: (i) oxidation of the Fe^{II} catalyst to an Fe^{III} imido radical by the alkyl azide substrate, (ii) intramolecular H-atom abstraction to generate an alkyl radical and an Fe^{III} amide (path Ia), and (iii) radical recombination to form the observed N-heterocyclic product (path Ib). Alternatively, a direct C–H bond insertion by the Fe^{III} imido radical intermediate cannot be excluded (path II). Both mechanisms require that the substrate C–H bond be brought into close proximity to the reactive Fe-imido radical. Based on our previous findings, the imido radical likely resides in the plane defined by the iron and the dipyrin ligand, flanked by large pyrrolide adamantyl substituents. Such a conformation requires that the C–H bond substrate approach the imido radical opposite the chloride ligand. We expect that once this orientation is obtained, C–H bond functionalization is rapid. This hypothesis is supported by the retention of stereochemical information during the cyclization of (*R*)-2-phenyl-5-azidopentane

(Scheme 4.4a). This stereoretention probably reflects the spatial constraints imposed by the ligand adamantyl units to inhibit racemization of the carboradical intermediate. Additionally, ligand adamantyl units to inhibit racemization of the carboradical intermediate. Additionally,



Scheme 4.3. Mechanistic possibilities. Proposed mechanistic pathways for intramolecular C–H amination of linear alkyl azides with Fe catalyst **4.1** or **4.2** to form N-heterocycles. Pyrrolidine formation is depicted, although azetidine and piperidine products are also accessible.



Scheme 4.4 Mechanistic probes. Substrates designed to probe the mechanism of C–H functionalization and distinguish between paths I and II (Scheme 4.3).

cyclization of 1-azido-4-deutero-4-phenylbutane provides an intramolecular kinetic isotope effect of 5.3 at 25°C and 5.1(2) at 65°C (Scheme 4.4b). This value is similar to the kinetic isotope effect (KIE) observed in the hydroxylation of 1,3-dideuteroadamantane catalyzed by tetramesitylporphyrin iron with oxone (KIE = 4.1).¹⁶⁰ Finally, addition of the radical clock substrate (2-(4-azidobutyl)cyclopropyl)benzene to **4.2** exclusively furnishes the pyrrolidine product 1-Boc-2-(2-phenylcyclopropyl)pyrrolidine with the cyclopropyl unit intact (Scheme 4.4c). The nonunity intramolecular kinetic isotope effect suggests a stepwise mechanism for benzylic substrates (Scheme 4.3, path I), which is consistent with our previously reported intermolecular amination reaction. The stereospecificity of the cyclization and the preservation of the cyclopropyl unit in the radical clock experiment suggest that if a stepwise mechanism is operative, the radical intermediate following H-atom abstraction is short-lived (recombination rate $> 10^{11} \text{ s}^{-1}$).³⁵ Alternatively, the reaction mechanism may change to a direct-insertion pathway (Scheme 4.3, path II) when stronger substrate C–H bonds are functionalized.

4.6 Conclusions

The foregoing results have demonstrated the oxidative potency of the transiently formed, high-spin iron imido radical for the functionalization of both activated and unactivated aliphatic C–H bond substrates. This iron-mediated cyclization of linear azides provides facile entry into complex N-heterocyclic products from readily available substrates that cannot be achieved by azide photolysis¹⁶¹ or via classic Hoffmann-Löffler-Freytag methodologies.¹⁶² We anticipate the methodology described herein can be extended to produce a wide variety of saturated, cyclic

159. Sorokin, A.; Robert, A.; Meunier, B. *J. Am. Chem. Soc.* **1993**, *115*, 7293.

160. Barton, D. H. R.; Starratt, A. N. *J. Chem. Soc.* **1965**, 2444.

structures. The oxidative amination of aliphatic C–H bonds over more electron-rich C–H bonds (olefinic and aromatic) is made possible by the unique electronic structure of the putative iron-stabilized imido radical intermediate. Indeed, first-row transition metal catalysis is undergoing a renaissance, as the interplay between electronic structure and function are becoming better understood.

4.7 Experimental Methods.

4.7.1 General Considerations

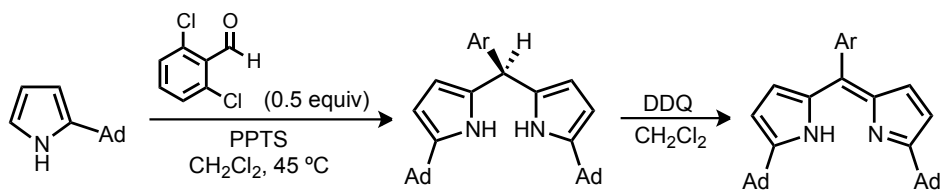
All manipulations of metal complexes were carried out in the absence of water and dioxygen using standard Schlenk techniques, or in an MBraun inert atmosphere drybox under a dinitrogen atmosphere. Ligand, ligand precursor syntheses, and substrate syntheses were carried out in air, except where noted. All glassware was oven dried for a minimum of 1 h and cooled in an evacuated antechamber prior to use in the drybox. Benzene, diethyl ether, *n*-hexane, and tetrahydrofuran were dried and deoxygenated on a Glass Contour System (SG Water USA, Nashua, NH) and stored over 4 Å molecular sieves (Strem) prior to use. Dimethylsulfoxide, hydrobromic acid (48%), pyridine (anhydrous), pentane (anhydrous), methanol, and dimethylformamide were purchased from VWR and used as received. Chloroform-*d* was purchased from Cambridge Isotope Labs and used as received. Benzene-*d*₆ was purchased from Cambridge Isotope Labs and was degassed and stored over 4 Å molecular sieves prior to use. 2,6-dichlorobenzaldehyde, pyridinium *p*-toluenesulfonate, dichlorodicyanoquinone, sodium azide, 6-bromo-1-hexene, 7-bromo-1-heptene, 8-bromo-1-octene, 1-bromohexane, 1-bromo-5-methylhexane, 1-bromobutane, benzyl 2-bromoethyl ether, 4-phenylbutanol, 5-phenylpentanol, (*S*)-2-phenyl-propan-1-ol, ethyl 5-bromovalerate, ethyl levulinate, methyl lithium (1.6 M in

Et₂O), boron trifluoride diethyl etherate, azidotrimethylsilane, 2-methyl-2-pentanol, propylene oxide (2.5 M in THF), styrene oxide, *cis*-2,3-epoxybutane, (Cyclohexylmethyl)magnesium bromide, isobutylmagnesium bromide, 3-butenylmagnesium bromide, 3-pentylmagnesium bromide, cyclopropylmagnesium bromide (0.5 M in THF), acetyl chloride, lithium chloride, tosyl chloride, *d*₁-benzaldehyde, Palladium on Carbon (10 wt%), 5-bromopentyl acetate, triphenylphosphine, lithium hexamethyldisilazide (solid), benzaldehyde, *tert*-butyldimethylsilyl chloride, imidazole, trifluoroacetic acid, diiodomethane, and tetrabutyl ammonium fluoride (1.0 M in THF) were purchased from Aldrich and used as received. Anhydrous iron(II) chloride, copper(II) chloride, and diethyl zinc (10% w/w in hexanes) were purchased from Strem and used as received. Celite® 545 (J. T. Baker) was dried in a Schlenk flask for 24 h under dynamic vacuum while heating to at least 150 °C prior to use in a drybox. Silica gel 32-63 μ (AIC, Framingham, MA) was used as received.

4.7.2 Characterization and Physical Methods

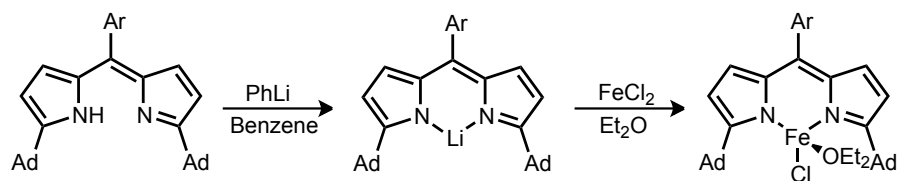
¹H, ¹³C, and were recorded on Varian Mercury 400 MHz or Varian Unity/Inova 500 MHz spectrometers. ¹H and ¹³C{¹H} NMR chemical shifts are reported relative to SiMe₄ using the chemical shift of residual solvent peaks as reference. Infrared (FTIR) spectra were recorded on a Varian 1000 Scimitar FT-IR spectrophotometer referenced to a polystyrene standard. Gas chromatography/mass spectrometry (GC/MS) was performed on a Shimadzu GCMS-QP2010S. GC analysis of enantiomeric excess was performed using an Agilent 7890A GC system with commercially available Chiraldex or Agilent columns. HPLC analysis of enantiomeric excess was performed using an Agilent 1200 series quaternary HPLC system with commercially available Chiraltech analytical columns (4.6 × 250 mm). Elemental analyses were carried out by Complete Analysis Laboratories, Inc. (Parsippany, NJ).

4.7.3 Ligand Synthesis



1,9-di(1-adamantyl)-5-(2,6-dichloro)benzene-dipyrromethene (^{Ad}L_{Cl₂})H: A 500 mL round-bottomed flask was charged with 2-(1-adamantyl)-1*H*-pyrrole (12.3 g, 60.9 mmol), 2,6-dichlorobenzaldehyde (5.30 g, 30.4 mmol, 0.5 equiv.), and 240 mL of dry CH₂Cl₂. After stirring until all materials were dissolved, pyridinium *p*-toluenesulfonate (1.249 g, 4.971 mmol, 0.1 equiv.) was added. The reaction was refluxed at 40 °C for 12 h. The solution was concentrated *in vacuo* and filtered through a plug of silica gel in a medium porosity frit (30 mL) with CH₂Cl₂ to give a pale yellow filtrate. Solvent was removed *in vacuo* affording 1,9-di(1-adamantyl)-5-(2,6-dichloro)benzene-dipyrromethane (14.9 g, 88%) as a pale yellow powder. ¹H NMR (500 MHz, CDCl₃) δ: 8.05 (br. s., 2 H), 7.28–7.38 (m, 2 H), 7.12 (t, *J* = 8.0 Hz, 1 H), 6.41 (s, 1 H), 5.87–5.93 (m, 2 H), 5.85 (t, *J* = 3.0 Hz, 2 H), 2.05 (br. s., 6 H), 1.86 (br. d, *J* = 2.3 Hz, 12 H), 1.68–1.81 (m, 12 H). ¹³C{¹H} NMR (125 MHz, CDCl₃) δ: 142.0, 137.4, 128.3, 127.6, 106.6, 101.7, 42.9, 40.1, 36.8, 33.2, 28.6. The product (14.9 g, 26.7 mmol) was dissolved in 270 mL CH₂Cl₂. The oxidant, 2,3-dichloro-5,6-dicyanoquinone (DDQ) (6.03 g, 26.7 mmol, 1 equiv.), was added to immediately give a dark brown solution. After stirring for 2 h, the solution was concentrated *in vacuo* and filtered through a plug of alumina in a medium porosity frit (30 mL). The product was loaded onto the alumina with minimal amounts of benzene and eluted with 10:1 hexanes:ethyl acetate to give an orange filtrate. Solvent was removed *in vacuo* to give (^{Ad}L)H (10.5 g, 71%) as a bright yellow-orange solid. ¹H NMR (500 MHz, CDCl₃) δ: 13.02 (br. s, 1 H), 7.36–7.44(m, 2 H), 7.27–7.33 (m, 1 H), 6.22–6.29 (m, 4 H), 2.13 (br. s., 6 H), 2.07 (s, 12 H),

1.77–1.88 (m, 12 H). $^{13}\text{C}\{\text{1H}\}$ NMR (125 MHz, CDCl_3) δ : 166.7, 138.3, 136.0, 135.1, 129.6, 127.7, 125.9, 113.8, 41.8, 36.9, 35.4, 28.5. HRMS (ESI⁺) m/z Calc. 557.2485 [$\text{C}_{35}\text{H}_{38}\text{N}_2\text{Cl}_2+\text{H}$]⁺, Found 557.2499 [$\text{M}+\text{H}$]⁺.



($^{\text{Ad}}\text{L}_{\text{Cl}_2}$)Li(OEt₂): In a 200 mL round-bottomed flask ($^{\text{Ad}}\text{L}_{\text{Cl}_2}$)H (2.00 g, 3.60 mmol) was dissolved in 40 mL diethyl ether and placed in a liquid nitrogen cooled cold well until partially frozen. Phenyl lithium (0.394 g, 4.68 mmol, 1.3 equiv.) was added as a solid. The solution was allowed to stir overnight and became a dark orange slurry. ($^{\text{Ad}}\text{L}_{\text{Cl}_2}$)Li(OEt₂) was collected as a bright orange powder on a medium porosity glass frit (1.25 g, 54%). ^1H NMR (500 MHz, C_6D_6) δ : 7.05 (d, J = 8.0 Hz, 2 H) 6.76 (d, J = 3.8 Hz, 2 H) 6.60 (t, J = 8.0 Hz, 1 H) 6.49 (d, J = 3.8 Hz, 2 H) 3.26 (br. s, 4 H) 1.94–2.03 (m, 9 H) 1.69 (br. s, 6 H) 1.00 (br. s, 6 H).

($^{\text{Ad}}\text{L}_{\text{Cl}_2}$)FeCl(OEt₂), **4.2**: A 100 mL oven-dried, round-bottomed flask was charged with ($^{\text{Ad}}\text{L}_{\text{Cl}_2}$)Li(OEt₂) (2.000 g, 3.14 mmol) and 31 mL of diethyl ether. Finely ground FeCl₂ (0.475 g, 3.77 mmol, 1.2 equiv.) was added to the slurry of ($^{\text{Ad}}\text{L}_{\text{Cl}_2}$)Li(OEt₂) at room temperature. After stirring for 3 hours, the dark brown reaction mixture was initially filtered through a medium porosity glass frit with Celite. A dark brown solid collects on top of celite and is rinsed with 10 mL Et₂O to remove any ($^{\text{Ad}}\text{L}_{\text{Cl}_2}$)H generated during the reaction. The filter flask is then replaced with a new 250 mL filter flask and the dark brown solid is dissolved and filtered with benzene to remove excess FeCl₂ and LiCl formed during the reaction. Sublimation of the benzene *in vacuo* yields ($^{\text{Ad}}\text{L}_{\text{Cl}_2}$)FeCl(OEt₂) (1.20 g, 53%) as a red brown powdery solid. Crystals suitable for x-ray diffraction were grown from an Et₂O solution of ($^{\text{Ad}}\text{L}_{\text{Cl}_2}$)FeCl(OEt₂) at room temperature. ^1H

NMR (500 MHz, C₆D₆) δ : 60.97 (s), 30.38 (br. s), 12.45 (s), 7.71 (s), 4.67 (br. s), 1.33 (s), -1.44 (br. s), -3.85 (br. s). **Anal.** Calc. for C₃₉H₄₇Cl₃FeN₂O: C 64.88, H 6.56, N 3.88; Found: C 64.98, H 6.65, N 3.97.

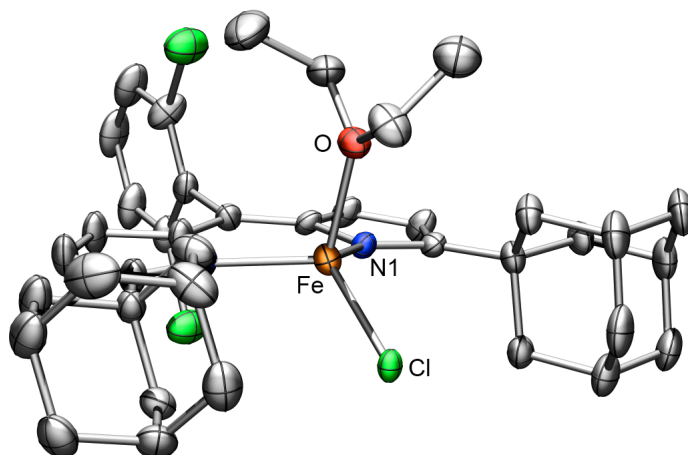
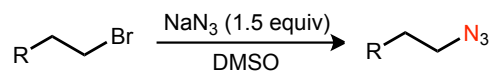


Figure 4.6 X-ray structure of 4.2. Thermal ellipsoids at 50% probability level. Hydrogens and disorder omitted for clarity.

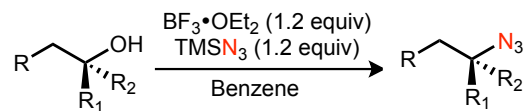
4.7.4 Substrate Syntheses

CAUTION: Organic azides are known to be potentially explosive compounds. While we did not encounter any issues during their synthesis, proper precautions were taken. All azidation reactions and subsequent workups were performed behind a blast shield. Once isolated, organic azides were stored in a -33 °C freezer.

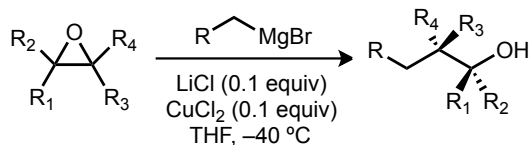


Procedure A: To a solution of the desired alkyl bromide (20 mmol, 1 equiv) in DMSO (0.5 M) was added sodium azide (1.5 equiv.), and the solution was stirred for 42h at room temperature. A 1:1 mixture of H₂O/diethyl ether was added to the reaction mixture, and the aqueous phase was extracted three times with 20 mL Et₂O. The combined organic phases were washed twice with 20 mL H₂O, 20 mL brine, and dried over MgSO₄. After removal of the solvent under reduced

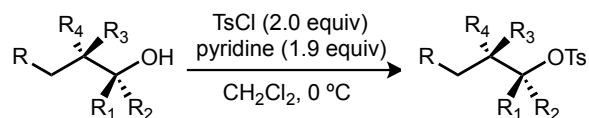
pressure, a colorless oil was obtained. Azides were purified through a silica gel plug using hexanes as the eluent.



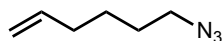
Procedure B: Boron trifluoride etherate (1.2 equiv.) was added dropwise at 25 °C to a stirring solution of tertiary (or benzylic) alcohol (15 mmol, 1 equiv.) and trimethylsilyl azide (1.2 equiv.) in benzene (0.5 M) under N₂. After 24 hours, the mixture is poured into water. The aqueous phase was extracted three times with 10 mL Et₂O. The combined organic phases were washed with 50 mL H₂O and dried over MgSO₄, filtered and concentrated. The crude products were purified via silica gel chromatography.



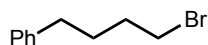
Procedure C: An oven-dried 100 mL RBF was charged with anhydrous LiCl (0.1 equiv) and CuCl₂ (0.1 equiv) and dissolved in THF (0.67 M). The flask was cooled to -40 °C and the Grignard reagent (1.2 equiv) was added dropwise. After 10 minutes, desired epoxide (20 mmol, 1 equiv.) is added dropwise and the reaction is maintained at -40 °C. The reaction was monitored by TLC and worked up once starting material was consumed (typically 4-5 hrs). Once complete, the reaction is quenched with a saturated aqueous solution of NH₄Cl and diluted with water. The aqueous phase was extracted three times with Et₂O. The combined organic phases were washed once with brine, dried over MgSO₄, filtered and concentrated. The crude products were purified via silica gel chromatography.



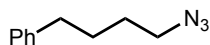
Procedure D: To a stirring solution of primary or secondary alcohol (15 mmol, 1 equiv) in dichloromethane (1.3 M) at 0 °C, tosyl chloride (2.0 equiv) and pyridine (1.9 equiv) are added. The reaction is stirred overnight at 0 °C. The reaction is warmed to room temperature and quenched with water. The aqueous phase was extracted three times with DCM. The combined organic phases were washed with a saturated aqueous solution of NaHCO₃ and brine, dried over MgSO₄, filtered and concentrated. The crude products were purified via silica gel chromatography to remove excess tosyl chloride. The tosylate is then subjected to the same conditions as Procedure A to generate the desired azide.



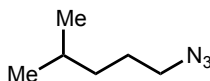
6-azido-1-hexene: Synthesized following Procedure A from 6-bromo-1-hexene. Yield: 65%. ¹H NMR (500 MHz, C₆D₆) δ: 5.56–5.67 (m, 1 H), 4.95 (dt, *J* = 2.6, 1.4 Hz, 1 H), 4.92 (d, *J* = 1.4 Hz, 1 H), 2.66 (t, *J* = 6.6 Hz, 2 H), 1.77 (q, *J* = 6.8 Hz, 2 H), 1.00–1.25 (m, 4 H). ¹³C{¹H} NMR (125 MHz, C₆D₆) δ: 138.3, 114.9, 51.1, 33.3, 28.3, 26.0. IR (thin film) ν = 3079, 2938, 2862, 2097, 1642, 994, 913 cm⁻¹. GCMS (EI) t_R = 5.2 min; *m/z*: 42, 69, 97 (–N₂); t_R = 5.5 min; *m/z*: 41, 69, 96 (–N₂–H⁺).



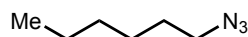
4-bromo-1-phenylbutane: ¹⁶³ 4-phenyl-1-butanol (3.00 g, 20.0 mmol) was added to 48% HBr (aq) (10 mL) and the mixture was stirred and heated to 120 °C for 30 minutes. Upon cooling, the aqueous layer was extracted three times with 10 mL Et₂O. The combined organic phases were dried over MgSO₄. Removal of the solvent under reduced pressure resulted in a colorless oil (3.59 g, 85%) that was used in the subsequent step without any further purification.



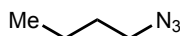
4-azido-1-phenylbutane: Synthesized following Procedure A from 4-bromo-1-phenylbutane. Yield: 0.420g, 34%. $^1\text{H NMR}$ (500 MHz, C_6D_6) δ : 7.24–7.29 (m, 2 H), 7.18 (d, $J = 7.3$ Hz, 1 H), 7.06–7.11 (m, 2 H), 2.74 (t, $J = 6.8$ Hz, 2 H), 2.39 (t, $J = 7.8$ Hz, 2 H), 1.38–1.47 (m, 2 H), 1.22–1.31 (m, 2 H). $^{13}\text{C}\{^1\text{H}\}$ NMR (125 MHz, C_6D_6) δ : 142.1, 128.6, 128.6, 126.2, 51.1, 35.5, 28.5, 28.4. IR (thin film) $\nu = 3027, 2940, 2861, 2097$ cm^{-1} . GCMS (EI) $t_{\text{R}} = 7.5$ min; m/z : 40, 51, 65, 77, 91, 104, 145($-\text{N}_2 + \text{H}^+$); $t_{\text{R}} = 7.8$ min; m/z : 41, 65, 91, 104, 118, 146($-\text{N}_2 + 2\text{H}^+$).



1-azido-4-methylpentane: Synthesized following Procedure A from 1-bromo-4-methylpentane. Yield: 65%. $^1\text{H NMR}$ (500 MHz, C_6D_6) δ : 2.68 (t, $J = 7.1$ Hz, 2 H), 1.15–1.33 (m, 3 H), 0.88–0.97 (m, 2 H), 0.75 (d, $J = 6.4$ Hz, 6 H). $^{13}\text{C}\{^1\text{H}\}$ NMR (125 MHz, C_6D_6) δ : 51.5, 35.9, 27.8, 26.8, 22.4. IR (thin film) $\nu = 2964, 2936, 2096$ cm^{-1} . GCMS (EI) $t_{\text{R}} = 5.6$ min; m/z : 43, 56, 71, 84, 98 ($-\text{N}_2 - \text{H}^+$).

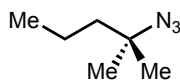


1-azidohexane: Synthesized following Procedure A from 1-bromohexane. Yield: 1.11g, 72%. $^1\text{H NMR}$ (500 MHz, C_6D_6) δ : 2.69 (t, $J = 7.1$ Hz, 2 H), 1.09–1.23 (m, 4 H), 0.98–1.08 (m, 4 H), 0.82 (t, $J = 7.3$ Hz, 2 H). $^{13}\text{C}\{^1\text{H}\}$ NMR (125 MHz, C_6D_6) δ : 51.3, 31.5, 28.9, 26.5, 11.8, 14.1. IR (thin film) $\nu = 2958, 1932, 2861, 2096, 1467, 1266$ cm^{-1} . GCMS (EI) $t_{\text{R}} = 5.8$ min; m/z : 41, 43, 56, 70, 84, 98, 115.

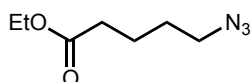


1-azidobutane: Synthesized following procedure A from 1-bromobutane.¹⁶⁴

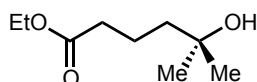
162. Shahid, I.; Patel, C. H.; Dhanani, S.; Owen, C. P.; Ahmed, S. *J. Steroid Biochem. Mol. Biol.* **2008**, *110*, 18.



2-azido-2-methylpentane: Synthesized following Procedure B from 2-methylpentan-2-ol. 46%
 $^1\text{H NMR}$ (500 MHz, CDCl_3) δ : 1.45–1.51 (m, 2 H), 1.35–1.42 (m, 2 H), 1.26 (s, 6 H), 0.95 (t, J = 7.1 Hz, 3 H). $^{13}\text{C}\{^1\text{H}\}$ NMR (125 MHz, CDCl_3) δ : 61.7, 43.7, 26.0, 17.5, 14.4. **IR** (thin film) ν = 2963, 2934, 2874, 2093, 1266 cm^{-1} . **GCMS** (EI) t_R = 5.0 min; m/z : 41, 43, 56, 70, 85.



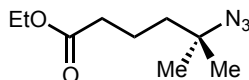
Ethyl 5-azidopentanoate: Synthesized following procedure A from ethyl 5-bromopentanoate.
 Yield: 95%.¹⁶⁵



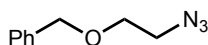
Ethyl 5-hydroxy-5-methylhexanoate¹⁶⁶: In an inert atmosphere, TiCl_4 (1.90 g, 10 mmol, 1 equiv.) was added to 50 mL of cooled ($-78\text{ }^\circ\text{C}$) Et_2O in a 100 mL pear shaped flask, resulting in partial precipitation of the yellow TiCl_4 -bis-etherate. An ethereal solution of MeLi (1.6 M in Et_2O , 10 mmol, 1 equiv.) was added slowly, which caused a color change to dark purple. The mixture was allowed to warm to $-30\text{ }^\circ\text{C}$, and was added *via* cannula to a $-30\text{ }^\circ\text{C}$ solution of ethyl 4-acetylbutyrate (1.58 g, 10.0 mmol) in 50 mL Et_2O . After reacting for four hours at $-30\text{ }^\circ\text{C}$, the solution was poured into H_2O (100 mL). The aqueous phase was extracted three times with 50 mL Et_2O . The combined organic phases were washed with 100 mL H_2O and dried over MgSO_4 . The crude product was isolated as a clear, colorless oil (1.170 g, 67%) and was subjected to the next reaction without any further purification.

163. For spectroscopic and physical characterization, see: Nguyen, D. M.; Miles, D. H. *Synth. Commun.* **2011**, *41*, 1759.

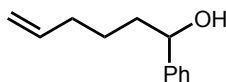
164. For spectroscopic and physical characterization, see: Khouki, N.; Vaultier, M.; Carrie, R. *Tetrahedron* **1987**, *43*, 1811.



Ethyl 5-azido-5-methylhexanoate¹⁶⁷: Synthesized following Procedure B from ethyl 5-hydroxy-5-methylhexanoate. Yield: 38% **¹H NMR** (500 MHz, C₆D₆) δ: 3.96 (q, *J* = 7.2 Hz, 2 H), 2.00 (t, *J* = 7.3 Hz, 2 H), 1.47–1.55 (m, 2 H), 1.14–1.21 (m, 2 H), 0.97 (t, *J* = 7.1 Hz, 3 H), 0.90 (s, 6 H). **¹³C{¹H} NMR** (125 MHz, C₆D₆) δ: 172.5, 61.1, 60.1, 40.8, 34.2, 25.5, 19.9, 14.3. **IR** (thin film) ν_{max} = 2979, 2940, 2877, 2097, 1737, 1465, 1371, 1259, 1187 cm⁻¹. **GCMS** (EI) *t_R* = 6.2 min; *m/z*: 41, 56, 83, 87, 111, 115, 142, 157, 172.



Benzyl 2-azidoethyl ether: Synthesized following Procedure A from benzyl 2-bromoethyl ether. Yield: 88%. **¹H NMR** (500 MHz, C₆D₆) δ: 7.30–7.34 (m, 2 H), 7.23–7.28 (m, 2 H), 7.18 (d, *J* = 7.3 Hz, 1 H), 4.25–4.31 (m, 2 H), 3.14–3.21 (m, 2 H), 2.84 (t, *J* = 4.9 Hz, 2 H). **¹³C{¹H} NMR** (125 MHz, C₆D₆) δ: 138.5, 128.6, 128.2, 127.7, 73.1, 68.9, 50.7. **IR** (thin film) ν = 3065, 3032, 2927, 2863, 2102 cm⁻¹. **GCMS** (EI) *t_R* = 7.3 min; *m/z*: 41, 51, 65, 79, 91, 106, 118, 147 (–N₂ – 2H⁺); *t_R* = 7.6 min; *m/z*: 40, 51, 65, 77, 91, 104, 118, 149 (–N₂); *t_R* = 7.7 min; *m/z*: 40, 51, 65, 91, 105, 148 (–N₂ – H⁺).

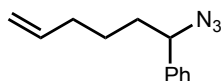


1-phenylhex-5-en-1-ol: Synthesized following Procedure C using styrene oxide and 3-butenylmagnesium bromide. 71% (38% depicted regioisomer). **¹H NMR** (500 MHz, CDCl₃) δ: 7.34–7.40 (m, 3 H), 7.27–7.32 (m, 2 H), 5.79 (ddt, *J* = 17.1, 10.3, 6.6 Hz, 1 H), 4.92–5.04 (m, 2 H), 4.69 (t, *J* = 6.8 Hz, 1 H), 2.06–2.13 (m, 2 H), 1.69–1.88 (m, 2 H), 1.49–1.60 (m, 1 H), 1.34–1.45 (m, 1 H). **¹³C{¹H} NMR** (125 MHz, CDCl₃) δ: 144.8, 138.5, 128.5, 127.5, 125.9, 114.7,

165. Reaction procedure modified from: Reetz, M. T.; Kyung, S. H.; Hullmann, M. *Tetrahedron* **1986**, *42*, 2931.

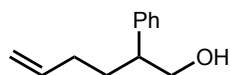
74.5, 38.5, 33.6, 25.1. **IR** (thin film) $\nu = 3606, 3069, 2979, 2934, 2863, 1641, 1455, 1265 \text{ cm}^{-1}$.

HRMS (ESI⁺) m/z Calc. 177.1279 [C₁₂H₁₆O+H]⁺, Found 176.9922 [M+H]⁺.



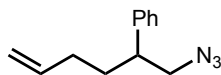
1-azido-1-phenylhex-5-ene: Synthesized following Procedure B from 1-phenylhex-5-en-1-ol.

79% **¹H NMR** (500 MHz, CDCl₃) δ : 7.28–7.42 (m, 5 H), 5.77 (ddt, $J = 17.1, 10.3, 6.5, 6.5$ Hz, 1 H), 4.94–5.05 (m, 2 H), 4.43 (t, $J = 7.3$ Hz, 1 H), 2.06–2.12 (m, 2 H), 1.82–1.90 (m, 1 H), 1.73–1.81 (m, 1 H), 1.48–1.57 (m, 1 H), 1.35–1.44 (m, 1 H). **¹³C{¹H} NMR** (125 MHz, CDCl₃) δ : 139.8, 138.1, 128.8, 128.2, 126.9, 115.0, 66.3, 35.6, 33.3, 25.4. **IR** (thin film) $\nu = 3074, 3031, 2945, 2864, 2099, 1246 \text{ cm}^{-1}$. **GCMS** (EI) $t_r = 7.9$ min; m/z : 40, 51, 65, 77, 91, 104, 115, 130, 144, 158, 173.



2-phenylhex-5-en-1-ol: Synthesized following Procedure C using styrene oxide and 3-

butenylmagnesium bromide. 71% (33% depicted regioisomer). **¹H NMR** (500 MHz, CDCl₃) δ : 7.32–7.39 (m, 2 H), 7.20–7.26 (m, 3 H), 5.79 (ddt, $J = 17.0, 10.4, 6.6$ Hz, 1 H), 4.92–5.00 (m, 2 H), 3.70–3.83 (m, 2 H), 2.79–2.88 (m, 1 H), 1.97 (dt, $J = 14.3, 6.8$ Hz, 2 H), 1.76–1.87 (m, 1 H), 1.65–1.76 (m, 1 H). **¹³C{¹H} NMR** (125 MHz, CDCl₃) δ : 142.0, 138.3, 128.7, 128.1, 126.8, 114.8, 67.5, 48.0, 31.3, 31.1. **IR** (thin film) $\nu = 3616, 3031, 2931, 1640, 1495, 1454, 1386, 1265 \text{ cm}^{-1}$. **HRMS** (ESI⁺) m/z Calc. 177.1279 [C₁₂H₁₆O+H]⁺, Found 177.0056 [M+H]⁺.

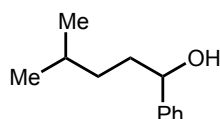


1-azido-2-phenylhex-5-ene: Synthesized following Procedure D from 2-phenylhex-5-en-ol.

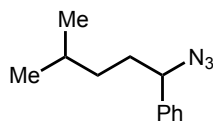
51% over 2 steps. **¹H NMR** (500 MHz, CDCl₃) δ : 7.31–7.38 (m, 2 H), 7.24–7.30 (m, 1 H), 7.21

166. For reaction procedure, see: Koziara, A.; Zwierzak, A. *Tetrahedron Lett.* **1987**, 28, 6513.

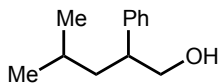
(d, $J = 7.3$ Hz, 2 H), 5.71–5.82 (m, 1 H), 4.93–5.01 (m, 2 H), 3.42–3.53 (m, 2 H), 2.82–2.90 (m, 1 H), 1.81–2.04 (m, 3 H), 1.68–1.79 (m, 1 H). $^{13}\text{C}\{^1\text{H}\}$ NMR (125 MHz, CDCl_3) δ : 141.7, 137.9, 128.7, 127.8, 127.0, 115.1, 57.1, 45.2, 40.3, 32.2, 31.2. IR (thin film) $\nu = 3156, 3031, 2928, 2850, 2102, 1268$ cm^{-1} . GCMS (EI) $t_{\text{R}} = 8.08$ min; m/z : 42, 69, 77, 91, 104, 115, 145, 173.



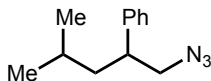
4-methyl-1-phenylpentanol: Synthesized following Procedure C from styrene oxide and 2-methylpropylmagnesium bromide. 68% (41% depicted regioisomer). ^1H NMR (500 MHz, CDCl_3) δ : 7.39–7.34 (m, 4 H), 7.29 (dd, $J = 9.0, 4.6$ Hz, 1 H), 4.68–4.63 (m, 1 H), 1.86–1.68 (m, 2 H), 1.56 (dq, $J = 13.3, 6.7$ Hz, 1 H), 1.34 (dddd, $J = 13.2, 11.4, 6.7, 4.9$ Hz, 1 H), 1.15 (dddd, $J = 13.2, 11.4, 6.7, 4.9$ Hz, 1 H), 0.88 (dd, $J = 6.6, 2.7$ Hz, 6 H). $^{13}\text{C}\{^1\text{H}\}$ NMR (125 MHz, CDCl_3) δ : 144.9, 128.4, 127.5, 125.9, 75.0, 37.0, 34.9, 28.0, 22.6. IR (thin film) $\nu = 3607, 3034, 2960, 2938, 2872, 1494, 1455, 1386, 1265$ cm^{-1} . GCMS (EI) $t_{\text{R}} = 7.70$ min; m/z : 41, 65, 79, 91, 107, 117, 145, 160, 178.



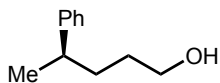
4-methyl-1-phenylpentylazide: Synthesized following procedure B from 4-methyl-1-phenylpentanol. 78%. ^1H NMR (500 MHz, CDCl_3) δ : 7.37–7.43 (m, 2 H), 7.29–7.36 (m, 3 H), 4.38 (t, $J = 7.3$ Hz, 1 H), 1.71–1.90 (m, 2 H), 1.51–1.61 (m, 1 H), 1.08–1.36 (m, 2 H), 0.89 (dd, $J = 6.6, 2.1$ Hz, 6 H). $^{13}\text{C}\{^1\text{H}\}$ NMR (125 MHz, CDCl_3) δ : 139.9, 128.7, 128.1, 126.9, 66.7, 35.3, 34.1, 27.8, 22.5. IR (thin film) $\nu = 3032, 2959, 2872, 2098, 1243$ cm^{-1} . GCMS (EI) $t_{\text{R}} = 7.90$ min; m/z : 41, 57, 71, 91, 105, 117, 132, 144, 160, 175, 187.



4-methyl-2-phenylpentanol: Synthesized following Procedure C from styrene oxide and 2-methylpropylmagnesium bromide. 68% (27% depicted regioisomer). $^1\text{H NMR}$ (500 MHz, CDCl_3) δ : 7.37–7.32 (m, 2 H), 7.27–7.22 (m, 2 H), 3.81–3.65 (m, 2 H), 2.96–2.86 (m, 1 H), 1.64–1.53 (m, 1 H), 1.51–1.37 (m, 2 H), 0.94–0.84 (m, 6 H). $^{13}\text{C}\{^1\text{H}\}$ NMR (125 MHz, CDCl_3) δ : 142.4, 128.6, 128.1, 126.7, 68.0, 46.4, 41.1, 25.2, 23.5, 21.8. IR (thin film) ν = 3358, 3029, 2955, 2930, 2869, 1494, 1454, 1367 cm^{-1} . GCMS (EI) m/z : 41, 65, 77, 91, 105, 115, 131, 147, 178.

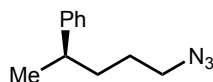


4-methyl-2-phenylpentylazide: Synthesized following Procedure D from 4-methyl-2-phenylpentanol. $^1\text{H NMR}$ (500 MHz, CDCl_3) δ : 7.34–7.39 (m, 2 H), 7.28–7.31 (m, 1 H), 7.22–7.26 (m, 2 H), 3.38–3.51 (m, 2 H), 2.90–3.00 (m, 1 H), 1.60–1.69 (m, 1 H), 1.49–1.56 (m, 1 H), 1.37–1.48 (m, 1 H), 0.91 (d, J = 6.3 Hz, 3 H), 0.89 (d, J = 6.3 Hz, 3 H). $^{13}\text{C}\{^1\text{H}\}$ NMR (125 MHz, CDCl_3) δ : 142.1, 128.6, 127.7, 126.9, 57.6, 43.6, 42.3, 25.2, 23.5, 21.6. IR (thin film) ν = 3156, 2960, 2928, 2871, 2102, 1469, 1383, 1096 cm^{-1} . GCMS (EI) t_R = 7.88 min; m/z : 41, 77, 91, 105, 119, 147.

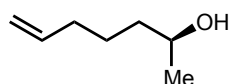


(R)-5-phenylhexanol: Synthesized following procedure C using ethylene oxide and (*R*)-2-phenylpropylmagnesium bromide. Grignard reagent was made from corresponding bromide¹⁶⁸ with activated magnesium. Yield: 93%. $^1\text{H NMR}$ (400 MHz, CDCl_3) δ : 7.15–7.23 (m, 3 H), 7.06–7.13 (m, 2 H), 3.50 (t, J = 6.6 Hz, 2 H), 2.61 (sxt, J = 7.0 Hz, 3 H), 1.50–1.63 (m, 2 H),

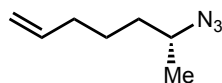
1.26–1.50 (m, 2 H), 1.17 (d, $J = 6.6$ Hz, 3 H). $^{13}\text{C}\{\text{1H}\}$ NMR (125 MHz, CDCl_3) δ : 128.4, 127.0, 125.9, 110.7, 63.1, 39.8, 34.4, 31.0, 22.4. IR (thin film) $\nu = 3339, 3086, 3062, 3027, 2958, 2927, 2855, 1494, 1452, 1377, 1059, 1031$ cm^{-1} . GCMS (EI) $t_{\text{R}} = 9.51$ min; m/z : 51, 57, 65, 71, 91, 105, 118, 131, 146, 164.



(R)-1-azido-5-phenylhexane: Synthesized following procedure D from (*R*)-5-phenylhexanol. Yield: 64% over two steps. ^1H NMR (600 MHz, CDCl_3) δ : 7.28–7.34 (m, 2 H), 7.17–7.23 (m, 3 H), 3.23 (t, $J = 6.9$ Hz, 2 H), 2.71 (qt, $J = 7.1$ Hz, 1 H), 1.63–1.70 (m, 2 H), 1.42–1.60 (m, 17 H), 1.28 (d, $J = 7.0$ Hz, 3 H). $^{13}\text{C}\{\text{1H}\}$ NMR (100 MHz, CDCl_3) δ : 146.8, 128.4, 126.9, 126.1, 51.5, 39.6, 35.3, 27.1, 22.4. IR (thin film) $\nu = 3027, 2960, 2930, 2872, 2096, 1494, 1452, 1350, 1277, 1256$ cm^{-1} . GCMS (EI) $t_{\text{R}} = 8.07$ min; m/z : 43, 65, 77, 91, 105, 117, 132, 146, 160. This material was determined to be 95% ee by chiral HPLC analysis (ChiralPak IB, Hexanes, 1 mL/min, 210nm, $t_{\text{r}}(\text{minor}) = 7.2$ min, $t_{\text{r}}(\text{major}) = 7.5$ min).



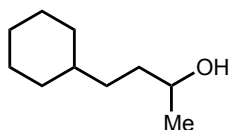
(S)-Hept-6-en-2-ol¹⁶⁹: Synthesized following Procedure C from (*S*)-propyleneoxide and 3-butenylmagnesium bromide. Yield: 80%.



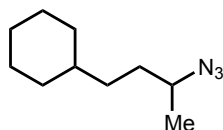
(R)-6-azido-1-heptene: Synthesized following Procedure D using (*S*)-Hept-6-en-2-ol. 73%. ^1H NMR (500 MHz, C_6D_6) δ : 5.65 (ddt, $J = 17.0, 10.4, 6.8, 6.8$ Hz, 1 H), 4.96–5.00 (m, 1 H), 4.93–4.96 (m, 1 H), 3.26 (q, $J = 7.2$ Hz, 1 H), 1.81 (q, $J = 7.8$ Hz, 2 H), 0.99–1.31 (m, 4 H), 0.83 (d, J

167. Prins, L. J.; Hulst, R.; Timmerman, P.; Reinhoudt, D. N. *Chemistry* **2002**, 8, 2288.

= 6.3 Hz, 3 H). $^{13}\text{C}\{^1\text{H}\}$ NMR (125 MHz, C_6D_6) δ : 138.4, 114.9, 57.8, 35.7, 33.6, 25.5, 19.2. IR (thin film) ν = 3079, 2975, 2938, 2860, 2106, 1642, 1477, 1447, 1380, 1325, 1250 cm^{-1} . GCMS (EI) t_{R} = 5.4 min; m/z : 42, 68, 83, 96, 111. This material was determined to be 85% ee by chiral GC analysis (β -PH, 40–100 $^{\circ}\text{C}$, 7 psi, $t_{\text{r}}(\text{major})$ = 49.7 min, $t_{\text{r}}(\text{minor})$ = 50.5 min).

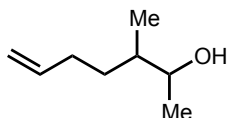


4-cyclohexylbutan-2-ol: Synthesized following Procedure C from (Cyclohexylmethyl)-magnesium bromide and propylene oxide. Yield: 90%. ^1H NMR (500 MHz, CDCl_3) δ : 3.76 (sxt, J = 6.3 Hz, 1 H), 1.58–1.74 (m, 5 H), 1.35–1.52 (m, 3 H), 1.06–1.33 (m, 8 H), 0.77–0.95 (m, 2 H). $^{13}\text{C}\{^1\text{H}\}$ NMR (125 MHz, CDCl_3) δ : 68.5, 37.7, 36.7, 33.4, 33.3, 26.7, 26.4, 23.5. IR (thin film) ν = 3053, 2987, 2928, 2851, 1265 cm^{-1} . GCMS (EI) t_{R} = 7.13 min; m/z : 41, 45, 67, 81, 96, 110, 123, 138, 141.

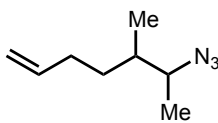


1-azido-4-cyclohexylbutane: Synthesized following Procedure D from 4-cyclohexylbutan-2-ol. 46% over two steps. ^1H NMR (500 MHz, CDCl_3) δ : 2.93 (sxt, J = 6.3 Hz, 1 H), 1.42–1.70 (m, 6 H), 1.22–1.34 (m, 1 H), 1.06–1.22 (m, 4 H), 0.94–1.05 (m, 2 H), 0.89 (dd, J = 6.3, 1.0 Hz, 3 H), 0.60–0.83 (m, 2 H). $^{13}\text{C}\{^1\text{H}\}$ NMR (100 MHz, CDCl_3) δ : 58.4, 37.5, 33.7, 33.5, 33.3, 26.6, 26.3, 19.5. IR (thin film) ν = 2928, 2854, 2101, 1450, 1249 cm^{-1} . GCMS (EI) t_{R} = 7.51 min; m/z : 42, 57, 70, 84, 110, 124, 152.

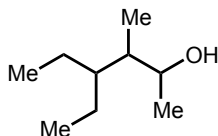
168. For spectroscopic and physical characterization, see: Dixon, D. J.; Ley, S. V.; Tate, E. W. *J. Chem. Soc. Perkin Trans. 1* **2000**, 2385.



3-methylhept-6-en-2-ol: Synthesized following Procedure C from *cis*-2,3-epoxybutane and 3-butenylmagnesium bromide. Yield: 78%. **¹H NMR** (500 MHz, CDCl₃) δ: 5.82 (ddt, *J* = 16.8, 10.3, 6.7, 6.7 Hz, 1 H), 5.03 (dd, *J* = 17.1, 2.4 Hz, 1 H), 4.96 (dd, *J* = 10.3, 1.0 Hz, 1 H), 3.64–3.72 (m, 1 H), 2.12–2.23 (m, 1 H), 1.96–2.05 (m, 1 H), 1.49, 1.62 (m, 2 H), 1.29 (br. s, 1 H), 1.17–1.25 (m, 1 H), 1.14 (d, *J* = 6.3 Hz, 3 H), 0.90 (d, *J* = 6.8 Hz, 3 H). **¹³C{¹H} NMR** (125 MHz, CDCl₃) δ: 138.9, 114.4, 71.7, 39.4, 31.7, 31.4, 19.4, 14.4. **IR** (thin film) ν = 3617, 3079, 2977, 2932, 2879, 1732, 1640, 1460, 1381, 1251 cm⁻¹. **GCMS** (EI) *t*_R = 6.10 min; *m/z*: 41, 45, 56, 81, 95, 110.

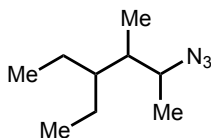


2-azido-3-methylhept-6-ene: Synthesized following Procedure D from 3-methylhept-6-en-2-ol. Yield: 25% over two steps. **¹H NMR** (500 MHz, C₆D₆) δ: 5.68 (ddt, *J* = 17.1, 10.3, 6.8, 6.8 Hz, 1 H), 4.91–5.05 (m, 2 H), 2.92–3.02 (m, 1 H), 1.74–1.96 (m, 2 H), 1.28–1.42 (m, 1 H), 1.14–1.26 (m, 1 H), 0.99–1.12 (m, 1 H), 0.81–0.88 (m, 3 H), 0.64–0.72 (m, 3 H). **¹³C{¹H} NMR** (125 MHz, C₆D₆) δ: 138.7, 114.7, 62.0, 37.7, 32.5, 31.5, 16.1, 14.5. **IR** (thin film) ν = 3079, 2974, 2932, 2881, 2101, 1642, 1457, 1381, 1257 cm⁻¹. **GCMS** (EI) *t*_R = 6.0 min; *m/z*: 41, 68, 83, 110, 125, 153.

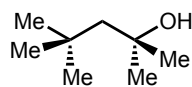


4-ethyl-3-methylhexan-2-ol: Synthesized following Procedure C from *cis*-2,3-epoxybutane and 2-methylpropylmagnesium bromide. Yield: 55%. **¹H NMR** (500 MHz, CDCl₃) δ: 3.73 (dq, *J* =

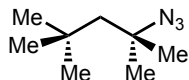
6.6 Hz, 5 H), 1.34–1.58 (m, 4 H), 1.19–1.24 (m, 1 H), 1.17 (dd, $J = 5.4, 1.0$ Hz, 3 H), 1.01–1.11 (m, 1 H), 0.85–0.92 (m, 6 H), 0.74 (d, $J = 7.3$ Hz, 3 H). $^{13}\text{C}\{\text{1H}\}$ NMR (125 MHz, CDCl_3) δ : 69.5, 41.7, 41.3, 23.4, 21.7, 21.0, 12.3, 11.8, 10.5. IR (thin film) $\nu = 3613, 2967, 2935, 2877, 1734, 1460, 1378, 1247$ cm^{-1} . GCMS (EI) $t_{\text{R}} = 6.40$ min; m/z : 41, 45, 57, 70, 97, 115, 143.



2-azido-4-ethyl-3-methylhexane: Synthesized following Procedure D from 4-ethyl-3-methylhexan-2-ol. Yield: 23% over two steps. ^1H NMR (500 MHz, CDCl_3) δ : 3.45 (qd, $J = 6.6$ Hz, 1 H), 1.33–1.56 (m, 3 H), 1.29 (d, $J = 6.3$ Hz, 3 H), 1.06–1.27 (m, 3 H), 0.84–0.90 (m, 9 H). $^{13}\text{C}\{\text{1H}\}$ NMR (100 MHz, CDCl_3) δ : 61.3, 42.7, 39.8, 23.2, 21.6, 17.9, 12.0, 11.7, 11.0. IR (thin film) $\nu = 2966, 2933, 2878, 2106, 1464, 1380, 1257$ cm^{-1} . GCMS (EI) $t_{\text{R}} = 6.80$ min; m/z : 41, 43, 57, 71, 84, 98, 112, 126, 140, 157.

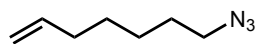


2,4,4-trimethylpentan-2-ol: Synthesized following procedure C from *tert*-butyl magnesium chloride and 2,2-dimethyloxirane. Grignard reagent was made from corresponding chloride. Yield: 29%. ^1H NMR (600 MHz, CDCl_3) δ : 1.53 (s, 2 H), 1.30 (s, 6 H), 1.04 (s, 9 H). $^{13}\text{C}\{\text{1H}\}$ NMR (125 MHz, CDCl_3) δ : 72.5, 55.8, 31.7, 31.4, 31.3. IR (thin film) $\nu = 3398, 2955, 2906, 1477, 1366, 1215, 1124$ cm^{-1} . GCMS (EI) $t_{\text{R}} = 5.08$ min; m/z : 41, 59, 83, 97, 115.



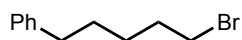
2-azido-2,4,4-trimethylpentane: Synthesized following procedure D from 2,4,4-trimethylpentan-2-ol. Yield: 65%. ^1H NMR (600 MHz, CDCl_3) δ : 1.53 (s, 2 H), 1.33 (s, 6 H),

1.04 (s, 9 H). $^{13}\text{C}\{^1\text{H}\}$ NMR (125 MHz, CDCl_3) δ : 52.9, 31.4, 31.1, 28.4. IR (thin film) ν = 2959, 2908, 2100, 1389, 1369 cm^{-1} . GCMS (EI) t_{R} = 6.00 min; m/z : 41, 57, 71, 84, 98, 112, 127.

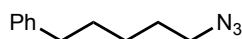


7-azido-1-heptene: Synthesized following Procedure A from 7-bromo-1-heptene. Yield: 78%.

^1H NMR (500 MHz, C_6D_6) δ : 5.69 (ddt, J = 17.1, 10.3, 6.8 Hz, 1 H) 4.99–5.01 (m, 1 H) 4.94–4.99 (m, 1 H) 2.67 (t, J = 6.8 Hz, 2 H) 1.79–1.92 (m, 2 H) 1.06–1.20 (m, 4 H) 0.99–1.06 (m, 2 H). $^{13}\text{C}\{^1\text{H}\}$ NMR (125 MHz, C_6D_6) δ : 138.7, 114.7, 51.2, 33.8, 28.8, 28.5, 26.3. IR (thin film) ν = 3078, 2934, 2860, 2097, 1641, 994, 911 cm^{-1} . GCMS (EI) t_{R} = 6.4 min; m/z : 41, 55, 70, 96, 110 ($-\text{N}_2 - \text{H}^+$).

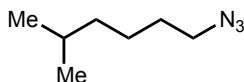


5-bromo-1-phenylpentane: 5-phenyl-1-pentanol (3.28 g, 20.0 mmol) was added to 48% HBr (aq) (10 mL) and the mixture was stirred and heated to 120 °C for 30 minutes. Upon cooling, the aqueous layer was extracted three times with 10 mL Et_2O . The combined organic phases were dried over MgSO_4 . Removal of the solvent under reduced pressure, a colorless oil (3.53 g, 78%) was obtained that was used in the subsequent step without any further purification.¹⁶³



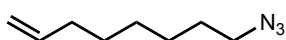
5-azido-1-phenylpentane: Synthesized following Procedure A from 5-bromo-1-phenylpentane.

Yield: 0.740 g, 59%. ^1H NMR (500 MHz, C_6D_6) δ : 7.16–7.22 (m, 2 H) 7.06–7.12 (m, 1 H) 7.03 (d, J = 6.8 Hz, 2 H) 2.61 (t, J = 7.1 Hz, 2 H) 2.35 (t, J = 7.6 Hz, 2 H) 1.31 (dt, J = 15.3, 7.8 Hz, 2 H) 1.09–1.18 (m, 2 H) 0.96–1.05 (m, 2 H). $^{13}\text{C}\{^1\text{H}\}$ NMR (125 MHz, C_6D_6) δ : 128.7, 128.6, 126.1, 51.2, 36.0, 31.1, 28.8, 26.4. IR (thin film) ν = 3085, 3026, 2934, 2859, 2094 cm^{-1} . GCMS (EI) t_{R} = 7.9 min; m/z : 40, 51, 65, 77, 91, 105, 144, 159 ($-\text{N}_2 - \text{H}^+$). t_{R} = 8.1 min; m/z : 41, 65, 77, 91, 104, 118, 132, 143, 160 ($-\text{N}_2 - 2\text{H}^+$).

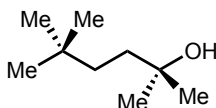


1-azido-5-methylhexane: Synthesized following Procedure A from 1-bromo-5-methylhexane.

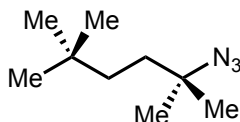
Yield: 78%. $^1\text{H NMR}$ (500 MHz, CDCl_3) δ : 3.27 (t, $J = 7.1$ Hz, 2 H), 1.49–1.63 (m, 3 H), 1.33–1.41 (m, 2 H), 1.17–1.23 (m, 2 H), 0.89 (d, $J = 6.3$ Hz, 6 H). $^{13}\text{C}\{^1\text{H}\}$ NMR (125 MHz, CDCl_3) δ : 51.8, 38.7, 29.3, 28.1, 24.8, 22.8. **IR** (thin film) $\nu = 3054, 2958, 2870, 2100, 1265$ cm^{-1} . **GCMS** (EI) $t_{\text{R}} = 6.2$ min; m/z : 41, 43, 56, 70, 84, 98, 112, 132.



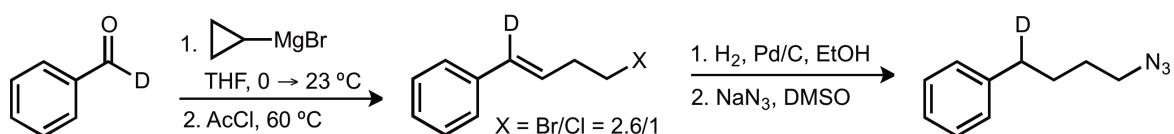
8-azido-1-octene: Synthesized following Procedure A. Yield: 0.769g, 95%. $^1\text{H NMR}$ (500 MHz, C_6D_6) δ : 5.74 (ddt, $J = 17.1, 10.3, 6.8$ Hz, 1 H), 4.91–5.09 (m, 2 H), 2.68 (t, $J = 7.1$ Hz, 2 H), 1.91 (q, $J = 7.2$ Hz, 2 H), 1.13–1.23 (m, 4 H), 0.98–1.06 (m, 4 H). $^{13}\text{C}\{^1\text{H}\}$ NMR (125 MHz, C_6D_6) δ : 139.0, 114.6, 51.2, 34.0, 29.0, 28.9, 28.8, 26.7. **IR** (thin film) $\nu = 3078, 2933, 2859, 2098, 1641, 1458, 1350$ cm^{-1} . **GCMS** (EI) $t_{\text{R}} = 5.8$ min; m/z : 41, 55, 70, 96, 110, 124.



2,5,5-trimethylhexan-2-ol: Synthesized following procedure C from 2,2-dimethyloxirane and 2,2-dimethylpropylmagnesium bromide. Grignard reagent was made from corresponding bromide with activated magnesium. Yield: 66%. $^1\text{H NMR}$ (500 MHz, CDCl_3) δ : 1.60 (br. s, 1 H), 1.41–1.47 (m, 2 H), 1.19–1.28 (m, 8 H), 0.89 (s, 9 H). $^{13}\text{C}\{^1\text{H}\}$ NMR (125 MHz, CDCl_3) δ : 71.0, 38.5, 38.1, 29.9, 29.3, 29.1. **IR** (thin film) $\nu = 3390, 2941, 2868, 1473, 1365, 1291, 1261, 1202$ cm^{-1} . **GCMS** (EI) $t_{\text{R}} = 5.75$ min; m/z : 41, 59, 71, 85, 111, 129.



2-azido-2,5,5-trimethylhexane: Synthesized following procedure D from 2,5,5-trimethylhexan-2-ol. Yield: 43%. $^1\text{H NMR}$ (500 MHz, CDCl_3) δ : 71.44–1.49 (m, 2 H), 1.21–1.27 (m, 8 H), 0.90 (s, 9 H). $^{13}\text{C}\{^1\text{H}\}$ NMR (100 MHz, CDCl_3) δ : 61.7, 37.9, 36.1, 30.0, 29.3, 26.0. IR (thin film) ν = 2959, 2869, 2096, 1473, 1388, 1369, 1260 cm^{-1} . GCMS (EI) t_R = 7.40 min; m/z : 41, 56, 71, 84, 111, 127.

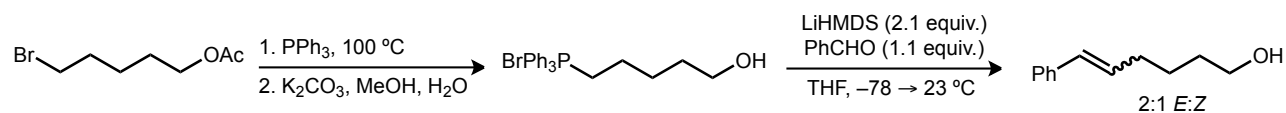


(E)-4-chloro(bromo)-1-deutero-1-phenylbut-1-ene¹⁷⁰: $^1\text{H NMR}$ (500 MHz, CDCl_3) δ : 7.30–7.45 (m, 4 H), 7.21–7.29 (m, 1 H), 6.16–6.29 (m, 1 H), 3.64 (t, J = 6.8 Hz, 0.55 H), 3.49 (t, J = 7.1 Hz, 1.45 H), 2.79 (q, J = 7.0 Hz, 0.55 H), 2.70 (q, J = 7.0 Hz, 1.45 H). $^{13}\text{C}\{^1\text{H}\}$ NMR (125 MHz, CDCl_3) δ : 139.9, 128.6, 127.4, 126.5, 126.1, 125.7, 44.0 (X=Cl) 36.2 (X=Br), 36.1 (X=Cl) 32.3 (X=Br). IR (thin film) ν = 3080, 3059, 3023, 2961, 2930, 2856, 1598, 1576, 1495, 1447, 1269, 1208, 1075, 1027 cm^{-1} . GCMS (EI) X=Cl t_R = 7.59 min; m/z : 40, 51, 65, 78, 92, 105, 118, 129, 167; X=Br t_R = 7.87 min; m/z : 40, 51, 64, 77, 92, 103, 118, 132, 211.

4-chloro(bromo)-1-deutero-1-phenylbutane: To a solution of (E)-4-chloro(bromo)-1-deutero-1-phenylbut-1-ene (635 mg) in ethanol (0.4 M) was added Pd/C (64 mg) with vigorous stirring under a balloon of H_2 for 3 hours. Upon reaction completion, the reaction mixture was filtered over Celite with Et_2O and concentrated. The crude product (564 mg) was taken on to the next step without any further purification. $^1\text{H NMR}$ (600 MHz, CDCl_3) δ : 7.30 (t, J = 1.0 Hz, 2 H), 7.17–7.24 (m, 3 H), 3.56 (t, J = 6.4 Hz, 0.6 H), 3.43 (t, J = 6.7 Hz, 1.4 H), 2.60–2.69 (m, 1 H),

1.86–1.96 (m, 1.2 H), 1.74–1.86 (m, 2.8 H). $^{13}\text{C}\{\text{1H}\}$ NMR (125 MHz, CDCl_3) δ : 141.7, 128.4, 125.9, 44.9 (X= Cl) 34.6 (X=Br), 33.6, 32.2 (X= Cl) 32.1 (X=Br), 29.7 (X=Cl) 28.5 (X=Br). **IR** (thin film) ν = 3087, 3061, 3025, 2934, 2863, 1496, 1450, 1247 cm^{-1} . **GCMS** (EI) X=Cl t_{R} = 7.42 min; m/z : 40, 51, 66, 78, 92, 105, 133, 169. X=Br t_{R} = 7.71 min; m/z : 440, 51, 66, 78, 92, 105, 134, 213.

4-azido-1-deutero-1-phenylbutane: Synthesized following Procedure A. Yield: 353 mg. ^1H NMR (500 MHz, CDCl_3) δ : 7.28–7.33 (m, 2 H), 7.17–7.24 (m, 3 H), 3.30 (t, J = 6.8 Hz, 2 H), 2.61–2.70 (m, 1 H), 1.61–1.76 (m, 4 H). $^{13}\text{C}\{\text{1H}\}$ NMR (125 MHz, CDCl_3) δ : 141.8, 128.4, 128.3, 125.9, 51.3, 35.1 (q), 28.4, 28.3. **IR** (thin film) ν = 3084, 3062, 3027, 2936, 2864, 2097, 1496, 1451, 1283, 1256, 913 cm^{-1} . **GCMS** (EI) t_{R} = 7.81 min; m/z : 41, 43, 66, 71, 92, 104, 119, 129, 147.

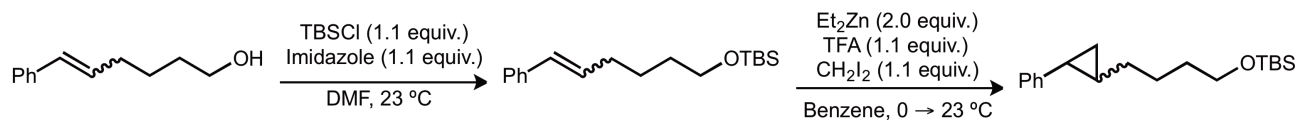


6-phenylhex-5-en-1-ol¹⁷¹: To a suspension of 5-hydroxypentyltriphenylphosphonium bromide¹⁷² in 26 mL (0.5 M) THF was added LiHMDS (4.90 g, 29.3 mmol, 2.2 equiv.) in a dry box at room temperature. After 30 min, the red, clear solution was removed from the drybox and cooled to –78 °C under nitrogen and benzaldehyde (1.41 g, 13.3 mmol) was slowly added. The solution was allowed to warm slowly to 23 °C and stirred for an additional hour. The reaction was quenched with 25 mL water and extracted (3 x 25 mL) with diethyl ether. The combined organics were then washed with brine (1 x 25 mL), dried with MgSO_4 , filtered, and concentrated. The product

169. For spectroscopic and physical characterization, see: Wong, K.-T.; Hung, Y.-Y. *Tetrahedron Lett.* **2003**, *44*, 8033.

170. For experimental procedure and spectroscopic characterization data, see: Maryanoff, B. E.; Reitz, A. B.; Duhl-Emswiler, B. A. *J. Am. Chem. Soc.* **1985**, *107*, 217.

was purified by silica gel column chromatography and isolated as a colorless oil (2.12 g, 91%, 2:1 *E:Z*). **¹H NMR** (500 MHz, CDCl₃) δ: 7.14–7.42 (m, 5 H), 6.33–6.50 (m, 1 H), 6.23 (dt, *J* = 16.0, 6.9 Hz, 0.67 H), 5.67 (dt, *J* = 11.7, 7.3 Hz, 0.33 H), 3.58–3.76 (m, 2 H), 2.20–2.45 (m, 2 H), 1.47–1.74 (m, 4 H), 1.28–1.47 (m, 1 H). **¹³C{¹H} NMR** (125 MHz, CDCl₃) δ: 137.7, 132.6, 130.5, 130.1, 129.1, 128.7, 128.5, 128.1, 126.9, 126.5, 125.9, 62.8, 32.7, 32.3, 28.2, 26.1, 25.5. **IR** (thin film) ν = 3343, 3081, 3058, 3025, 2933, 2860, 1494, 1448, 1070, 965 cm⁻¹. **GCMS** (EI) *t_R* = 10.1 min; *m/z*: 51, 57, 65, 71, 77, 85, 91, 98, 104, 115, 130, 143, 158, 176. *t_R* = 10.4 min; *m/z*: 51, 57, 65, 71, 77, 85, 91, 98, 104, 115, 117, 130, 143, 158, 176.

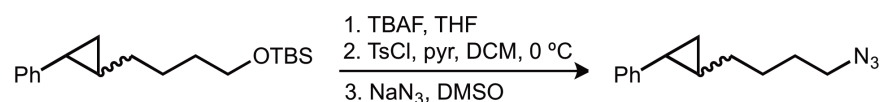


1-*tert*-Butyl-dimethylsiloxy-6-phenylhex-5-ene: To a stirring solution of alcohol (2.12 g, 12.0 mmol) in dimethylformamide (25 mL, 0.5 M) was added imidazole (0.90 g, 13.2 mmol, 1.1 equiv.) followed by *tert*-butyldimethylsilyl chloride (1.99 g, 13.2 mmol, 1.1 equiv.). The reaction was allowed to stir for two hours and was then diluted with water (25 mL) and extracted with ethyl acetate (3 x 25 mL). The combined organics were then washed with brine (4 x 10 mL), dried with MgSO₄, filtered and concentrated. The product was purified by silica gel column chromatography and isolated as a colorless oil (2.56 g, 74%). **¹H NMR** (500 MHz, CDCl₃) δ: 7.25–7.39 (m, 4 H), 7.16–7.26 (m, 1 H), 6.36–6.47 (m, 1 H), 6.18–6.28 (m, 0.67 H), 5.62–5.72 (m, 0.33 H), 3.58–3.69 (m, 2 H), 2.31–2.41 (m, 0.66 H), 2.20–2.28 (m, 1.34 H), 1.47–1.64 (m, *J* = 1.5 Hz, 4 H), 0.88–0.93 (m, 9 H), 0.03–0.08 (m, 6 H). **¹³C{¹H} NMR** (100 MHz, CDCl₃) δ: 137.9, 133.0, 130.9, 129.9, 128.9, 128.7, 128.4, 128.1, 126.8, 126.4, 125.9, 63.1, 32.8, 32.4, 28.3, 26.2, 26.0, 25.6, 18.4, -5.3. **IR** (thin film) ν = 3082, 3062, 3026, 2954, 2929, 2896, 2957, 1495,

171. For the experimental procedure, see: Baldwin, J. E.; Claridge, T. D. W.; Culshaw, A. J.; Heupel, F. A.; Lee,

1472, 1448, 1389, 1361, 1256, 1101, 1006, 964 cm^{-1} . **HRMS** (ESI⁺) m/z Calc. 291.2144 [C₁₈H₃₀OSi+H]⁺, Found 291.2147 [M+H]⁺.

1-tert-Butyl-dimethylsiloxy-4-(2-phenylcyclopropyl)butane:¹⁷³ Yield: 933 mg, 89%. **¹H NMR** (500 MHz, CDCl₃) δ : 7.24–7.33 (m, 2 H), 7.12–7.23 (m, 1 H), 7.07 (d, J = 6.8 Hz, 1 H), 3.64 (t, J = 6.6 Hz, 1.40 H), 3.47–3.56 (m, 0.60 H), 1.26–1.68 (m, 6 H), 0.96–1.22 (m, 2 H), 0.93 (s, 6.3 H), 0.90 (s, 2.7 H), 0.64–0.82 (m, 1 H), 0.08 (s, 4.2 H), 0.04 (s, 1.8 H). **¹³C{¹H} NMR** (125 MHz, CDCl₃) δ : 144.0, 129.0, 128.2, 127.8, 125.6, 125.5, 125.1, 63.2, 34.2, 32.7, 28.3, 26.0, 25.6, 23.8, 23.2, 21.0, 19.0, 18.4, 16.1, 9.6, -5.3. **IR** (thin film) ν = 3065, 3027, 2999, 2929, 2857, 1497, 1463, 1388, 1361, 1256, 1101, 836 cm^{-1} . **HRMS** (ESI⁺) m/z Calc. 305.2301 [C₁₉H₃₂OSi+H]⁺, Found 305.2311 [M+H]⁺.



4-(2-phenylcyclopropyl)butan-1-ol: To a stirring solution of TBS-protecting alcohol (933 mg, 3.06 mmol) in THF (12 mL, 0.25M) was added a 1.0 M solution of tetrabutylammonium fluoride in THF (4.60 mL, 1.5 equiv.). The solution was stirred overnight and then diluted with water (10 mL) and extracted with ethyl acetate (3 x 10 mL). The combined organics were then washed with brine (1 x 20 mL), dried with MgSO₄, filtered and concentrated. The product was purified by silica gel column chromatography and isolated as a colorless oil (570 mg, 98%). **¹H NMR** (500 MHz, CDCl₃) δ : 7.14–7.34 (m, 4 H), 7.08 (d, J = 7.3 Hz, 1 H), 3.70 (t, J = 6.6 Hz, 1.35 H), 3.53 (q, J = 6.8 Hz, 0.65 H), 1.32–1.73 (m, 6 H), 0.88–1.26 (m, 3 H), 0.81 (dt, J = 8.3, 5.1 Hz, 0.68 H), 0.71 (q, J = 5.4 Hz, 0.32 H). **¹³C{¹H} NMR** (125 MHz, CDCl₃) δ : 143.9, 128.9, 128.2, 127.8, 125.5, 125.1, 63.0, 62.8, 31.2, 32.6, 32.4, 28.1, 25.6, 25.3, 23.6, 23.2, 20.9, 19.0, 16.1, 9.6. **IR**

(thin film) $\nu = 3338, 3063, 3026, 2998, 2932, 2857, 1605, 1497, 1460, 1067, 1029$. **GCMS** (EI) $t_R = 10.4$ min; m/z : 51, 58, 65, 78, 91, 104, 117, 129, 143, 157, 165, 172, 190; $t_R = 10.6$ min; m/z : 51, 58, 65, 74, 81, 91, 104, 117, 129, 136, 143, 157, 165, 172, 190.

1-(4-methylbenzene)sulfonyl-4-(2-phenylcyclopropyl)butane: Synthesized following procedure D. Yield: 745 mg, 72%. **^1H NMR** (600 MHz, CDCl_3) δ : 7.78–7.82 (m, 1.3 H), 7.75–7.78 (m, 0.7 H), 7.32–7.36 (m, 2 H), 7.22–7.28 (m, 2 H), 7.11–7.19 (m, 2 H), 7.00–7.04 (m, 1 H), 4.04 (t, $J = 6.4$ Hz, 1.3 H), 3.90 (t, $J = 6.6$ Hz, 0.7 H), 2.42–2.48 (m, 3 H), 1.66–1.74 (m, 1.3 H), 1.57 (dt, $J = 8.7, 4.6$ Hz, 0.7 H), 1.53 (ddq, $J = 10.8, 6.5, 2.2, 2.2, 2.2$ Hz, 0.7 H), 1.43–1.50 (m, 1.3 H), 1.32–1.38 (m, 1 H), 1.22–1.31 (m, 0.35 H), 0.98–1.14 (m, 0.65 H), 0.92–0.98 (m, 1 H), 0.87 (m, $J = 8.3, 4.9, 4.9$ Hz, 1 H), 0.72 (ddd, $J = 8.6, 5.5, 4.7$ Hz, 0.65 H), 0.61 (q, $J = 5.9$ Hz, 0.35 H). **$^{13}\text{C}\{^1\text{H}\}$ NMR** (125 MHz, CDCl_3) δ : 144.6, 143.6, 133.2, 129.8, 128.9, 128.2, 127.9, 125.5, 125.2, 70.6, 33.6, 28.6, 28.5, 27.7, 25.2, 25.1, 23.3, 23.2, 21.6, 20.9, 18.7, 16.0, 9.5. **IR** (thin film) $\nu = 3063, 3027, 2997, 2925, 2858, 1599, 1497, 1460, 1359, 1176, 1098, 1020$ cm^{-1} . **$^1\text{HRMS}$** (ESI⁺) m/z Calc. 367.1338 [$\text{C}_{20}\text{H}_{24}\text{O}_3\text{S}+\text{Na}$]⁺, Found 367.1354 [$\text{M}+\text{Na}$]⁺.

4-(2-phenylcyclopropyl)-1-azidobutane: Synthesized following procedure D. Yield: 391 mg, 84%. **^1H NMR** (500 MHz, CDCl_3) δ : 7.13–7.34 (m, 4 H), 7.07 (d, $J = 7.3$ Hz, 1 H), 3.23–3.38 (m, 1.35 H), 3.08–3.19 (m, 0.65 H), 2.16 (td, $J = 8.5, 6.0$ Hz, 0.3 H), 1.26–1.76 (m, 6 H), 0.89–1.24 (m, 2.6 H), 0.64–0.85 (m, 1 H). **$^{13}\text{C}\{^1\text{H}\}$ NMR** (125 MHz, CDCl_3) δ : 143.7, 128.9, 128.2, 127.8, 125.6, 125.2, 51.5, 51.3, 33.9, 28.6, 28.5, 27.9, 26.6, 26.5, 23.5, 23.2, 21.0, 18.8, 16.1, 9.5. **IR** (thin film) $\nu = 3064, 3027, 2999, 2934, 2857, 2095, 1605, 1497, 1457, 1350, 1272, 1029$ cm^{-1} . **GCMS** (EI) $t_R = 10.9$ min; m/z : 56, 65, 83, 91, 104, 115, 129, 144, 156, 172, 186; $t_R = 11.0$ min; m/z : 56, 65, 83, 91, 104, 117, 129, 144, 156, 170, 186.

172. For experimental procedure, see: Lorenz, J. C.; Long, J.; Yang, Z.; Xue, S.; Xie, Y.; Shi, Y. *J. Org. Chem.*

4.7.5 Stoichiometric N-Heterocycle Forming Reactions: Lewis Acid/Base Pair with Fe-Complex

Under an inert N₂ atmosphere, (^{Ad}L_{Mes})FeCl(OEt₂) (**4.1**) or (^{Ad}L_{Cl₂})FeCl(OEt₂) (**4.2**) (0.056 mmol) was added to a stirring solution of the desired azide (1 equiv) in 2 mL of benzene in a 5 mL scintillation vial. The resultant inky, dark red solution was then allowed to stir for 3 hours in the glove box. The reaction mixture was then concentrated to a red/brown powder *in vacuo* and a paramagnetic ¹H NMR in C₆D₆ was obtained to ensure reaction completion. The resultant mixture was redissolved in hexanes, filtered to remove any insoluble material and left to crystallize at room temperature.

1+(2-phenylpyrrolidine) (4.3): ¹H NMR (500 MHz, C₆D₆): 134.6, 96.6, 73.5, 55.7, 54.9, 26.3, 20.7, 17.7, 15.6, 11.8, 9.6, 5.5, 4.5, 3.4, 1.9, 1.1, 0.6, -2.9, -3.4, -17.2, -22.1, -24.2.

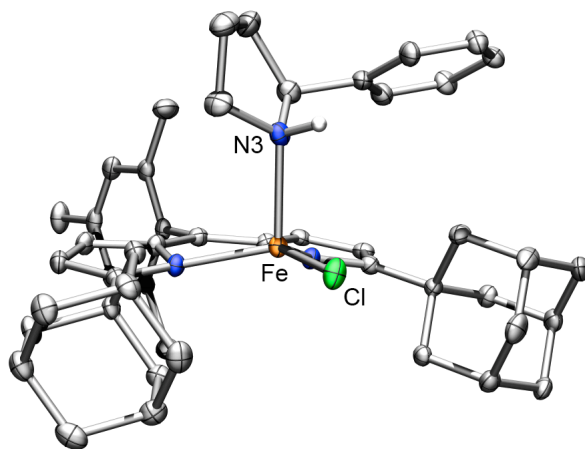


Figure 4.7. X-ray structure of **4.3**. Thermal ellipsoids at 50% probability level. Hydrogens and pyrrolidine disorder omitted for clarity.

1+(2-vinylpyrrolidine) (4.4): ¹H NMR (500 MHz, C₆D₆): 55.4, 55.0, 47.1, 28.2, 22.4, 18.8, 16.5, 14.5, 11.5, 9.4, 5.6, 4.4, 3.6, 2.2, 2.1, 1.7, 1.3, 0.9, 0.6, -1.5, -2.8, -4.4, -7.3, -17.0, -18.1, -21.0, -23.3.

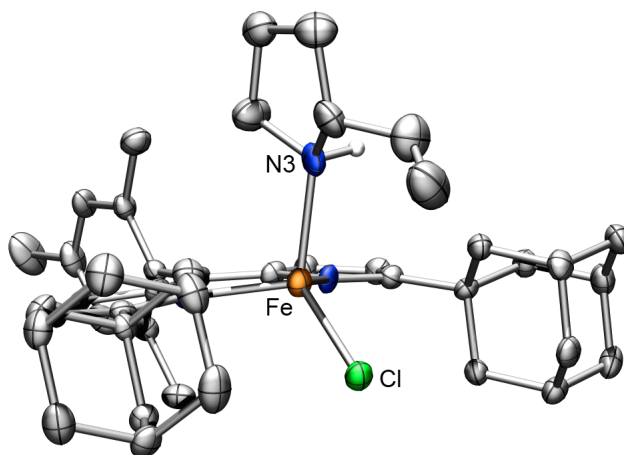


Figure 4.8. X-ray structure of 4.4. Thermal ellipsoids at 50% probability level. Hydrogens and pyrrolidine disorder omitted for clarity.

1+(2,2-dimethylpyrrolidine) (4.5, 4.7): $^1\text{H NMR}$ (500 MHz, C_6D_6): $^1\text{H NMR}$ (500 MHz, C_6D_6): 70.0, 66.2, 58.3, 55.1, 41.5, 25.7, 18.9, 13.4, 10.6, 9.9, 5.4, 2.7, 0.5, -2.2, -3.0, -5.3, -7.7, -16.0, -18.5, -24.4, -27.0.

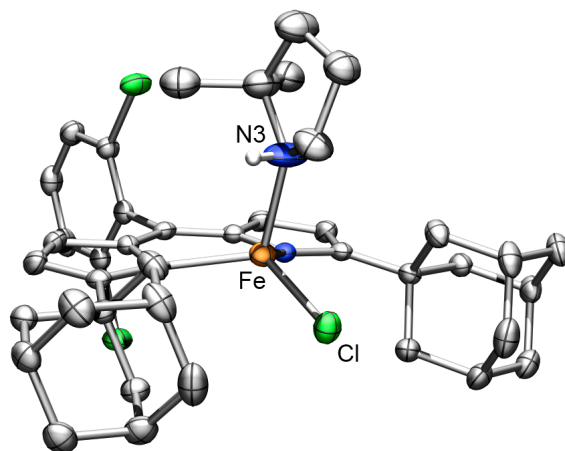


Figure 4.9. X-ray structure of 4.7. Thermal ellipsoids at 50% probability level. Hydrogens omitted for clarity.

1+(2-ethylpyrrolidine) (4.6): $^1\text{H NMR}$ (500 MHz, C_6D_6): $^1\text{H NMR}$ (500 MHz, C_6D_6): 156.7, 94.4, 63.1, 55.8, 49.2, 47.5, 24.8, 18.0, 12.6, 10.3, 9.4, 5.5, 4.8, 2.9, 2.7, 2.0, 0.3, -2.0, -5.9, -9.3, -12.2, -17.4, -19.7, -23.8.

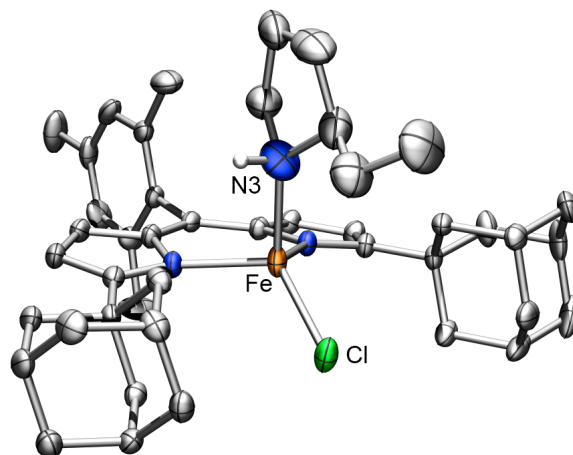


Figure 4.10. *X-ray structure of 4.6.* Thermal ellipsoids at 50% probability level. Hydrogens and pyrrolidine disorder omitted for clarity.

1+((*S*)-2-methyl-2-phenylpyrrolidine) (4.8):

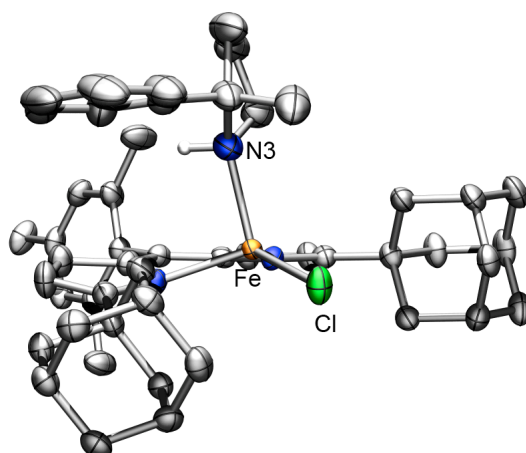


Figure 4.11. *X-ray structure of 4.8.* Thermal ellipsoids at 50% probability level. Hydrogens omitted for clarity. The structure possesses positional disorder with a second Fe and pyrrolidine (19% occupancy, opposite the depicted Fe–N bond vector). The second Fe is assigned in the refinement, but the weakness of the reflections of the pyrrolidine carbons did not allow for full refinement of the second ring.

1+(2-vinylpiperidine) (4.9):

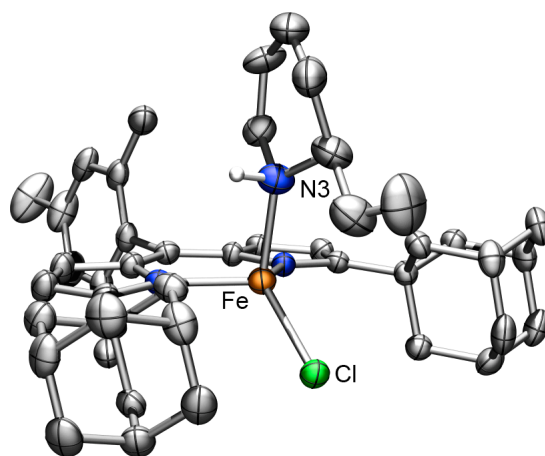


Figure 4.12. X-ray structure of 4.9. Thermal ellipsoids at 50% probability level. Hydrogens and piperidine disorder omitted for clarity.

1+(2,2-dimethyl-4-*tert*-butylazetidide)+(2,2-dimethyl-5,5-dimethylpiperidine) (4.10, 4.11):

^1H NMR (500 MHz, C_6D_6): 67.8, 50.2, 48.3, 47.2, 41.1, 19.9, 18.1, 13.4, 9.8, 8.2, 6.0, 5.2, 4.2, 3.6, 2.6, -1.7, -4.4, -4.7, -6.8, -10.0, -15.9.

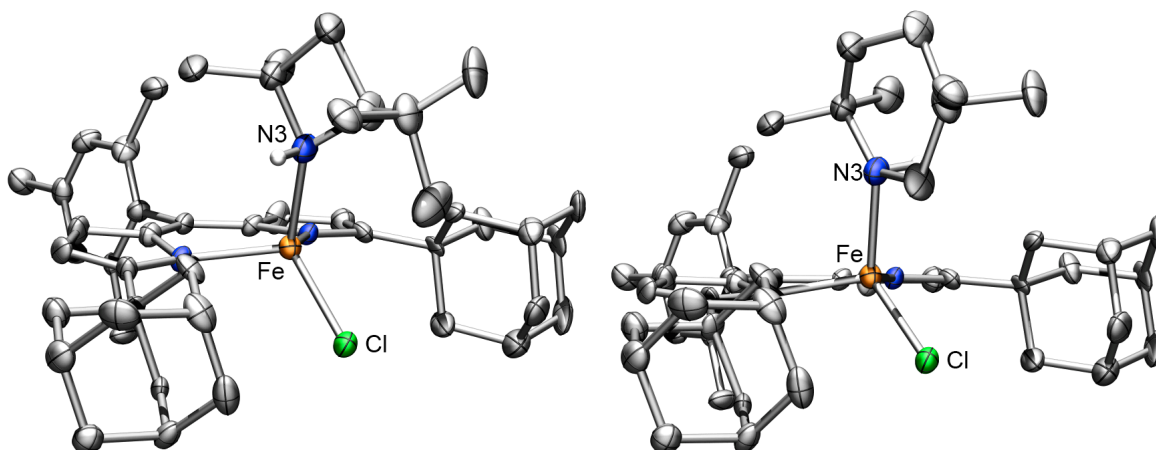
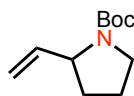


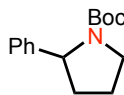
Figure 4.13. X-ray structures for 4.10, 4.11. **Right.** Solid-state molecular structure for 4.11 with thermal ellipsoids at 50% probability level. Hydrogens and second Fe complex in unit cell omitted for clarity. **Left.** Solid-state molecular structure for 4.10 with thermal ellipsoids at 50% probability level. Piperidine ring is at half occupancy, with the remaining electron density belonging to the half occupied 4-membered ring. Hydrogens, second Fe complex in unit cell, and disorder in Fe-bound heterocycle omitted for clarity.

4.7.6 Catalytic *N*-Heterocycle Forming Reactions

Under an inert N₂ atmosphere, (^{Ad}L_{Cl₂)FeCl(OEt₂) (**4.2**) (40.0 mg, 0.0556 mmol) and di-*tert*-butyl dicarbonate (1-10 equiv, depending on substrate) were added to a stirring solution of the desired azide (1-10 equiv, depending on substrate) in 3 mL of benzene in a 5 mL scintillation vial. The resultant inky, dark red solution was then transferred to a pressure vessel and heated to 65 °C for 12 hours. The reaction mixture was then flash chromatographed through a short pipette of deactivated silica gel using a 20:1 mixture of CH₂Cl₂ and MeOH as eluent to give a clear bright orange solution in order to remove paramagnetic materials. The solution was concentrated via rotary evaporation. The internal standard trimethoxybenzene or ferrocene (0.0556 mmol, 1 equiv) was added to the reaction mixture, followed by 1 mL of CDCl₃ in order to dissolve the contents of the entire flask into a homogenous solution. ¹H NMR yields were then determined via integration of the trimethoxybenzene or ferrocene peaks and the diagnostic α-H peaks of the newly formed *N*-heterocycle. The crude products were purified via silica gel chromatography using hexanes and ethyl acetate as eluent.}



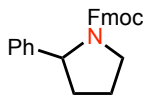
tert-Butyl 2-vinylpyrrolidine-1-carboxylate¹⁷⁴



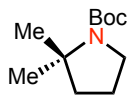
tert-Butyl 2-phenylpyrrolidine-1-carboxylate¹⁷⁵

173. For spectroscopic and physical characterization, see: Molander, G. A.; Romero, J. A. C. *Tetrahedron* **2005**, *61*, 2631.

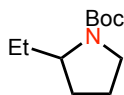
174. For spectroscopic and physical characterization, see: Barker, G.; O'Brien, P.; Campos, K. R. *Org. Lett.* **2010**, *12*, 4176.



(9H-fluoren-9-yl)methyl-2-phenylpyrrolidine-1-carboxylate: ^1H NMR (600 MHz, CDCl_3) δ (70:30 mixture of rotamers): 7.57–7.75 (m, 2 H), 7.00–7.47 (m, 11 H), 5.31 (s, 0.3 H), 4.99–5.06 (m, 0.7 H), 4.32–4.51 (m, 1.4 H), 4.23–4.30 (m, 0.3 H), 4.16–4.22 (m, 0.7 H), 3.97–4.03 (m, 0.6 H), 3.58–3.80 (m, 2 H), 2.25–2.45 (m, 1 H), 1.81–1.99 (m, 2 H), 1.70 – 1.83 (m, 1 H). $^{13}\text{C}\{\text{1H}\}$ NMR (125 MHz, CDCl_3) δ (rotamers): 155.3, 144.2, 144.0(143.9), 141.1(141.0), 128.6(128.4), 127.6, 127.4, 126.9(127.0), 125.4, 125.1(125.0), 119.9(119.7), 67.5(66.9), 61.0(61.2), 47.7(47.2), 35.8(36.8), 28.6, 22.5(23.6). IR (thin film) ν = 3064, 3029, 2971, 2902, 1702, 1451, 1414, 1348, 1270, 1245, 1114, 1031 cm^{-1} . HRMS (ESI⁺) m/z Calc. 360.4636 [$\text{C}_{23}\text{H}_{25}\text{NO}_2+\text{H}$]⁺, Found 370.4629 [M+H]⁺.

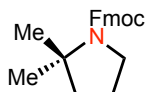


tert-Butyl 2,2-dimethylpyrrolidine-1-carboxylate: ^1H NMR (500 MHz, CDCl_3) δ (60:40 mixture of rotamers): 3.45 (t, J = 6.3 Hz, 1.2 H), 3.37 (br. s, 0.8 H), 1.80–1.74 (m, 4H), 1.48 (s, 5.4 H), 1.44 (s, 3.6 H), 1.39, (s, 2.4), 1.33 (s, 3.6 H). $^{13}\text{C}\{\text{1H}\}$ NMR (125 MHz, CDCl_3) δ (rotamers): 154.6, 79.0, 59.4(60.0), 48.1, 42.9(41.0), 36.7, 28.6, 27.1(27.4), 26.1, 21.6(22.0). IR (thin film) ν = 2968, 2930, 2873, 1696, 1392, 1180, 1152, 1069 cm^{-1} . GCMS (EI) t_R = 12.8 min; m/z : 199, 184, 166, 142, 128, 98, 84, 57, 41.

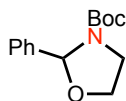


tert-butyl 2-ethylpyrrolidine-1-carboxylate: ^1H NMR (500 MHz, CDCl_3) δ : 3.59–3.78 (m, 1 H), 3.25–3.50 (m, 2 H), 1.74–1.98 (m, 4 H), 1.66 (br. s., 2 H), 1.47 (s, 9 H), 1.33 (br. s., 2 H), 0.87 (t, J = 1.0 Hz, 3 H). $^{13}\text{C}\{\text{1H}\}$ NMR (125 MHz, CDCl_3) δ : 154.7, 78.8, 58.6, 46.5(46.1),

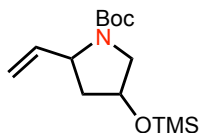
30.2(29.3), 28.5(28.4), 27.4(26.7, 26.5), 23.8(23.1, 22.6), 10.5. **IR** (thin film) $\nu = 2970, 2930, 1694, 1675, 1393, 1172, 1111, 913 \text{ cm}^{-1}$. **GCMS** (EI) m/z : $t_R = 7.40 \text{ min}$; 41, 57, 70, 84, 98, 114, 126, 144, 170, 199.



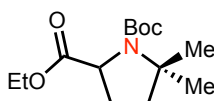
(9H-fluoren-9-yl)methyl 2,2-dimethylpyrrolidine-1-carboxylate: **^1H NMR** (500 MHz, CDCl_3) δ (65:35 mixture of rotamers): 7.73–7.81 (m, 2 H), 7.57–7.65 (m, 2 H), 7.35–7.44 (m, 2 H), 7.32 (m, 2 H), 4.68 (d, $J = 4.4 \text{ Hz}$, 0.7 H), 4.36 (d, $J = 7.3 \text{ Hz}$, 1 H), 4.25 (t, $J = 6.3 \text{ Hz}$, 1.3 H), 3.46–3.54 (m, 1.3 H), 3.41 (t, $J = 6.3 \text{ Hz}$, 0.7 H), 1.78–1.87 (m, 2 H), 1.60–1.70 (m, 2 H), 1.43 (s, 6 H), 1.22–1.35 (m, 2 H). **$^{13}\text{C}\{^1\text{H}\}$ NMR** (125 MHz, CDCl_3) δ (rotamers): 153.7, 144.3(144.4), 141.3(141.5), 127.5, 127.0, 125.1, 124.5, 119.9, 66.2(66.1), 60.7(59.8), 47.5(47.7), 41.7(42.8), 26.0(26.3), 22.2(21.7). **IR** (thin film) $\nu = 3066, 1042, 2964, 2895, 1701, 1451, 1406, 1350, 1151, 1083 \text{ cm}^{-1}$. **GCMS** (EI) m/z : $t_R = 15.4 \text{ min}$; 178, 153, 83, 55, 40.



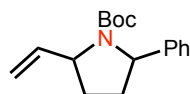
tert-butyl 2-phenyloxazolidine-3-carboxylate: *Note: The oxazolidine is unstable to moisture and silica gel. The reaction was worked up in the glove-box by trituration with pentane, filtration over Celite to remove Fe, and concentration of pentane filtrate.* **^1H NMR** (500 MHz, C_6D_6) δ : 7.89 (br. s, 1 H), 7.66 (br. s, 2 H), 7.07 (br. s, 3 H), 4.36 (br. s, 2 H), 3.53 (br. s, 2 H), 1.30 (s, 9 H). **$^{13}\text{C}\{^1\text{H}\}$ NMR** (100 MHz, C_6D_6) δ : 162.9, 154.5, 131.0, 129.0, 128.9, 128.7, 81.5, 66.9, 60.4, 28.0. **IR** (thin film) $\nu = 2979, 1740, 1649, 1279, 1254, 1162, 1119 \text{ cm}^{-1}$. **HRMS** (ESI⁺) m/z Calc. 250.1438 [$\text{C}_{38}\text{H}_{46}\text{N}_2+\text{H}$]⁺, Found 250.1445 [$\text{M}+\text{H}$]⁺.



tert-butyl 4-((trimethylsilyl)oxy)-2-vinylpyrrolidine-1-carboxylate: 176 ^1H NMR (500 MHz, C_6D_6) δ : 5.61–6.10 (m, 1 H), 4.89–5.27 (m, 2 H), 4.00–4.52 (m, 2 H), 3.09–3.81 (m, 2 H), 1.93–2.37 (m, 1 H), 1.65–1.90 (m, 1 H), 1.46 (br. s, 9 H), 0.12 (s, 9 H). $^{13}\text{C}\{1\text{H}\}$ NMR (125 MHz, C_6D_6) δ : 155.1, 140.4(139.7), 114.1, 79.6, 70.0(70.7, 69.4), 59.5(58.3), 54.4(55.1), 41.8(40.9), 28.7(29.9, 28.0), 0.22. IR (thin film) ν = 3082, 2993, 2981, 2933, 1699, 1479, 1455, 1394, 1366, 1252, 1172, 1113 cm^{-1} . HRMS (ESI $^+$) m/z Calc. 308.1658 [$\text{C}_{14}\text{H}_{27}\text{NO}_3\text{Si}+\text{Na}$] $^+$, Found 308.1629 [$\text{M}+\text{H}$] $^+$.



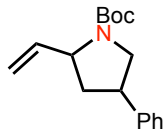
tert-butyl 2-ethyl 5,5-dimethylpyrrolidine-1,2-dicarboxylate: ^1H NMR (500 MHz, C_6D_6) δ (mixture of rotamers): 4.40 (dd, J = 8.8, 2.9 Hz, 0.6 H), 4.29 (dd, J = 9.0, 2.7 Hz, 0.4 H), 4.10–4.24 (m, 2 H), 2.08–2.21 (m, 1 H), 1.86 (s, 2 H), 1.70–1.81 (m, 1 H), 1.49 (s, 6 H), 1.39 (s, 9 H), 1.24–1.30 (m, 3 H). $^{13}\text{C}\{1\text{H}\}$ NMR (125 MHz, CDCl_3) (mixture of rotamers) δ : 173.6(173.1), 152.2(154.1), 79.8, 79.3, 61.6(61.5), 60.8(60.7), 40.8(40.0), 28.5(28.4), 27.4(26.8), 26.3(26.2), 25.9, 14.2(14.1). IR (thin film) ν = 2980, 2930, 1742, 1697, 1678 cm^{-1} . HRMS (ESI $^+$) m/z Calc. 294.1676 [$\text{C}_{14}\text{H}_{25}\text{N}_1\text{O}_4+\text{Na}$] $^+$, Found 294.1677 [$\text{M}+\text{Na}$] $^+$.



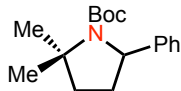
tert-butyl 2-phenyl-5-vinylpyrrolidine-1-carboxylate: ^1H NMR (500 MHz, d_6 -DMSO) δ (mixture of rotamers and diastereomers): 7.27–7.35 (m, 2 H), 7.10–7.26 (m, 3 H), 5.79–6.07 (m,

175. Azide substrate was prepared following the report in: Sinou, D.; Emziane, M. *Tetrahedron Lett.* **1986**, 27, 4423.

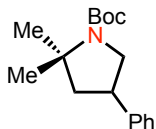
1 H), 5.16 (m, 2 H), 4.64–4.96 (m, 1 H), 4.26–4.61 (m, 1 H), 2.18–2.37 (m, 1 H), 1.94–2.07 (m, 1 H), 1.66–1.81 (m, 2 H), 0.99 – 1.42 (m, 9 H). $^{13}\text{C}\{\text{1H}\}$ NMR (125 MHz, d_6 -DMSO) δ (rotamers of diastereomers): 153.9(153.1, 152.8), 145.4(144.3), 139.6(139.1, 138.5), 128.3(128.1, 128.0), 126.3, 125.6, 125.2(125.1), 114.9(113.6), 78.4(78.0), 62.3(61.1), 60.3(59.8, 59.2), 34.4(33.4), 29.9, 28.3(27.8, 27.5). IR (thin film) ν = 3064, 3031, 2976, 2932, 1697, 1604, 1479, 1454, 1385, 1365, 1256, 1167, 1108 cm^{-1} . GCMS (EI) t_R = 8.92 min (diastereomer 1); m/z : 41, 57, 77, 91, 104, 129, 145, 163, 188, 207, 217. t_R = 8.96 min (diastereomer 2); m/z : 41, 57, 77, 91, 104, 129, 145, 163, 188, 207, 217.



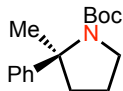
tert-butyl 4-phenyl-2-vinylpyrrolidine-1-carboxylate: ^1H NMR (500 MHz, d_6 -DMSO) δ (1.4:1 mixture of diastereomers): 7.27–7.36 (m, 3 H), 7.19–7.26 (m, 2 H), 5.76–5.94 (m, 1 H), 4.99–5.16 (m, 2 H), 4.30–4.46 (m, 0.65 H), 4.15–4.29 (m, 0.45 H), 3.90 (t, J = 8.3 Hz, 0.65 H), 3.71 (dd, J = 10.0, 8.1 Hz, 0.45 H), 3.09–3.32 (m, 2 H), 2.40–2.49 (m, 0.65 H), 2.14–2.27 (m, 0.45 H), 1.92–2.08 (m, 0.45 H), 1.70–1.86 (m, 0.65 H), 1.31–1.46 (br. s, 9 H). $^{13}\text{C}\{\text{1H}\}$ NMR (125 MHz, d_6 -DMSO) δ (diastereomers): 153.4, 140.5, 139.0, 128.4, 127.2, 126.6 114.2(113.9), 78.4(78.3), 60.1(59.8), 53.0(52.5), 41.8(40.2), 38.5(37.2), 28.1(27.4). IR (thin film) ν = 3368, 3084, 3064, 3030, 2976, 2932, 2876, 1695, 1604, 1479, 1456, 1396, 1255 cm^{-1} . GCMS (EI) t_R = 9.31 (diastereomer 1); m/z : 41, 57, 77, 91, 104, 129, 144, 172, 188, 217, 273; t_R = 9.41 min (diastereomer 2); m/z : 41, 57, 77, 91, 104, 129, 144, 172, 188, 217, 273.



tert-butyl 2,2-dimethyl-5-phenylpyrrolidine-1-carboxylate: $^1\text{H NMR}$ (500 MHz, CDCl_3) δ (mixture of rotamers): 7.30 (t, $J = 7.8$ Hz, 2 H), 7.20 (d, $J = 7.8$ Hz, 3 H), 5.07 (br. d, $J = 6.3$ Hz, 0.4 H), 4.87 (br. d, $J = 5.9$ Hz, 0.6 H), 2.31 (br. s, 1 H), 1.86 (br. s., 1 H), 1.64–1.76 (m, 2 H), 1.36–1.63 (m, 9 H), 1.14 (br. s, 6 H). $^{13}\text{C}\{^1\text{H}\}$ NMR (125 MHz, CDCl_3) δ (mixture of rotamers): 153.4, 145.6(144.3), 128.2(128.0), 126.2, 125.4, 79.3(78.6), 63.5(63.3), 61.3(59.9), 39.9(39.4), 32.2(31.5), 28.5(28.1), 27.0(26.2, 25.3), 22.4(22.2). IR (thin film) $\nu = 3047, 3029, 2968, 2931, 1695, 1454, 1364, 1247$ cm^{-1} . GCMS (EI) $t_{\text{R}} = 9.15$ min m/z : 41, 57, 82, 91, 104, 117, 128, 143, 160, 174, 204, 219, 260, 275.

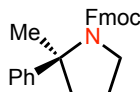


tert-butyl 2,2-dimethyl-4-phenylpyrrolidine-1-carboxylate: $^1\text{H NMR}$ (500 MHz, CDCl_3) δ : 7.29–7.37 (m, 2 H), 7.21–7.28 (m, 3 H), 3.84–4.06 (m, 1 H), 3.25–3.42 (m, 2 H), 1.95–2.21 (m, 2 H), 1.36–1.62 (m, 15 H). $^{13}\text{C}\{^1\text{H}\}$ NMR (125 MHz, CDCl_3) δ (mixture of rotamers): 154.3(153.2), 141.1(140.9), 128.5, 127.2(127.1), 126.7, 79.3(78.6), 60.6(60.0), 54.6(54.1), 50.2(49.2), 40.4(39.7), 28.6(28.5), 27.4(26.6, 25.6). IR (thin film) $\nu = 2964, 2932, 2872, 1733, 1674, 1404, 1375, 1250$ cm^{-1} . GCMS (EI) $t_{\text{R}} = 9.15$ min; m/z : 41, 57, 71, 91, 104, 128, 146, 160, 204, 218, 260, 275.

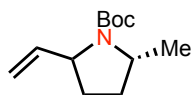


tert-butyl (S)-2-methyl-2-phenylpyrrolidine-1-carboxylate: $^1\text{H NMR}$ (600 MHz, CDCl_3) δ : 7.27–7.34 (m, 2 H), 7.23–7.27 (m, 1 H), 7.20 (d, $J = 6.4$ Hz, 2 H), 3.53–3.78 (m, 2 H), 1.98–2.15 (m, 2 H), 1.80–1.92 (m, 2 H), 1.76 (s, 3 H), 1.45 (s, 3 H), 1.13 (s, 6 H). $^{13}\text{C}\{^1\text{H}\}$ NMR (125

MHz, CDCl₃) δ (mixture of rotamers): 154.3, 148.4(146.9), 128.1(128.3), 125.9(126.0), 125.0(124.8), 79.0(78.8), 64.8(65.6), 48.6(48.7), 45.8(44.8), 28.1(28.5), 25.4(25.7), 22.0(21.8). **IR** (thin film) ν = 3060, 3026, 2973, 2930, 2876, 1688, 1601, 1494, 1479, 1447, 1392, 1366, 1255, 1163. **GCMS** (EI) t_R = 8.73 min; m/z : 41, 57, 77, 84, 103, 117, 128, 146, 160, 176, 190, 205, 216, 246, 261.

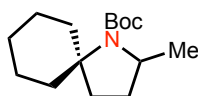


(9H-fluoren-9-yl)methyl (S)-2-methyl-2-phenylpyrrolidine-1-carboxylate: ¹H NMR (600 MHz, CDCl₃) δ : 7.80 (dd, J = 7.5, 3.4 Hz, 1 H), 7.62–7.70 (m, 2 H), 7.43 (q, J = 7.6 Hz, 1 H), 7.16–7.39 (m, 8 H), 6.91–7.15 (m, 2 H), 5.31 (s, 0.5 H), 4.36–4.54 (m, 1 H), 4.31 (d, J = 6.4 Hz, 1 H), 4.26 (t, J = 6.7 Hz, 0.5 H), 3.93 (t, J = 6.4 Hz, 0.5 H), 3.72–3.87 (m, 1 H), 3.62–3.71 (m, 1 H), 2.00–2.16 (m, 2 H), 1.69–1.90 (m, 5 H). ¹³C{**1H**} NMR (125 MHz, CDCl₃) δ (mixture of rotamers): 155.3(153.8), 147.2(146.4), 144.3(144.1, 143.9), 141.4(141.1), 128.4(128.2), 127.6(127.3), 127.0(126.9), 126.4(126.3), 125.0(124.9), 124.8(124.7), 119.9(119.7, 119.6), 67.2(66.3, 66.1, 65.4), 49.5(48.4, 47.6), 47.2(46.0, 44.5), 29.7, 26.2(25.5), 22.1(21.5). **IR** (thin film) ν = 3026, 2922, 1690, 1450, 1408, 1350, 1270, 1226, 1194, 1163, 1107, 1082, 1048, 1032. **HRMS** (ESI⁺) m/z Calc. 384.1964 [C₂₆H₂₆NO₂+H]⁺, Found 384.1976 [M+H]⁺. This material was determined to be 94% ee by chiral HPLC analysis (ChiralPak AS-H, 5% IPA in hexanes, 1 mL/min, 254nm, t_r (major) = 14.0 min, t_r (minor) = 16.6 min).

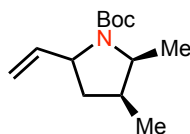


tert-Butyl 5-methyl-2-vinylpyrrolidine-1-carboxylate: ¹H NMR (500 MHz, *d*₆-DMSO) δ (syn:anti(+rotamers) 1.0:0.9): 5.65–5.83 (m, 1 H), 4.85–5.10 (m, 2 H), 4.11–4.27 (m, 1 H), 3.68–3.92 (m, 1 H), 1.85–2.18 (m, 2 H), 1.52–1.70 (m, 1 H), 1.45 (m, 1 H), 1.31–1.40 (br.s, 9 H), 1.17

(d, $J=6.3$ Hz, 3 H). $^{13}\text{C}\{\mathbf{1H}\}$ NMR (125 MHz, d_6 -DMSO) δ (diastereomer[rotamer]): 153.6(153.0[152.7]), 140.4(139.1[138.4]), 113.6(113.1), 78.0(77.9), 60.0(59.2[58.3]), 53.6(52.5[52.4]), 29.7(31.2), 28.8(28.6), 28.1(28.0), 19.3(20.4[21.0]). IR (thin film) $\nu = 3043, 2977, 1686, 1390, 1285, 1174, 698$ cm^{-1} . GCMS (EI) $t_{\text{R}} = 7.38$ min (syn diastereomer); m/z : 41, 57, 70, 96, 110, 140, 155, 168, 193, 211; $t_{\text{R}} = 7.41$ min (antidiastereomer); m/z : 41, 57, 70, 96, 110, 140, 155, 170, 191, 211. This material was determined to be 72% ee by chiral GC analysis (β -Cyclosil, 70 $^{\circ}\text{C}$ –100 $^{\circ}\text{C}$, 7 psi, t_{r} (major) = 79.1 min, t_{r} (minor) = 79.8 min).

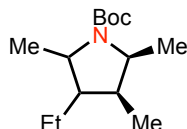


tert-butyl 2-methyl-1-azaspiro[4.5]decane-1-carboxylate: ^1H NMR (500 MHz, d_6 -DMSO) δ (2:1 mixture of rotamers): 4.03–4.14 (m, 0.5 H), 3.91–4.02 (m, 1 H), 2.64–2.81 (m, 1 H), 2.41–2.56 (m, 0.5 H), 2.29–2.40 (m, 1 H), 2.04–2.17 (m, 3 H), 1.80–1.94 (m, 1 H), 1.63–1.74 (m, 3.5 H), 1.39–1.52 (m, 13.5 H), 1.19–1.37 (m, 9 H), 1.13 (br. s., 4.5 H). $^{13}\text{C}\{\mathbf{1H}\}$ NMR (125 MHz, d_6 -DMSO) δ (2:1 mixture of rotamers): 153.4(152.3), 78.3(79.0), 64.7(64.2), 54.7, 37.2(38.2), 33.5(34.6), 30.8(32.1), 28.7(29.1), 25.0(25.4), 24.5(24.3), 21.2(20.4) IR (thin film) $\nu = 2970, 2927, 2866, 1692, 1456, 1367, 1322, 1301, 1255$ cm^{-1} . GCMS (EI) $t_{\text{R}} = 8.40$ min; m/z : 41, 57, 82, 97, 110, 141, 154, 180, 197, 253.

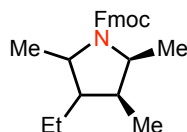


tert-Butyl 2,3-dimethyl-5-vinylpyrrolidine-1-carboxylate: ^1H NMR (500 MHz, d_6 -DMSO) δ (overlapping diastereomers and rotamers): 5.62–5.85 (m, 1 H), 4.87–5.08 (m, 2 H), 3.97–4.20 (m, 1 H), 3.82 (s, 1 H), 2.13 (br. s., 2 H), 1.54–1.87 (m, 1 H), 1.30–1.44 (m, 9 H), 0.94 (m, 3 H), 0.89 (d, $J = 6.9$ Hz, 3 H). $^{13}\text{C}\{\mathbf{1H}\}$ NMR (125 MHz, d_6 -DMSO) δ (diastereomer[rotamer]): 151.9,

141.6(139.8[139.1]), 113.4(113.1[113.0]), 78.0, 59.4(58.4[57.7]), 56.5(55.8[55.4]), 38.2(36.4[35.2]), 34.5(33.1[32.2]), 28.1, 15.2(14.4[13.7]), 13.9(13.6[13.3]). **IR** (thin film) $\nu = 2974, 2935, 2877, 1680, 1477, 1457, 1395, 1256, 1175 \text{ cm}^{-1}$. **GCMS** (EI) $t_R = 7.58 \text{ min}$ (major diastereomer); m/z : 41, 57, 83, 110, 124, 154, 169, 225; $t_R = 7.61 \text{ min}$ (minor diastereomer); m/z : 41, 57, 83, 110, 124, 154, 169, 225.

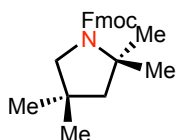


tert-Butyl 3-ethyl-2,4,5-trimethylpyrrolidine-1-carboxylate: **^1H NMR** (500 MHz, d_6 -DMSO) δ (mixture of 4 diastereomers): 4.06–4.12 (m, 0.2 H), 3.62–3.85 (m, 0.8 H), 3.46–3.60 (m, 0.3 H), 3.07–3.30 (m, 0.7 H), 1.65–1.98 (m, 1 H), 1.47–1.60 (m, 1 H), 1.39 (s, 9 H), 1.29–1.35 (m, 6 H), 1.23 (d, $J = 6.0 \text{ Hz}$, 3 H), 0.95 (d, $J = 6.4 \text{ Hz}$, 3 H), 0.81–0.92 (m, 3H). **$^{13}\text{C}\{^1\text{H}\}$ NMR** difficult to analyze due to mixture of diastereomers, synthesized Fmoc protected pyrrolidine (using FmocOSu and 2) and fully characterized this derivative. **IR** (thin film) $\nu = 2972, 2934, 2876, 1682, 1460, 1395, 1299, 1247, 1178 \text{ cm}^{-1}$. **GCMS** (EI) $t_R = 7.83 \text{ min}$ (major diastereomer); m/z : 41, 57, 71, 97, 115, 126, 140, 154, 170, 184, 225, 241; $t_R = 7.90 \text{ min}$ (diastereomer 2); m/z : 41, 57, 71, 97, 115, 126, 140, 154, 170, 184, 225, 241; $t_R = 8.00 \text{ min}$ (diastereomer 3); m/z : 41, 57, 71, 97, 115, 126, 140, 154, 170, 184, 225, 241; $t_R = 8.04 \text{ min}$ (minor diastereomer); m/z : 41, 57, 71, 97, 115, 126, 140, 154, 170, 184, 225, 241.

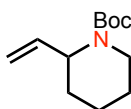


(9H-fluoren-9-yl)methyl 3-ethyl-2,4,5-trimethylpyrrolidine-1-carboxylate: Yield: 84%. **^1H NMR** (600 MHz, CDCl_3) δ (mixture of rotamers): 7.77 (d, $J = 7.3 \text{ Hz}$, 2 H), 7.62 (br. s., 2 H), 7.37–7.43 (m, 2 H), 7.29–7.36 (m, 2 H), 4.33–4.65 (m, 2 H), 4.26 (t, $J = 6.3 \text{ Hz}$, 1 H), 3.82–4.07

(m, 1 H), 3.18–3.81 (m, 3 H), 2.18 (s, 1 H), 1.66–2.04 (m, 1 H), 1.39–1.66 (m, 3 H), 0.83–1.37 (m, 11 H). $^{13}\text{C}\{\text{1H}\}$ NMR (125 MHz, CDCl_3) δ (mixture of rotamers): 154.8(154.7), 144.4(144.3), 141.4, 127.5, 126.9, 125.0, 119.9, 66.5(66.3), 57.3(58.5, 58.2, 56.2), 51.7(51.4, 51.0), 47.6(47.0, 46.1), 40.4(40.1), 37.0(36.7, 35.9), 29.7(31.6), 23.8(22.7, 21.7), 16.2(15.8, 14.4), 13.1, 11.4. IR (thin film) ν = 3066, 3041, 3018, 2964, 1933, 1696, 1559, 1540, 1451, 1409, 1340, 1293, 1117, 1058. HRMS (ESI⁺) m/z Calc. 364.2277 [$\text{C}_{24}\text{H}_{29}\text{NO}_2+\text{H}$]⁺, Found 364.2214 [$\text{M}+\text{H}$]⁺.

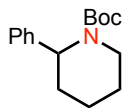


(9H-fluoren-9-yl)methyl 2,2,4,4-tetramethylpyrrolidine-1-carboxylate: ^1H NMR (600 MHz, CDCl_3) δ (1.3:0.7 mixture of rotamers): 7.72–7.82 (m, 2 H), 7.57–7.65 (m, 2 H), 7.28 – 7.46 (m, 4 H), 4.69 (d, J = 4.4 Hz, 0.7 H), 4.36 (d, J = 7.3 Hz, 1.3 H), 4.22– 4.30 (m, 1 H), 3.29 (s, 1.3 H), 3.21 (s, 0.7 H), 1.76 (s, 1.3 H), 1.61 (s, 0.7 H), 1.49 (br. s., 3.9 H), 1.15 (br. s., 3.9 H), 1.02 (s, 2.1 H), 0.85 (s, 2.1 H). $^{13}\text{C}\{\text{1H}\}$ NMR (125 MHz, CDCl_3) δ (mixture of rotamers): 153.9(155.2), 144.3(144.4), 127.8(127.5), 127.0(126.9), 125.1(124.5), 119.9(119.8), 66.2(66.1), 61.3(60.9), 60.4(60.2), 55.7(56.9), 47.5(41.8), 35.8(35.1), 28.0(28.2), 27.8(27.9). IR (thin film) ν = 3067, 3041, 4018, 2955, 2926, 2868, 1703, 1559, 1450, 1405, 1350, 1167. HRMS (ESI⁺) m/z Calc. 372.1934 [$\text{C}_{23}\text{H}_{28}\text{NO}_2+\text{Na}$]⁺, Found 372.1946 [$\text{M}+\text{Na}$]⁺.

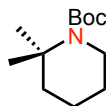


tert-butyl 2-vinylpiperidine-1-carboxylate¹⁷⁷

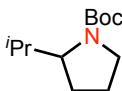
176. For spectroscopic and physical characterization, see: Hassner, A.; Maurya, R.; Padwa, A.; Bullock, W. H. *J. Org. Chem.* **1991**, *56*, 2775.



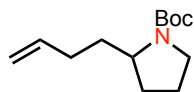
tert-butyl 2-phenylpiperidine-1-carboxylate¹⁷⁸



tert-butyl 2,2-dimethylpiperidine-1-carboxylate¹⁷⁹



tert-butyl 2-isopropylpyrrolidine-1-carboxylate¹⁸⁰



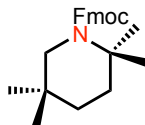
tert-butyl 2-(but-3-enyl)pyrrolidine-1-carboxylate: ¹H NMR (500 MHz, CDCl₃) δ: 5.73–5.89 (m, 1 H), 5.02 (d, *J* = 17.3 Hz, 1 H), 4.89–4.98 (m, 1 H), 3.67–3.87 (m, 1 H), 3.23–3.46 (m, 2 H), 2.04 (br. s., 2 H), 1.73–1.97 (m, 4 H), 1.66 (br. s., 2 H), 1.46 (s, 9 H). ¹³C{¹H} NMR (125 MHz, CDCl₃) (rotamers) δ: 154.6, 138.3, 114.4(114.2), 79.0, 56.7, 46.4(46.1), 34.6(34.5), 33.8(33.3), 30.7(29.7), 28.5(28.4), 25.3(23.7) 20.7(20.4). **IR** (thin film) ν = 3077, 2974, 2929, 1696, 1393, 1365, 1250, 1171, 1108, 909 cm⁻¹. **GCMS** (EI) *m/z*: *t*_R = 7.83 min; 41, 57, 70, 96, 110, 114, 127, 140, 169, 183.

In order to assist in chromatographic separation of isomers, the UV-active Fmoc-OSuc protecting reagent was used rather than the Boc₂O reported in main text.

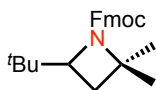
177. For spectroscopic and physical characterization, see: Andersson, H.; Gustafsson, M.; Bostrom, D.; Olsson, R.; Almqvist, F. *Angew. Chem., Int. Ed.* **2009**, *48*, 3288.

178. For spectroscopic and physical characterization, see: Wolckenhauer, S. A.; Rychnovsky, S. D. *Org. Lett.* **2004**, *6*, 2745.

179. For spectroscopic and physical characterization, see: Snead, D. R.; Inagaki, S.; Abboud, K. A.; Hong, S. *Organometallics* **2010**, *29*, 1729.



(9H-fluoren-9-yl)methyl 2,2,5,5-tetramethylpiperidine-1-carboxylate: $^1\text{H NMR}$ (600 MHz, CDCl_3) δ : 7.75 (d, $J = 7.6$ Hz, 2 H), 7.59 (dd, $J = 7.6, 0.9$ Hz, 2 H), 7.27–7.42 (m, 4 H), 4.40–4.51 (m, 2 H), 4.18–4.27 (m, 1 H), 3.02 (s, 2 H), 1.43 (s, 2 H), 1.20–1.34 (m, 8 H), 0.87 (s, 6 H). $^{13}\text{C}\{^1\text{H}\}$ NMR (125 MHz, CDCl_3) δ : 154.2, 144.4, 141.4, 127.5, 126.9, 124.8, 119.9, 66.3, 54.7, 52.2, 27.5, 37.0, 33.0, 29.7, 27.3, 25.8. **IR** (thin film) $\nu = 3067, 3042, 3018, 2954, 2931, 2867, 1703, 1478, 1451, 1403, 1367, 1289, 1199, 1186, 1105, 1079$. **HRMS** (ESI $^+$) m/z Calc. 402.1830 $[\text{C}_{24}\text{H}_{29}\text{NO}_2+\text{K}]^+$, Found 402.1827 $[\text{M}+\text{K}]^+$.



(9H-fluoren-9-yl)methyl 4-(tert-butyl)-2,2-dimethylazetidide-1-carboxylate: $^1\text{H NMR}$ (600 MHz, CDCl_3) δ : 7.76 (dd, $J = 7.3, 3.2$ Hz, 2 H), 7.61 (t, $J = 6.6$ Hz, 6 H), 7.36–7.42 (m, 2 H), 7.29–7.35 (m, 2 H), 4.60–4.77 (m, 0.7 H), 4.33–4.52 (m, 1.3 H), 4.20 – 4.29 (m, 1 H), 3.65 – 3.94 (m, 0.6 H), 3.03 (s, 0.4 H), 1.75 (d, $J = 7.3$ Hz, 2 H), 1.26 (s, 3 H), 0.97 – 1.11 (m, 3 H), 0.84 – 0.95 (m, 9 H). $^{13}\text{C}\{^1\text{H}\}$ NMR (125 MHz, CDCl_3) δ (mixture of rotamers): 153.9 (154.2), 144.3, 141.5, 127.5, 127.0, 124.8(124.7), 119.9(119.8), 65.5(66.3), 52.2, 47.5, 36.9, 33.5(33.2), 29.7(30.6), 27.3(27.0), 26.1(25.7). **IR** (thin film) $\nu = 3067, 3042, 3018, 2960, 2904, 1699, 1558, 1451, 1397, 1368, 1329, 1264, 1220, 1200, 1168, 1131$. **HRMS** (ESI $^+$) m/z Calc. 364.2271 $[\text{C}_{24}\text{H}_{29}\text{NO}_2+\text{H}]^+$, Found 364.2287 $[\text{M}+\text{H}]^+$.

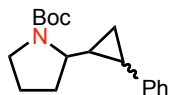
4.7.7 ¹H NMR Experiment to Monitor Activation of 1° and 3° C–H Bonds

Under an inert N₂ atmosphere, (^{Ad}L_{Cl₂})FeCl(OEt₂) (20.0 mg, 0.0278 mmol) was dissolved in 1 mL C₆D₆ and transferred to an NMR tube. The dark red solution was frozen in a liquid nitrogen cooled cold well. A solution of desired azide (1 drop) in C₆D₆ (~0.25 mL) was placed atop the frozen layer in the NMR tube and then re-deposited in cold well. Once both layered solutions were completely frozen, the NMR tube was capped and removed from the dry box and placed in a -78 °C dewer for transport. The NMR tube was immediately placed in the spectrometer and spectra were taken at various time points.

4.7.8 Kinetic Isotope Experiment

Under an inert N₂ atmosphere, (^{Ad}L_{Cl₂})FeCl(OEt₂) (20.0 mg, 0.0278 mmol) and di-*tert*-butyl dicarbonate (60.9 mg, 0.278 mmol, 10 equiv.) were added to a stirring solution of 4-azido-1-deutero-1-phenylbutane (49.0 mg, 0.278 mmol, 10 equiv) in 3 mL of benzene in a 5 mL scintillation vial. The resultant inky, dark red solution was then transferred to a 25 mL storage vessel and heated to 65 °C in an oil bath for 12 hours. The reaction mixture was then flash chromatographed through a short pipette of deactivated silica gel using a 20:1 mixture of CH₂Cl₂ and MeOH as eluent to give a clear bright orange solution. The ratio of k_H/k_D was determined by ¹H NMR integration of the methine proton against the methylene protons at the 2- and 4-positions respectively.

4.7.9 Radical Clock Experiment



Under an inert N₂ atmosphere, (^AdL_{Cl2})FeCl(OEt₂) (40.0 mg, 0.0555 mmol) and di-*tert*-butyl dicarbonate (60.9 mg, 0.278 mmol, 5 equiv.) were added to a stirring solution of 4-(2-phenylcyclopropyl)-1-azidobutane (60.0 mg, 0.278 mmol, 5 equiv) in 3 mL of benzene in a 25 mL storage vessel. The resultant inky, dark red solution was removed from the glove box and placed in a 65 °C oil bath for 12 hours. The reaction mixture was then purified by silica gel chromatography to isolate the cyclopropyl-substituted pyrrolidine as the major product (58.2 mg, 73%). ¹H NMR (600 MHz, CDCl₃) δ: 7.22–7.30 (m, 2 H), 7.12–7.20 (m, 1 H), 7.05 (d, *J* = 8.2 Hz, 2 H), 3.04–3.85 (m, 3 H), 1.68–2.22 (m, 4 H), 1.46–1.66 (m, 9 H), 1.44 (d, *J* = 6.7 Hz, 1 H), 0.78–1.24 (m, 3 H). ¹³C{¹H} NMR (125 MHz, CDCl₃) δ(mixture of rotamers): 155.1(154.9), 138.8, 128.7(128.3), 128.0, 125.7(125.4), 79.2, 60.4(57.3), 46.6, 31.6, 28.6, 24.3, 23.2, 20.2, 16.1(15.8), 9.6. IR (thin film) ν = 3082, 3028, 2975, 2929, 1692, 1604, 1497, 1454, 1391, 1370, 1248, 1168, 1109. GCMS (EI) *m/z*: *t*_R = 12.5 min; 57, 70, 83, 96, 104, 114, 127, 143, 164, 186, 214, 231; *t*_R = 12.6 min; 57, 70, 83, 91, 104, 114, 127, 140, 156, 164, 186, 214, 231.

4.7.10 X-Ray Diffraction Techniques

For equipment and software details, see Section 2.6.6.

(^AdL_{Cl2})FeCl(OEt₂) (**4.2**) The structure was solved in the monoclinic space group *P*2₁/*n* with 4 molecules per unit cell. The structure exhibited full body disorder and was refined using similarity constraints.

(^{Ad}L_{Mes})FeCl(2-phenylpyrrolidine) (4.3) The structure was solved in the monoclinic space group *C2/c* with 8 molecules per unit cell. The crystal was twinned. The phenyl pyrrolidine fragment exhibited positional disorder and was refined using similarity constraints.

(^{Ad}L_{Mes})FeCl(2-vinylpyrrolidine) (4.4) The structure was solved in the monoclinic space group *P2₁/n* with 4 molecules per unit cell. The vinyl pyrrolidine fragment exhibited positional disorder and was refined using similarity constraints.

(^{Ad}L_{Mes})FeCl(2-ethylpyrrolidine) (4.6) The structure was solved in the monoclinic space group *P2₁/n* with 4 molecules per unit cell. The ethyl pyrrolidine fragment exhibited positional disorder and was refined using similarity constraints.

(^{Ad}L_{Cl2})FeCl(2,2-dimethylpyrrolidine) (4.7) The structure was solved in the orthorhombic space group *Pnma* with 8 molecules per unit cell.

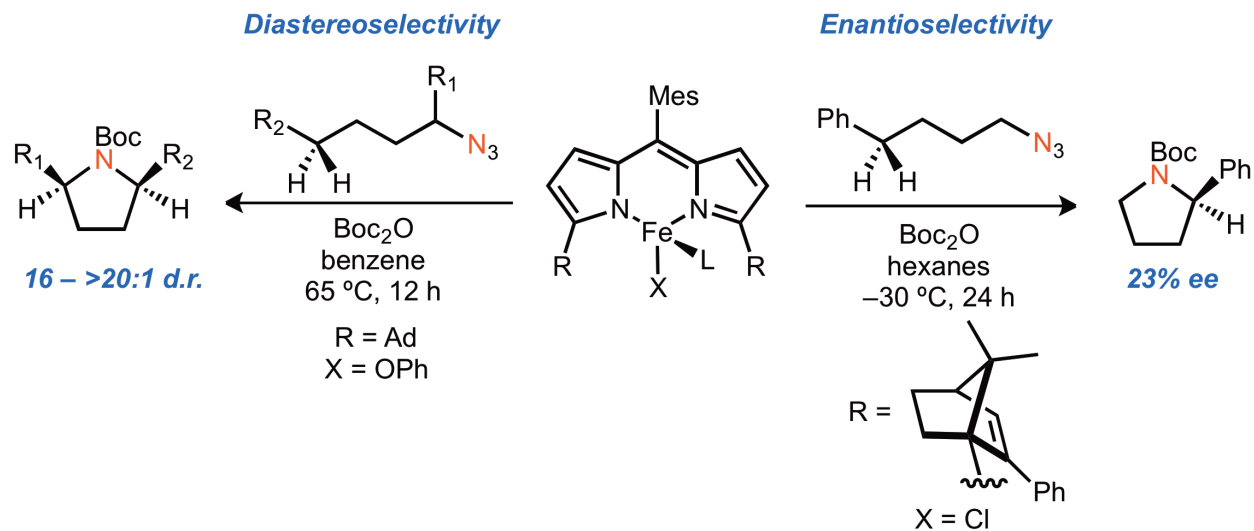
(^{Ad}L_{Mes})FeCl((*S*)-2-methyl-2-phenylpyrrolidine) (4.8) The structure was solved in the orthorhombic space group *P2₁2₁2₁* with 4 molecules per unit cell.

(^{Ad}L_{Mes})FeCl(2-vinylpiperidine) (4.9) The structure was solved in the monoclinic space group *P2₁/n* with 4 molecules per unit cell. The vinyl piperidine fragment exhibited positional disorder and was refined using similarity constraints.

(^{Ad}L_{Mes})FeCl(2,2-dimethyl-4,4-dimethylpiperidine)+(2,2-dimethyl-4-*tert*-butylazetidine) (4.10, 4.11) The structure was solved in the monoclinic space group *P2₁* with 2 molecules per unit cell. One Fe in the asymmetric unit is solely bound to the azetidine ring. The second Fe in the asymmetric unit exhibits occupational disorder between the azetidine and piperidine rings. The occupancy between the two bound heterocycles was freely refined.

Table 4.3. X-ray crystallographic experimental properties.^{a,b}

	4.4	4.3	4.6	4.9	4.2	4.7	4.10+4.11	4.8
CCDC Deposit Number	905455	905456	905457	905460	905454	905458	905461	905459
Moiety Formula	C ₄₄ H ₅₆ ClFeN ₃	C ₄₈ H ₆₀ ClFeN ₃	C ₄₄ H ₅₈ ClFeN ₃	C ₄₅ H ₅₈ ClFeN ₃	C ₃₉ H ₄₇ Cl ₃ FeN ₂ O	C ₄₁ H ₅₀ Cl ₃ FeN ₃	C ₉₄ H ₁₂₈ Cl ₂ Fe ₂ N ₆	C ₄₉ H ₆₀ ClFeN ₃
FW	718.22	770.29	720.23	732.24	721.99	747.04	1524.62	782.30
Crystal System	mono clinic	mono clinic	mono clinic	mono clinic	mono clinic	ortho rhombic	mono clinic	ortho rhombic
Space Group (Z)	P2 ₁ /c (4)	C2/c (8)	P2 ₁ /c (4)	P2 ₁ /c (4)	P2 ₁ /c (4)	Pnma (4)	P2 ₁ (2)	P2 ₁ 2 ₁ 2 ₁ (4)
a (Å)	17.052(4)	20.1132(7)	13.4207(9)	17.4113(12)	21.431(3)	15.6799(19)	11.747(3)	14.9212(2)
b (Å)	19.164(4)	15.9506(5)	22.3138(15)	19.5961(14)	12.2933(15)	17.639(2)	21.852(6)	16.2956(2)
c (Å)	11.793(3)	24.4531(8)	13.0454(10)	11.7524(8)	14.2350(17)	13.0347(16)	16.318(4)	16.6843(2)
α (°)	90	90	90	90	90	90	90	90
β (°)	108.058(4)	96.583(2)	117.379(1)	107.709(1)	107.720(2)	90	104.774(5)	90
γ (°)	90	90	90	90	90	90	90	90
Volume (Å ³)	3663.9(13)	7783.3(2)	3735.0(4)	3819.8(5)	3572.5(7)	3605.1(7)	4050.4(19)	4056.79(9)
Calc. ρ (mg/m ³)	1.302	1.315	1.281	1.278	1.342	1.376	1.250	1.281
μ (mm ⁻¹)	0.52	4.02	0.51	0.50	0.680	0.68	0.48	3.87
Crystal Size (mm)	0.28×0.02×0.020.24×0.19×0.180.22×0.18×0.090.3×0.15×0.020.4×0.15×0.120.21×0.16×0.050.24×0.11×0.060.07×0.07×0.06							
Reflections	7036	10637	9940	7287	6804	3562	14083	7060
GOF on F ²	1.006	1.048	1.062	1.018	1.036	1.04	1.08	1.05
R1, wR2 [§] [I>2σ(I)]	0.0603, 0.1420	0.0449, 0.1120	0.0541, 0.1331	0.0544, 0.1380	0.0621, 0.1611	0.043, 0.112	0.067, 0.117	0.050, 0.123
Flack parameter	-0.018(5)							



Chapter 5: Advances in the Diastereoselectivity and Enantioselectivity of *N*-Heterocycle Formation

5.1 Introduction

Pyrrolidines, piperidines, and other saturated *N*-heterocycles are common structures in both natural products and pharmaceuticals.^{181,182} Additionally, *N*-heterocyclic units are critical components of organocatalysts¹⁸³ and ligands¹⁸⁴ for transition metals. As such, efficient generation of *N*-heterocycles has been of interest since the turn of the twentieth century. In 1906, Hofmann, Löffler, and Freytag developed a pyrrolidine synthesis derived from *N*-halogenated alkylamines.¹⁶² Irradiation of the *N*-haloamine under strongly acidic conditions generates a *N*-based radical that abstracts a H-atom from the δ -carbon and ultimately cyclizes to form the cyclic amine.

180. Michael, J. P. *Nat. Prod. Rep.* **2005**, *22*, 603.

181. O'Hagan, D. *Nat. Prod. Rep.* **2000**, *17*, 435.

182. Dalko, P. I.; Moisan, L. *Angew. Chem., Int. Ed.* **2004**, *43*, 5138.

Over the past 15 years, research has targeted the discovery of more tolerant and selective transition metal-catalyzed methods for *N*-heterocycle formation.^{185,186} Asymmetric reductions of cyclic enamines, pyrroles, and succinimides have proven to be simple and successful ways of accessing the saturated *N*-heterocycle counterparts with good enantioselectivities.¹⁸⁷⁻¹⁹⁰ Following the development of Overman's Aza-cope Mannich cascade to generate 3-acylpyrrolidines¹⁹¹ various classes of pericyclic reactions yielding highly substituted pyrrolidines with excellent stereocontrol have been developed.^{192,193} Intramolecular hydroamination,¹⁹⁴⁻¹⁹⁶ and aza-Wacker reactions¹⁹⁷ have dominated the pyrrolidine and piperidine literature, but there are few established asymmetric variants.¹⁹⁴ Additionally, recent advances in the C-H functionalization

183. Fache, F.; Schulz, E.; Tommasino, M. L.; Lemaire, M. *Chem. Rev.* **2000**, *100*, 2159.

184. Nakamura, I.; Yamamoto, Y. *Chem. Rev.* **2004**, *104*, 2127.

185. Patil, N. T.; Yamamoto, Y. *Chem. Rev.* **2008**, *108*, 3395.

186. Wojcik, B.; Adkins, H. *J. Am. Chem. Soc.* **1934**, *56*, 2419.

187. Karrer, P.; Portmann, P. *Helv. Chim. Acta* **1948**, *31*, 2088.

188. Hou, G.-H.; Xie, J.-H.; Yan, P.-C.; Zhou, Q.-L. *J. Am. Chem. Soc.* **2009**, *131*, 1366.

189. Jiang, C.; Frontier, A. *J. Org. Lett.* **2007**, *9*, 4939.

190. Overman, L. E.; Kakimoto, M.-A. *J. Am. Chem. Soc.* **1979**, *101*, 1310.

191. Rhee, J. U.; Krische, M. J. *J. Am. Chem. Soc.* **2006**, *128*, 10674.

192. Trost, B. M.; Silverman, S. M. *J. Am. Chem. Soc.* **2012**, *134*, 4941.

193. An example of an enantioselective hydroamination reaction: LaLonde, R. L.; Sherry, B. D.; Kang, E. J.; Toste, F. D. *J. Am. Chem. Soc.* **2007**, *129*, 2452.

194. Shen, H. C. *Tetrahedron* **2008**, *64*, 3885.

195. Pronin, S. V.; Tabor, M. G.; Jansen, D. J.; Shenvi, R. A. *J. Am. Chem. Soc.* **2012**, *134*, 2012.

196. Kotov, V.; Scarborough, C. C.; Stahl, S. S. *Inorg. Chem.* **2007**, *46*, 1910.

chemistry of high-valent Pd-complexes has led several groups to explore the potential to form saturated *N*-heterocycles via oxidative addition and reductive elimination pathways.^{198,199}

C–N bond formation from metal-nitrenoid intermediates has also been a significant area of research. Driver and co-workers have extended dirhodium nitrenoid chemistry to indole and indoline formation using aryl azides as the nitrene precursor. Azide decomposition to form a Rh-bound nitrenoid initiates a 4π -electron, 5-atom electrocyclization resulting in a new C–N bond.¹⁵⁴ More recently, Driver has employed FeBr₂ in concert with aryl azides to promote intramolecular C–H amination of ethereal C–H bonds to give indole products via hydride transfer, followed by amine attack of the resultant oxocarbenium ion.¹⁵⁶ Similarly, in 2010, Che and co-workers discovered that Fe-porphyrin complexes could catalyze indole formation from aryl azide substrates, albeit through an H-atom abstraction/radical rebound mechanism.²⁰⁰

Despite advances in transition metal-catalyzed *N*-heterocycle formation, the ability to construct C–N bonds in a single operation from a minimally decorated alkyl chain in a single operation is still epitomized by the Hofman-Löffler-Freytag reaction. Because the reaction requires strongly acidic conditions and generates promiscuous radical intermediates, it has not been implemented broadly in chemical synthesis.²⁰¹ C–H amination using high spin Fe-dipyrrinato complexes and organic azides provides a synthetically appealing analog to this reaction. As discussed in Chapter 4, we have developed an intramolecular C–H amination/cyclization reaction that allows access to a wide range of substituted pyrrolidine and

197. Nadres, E. T.; Daugulis, O. *J. Am. Chem. Soc.* **2012**, *134*, 7.

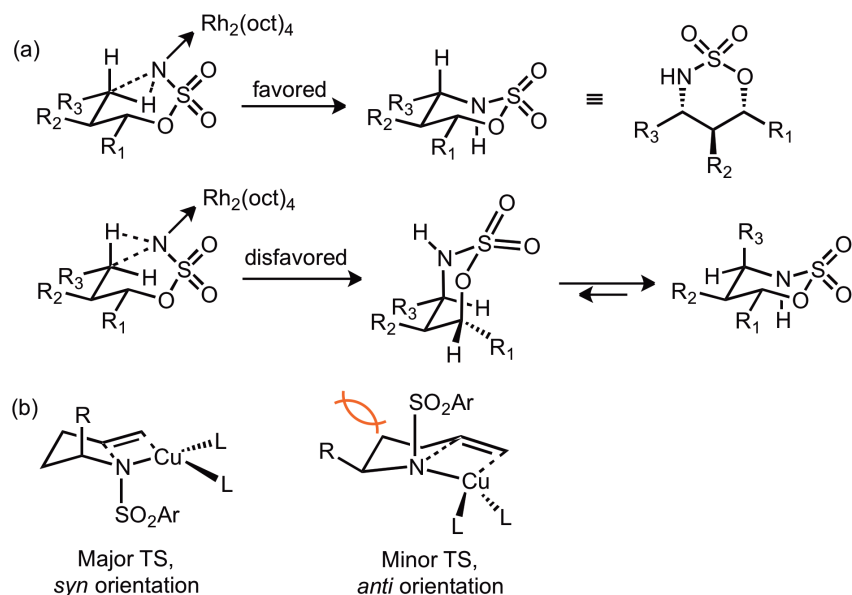
198. He, G.; Zhao, Y.; Zhang, S.; Lu, C.; Chen, G. *J. Am. Chem. Soc.* **2012**, *134*, 3.

199. Liu, Y.; Wei, J.; Che, C.-M. *Chem. Commun.* **2010**, *46*, 6926.

200. Modifications have been made to run the reaction under milder conditions, most successfully: Hernández, R.; Rivera, A.; Salazar, J. A.; Suárez, E. *J. Chem. Soc., Chem. Commun.* **1980**, 958.

piperidine structures from simple linear alkyl azide precursors under mild conditions. Herein we report the recent advances towards enhancing the functional group tolerance, diastereoselectivity, and enantioselectivity of the reaction.

5.2 Diastereoselective *N*-Heterocycle Formation²⁰²



Scheme 5.1. Stereochemical models for predicting diastereoselectivity. (a) $\text{Rh}_2(\text{oct})_4$ catalyzed C–H insertion proceeds through a chair-like transition state, placing each substituent in pseudo-equatorial positions. (b) $\text{Cu}(\text{II})$ -catalyzed carboamination of alkenes requires a trans orientation of substituent R at α -carbon and sulfonyl group, ultimately resulting in a favored *syn* orientation of substituents in pyrrolidine product.

In efforts to gear our catalysis towards the formation of more synthetically attractive products with higher levels of stereocontrol, we investigated the design elements that dictate the diastereoselectivity of cyclization. Typically, *N*-heterocycle cyclizations occur via chair-like transition states in the absence of any over-riding external factors. Therefore, 2,5-disubstitution innately favors an *anti*-orientation and 2,4-disubstitution favors a *syn* orientation. Indeed, the $\text{Rh}_2(\text{oct})_4$ catalyzed C–H amination and cyclization reactions of chiral sulfamates afford high stereocontrol, dictated solely by staggering groups in equatorial positions, minimizing the gauche

201. This section describes work done in collaboration with Diana Iovan.

interactions between the substituents (Scheme 5.1a).²⁰³ Despite this thermodynamic preference, several catalytic systems demonstrate high levels of diastereoselectivity that would not be anticipated from a simple chair-like transition state. For example, Chemler and co-workers developed a Cu(II)-catalyzed carboamination of unactivated olefins to form *cis*-2,5-disubstituted pyrrolidine products.²⁰⁴ The destabilizing steric interaction between the sulfonyl substituent on the N-atom and the R group at the α -carbon requires that they orient *trans* to one another, forcing the R substituent in a pseudo-axial position (Scheme 5.1b). Given the wide-ranging effects that both the nitrene precursor and catalyst can have on the diastereoselectivity of cyclization, we were interested in investigating our system's inherent selectivity with the hope of introducing catalyst modifications to increase stereocontrol.

We previously reported⁷⁶ that exposure of 1-azido-2-phenyl-5-hexene to $^{\text{Ad}}\text{L}_{\text{Cl}_2}\text{FeCl}(\text{OEt}_2)$ (**5.1**) in the presence of Boc_2O generated 1-Boc-4-phenyl-2-vinylpyrrolidine in good yield with poor diastereoselectivity (Table 5.1, entry 1, 2:1 d.r.). To assist in the stereochemical assignment, removal of the Boc-group under acidic conditions resulted in the isolation of a mixture of *cis*-4-phenyl-2-vinylpyrrolidine and *trans*-4-phenyl-2-vinylpyrrolidine. 1D NOE studies of the crude reaction mixture indicated that the *syn* isomer is the major diastereomer. This preference can be rationalized using a predictive model for 2,4-substitution on the alkyl azido substrate (Figure 5.2). In this model we propose the following: (1) the alkyl imido bisects the plane of the dipyrin ligand; (2) the cyclization occurs through a chair-like transition state; and (3) the C–H bond to be functionalized approaches the imido opposite the chloride ligand. Given this proposal, placing the 4-vinyl and 2-phenyl substituents in pseudo-equatorial positions in the transition state

202. When, P. M.; Lee, J.; Du Bois, J. *Org. Lett.* **2003**, *5*, 4823.

203. Sherman, E. S.; Fuller, P. H.; Kasi, D.; Chemler, S. R. *J. Org. Chem.* **2007**, *72*, 3896.

Table 5.1. Diastereoselectivities of disubstituted pyrrolidine products.

Entry	Product	Yield (%) ^a	d.r. (<i>syn:anti</i>) ^b	Entry	Product	Yield (%) ^a	d.r. (<i>syn:anti</i>) ^b
1		66 ^c 74 ^d	2:1 ^c 2:1 ^d	7		59 ^c 85 ^d	4:1 ^c >20:1 ^d
2		72 ^c	4:1 ^c	8		45 ^c 65 ^d	>20:1 ^c >20:1 ^d
3		63 ^c 78 ^d	3:1 ^c >20:1 ^d	9		30 ^{c,e} 46 ^d	>20:1 ^c >20:1 ^d
4		54 ^d	16:1 ^d	10		38 ^c 63 ^d	>20:1 ^c >20:1 ^d
5		49 ^c 48 ^d	3:1 ^c 17:1 ^d	11		30 ^c 31 ^d	>20:1 ^c >20:1 ^d
6		47 ^c 61 ^d	4:1 ^c >20:1 ^d				

^a ¹H NMR yield at 50 °C using ferrocene as an internal standard. ^b Diastereomeric ratio determined by GC/MS. Relative stereochemistry determined via 1D NOE analysis of crude reaction mixtures of deprotected pyrrolidine. ^c Reaction with catalyst 5.1. ^d Reaction with catalyst 5.4. ^e Reaction run with 10 mol% catalyst.

structure will result in the *cis*-pyrrolidine product (TS_a). The minor *anti*-diastereomer requires that either the phenyl or vinyl groups orient axially. With this substrate, the phenyl substituent is anchored in the equatorial position, given its larger A-value (3.0 *versus* 1.4 kcal/mol for phenyl and vinyl, respectively), and the vinyl substituent moves to the axial position (TS_b). By extension, the introduction of a larger substituent at the C4 carbon would likely enhance the diastereoselectivity.

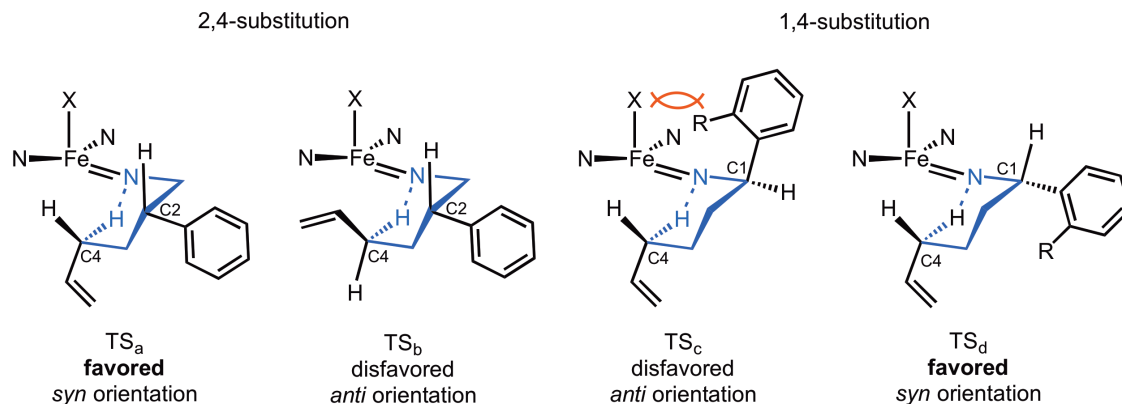
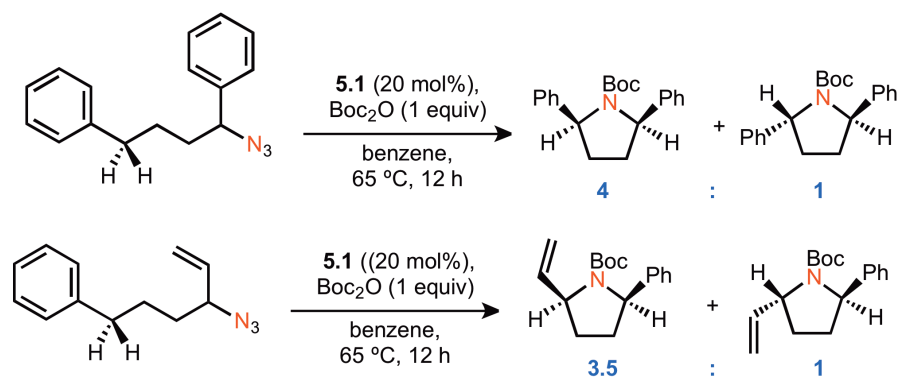


Figure 5.1. Transition state model. Competing chair-like transition states for the formation of 3,5- and 2,5-disubstituted pyrrolidines of either *syn* or *anti* orientation. **2,4-substitution:** TS_a illustrates a chair-like arrangement of the alkyl chain places the phenyl and vinyl substituents in pseudo-equatorial positions, minimizing gauche interactions and favoring a *syn* orientation. TS_b is slightly higher in energy and results in the minor product diastereomer, as it requires a pseudo-axial arrangement of the vinyl substituent. **1,4-substitution:** TS_c highlights the destabilizing interaction between the anionic ligand (X) and the phenyl substituent at C2. The favored TS_d places the phenyl substituent in a pseudo-axial orientation, relieving the interaction with the bulky anion.

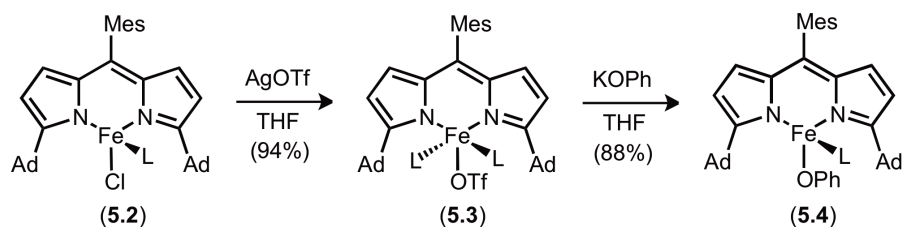
We next applied this model to substrates where the phenyl substituent has shifted from C2 to C1 (Table 5.1, entry 2) on the alkyl azido substrate. Given that the identity of the two substituents has not changed from the previous example, we did not expect to see a shift in the diastereomeric ratio. However, the selectivity has doubled (entry 1, 2:1 d.r. vs. entry 2, 4:1 d.r.) upon formation of 1-Boc-5-phenyl-2-vinylpyrrolidine. Similarly, we anticipated that TS_c (Figure 5.1), where both substituents are in equatorial positions, would lead to the major *anti* diastereomer. Nonetheless, 1D NOE analysis of the deprotected pyrrolidine indicated that the major diastereomer has a *syn* configuration. Such disparities suggested that an additional interaction has been introduced with this different substitution pattern. To further investigate this phenomenon, we synthesized a series of hexenylazide substrates with various aryl groups at the C1 position. Substrates with *para*- and *meta*- substitution (entries 3-7) on the aryl unit led to similar diastereoselectivities as seen with the phenyl derivative upon cyclization in the presence of **5.1** and Boc₂O. However, introduction of *ortho*-substitution on the aryl component (entries 8-10) led to the formation of the pyrrolidine as a single diastereomer. Increasing the size of the substituent at the *ortho* carbon from hydrogen to either a halide or a trifluoromethyl group



Scheme 5.2. Variations in substituent identity. Variation in C4 substitution has limited effect on the diastereoselectivity. These 1,4-disubstituted substrates reinforce that the dominant interaction that dictates the diastereomeric ratio is the interaction between the C1 substituent and the anionic ligand on the Fe catalyst.

enhances the significant destabilizing interaction between the aryl unit and the chloride bound to the Fe center to the point where the aryl substituent exclusively favors the pseudo-axial position in the transition state (TS_d, Figure 5.1). Such an orientation results in the formation of the *cis*-2,5-disubstituted pyrrolidine. Furthermore, a bulky *tert*-butyl substituent at the C1 position similarly favors exclusive formation of the *cis*-pyrrolidine product (entry 11).

Variation of the C4 substitution from the vinyl substituent to a phenyl substituent (Scheme 5.2) in 1,4-disubstituted azide substrates provides further support for our TS model (Figure 5.2). The synthesis of 1-Boc-2,5-diphenylpyrrolidine by exposure of **5.1** to 1-azido-1,4-diphenylbutane and Boc₂O proceeded in moderate yield (34 %) and moderate diastereoselectivity (5:1 d.r.). Despite an increase in the steric bulk at the C4 position, there is no improved diastereoselectivity as compared to 1-Boc-2-phenyl-5-vinylpyrrolidine (Table 5.1, entry 2, 4:1 d.r.). We see a similar effect when comparing the diastereoselectivities arising from azide substrates in which the positions of the phenyl and vinyl substituents are inverted. The synthesis of 1-Boc-2-phenyl-5-vinylpyrrolidine arising from addition of 3-azido-6-phenyl-hex-1-ene to **5.1** and Boc₂O proceeds in slightly lower diastereoselectivity (3.5:1 d.r.) than the synthesis of the same pyrrolidine derived from 1-azido-1-phenyl-hex-5-ene (4:1 d.r.). Less stereocontrol is



Scheme 5.3. Synthesis of phenoxide bound catalyst **5.4**.

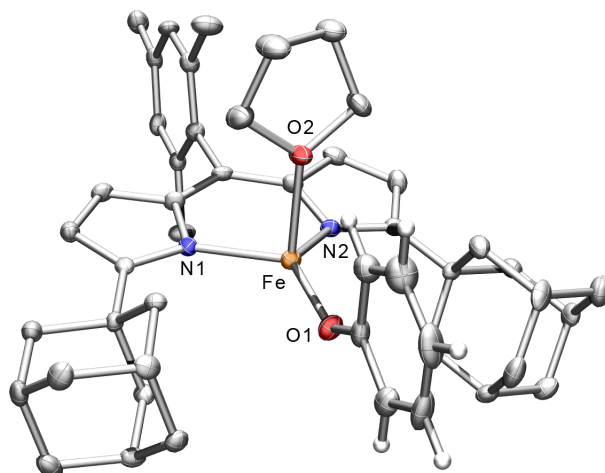


Figure 5.2. X-ray structure of **5.4**. Thermal ellipsoids set at the 50% probability level (Fe, orange; C, gray; H, white; N, blue; O, red). Bond lengths (Å): Fe-N1, 2.042(3); Fe-N2, 2.058(3); Fe-O1, 1.884(2); Fe-O2, 2.119(2). X-ray structure obtained by Diana Iovan.

observed when this smaller vinyl substituent is placed at the C1 position and the bulkier phenyl substituent is placed at the C5 position of the azide substrate. These results suggest that the dominant interaction dictating diastereoselectivity is not the orientation of the C4 substituent, but truly the interaction between the C1 substituent and the anionic ligand on the Fe catalyst.

With the realization that a significant destabilizing interaction between the Fe-bound anion and the substrate's C1-substituent exists, we set out to design catalysts with bulkier anions to enhance this effect (Scheme 5.3). Addition of silver triflate to $\text{Ad}^{\text{L}}\text{L}_{\text{Mes}}\text{FeCl}(\text{OEt}_2)$ (**5.2**) in THF results in the formation of the inner-sphere triflate species **5.3**, a useful anion metathesis synthon. Initially, we subjected **5.3** to a variety of bulky alkoxide salts, but found their catalytic activity to be significantly poorer than the chloride counterpart **5.1**. On the other hand, addition of potassium phenoxide to **5.3** cleanly generates the phenoxide bound complex **5.4** (Figure 5.2),

which has proven to be a markedly improved catalyst for the cyclization chemistry (Table 5.1).²⁰⁵

Additionally, catalyst **5.4** is extremely diastereoselective for all of the 2,5-disubstituted pyrrolidines generated (entries 2-13), regardless of the substitution pattern along the aryl ring. The added steric bulk from the phenoxide anion destabilizes TS_c such that even in substrates bearing no *ortho* substitution the diastereomer resulting from TS_d is formed with very high selectivity (entries 3-5, 7-8). Notably, the selectivity with catalyst **5.4** is not improved for the 2,4-disubstituted pyrrolidine (entry 1), as the phenoxide ligand does not project far enough to influence the orientation of the substituent at the C2 position.

5.3 Progress towards an Enantioselective Catalyst

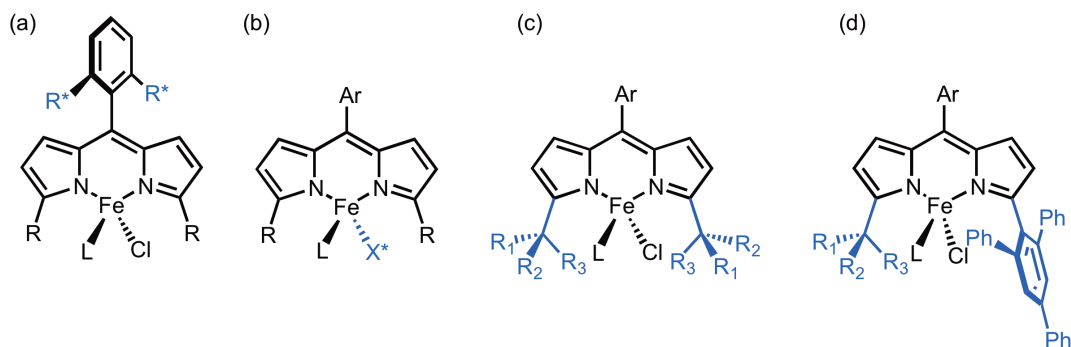


Figure 5.3. Asymmetric dipyrromethene complexes. Potential strategies to introduce asymmetry into the dipyrromethene ferrous complexes: (a) Asymmetric *meso* position; (b) Asymmetric anion; (c) Chiral alkyl substituents at the 2-position of pyrrole to generate a C_2 symmetric complex; (d) Asymmetric dipyrromethene synthesis to generate a complex that is chiral at the Fe center.

In designing a catalyst for asymmetric *N*-heterocycle formation, we considered four different approaches (Figure 5.3): (1) synthesis of a dipyrinato Fe complex with chiral substituents at the *meso* position; (2) synthesis of a dipyrinato Fe complex with an inner-sphere chiral anion; (3) synthesis of a C_2 symmetric dipyrinato Fe complex with chiral substituents at

204. Our current hypothesis for the improved catalytic activity of **5.3** is that the bulkier anionic ligand decelerates *t*BuOH coordination to the Fe-center, thereby decelerating the protonation of the dipyririn ligand and decomposition of the complex.

the 2-position of the pyrrole; (4) synthesis of an asymmetric dipyrinato Fe complex to generate a stereogenic Fe center.

Strategy 1 has been popularized in asymmetric catalysis with porphyrin ligands. Most notably, Zhang and co-workers have appended *ortho* chiral amides on the *meso* aryl ring to generate a D_2 symmetric chiral porphyrin cobalt(II) complex for asymmetric olefin cyclopropanation²⁰⁶ and aziridination.²⁰⁷ However, this did not seem a suitable approach for the pseudo-tetrahedral dipyrinato complexes, as we believe the site of C–N bond formation is fairly remote from the ligand *meso* position.

In the following sections, progress towards modifying the Fe-based catalyst XX discussed herein for asymmetric *N*-heterocycle formation will be discussed, focusing on strategies 2 and 3 above.

5.3.1 Strategy 2: Chiral Anionic Ligand

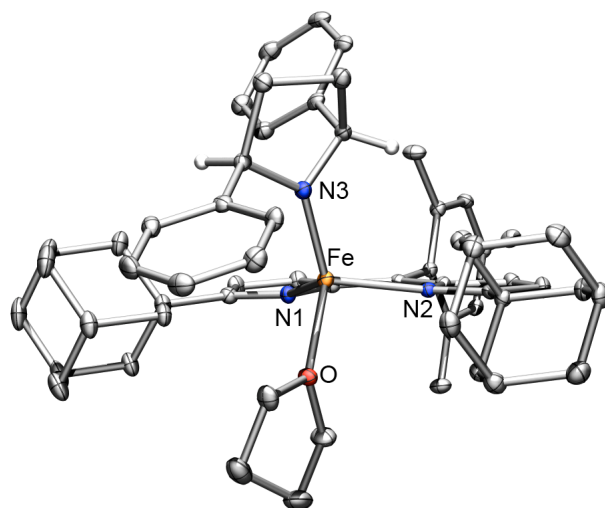
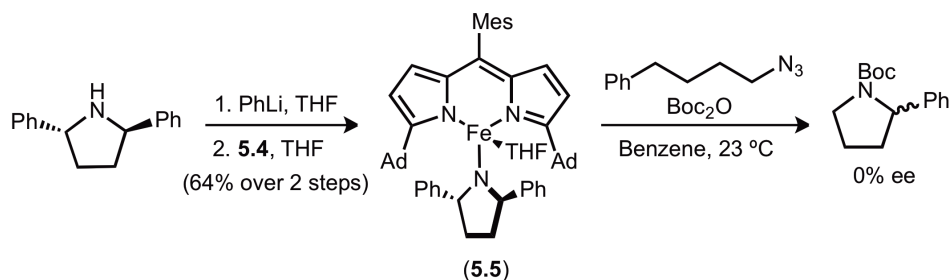


Figure 5.4. X-ray structure of 5.5. Thermal ellipsoids set at the 50% probability level (Fe, orange; C, gray; H, white; N, blue; Cl, green; O, red). Bond lengths (Å): Fe–N1, 2.0996(19); Fe–N2, 2.110(2); Fe–N3, 1.943(2); Fe–O, 2.0891(17).

205. Zhu, S.; Ruppel, J. V.; Lu, H.; Wojtas, L.; Zhang, X. P. *J. Am. Chem. Soc.* **2008**, *130*, 5042.

206. Subbarayan, V.; Ruppel, J. V.; Zhu, S.; Perman, J. A.; Zhang, X. P. *Chem. Commun.* **2009**, 4266.



Scheme 5.4. Synthesis of Fe-complex with chiral anionic ligand.

Strategy 2 is synthetically appealing; the introduction of a chiral anion can be achieved in a single anion metathesis step from the readily accessible chloride complex $^{Ad}L_{Mes}FeCl(OEt_2)$ (**5.2**). We envisioned that an anionic ligand with significant projection of its stereo-information could influence the conformation the alkyl azide adopts prior to C–H functionalization. Thus, we targeted the incorporation of deprotonated, chiral C_2 pyrrolidines to the ferrous complex, given their success when applied as phosphoramidite ligands for asymmetric catalysis.^{208, 209} Deprotonation of the (2*R*,5*R*)-2,5-diphenylpyrrolidine with phenyl lithium, followed by introduction of the ferrous chloride complex **5.2** led to the isolation of **5.5** in quantitative yield (Figure 5.4, Scheme 5.4.). Unfortunately, stoichiometric²¹⁰ application of **5.5** to 1-azido-4-phenylbutane resulted in a racemic mixture of 2-phenylpyrrolidine, suggesting that the chiral information is too far from the C–N bond forming event.

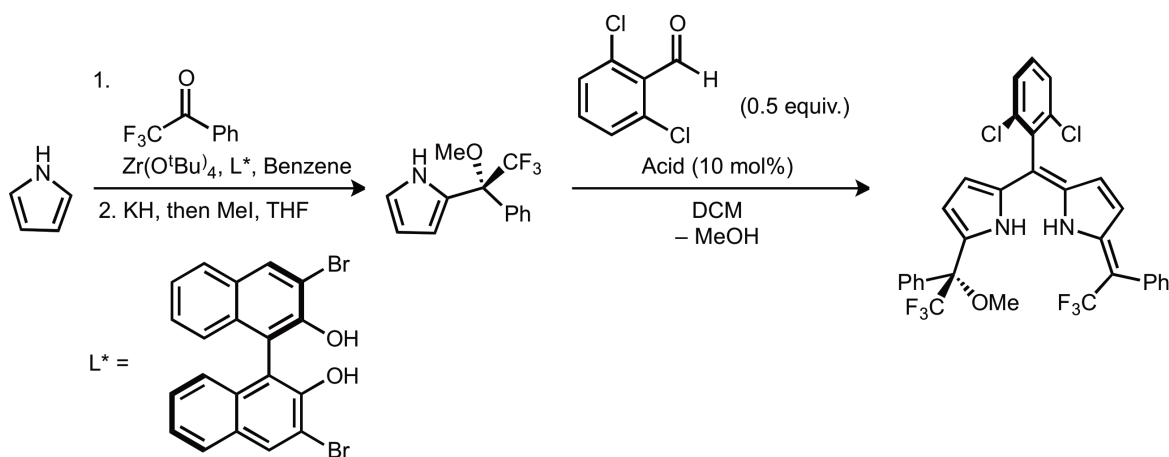
5.3.2 Strategy 3: C_2 Symmetric Chiral Catalyst

Next, we focused on synthesizing a C_2 -symmetric dipyrromethene ligand with chiral pyrrolide substituents. Based on our previous findings, the alkyl imido radical resides in the cleft between the flanking pyrrolide substituents, displacing the chloride ligand either above or below

207. Trost, B. M.; Silverman, S. M.; Stambuli, J. P. *J. Am. Chem. Soc.* **2011**, *133*, 19483.

208. Choi, Y. H.; Choi, J. Y.; Yang, H. Y.; Kim, Y. H. *Tetrahedron: Asymmetry* **2002**, *13*, 801.

209. This complex decomposes under catalytic conditions due to the instability of the pyrrolidinyl moiety with Boc_2O .



Scheme 5.5 *Asymmetric Friedel-Crafts alkylation.* Attempt to employ enantioselective Friedel-Crafts pyrrole alkylation to generate asymmetric dipyrin ligands.

the plane of the dipyrin. Such a conformation likely requires that the C–H bond substrate approach the imido radical opposite the chloride ligand. Given the uncertainty in the chloride’s position, it was necessary to design a C_2 -symmetric dipyrin ligand wherein the asymmetric environment is maintained above and below the ligand plane, generating homotopic chloride binding sites. This approach has proven widely successful in asymmetric transformations using chiral C_2 -symmetric Schiff base complexes²¹¹ and bis-oxazoline complexes.²¹²

There are only a handful of reports describing highly selective and readily accessible routes to chiral 2-substituted pyrroles. Initially, we pursued a Zr-catalyzed Friedel-Crafts alkylation of pyrroles with trifluoromethylketones (Scheme 5.5) that proceeds in excellent yields and enantioselectivities.²¹³ The resultant tertiary alcohol was then protected as the methyl ether and subjected to the typical acid catalyzed condensation conditions to generate the corresponding dipyrromethane (10 mol% PPTS, 0.5 equiv. ArCHO, DCM, 23 °C). However, the introduction of the electron-withdrawing trifluoromethyl substituent deactivated the pyrrole and no reaction was

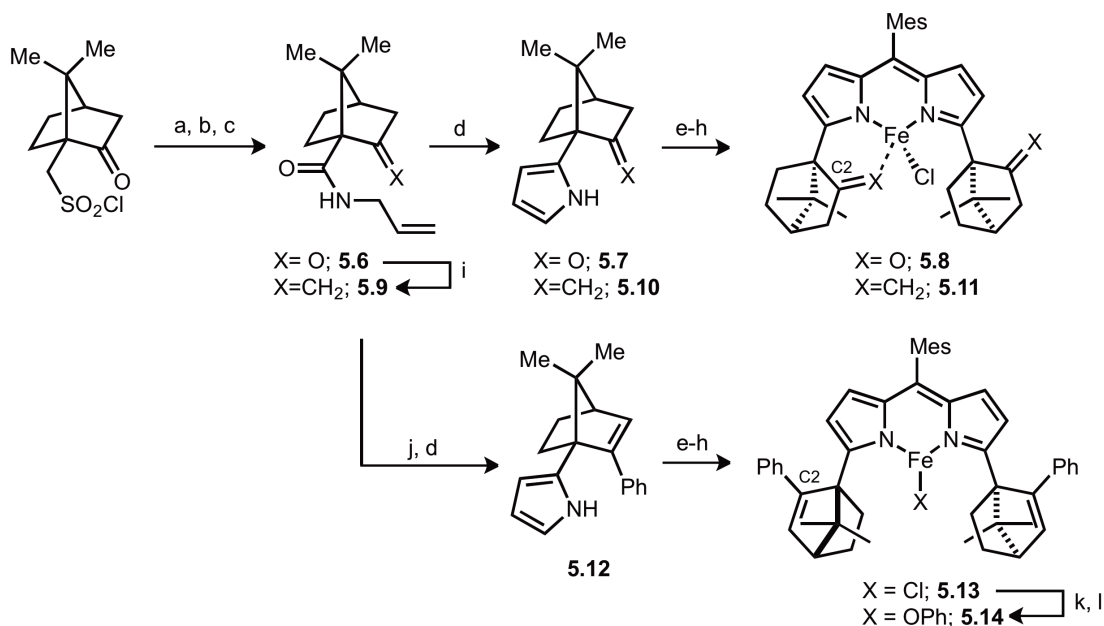
210. Seminal reference: Zhang, W.; Loebach, J. L.; Wilson, S. R.; Jacobsen, E. N. *J. Am. Chem. Soc.* **1990**, *112*, 2801.

211. Seminal reference: Evans, D. A.; Miller, S. J.; Lectka, T.; von Matt, P. *J. Am. Chem. Soc.* **1999**, *121*, 7559.

observed. While introduction of a stronger acid (10 mol% TsOH) initialized the condensation reaction, it also promoted methanol elimination to give the asymmetrically substituted dipyrin ligand (Scheme 5.5). A variety of Lewis acid catalysts were also screened (*eg.* AlCl₃, InCl₃, Ti(O^{*i*}Pr)₄), none of which resulted in clean conversion to the desired dipyrromethane. Similarly, variation of the protecting group on the tertiary alcohol from a methyl ether to a *tert*-butyldimethylsilyl ether did not have the desired effect.

Given the significant limitations in efficiently generating a chiral 2-substituted pyrrole through enantioselective catalysis, we chose to draw from the chiral pool in our next approach. We designed a (+)-camphor substituted dipyrin ligand starting from the commercially available (1*S*)-(+)-10-camphorsulfonyl chloride (Scheme 5.6). The sulfonyl chloride is readily converted to the *N*-allyl amide **5.6** via oxidation to (+)-ketopinonic acid, followed by a two-step amidation sequence through the acid chloride intermediate. Exposure of **5.6** to phosgene generates the imidoyl chloride, which is converted to 2-(+)-camphor-pyrrole **5.7** in the presence of potassium *tert*-butoxide.²¹⁴ We then employed typical condensation, oxidation, and deprotonation/metallation conditions to prepare the (+)-camphor substituted dipyrinato complex **5.8**. However, we found that **5.8** is unreactive towards alkyl azide substrates, even at elevated temperatures. Assuming that ketone ligation to the Fe-center was responsible for the lack of reactivity, we methenylated the ketone using standard Wittig conditions to generate **5.9**. The subsequent steps proceeded as anticipated and we isolated the Fe complex **5.11** in a straightforward manner. Exposure of **5.11** to a stoichiometric amount of 1-azido-5-hexene resulted in the formation of a clean, new paramagnetic species as determined by ¹H NMR. However, analysis of the reaction mixture by LC/MS indicated that the nitrene functionality was

212. Blay, G.; Fernández, I.; Monleón, A.; Pedro, J. R.; Vila, C. *Org. Lett.* **2009**, *11*, 441.



Scheme 5.6. Synthesis of camphor-derived dipyrromethene Fe complexes. Reagents and conditions: (a) excess KMnO_4 , excess Na_2CO_3 , H_2O , 80°C , 2 h (36%); (b) SOCl_2 , TEA, DCM, 3 h; (c) 2 equiv. allylamine, Et_2O , 1 h (67% steps b,c); (d) excess COCl_2 , cat. DMF, toluene, 12 h, then KO^tBu , THF, 10 min (20% for **5.7**; 88% for **5.10**); (e) 0.5 equiv $\text{MesCH}(\text{OMe})_2$, 0.1 equiv PPTS, DCE, 80°C , 6 h; (f) DDQ, hexanes, 6h (steps e and f, 59% towards **5.8**, 46% towards **5.11**, 70% towards **5.13**); (g) 1.2 equiv. PhLi , benzene; 2 h; (h) 1.2 equiv. FeCl_2 , Et_2O , 4 h (steps g and h, 91% for **5.8**, 70% for **5.11**, 88% for **5.13**); (i) 2.0 equiv. $\text{CH}_3\text{PPh}_3\text{Cl}$, 2.2 equiv. KO^tBu , THF, $0 \rightarrow 80^\circ\text{C}$, 7 h (69%); (j) 10 equiv. CeCl_3 , 5.0 equiv. PhLi , THF, -40°C , 2 h (68%); (k) 1.0 equiv. AgOTf , THF, 3 h (89%); (l) 1.0 equiv. KOPh , THF, 3 h (quant.).

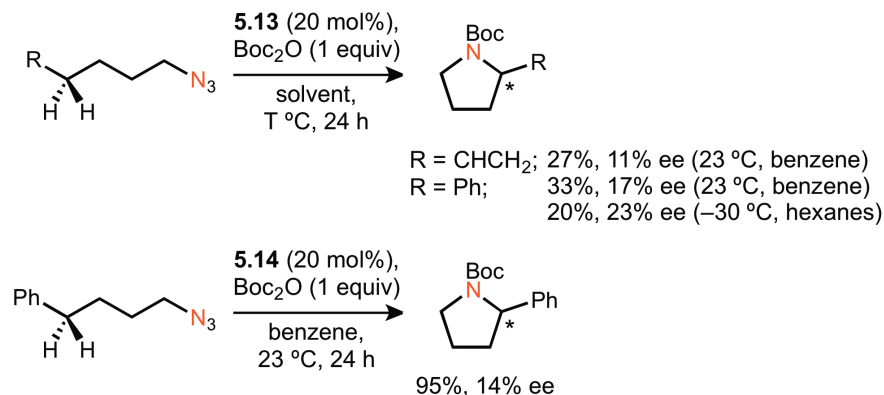
transferred to the ligand and the desired cyclization chemistry did not occur. We believe that the exposed terminal alkene is oriented proximal to the imido moiety and susceptible to intramolecular aziridination or amination.

In efforts to favor an alternate orientation where the C2 carbon of the camphor moiety is oriented away from the Fe center, we tried to generate tri- and tetra-substituted olefins using a variety of olefination conditions. Direct olefination of ketone **5.6** with bulkier phosphonium ylides was unsuccessful. However, 1,2-addition of aryl organometallic reagents to the ketone, followed by dehydration of the tertiary alcohol provided an indirect route to a tri-substituted internal olefin (Scheme 5.6). Use of excess phenyl magnesium bromide with **5.6** generated the desired tertiary alcohol, but with low conversion. Grignard additions to bulky ketones are known

to proceed in poor yield due to competitive enolate formation. However, transitioning to the less basic organocerium reagent led to full conversion and isolation of the tertiary alcohol in 70% yield.²¹⁵ Exposure of the alcohol to phosgene generates **5.12**, wherein both the alcohol dehydration and the pyrrole formation occurred in a single step. Pyrrole **5.12** was readily converted to the dipyrinato complex **5.13** in four steps. Although we have not been able to crystallize **5.13**, we believe that the bulky phenyl substituent prefers an orientation away from the Fe center, forcing the dipyrin to adopt C_2 symmetry.

Exposure of 1-azido-5-hexene to catalytic amounts of **5.13** and Boc_2O at 23 °C generated 1-Boc-2-vinylpyrrolidine in 27% yield with 11% enantiomeric excess (Scheme 5.7). Moving to a substrate with a slightly larger substituent, the cyclization of 1-azido-4-phenylbutane occurs with increased selectivity (17% ee at 23 °C, 23% ee at -30 °C), again with low yields (33% at 23 °C, 20% at -30 °C). The yield can be improved significantly with the phenoxide complex **5.14**, but without any concomitant improvement in selectivity (95% yield, 14% ee at 23 °C). We propose that the marginal selectivity arises from the difference in energy of the diastereomeric transition states TS_R and TS_S (Figure 5.5). In the higher energy transition state, the adopted chair conformation places the pseudo-axial proton H_R in close proximity to the *gem*-dimethyl unit on the bridgehead carbon, as opposed to the ethyl bridge in the opposing transition state TS_R . With this ligand design we will likely be limited to poor selectivities, as the difference in the steric interactions (ethyl bridge *versus* dimethyl bridgehead) is not significant enough to dramatically favor one transition state over another.

214. Dimitrov, V.; Bratovanov, S.; Simova, S.; Kostova, K. *Tetrahedron Lett.* **1994**, 35, 6713.



Scheme 5.7. Enantioselectivities of C–H functionalization/cyclization reactions.

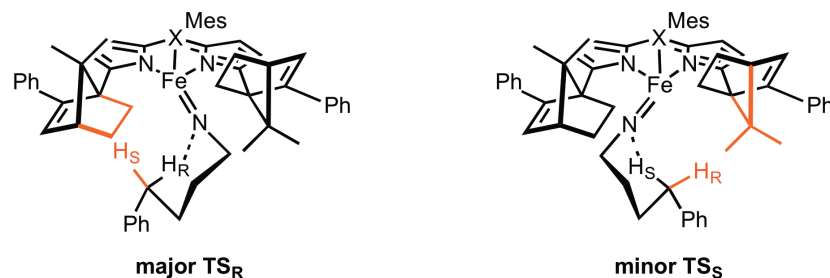


Figure 5.5. Proposed mechanism of enantioinduction. Diastereomeric transition states TS_R and TS_S lead to the (*R*) and (*S*) pyrrolidine enantiomers, respectively. The major steric interactions between the dipyrriin ligand and the enantiotopic protons are highlighted in red. TS_R highlights the interaction between H_S and the ethyl bridge of the norbornene. TS_S highlights the more destabilizing interaction between H_R and the *gem*-dimethyl bridgehead substituent.

Strategy 4 offers a method to introduce greater steric differentiation on the dipyrriin platform. This strategy has been employed recently by Chirik and co-workers for asymmetric alkene hydrogenation using an asymmetrically substituted bis(imino)pyridine cobalt complex.²¹⁶ The challenge with this approach on our ligand platform lies in the uncertainty of the anion binding. During the synthesis of the stereogenic Fe complex, we will form a mixture of both enantiomers where the anionic ligand can adopt one of the two remaining positions about the pseudo-tetrahedral Fe center. This issue could readily be circumvented through the introduction of a bulky chiral anionic ligand to generate a separable diastereomeric mixture.²¹⁷ Looking

215. Monfette, S.; Turner, Z. R.; Semproni, S. P.; Chirik, P. J. *J. Am. Chem. Soc.* **2012**, *134*, 4561.

216. For an example of a similar approach on a Mo-catalyst for enantioselective alkene metathesis, see: Malcolmson, S. J.; Meek, S. J.; Sattely, E. S.; Schrock, R. R.; Hoveyda, A. H. *Nature* **2008**, *456*, 933.

forward, this seems like a promising strategy to access a library of asymmetrically substituted dipyrin ligands.

5.4 Conclusions

In this chapter we have demonstrated the dramatic improvement in the diastereoselectivity of 2,5-disubstituted pyrrolidine formation through simple ligand modifications of catalyst **5.1**. Our current hypothesis predicts that the selectivity arises from destabilizing interactions between the substituent at the C2 carbon and the anionic Fe-bound ligand. We are currently exploring the synthesis of Fe-complexes with various phenoxide derivatives to optimize the catalyst for the diastereoselective synthesis of pyrrolidines with smaller substituents or different substitution patterns.

Additionally, we have synthesized new dipyrinato ferrous complexes for asymmetric pyrrolidine formation, targeting two different design strategies. The first strategy employed the introduction of a bulky chiral anionic ligand bound to the Fe-center and proved unsuccessful. However, the second strategy, design of a C_2 -symmetric chiral dipyrin ligand, revealed promising results. Incorporation of a modified camphor-substituent into the dipyrinato ligand scaffold generated a catalyst capable of inducing low-levels of enantioselectivity in the formation of 1-Boc-2-phenylpyrrolidine (23% ee) and 1-Boc-2-vinylpyrrolidine (11% ee). Despite these promising results, the natural product-derived substituent is amenable to only limited structural modification. Looking forward, we will pursue the synthesis of asymmetrically substituted dipyrin ligands with the hopes of generating a greater steric bias between diastereomeric transition states with relative synthetic ease.

5.5 Experimental Methods

5.5.1 General Considerations

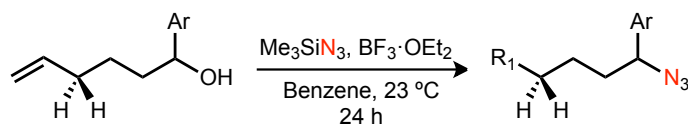
All manipulations of metal complexes were carried out in the absence of water and dioxygen using standard Schlenk techniques, or in an MBraun inert atmosphere drybox under a dinitrogen atmosphere. Ligand, ligand precursor syntheses, and substrate syntheses were carried out in air, except where noted. All glassware was oven dried for a minimum of 1 h and cooled in an evacuated antechamber prior to use in the drybox. Benzene, diethyl ether, *n*-hexane, and tetrahydrofuran were dried and deoxygenated on a Glass Contour System (SG Water USA, Nashua, NH) and stored over 4 Å molecular sieves (Strem) prior to use. Dimethylsulfoxide and dimethylformamide were purchased from VWR and used as received. Chloroform- d_1 was purchased from Cambridge Isotope Labs and used as received. Benzene- d_6 was purchased from Cambridge Isotope Labs and was degassed and stored over 4 Å molecular sieves prior to use. All reagents, unless otherwise specified, were purchased from Sigma Aldrich and used as received. Anhydrous iron(II) chloride and copper(II) chloride were purchased from Strem and used as received. Celite® 545 (J. T. Baker) was dried in a Schlenk flask for 24 h under dynamic vacuum while heating to at least 150 °C prior to use in a drybox. Silica gel 32-63 μ (AIC, Framingham, MA) was used as received.

5.5.2 Characterization and Physical Methods

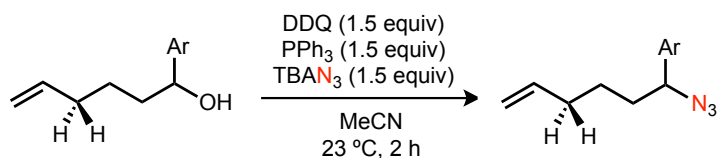
^1H , ^{13}C , and were recorded on Varian Mercury 400 MHz or Varian Unity/Inova 500 MHz spectrometers. ^1H and $^{13}\text{C}\{^1\text{H}\}$ NMR chemical shifts are reported relative to SiMe_4 using the chemical shift of residual solvent peaks as reference. Infrared (FTIR) spectra were recorded on a Varian 1000 Scimitar FT-IR spectrophotometer referenced to a polystyrene standard. Gas chromatography/mass spectrometry (GC/MS) was performed on an Agilent GC/MS 5975 Turbo

system. HPLC analysis of enantiomeric excess was performed using an Agilent 1200 series quaternary HPLC system with commercially available Chiraltech analytical columns (4.6 × 250 mm).

5.5.3 Synthesis and Characterization of Azide Substrates and Resultant *N*-Heterocycles



Procedure A: Boron trifluoride etherate (1.2 equiv.) was added dropwise at 25 °C to a stirring solution of benzylic alcohol²¹⁸ (15 mmol, 1 equiv.) and trimethylsilyl azide (1.2 equiv.) in benzene (0.5 M) under N₂. After 24 hours, the mixture is poured into water. The aqueous phase was extracted three times with 10 mL Et₂O. The combined organic phases were washed with 50 mL H₂O and dried over MgSO₄, filtered and concentrated. The crude products were purified via silica gel chromatography.

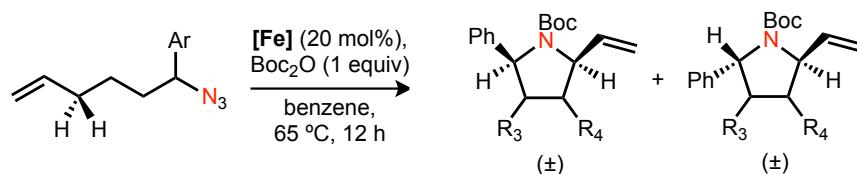


Procedure B²¹⁹: Portionwise addition of DDQ (1.5 equiv.) was added to a stirred solution of triphenylphosphine (1.5 equiv.) in DCM (0.44 M wrt to DDQ). After stirring for 2 min, tetrabutyl ammonium azide (1.5 equiv.) was added, followed by a solution of alcohol (1 equiv.) in DCM (1.5 M wrt to alcohol). The reaction was allowed to stir at RT for 1 h and then the mixture

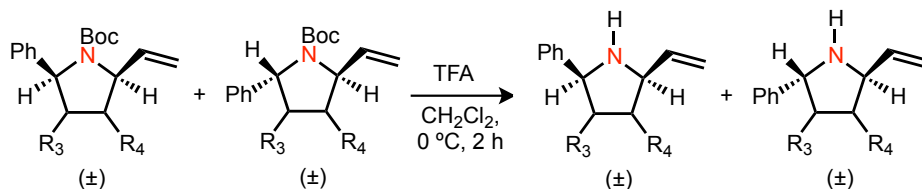
217. Synthetic procedure for benzylic alcohols can be found in Chapter 4, Experimental Methods.

218. Procedure adopted from: Brooks, H. B.; Crich, J. Z.; Henry, J. R.; Li, H.-Y.; Slater, M. K.; Wang, Y. U. *PCT Int. Appl.* 2008-144-223, Nov 27, 2008.

was loaded onto a silica plug, using 20% ethyl acetate in hexanes as eluent. Following the plug, the crude products were purified via silica gel chromatography.



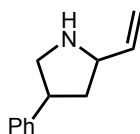
Procedure C: Under an inert N_2 atmosphere, Fe-catalyst (0.0556 mmol) and di-*tert*-butyl dicarbonate (1-10 equiv, depending on substrate) were added to a stirring solution of the desired azide (1-10 equiv, depending on substrate) in 3 mL of benzene in a 5 mL scintillation vial. The resultant inky, dark red solution was then transferred to a pressure vessel and heated to 65 °C for 12 hours. The reaction mixture was then flash chromatographed through a short pipette of deactivated silica gel using a 20:1 mixture of CH_2Cl_2 and MeOH as eluent to give a clear bright orange solution in order to remove paramagnetic materials. The solution was concentrated via rotary evaporation. The internal standard ferrocene (0.0556 mmol, 1 equiv) was added to the reaction mixture, followed by 1 mL of CDCl_3 in order to dissolve the contents of the entire flask into a homogenous solution. ^1H NMR yields were then determined via integration of the ferrocene peak and the diagnostic α -H peaks of the newly formed *N*-heterocycle. The crude products were purified via silica gel chromatography using hexanes and ethyl acetate as eluent.



Procedure D²²⁰: Trifluoroacetic acid (20 equiv.) was added dropwise at 0 °C to a stirring solution of boc-protected pyrrolidine in dichloromethane (0.05 M) under N_2 . After 2 hours, the

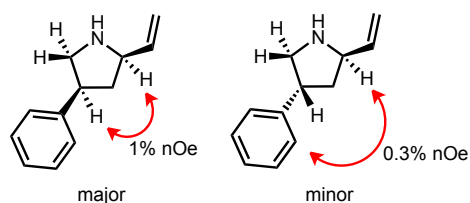
219. Procedure adopted from: Trost, B. M.; Silverman, S. M.; Stambuli, J. P. *J. Am. Chem. Soc.* **2011**, *133*, 19483.

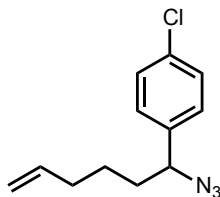
mixture was concentrated. The residual oil was diluted with ethyl acetate (3 mL) and quenched with 2N NaOH (3 mL). The biphasic mixture was extracted three times with 3 mL EtOAc. The combined organics were washed once with 3 mL saturated NH_4Cl and dried over MgSO_4 , filtered and concentrated. The crude material was analyzed without any further purification.



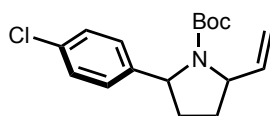
4-phenyl-2-vinylpyrrolidine: Synthesized via procedure D. $^1\text{H NMR}$ (600 MHz, C_6D_6) δ (1.9:1 mixture of diastereomers) ppm 7.08–7.15 (m, 4.6 H), 7.00–7.07 (m, 3.0 H), 6.59 (br. s., 0.5 H), 6.33 (br. s., 1 H), 6.01 (dddd, $J = 17.2, 10.2, 7.5, 5.0$ Hz, 1 H), 5.88 (dddd, $J = 17.1, 10.3, 6.9, 5.6$ Hz, 0.5 H), 5.14–5.24 (m, 1.5 H), 4.97–5.04 (m, 1.5 H), 3.78–3.86 (m, 0.5 H), 3.63–3.72 (m, 1 H), 3.36 (td, $J = 11.0, 7.9$ Hz, 0.5 H), 3.23–3.31 (m, 1 H), 3.19 (dq, $J = 17.2, 8.4$ Hz, 0.5 H), 3.05–3.11 (m, 1 H), 2.94–3.05 (m, 1 H), 2.88 (dt, $J = 10.6, 8.8$ Hz, 0.5 H), 1.85–1.93 (m, 1 H), 1.83 (q, $J = 8.0$ Hz, 1 H), 1.62–1.71 (m, 1 H). $^{13}\text{C}\{^1\text{H}\}$ NMR (125 MHz, CDCl_3) δ (minor diastereomer in parentheses): 141.9(143.0), 136.9(138.4), 128.9(128.8), 127.5(127.5), 127.0(126.8), 117.8(116.4), 62.5(61.3), 52.2(53.4), 44.7(43.7), 40.7(39.8). **GCMS** (EI) $t_r = 7.80$ min m/z : 51, 68, 78, 91, 104, 115, 129, 146, 160, 173.

1D NOESY (600 MHz, C_6D_6)

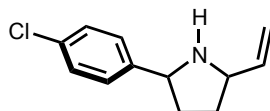




1-(1-azidohex-5-en-1-yl)-4-chlorobenzene: Synthesized via procedure A. $^1\text{H NMR}$ (600 MHz, CDCl_3) δ : 7.36 (dd, $J = 8.2, 2.0$ Hz, 5 H), 7.24 (dd, $J = 8.5, 1.7$ Hz, 2 H), 5.70–5.83 (m, 1 H), 5.01 (dt, $J = 17.0, 1.7$ Hz, 1 H), 4.97 (d, $J = 10.2$ Hz, 1 H), 4.41 (t, $J = 7.2$ Hz, 1 H), 2.07 (q, $J = 7.5$ Hz, 2 H), 1.77–1.88 (m, 1 H), 1.68–1.77 (m, 1 H), 1.44–1.54 (m, 1 H), 1.30–1.42 (m, 1 H). $^{13}\text{C}\{^1\text{H}\}$ NMR (125 MHz, CDCl_3) δ : 138.3, 137.9, 133.9, 129.0, 128.2, 115.1, 65.5, 35.6, 33.2, 25.3. GCMS (EI) $t_R = 10.28$ min m/z : 51, 64, 77, 91, 102, 113, 125, 141, 235.



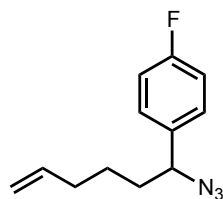
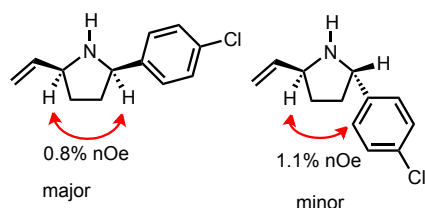
tert-butyl 2-(4-chlorophenyl)-5-vinylpyrrolidine-1-carboxylate: Synthesized via procedure C. $^1\text{H NMR}$ (500 MHz, C_6D_6 , 50 °C) δ (mixture of rotamers): 7.10–7.14 (m, 3 H), 7.02–6.89 (m, 2 H), 5.54–5.97 (m, 1 H), 5.21 (d, $J = 16.9$ Hz, 1 H), 4.86–5.10 (m, 1 H), 4.50–4.73 (m, 1 H), 4.20–4.47 (m, 1 H), 1.65–2.11 (m, 2 H), 1.36–1.61 (m, 2 H), 1.24–1.36 (m, 9 H). $^{13}\text{C}\{^1\text{H}\}$ NMR (125 MHz, C_6D_6 , 50 °C) δ (mixture of rotamers): 154.7, 143.5, 140.0, 132.5, 128.5, 127.8, 115.0, 79.2, 62.5, 61.0, 34.3, 30.3, 28.3. GCMS (EI) t_R (minor) = 10.40 min, t_R (major) = 10.46 min m/z : 57, 67, 77, 89, 103, 115, 125, 138, 153, 166, 179, 197, 207, 222, 234, 251, 281.



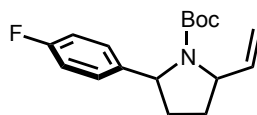
2-(4-chlorophenyl)-5-vinylpyrrolidine: Synthesized via procedure D. $^1\text{H NMR}$ (600 MHz, C_6D_6) δ (3.4:1 mixture of diastereomers): 7.11–7.20 (m, 6.3 H), 7.06 (d, $J = 8.2$ Hz, 0.6 H), 5.87 (ddd, $J = 17.0, 10.0, 7.0$ Hz, 1 H), 5.69 (ddd, $J = 17.2, 10.4, 7.0$ Hz, 0.3 H), 5.17 (d, $J = 15.3$ Hz,

1 H), 5.03 (d, $J = 17.0$ Hz, 0.3 H), 4.98 (dd, $J = 9.7, 1.5$ Hz, 1 H), 4.92 (d, $J = 10.0$ Hz, 0.3 H), 3.96 (t, $J = 7.6$ Hz, 0.3 H), 3.71 (q, $J = 7.0$ Hz, 1 H), 3.65–3.69 (m, 1 H), 3.29–3.37 (m, 1 H), 1.67–1.83 (m, 1.6 H), 1.57–1.67 (m, 1 H), 1.37–1.49 (m, 2 H), 1.25–1.37 (m, 0.6 H). $^{13}\text{C}\{\text{1H}\}$ NMR (125 MHz, CDCl_3) δ (minor diastereomer in parentheses): 143.6, 141.6(140.5), 132.7(132.9), 128.5(128.7), 128.5(128.4), 114.3(114.6), 61.6, 61.2(60.9), 34.2(34.9), 31.4(32.5).

1D NOESY (600 MHz, C_6D_6):

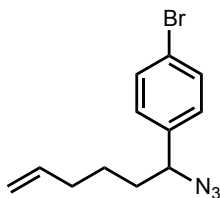


1-(1-azidohex-5-en-1-yl)-4-fluorobenzene: Synthesized via procedure A. ^1H NMR (600 MHz, CDCl_3) δ : 7.25–7.34 (m, 2 H), 7.04–7.14 (m, 2 H), 5.70–5.91 (m, 1 H), 4.91–5.13 (m, 2 H), 4.34–4.53 (m, 1 H), 2.01–2.19 (m, 2 H), 1.67–1.93 (m, 2 H), 1.32–1.55 (m, 2 H). $^{13}\text{C}\{\text{1H}\}$ NMR (125 MHz, CDCl_3) δ : 138.0, 135.6, 128.5, 128.3, 126.8, 115.6, 65.5, 35.6, 33.2, 25.3. **GCMS** (EI) $t_R = 11.05$ min m/z : 55, 77, 91, 109, 122, 135, 148, 161, 178, 191, 207, 219.

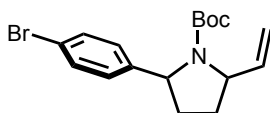


tert-butyl 2-(4-fluorophenyl)-5-vinylpyrrolidine-1-carboxylate: Synthesized via procedure C. ^1H NMR (600 MHz, C_6D_6) δ (mixture of rotamers): 7.06 (br. s., 2 H), 6.72–6.91 (m, 3 H), 5.52–6.05 (m, 1 H), 4.90–5.38 (m, 2 H), 4.17–4.75 (m, 2 H), 1.61–2.06 (m, 2 H), 1.14–1.58 (m, 11 H). **GCMS** (EI) (3.5:1 dr); $t_R = 11.13$ min (minor diastereomer) m/z : 57, 68, 82, 95, 109, 122, 135,

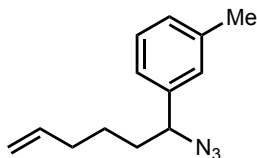
147, 163, 172, 181, 190, 206, 218, 235; $t_R = 11.18$ min (major diastereomer) m/z : 57, 68, 82, 95, 109, 122, 135, 147, 163, 172, 181, 190, 206, 218, 235.



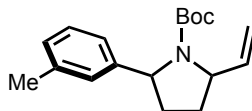
1-(1-azidohex-5-en-1-yl)-4-bromobenzene: Synthesized via procedure A. $^1\text{H NMR}$ (600 MHz, CDCl_3) δ : 7.48–7.60 (m, 2 H), 7.18 (d, $J = 8.8$ Hz, 2 H), 5.76 (ddt, $J = 17.0, 10.1, 6.7, 6.7$ Hz, 1 H), 4.94–5.09 (m, 2 H), 4.40 (t, $J = 6.5$ Hz, 1 H), 2.02–2.16 (m, 2 H), 1.68–1.90 (m, 2 H), 1.33–1.56 (m, 2 H). $^{13}\text{C}\{^1\text{H}\}$ NMR (125 MHz, CDCl_3) δ : 138.8, 137.9, 131.9, 128.5, 122.1, 115.1, 65.6, 35.5, 33.2, 25.3. **GCMS** (EI) $t_R = 11.00$ min m/z : 55, 68, 81, 96, 115, 128, 144, 157, 172, 184, 197, 210, 223, 236, 251, 279.



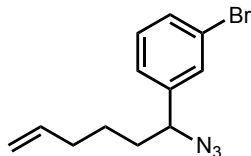
tert-butyl 2-(4-bromophenyl)-5-vinylpyrrolidine-1-carboxylate: Synthesized via procedure C. $^1\text{H NMR}$ (500 MHz, C_6D_6 , 50 °C) δ : 7.21 - 7.43 (m, 2 H), 6.86 - 7.08 (m, 2 H), 5.82 - 5.96 (m, 1 H), 5.21 (d, $J=16.94$ Hz, 1 H), 5.05 (d, $J=10.07$ Hz, 1 H), 4.60 (br. s., 1 H), 4.37 (br. s., 1 H), 1.80 - 2.03 (m, 1 H), 1.60 - 1.79 (m, 1 H), 1.22 - 1.56 (m, 11 H). $^{13}\text{C}\{^1\text{H}\}$ NMR (125 MHz, C_6D_6 , 50 °C) δ (mixture of rotamers): 155.0, 144.4, 140.3, 131.9, 128.5, 127.8, 120.9, 115.4, 79.6, 62.9, 61.4, 34.6, 30.8, 28.8. **GCMS** (EI) (16:1 dr); $t_R = 11.12$ min (minor diastereomer) m/z : 57, 68, 89, 95, 103, 115, 128, 144, 156, 169/171, 182/184, 195/197, 210/212, 223/225, 241/243, 250/252, 266/268, 280/282, 295/297; $t_R = 11.21$ min (major diastereomer) m/z : 57, 68, 89, 95, 103, 115, 128, 144, 156, 169/171, 182/184, 195/197, 210/212, 223/225, 241/243, 250/252, 266/268, 280/282, 295/297.



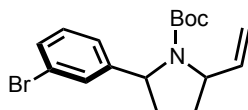
1-(1-azidohex-5-en-1-yl)-3-methylbenzene: Synthesized via procedure A. $^1\text{H NMR}$ (600 MHz, C_6D_6) δ : 7.06 (m, 1 H), 6.94 (m, 3 H), 5.57 - 5.66 (m, 1 H), 4.91 - 4.98 (m, 2 H), 3.99 - 4.05 (m, 1 H), 2.07 (s, 3 H), 1.83 (d, $J=7.63$ Hz, 2 H), 1.60 - 1.71 (m, 1 H), 1.47 - 1.56 (m, 1 H), 1.14 - 1.39 (m, 2 H). $^{13}\text{C}\{^1\text{H}\}$ NMR (125 MHz, C_6D_6) δ : 140.3, 139.0, 138.7, 129.5, 129.2, 128.9, 128.1, 124.5, 66.9, 36.2, 33.9, 26.1, 22.0. GCMS (EI) t_R = 8.37 min m/z : 51, 65, 77, 91, 105, 118, 131, 144, 158, 172, 187.



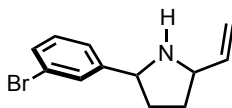
tert-butyl 2-(*m*-tolyl)-5-vinylpyrrolidine-1-carboxylate: Synthesized via procedure C. $^1\text{H NMR}$ (600 MHz, CDCl_3) δ (mixture of rotamers): 7.17–7.22 (m, 1 H), 7.05–7.08 (m, 1 H), 7.03 (d, $J = 7.6$ Hz, 1.7 H), 6.95 (t, $J = 6.5$ Hz, 0.3 H), 5.79–6.11 (m, 1 H), 5.00–5.42 (m, 2 H), 4.64–4.93 (m, 1 H), 4.29–4.58 (m, 1 H), 2.31–2.37 (m, 3 H), 2.25 (dd, $J = 13.2, 6.2$ Hz, 1 H), 2.02–2.11 (m, 1 H), 1.77–1.95 (m, 2 H), 1.08–1.35 (m, 9 H). $^{13}\text{C}\{^1\text{H}\}$ NMR (125 MHz, CDCl_3) δ (mixture of rotamers and diastereomers): 155.0(154.0), 144.3(145.2), 139.5(138.9), 137.6(138.2), 128.1, 127.2, 126.7(125.9), 122.8(122.5), 115.0(113.9), 79.4(79.2), 62.9(61.7), 61.0(59.8), 34.5, 30.6, 28.2, 21.5. GCMS (EI) (4.1:1 dr); t_R = 11.46 min (minor diastereomer) m/z : 57, 68, 79, 91, 105, 118, 129, 143, 159, 177, 188, 202, 214, 231, 287; t_R = 11.51 min (major diastereomer) m/z : 57, 68, 79, 91, 105, 118, 129, 143, 159, 177, 188, 202, 214, 231, 287.



1-(1-azidohex-5-en-1-yl)-3-bromobenzene: Synthesized via procedure A. $^1\text{H NMR}$ (500 MHz, C_6D_6) δ : 7.24 (t, $J=1.71$ Hz, 1 H), 7.02 - 7.19 (m, 1 H), 6.75 - 6.83 (m, 1 H), 6.63 - 6.71 (m, 1 H), 5.50 - 5.58 (m, 1 H), 4.86 - 4.95 (m, 2 H), 3.74 (dd, $J=7.81, 5.86$ Hz, 1 H), 1.69 - 1.79 (m, 2 H), 1.35 - 1.45 (m, 1 H), 1.12 - 1.32 (m, 2 H), 0.97 - 1.08 (m, 1 H). $^{13}\text{C}\{^1\text{H}\}$ NMR (125 MHz, C_6D_6) δ : 143.1, 138.5, 131.7, 130.1, 130.6, 125.8, 123.5, 115.5, 66.0, 36.2, 33.8, 25.8. **GCMS** (EI) t_{R} = 9.38 min m/z : 55, 67, 77, 89, 103, 115, 129, 144, 157, 172, 182/184, 192, 208/210, 222/224, 236/238, 249/250, 251/253.

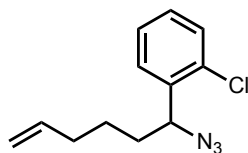
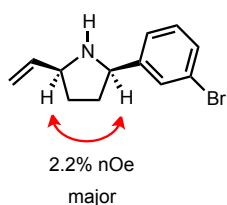


tert-butyl 2-(3-bromophenyl)-5-vinylpyrrolidine-1-carboxylate: Synthesized via procedure C. $^1\text{H NMR}$ (500 MHz, C_6D_6 , 50 °C) δ (mixture of rotamers): 7.47 - 7.49 (m, 1 H), 7.18 (m, 1 H), 7.07 (d, $J=7.32$ Hz, 1 H), 6.79 - 6.83 (m, 1 H), 5.89 (br. s., 1 H), 5.21 (d, $J=17.58$ Hz, 1 H), 5.04 (m, 1 H), 4.57 (br. s., 1 H), 4.37 (br. s., 1 H), 1.27 - 1.70 (m, 11 H). $^{13}\text{C}\{^1\text{H}\}$ NMR (125 MHz, C_6D_6 , 50 °C) δ (mixture of rotamers): 155.0, 148.0, 140.2, 130.4, 130.3, 130.2, 125.2, 123.1, 115.5, 79.7, 63.0, 61.4, 34.6, 30.6, 28.7. **GCMS** (EI) t_{R} = 10.97 min (major diastereomer) m/z : 57, 68, 77, 89, 96, 115, 128, 144, 157, 169/171, 182/184, 195/197, 210, 223/225, 241/243, 250/252, 251/253, 268, 295/297.

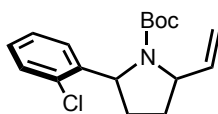


2-(3-bromophenyl)-5-vinylpyrrolidine: Synthesized via procedure D. $^1\text{H NMR}$ (600 MHz, C_6D_6) δ : 7.55 (m, 1 H), 7.12–7.22 (m, 2 H), 6.72–6.77 (m, 1 H), 5.66–5.75 (m, 1 H), 5.00 (d, $J = 17.09$ Hz, 1 H), 4.83 (d, $J = 10.25$ Hz, 1 H), 3.79–3.86 (m, 1 H), 3.48 (d, $J = 7.81$ Hz, 1 H), 1.53–1.69 (m, 2 H), 1.31–1.42 (m, 2 H).

1D NOESY (600 MHz, C_6D_6):

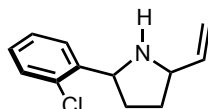


1-(1-azidohex-5-en-1-yl)-2-chlorobenzene: Synthesized via procedure B. $^1\text{H NMR}$ (500 MHz, C_6D_6) δ : 7.18–7.23 (m, 1 H), 7.06–7.09 (m, 1 H), 6.82–6.87 (m, 1 H), 6.68–6.73 (m, 1 H), 5.56–5.66 (m, 1 H), 4.86–4.98 (m, 3 H), 1.79–1.86 (m, 2 H), 1.52–1.59 (m, 2 H), 1.32–1.44 (m, 1 H), 1.18–1.29 (m, 1 H). $^{13}\text{C}\{^1\text{H}\}$ NMR (125 MHz, CDCl_3) δ : 138.6, 138.5, 133.5, 130.3, 129.5, 127.8, 127.5, 115.5, 62.8, 35.4, 33.8, 25.8. **GCMS** (EI) $t_{\text{R}} = 8.68$ min m/z : 51, 63, 77, 89, 103, 115, 125, 138/140, 144, 155, 172, 192, 207/209.



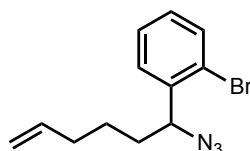
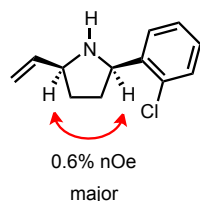
tert-butyl 2-(2-chlorophenyl)-5-vinylpyrrolidine-1-carboxylate: Synthesized via procedure C. $^1\text{H NMR}$ (500 MHz, C_6D_6 , 50 °C) δ (mixture of rotamers): 7.41–7.48 (m, 1 H), 7.14–7.21 (m, 1 H), 6.93–7.02 (m, 1 H), 6.74–6.84 (m, 1 H), 5.96–6.11 (m, 1 H), 5.20–5.41 (m, 2 H), 5.08

(dd, $J=10.25, 0.98$ Hz, 1 H), 4.43 (br. s., 1 H), 1.99 - 2.13 (m, 2 H), 1.21 - 1.59 (m, 11 H). $^{13}\text{C}\{^1\text{H}\}$ NMR (125 MHz, C_6D_6 , 50 °C) δ (mixture of rotamers): 154.9, 143.1, 134.2, 132.9, 130.0, 127.4, 127.3, 115.5, 79.6, 61.5, 61.0, 33.1, 30.4, 28.7. GCMS (EI) $t_{\text{R}} = 10.11$ min (major diastereomer) m/z : 57, 68, 82, 96, 115, 125, 144, 154, 166, 179/181, 191, 206, 216, 234/236, 251/253, 272.



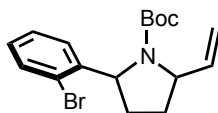
2-(2-chlorophenyl)-5-vinylpyrrolidine: Synthesized via procedure D. ^1H NMR (600 MHz, C_6D_6) δ : 7.91 (dd, $J=7.63, 1.76$ Hz, 1 H), 7.20 (dd, $J=7.63, 1.17$ Hz, 1 H), 6.99 - 7.04 (m, 1 H), 6.81 (td, $J=7.63, 1.76$ Hz, 1 H), 5.90 (ddd, $J=17.31, 10.27, 7.04$ Hz, 1 H), 5.15 - 5.20 (m, 1 H), 4.96 - 5.00 (m, 1 H), 4.39 - 4.44 (m, 1 H), 3.29 - 3.35 (m, 1 H), 2.09 - 2.17 (m, 1 H), 1.58 - 1.64 (m, 1 H), 1.39 - 1.50 (m, 2 H).

1D NOESY (600 MHz, C_6D_6):



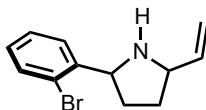
1-(1-azidohex-5-en-1-yl)-2-bromobenzene: Synthesized via procedure B. ^1H NMR (500 MHz, C_6D_6) δ : 7.25 - 7.29 (m, 1 H), 7.20 (dd, $J=7.78, 1.37$ Hz, 1 H), 6.85 - 6.90 (m, 1 H), 6.59 - 6.65 (m, 1 H), 5.57 - 5.67 (m, 1 H), 4.87 - 4.98 (m, 3 H), 1.81 - 1.89 (m, 2 H), 1.51 - 1.59 (m, 2 H), 1.34 - 1.44 (m, 1 H), 1.22 - 1.33 (m, 1 H). $^{13}\text{C}\{^1\text{H}\}$ NMR (125 MHz, C_6D_6) δ : 140.1, 138.36, 133.6, 129.9, 128.5, 128.4, 123.9, 115.5, 65.2, 35.6, 33.8, 25.8. GCMS (EI) $t_{\text{R}} = 9.19$ min m/z :

51, 63, 77, 89, 103, 115, 128/130, 144, 157, 172, 180/182, 194/196, 208/210, 222/224, 236/238, 251/253.



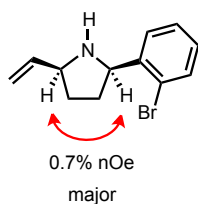
tert-butyl 2-(2-bromophenyl)-5-vinylpyrrolidine-1-carboxylate: Synthesized via procedure C.

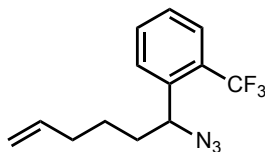
¹H NMR (500 MHz, C₆D₆, 50 °C) δ(mixture of rotamers): 7.42 (d, *J*=7.81 Hz, 1 H), 7.36 (dd, *J*=8.30, 0.98 Hz, 1 H), 6.95 - 7.01 (m, 1 H), 6.67 - 6.72 (m, 1 H), 5.97 - 6.09 (m, 1 H), 5.25 (d, *J*=15.63 Hz, 2 H), 5.08 (d, *J*=10.25 Hz, 1 H), 4.42 (br. s., 1 H), 2.01 - 2.11 (m, 2 H), 1.21 - 1.56 (m, 11 H). **¹³C{¹H} NMR** (125 MHz, C₆D₆, 50 °C) δ (mixture of rotamers): 154.9, 144.9, 140.2, 133.3, 128.6, 127.9, 127.5, 123.1, 115.6, 79.6, 63.4, 61.6, 33.3, 30.3, 28.7. **GCMS** (EI) *t_R* = 10.68 min (major diastereomer) *m/z*: 57, 68, 82, 96, 115, 128, 144, 156, 169/171, 182/184, 195, 216, 223/225, 235/237, 250/252, 295/297.



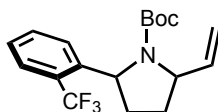
2-(2-bromophenyl)-5-vinylpyrrolidine: Synthesized via procedure D. **¹H NMR** (600 MHz, C₆D₆) δ: 7.88 (dd, *J*=7.63, 1.76 Hz, 1 H), 7.38 (d, *J*=7.63 Hz, 1 H), 7.04 (t, *J*=7.92 Hz, 1 H), 6.70 - 6.74 (m, 1 H), 5.90 (ddd, *J*=17.31, 10.27, 7.04 Hz, 1 H), 5.14 - 5.19 (m, 1 H), 4.94 - 4.99 (m, 1 H), 4.38 - 4.43 (m, 1 H), 3.33 (q, *J*=7.63 Hz, 1 H), 2.08 - 2.14 (m, 1 H), 1.55 - 1.61 (m, 1 H), 1.40 - 1.50 (m, 2 H).

1D NOESY (600 MHz, C₆D₆):

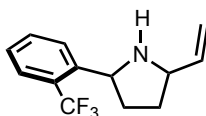




1-(1-azidohex-5-en-1-yl)-2-trifluoromethylbenzene: Synthesized via procedure B. $^1\text{H NMR}$ (500 MHz, C_6D_6) δ : 7.29 (d, $J=3.21$ Hz, 2 H), 6.96 - 7.03 (m, 1 H), 6.72 - 6.79 (m, 1 H), 5.55 - 5.65 (m, 1 H), 4.85 - 4.98 (m, 3 H), 1.82 (m, 2 H), 1.34 - 1.61 (m, 2 H), 1.12 - 1.22 (m, 2 H). $^{13}\text{C}\{^1\text{H}\}$ NMR (125 MHz, C_6D_6) δ : 140.0, 138.5, 133.0, 128.8, 128.7, 128.5, 126.3, 126.1 (q, $J = 5.5$ Hz), 115.5, 61.9, 36.9, 33.8, 26.1. **GCMS** (EI) $t_{\text{R}} = 7.73$ min m/z : 51, 68, 77, 87, 96, 107, 122, 135, 144, 159, 172, 186, 198, 212, 222, 241.



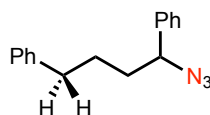
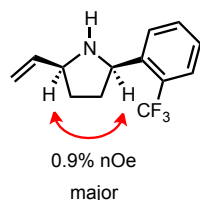
tert-butyl 2-(2-trifluoromethylphenyl)-5-vinylpyrrolidine-1-carboxylate: Synthesized via procedure C. $^1\text{H NMR}$ (500 MHz, C_6D_6 , 50 °C) δ (mixture of rotamers): 7.60 (d, $J=7.81$ Hz, 1 H), 7.43 (d, $J=7.81$ Hz, 1 H), 7.12 (t, $J=7.57$ Hz, 1 H), 6.86 (t, $J=7.32$ Hz, 1 H), 6.02 - 6.12 (m, 1 H), 5.28 (d, $J=17.09$ Hz, 1 H), 5.21 (br. s., 1 H), 5.07 - 5.13 (m, 1 H), 4.46 (br. s., 1 H), 1.98 - 2.06 (m, 2 H), 1.21 - 1.52 (m, 11 H). $^{13}\text{C}\{^1\text{H}\}$ NMR (125 MHz, C_6D_6 , 50 °C) δ (mixture of rotamers): 154.7, 145.6, 139.8, 132.5, 128.7, 127.3, 126.9, 126.2 (m), 115.6, 79.7, 61.2, 60.2, 35.6, 30.1, 28.6. **GCMS** (EI) $t_{\text{R}} = 9.12$ min (major diastereomer) m/z : 57, 68, 82, 96, 113, 134, 159, 163, 172, 192, 213, 226, 241, 268, 285, 341.



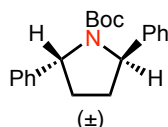
2-(2-trifluoromethylphenyl)-5-vinylpyrrolidine: Synthesized via procedure D. $^1\text{H NMR}$ (600 MHz, C_6D_6) δ : 8.06 (d, $J=7.63$ Hz, 1 H), 7.39 (d, $J=7.63$ Hz, 1 H), 7.13 - 7.17 (m, 4 H), 6.84 (t, $J=7.63$ Hz, 1 H), 5.89 (ddd, $J=17.02, 9.98, 7.04$ Hz, 1 H), 5.13 (d, $J=17.02$ Hz, 1 H), 4.93 (d,

$J=9.98$ Hz, 1 H), 4.53 (t, $J=7.34$ Hz, 1 H), 3.31 (q, $J=7.63$ Hz, 1 H), 1.93 - 2.00 (m, 1 H), 1.42 - 1.58 (m, 3 H).

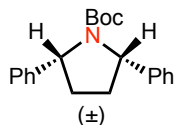
1D NOESY (600 MHz, C_6D_6):



(1-azidobutane-1,4-diyl)benzene: Synthesized via procedure B. 1H NMR (600 MHz, C_6D_6) δ : 7.12–7.15 (m, 2 H), 6.99–7.09 (m, 6 H), 6.95–6.98 (m, 2 H), 3.97 (dd, $J = 7.63, 6.46$ Hz, 1 H), 2.31–2.35 (m, 2 H), 1.59–1.66 (m, 1 H), 1.45–1.58 (m, 2 H), 1.33–1.41 (m, 1 H). $^{13}C\{^1H\}$ NMR (125 MHz, C_6D_6) δ : 142.4, 140.5, 129.3, 129.02, 129.0, 127.6, 127.5, 126.6, 66.8, 36.3, 36.0, 28.6. **GCMS** (EI) $t_R = 9.12$ min m/z : 51, 65, 77, 91, 104, 119, 132, 146, 165, 178, 194, 208, 222, 234, 253.

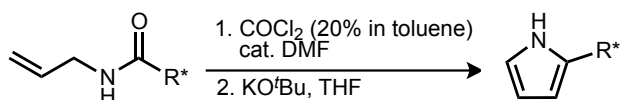


tert-butyl 2,5-diphenylpyrrolidine-1-carboxylate (*anti* isomer): Synthesized via Procedure C. 1H NMR (500 MHz, C_6D_6 , 50 °C) δ : 7.40 (br. s., 4 H), 7.17 - 7.21 (m, 4 H), 7.04 - 7.09 (m, 2 H), 4.94 (br. s., 2 H), 1.74 - 1.88 (m, 4 H), 1.16 - 1.26 (m, 9 H). $^{13}C\{^1H\}$ NMR (125 MHz, C_6D_6 , 50 °C) δ : 156.1, 144.9, 128.8, 127.4, 127.3, 79.6, 63.8, 34.0, 28.7. **GCMS** (EI) $t_R = 12.67$ min m/z : 57, 77, 91, 104, 117, 129, 146, 163, 195, 207, 222, 250, 267.



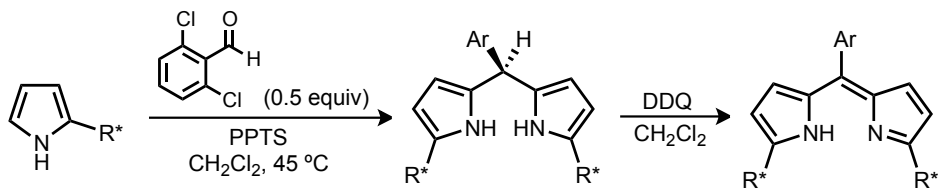
tert-butyl 2,5-diphenylpyrrolidine-1-carboxylate (*syn isomer*)²²¹: Synthesized via Procedure C.

5.5.4 Synthesis of Chiral Ligands

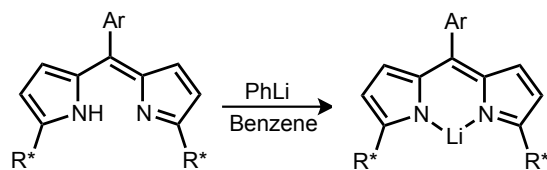


Procedure F: A 50 mL RBF equipped with a stir bar under N₂ was charged with allylamide (1 equiv) followed by 15% phosgene in toluene solution (0.4 M). Catalytic amount of anhydrous DMF (5 drops) was then added to initiate the reaction. Vigorous bubbling occurred. The reaction was allowed to stir for 12 hours. Toluene and excess phosgene were removed *in vacuo* and the remaining solid is re-dissolved in THF (10 mL) and placed in a 0 °C ice bath. The contents of the reaction mixture were then transferred via syringe to a separate 50 mL RBF equipped with a stir bar under N₂, containing a solution of potassium *tert*-butoxide (2.2 equiv) in THF (10 mL) at 0 °C. The reaction mixture was allowed to warm to room temperature over 15 minutes and was quenched with a saturated NH₄Cl solution (10 mL). The biphasic mixture was separated and the remaining aqueous layer was extracted with (2 x 10 mL). The combined organic layers were washed with H₂O (1 x 10 mL) and brine (1 x 10 mL), dried over MgSO₄ and concentrated to a brownish yellow oil. The crude mixture was purified by silica gel column chromatography (10:1 → 5:1 hexanes:ethyl acetate) to isolate a pale yellow oil (20–88%).

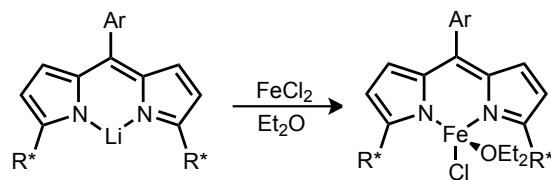
220. For physical and spectroscopic characterization, see: Durant, G. J.; Maillard, M.; Guo, J. Q. Preparation of *N*-amidinopiperidines and analogs as neuroprotectants. U. S. Patent 20030069274, April 2003.



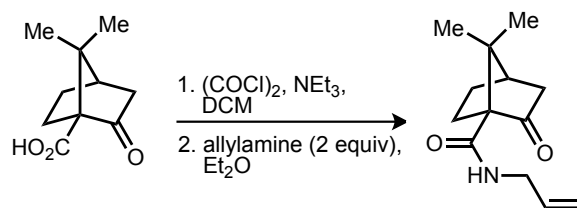
Procedure G: A round-bottomed flask was charged with pyrrole (**5.7,10,12**) (1.0 equiv), 2,6-dichlorobenzaldehyde or mesitaldehyde dimethyl acetal (0.5 equiv.), and DCE (0.2 M). After stirring until all materials were dissolved, pyridinium *p*-toluenesulfonate (0.1 equiv.) was added resulting in a color darkening. The flask was equipped with a reflux condenser and heated to 80 °C with an oil bath for 3 h. The solution was cooled to room temperature, concentrated *in vacuo*, and filtered through a plug of silica gel in a medium porosity frit with CH₂Cl₂ to give a pale yellow filtrate. Solvent was removed *in vacuo* and the yellow oil was re-dissolved in hexanes (0.1 M). The oxidant, 2,3-dichloro-5,6-dicyanoquinone (DDQ) (1 equiv.), was added to give a mustard yellow slurry that gradually reddened as the reaction progressed. After stirring for 12 h, the solution was filtered through a plug of silica gel in a medium porosity frit using a hexanes:ethyl acetate (10:1) solution to give a bright yellow filtrate. Solvent was removed *in vacuo* to afford dipyrromethene as a yellow powder.



Procedure H: Under an inert glove-box atmosphere, an oven-dried round-bottomed flask was charged with dipyrromethene (1.0 equiv) and benzene (0.1 M). Phenyl lithium (1.2 equiv.) was added to the stirring, yellow solution as a solid. The pink-orange solution was allowed to stir overnight and then passed through a pad of Celite. The benzene filtrate was lyophilized and collected as a fluffy, orange powder.

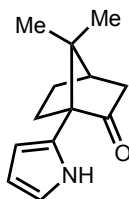


Procedure I: An oven-dried, round-bottomed flask was charged with $(R^*L_{Ar})Li(OEt_2)$ (2.000 g, 3.14 mmol) and 31 mL of diethyl ether. Finely ground $FeCl_2$ (0.475 g, 3.77 mmol, 1.2 equiv.) was added to the slurry of $(R^*L_{Ar})Li(OEt_2)$ at room temperature. After stirring for 3 hours, the dark brown reaction mixture was initially filtered through a medium porosity glass frit with Celite. A dark brown solid collects on top of Celite and is rinsed with 10 mL Et_2O to remove any $(AdL_{Cl_2})H$ generated during the reaction. The filter flask is then replaced with a new 250 mL filter flask and the dark brown solid is dissolved and filtered with benzene to remove excess $FeCl_2$ and $LiCl$ formed during the reaction. Sublimation of the benzene *in vacuo* yields $(R^*L_{Cl_2})FeCl(OEt_2)$ (1.20 g, 53%) as a red brown powdery solid.



5.6: DL-Ketopinic acid²²² (7.00 g, 38.4 mmol, 1.0 equiv) was dissolved in methylene chloride (77 mL, 0.5 M) at room temperature under ambient atmosphere. Oxalyl chloride (6.59 mL, 76.8 mmol, 2.0 equiv) was added to the reaction mixture, followed by the dropwise addition of triethylamine (7.99 mL, 57.6 mmol, 1.5 equiv). *Note: During the addition of triethylamine, a significant amount of white, fluffy triethylammonium chloride is generated.* Following the addition, the reaction was allowed to stir for 3 hours and then the solvent is removed *in vacuo*. The remaining solid was redissolved in diethyl ether (30 mL) and filtered through a Celite pad to

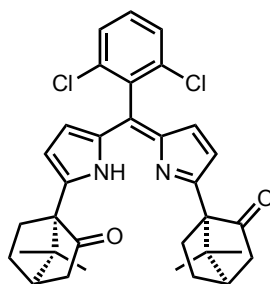
remove any insoluble material. The ether solution was then added via pipette to a stirring solution of allylamine (6.06 mL, 80.6 mmol, 2.1 equiv) in diethyl ether (77 mL). The reaction was stirred at room temperature for 1 hour and quenched with saturated NH_4Cl (20 mL). The biphasic mixture was separated and the remaining aqueous layer was extracted with diethyl ether (3 x 50 mL). The combined organics were washed with H_2O (1 x 50 mL) and brine (1 x 50 mL), dried over MgSO_4 , filtered, and concentrated to yellow oil (5.69 g, 25.7 mmol, 67% over two steps). $^1\text{H NMR}$ (600 MHz, C_6D_6) δ : 7.81 (br. s, 1 H), 5.69 (ddt, $J = 17.2, 10.3, 5.3, 5.3$ Hz, 1 H), 5.10 (dq, $J = 17.6, 1.8$ Hz, 0 H), 4.93 (dq, $J = 10.3, 1.5$ Hz, 1 H), 3.78–3.94 (m, 2 H), 2.46 (m, $J = 4.1$ Hz, 1 H), 2.05 (dt, $J = 18.3, 4.0$ Hz, 1 H), 1.60–1.69 (m, 1 H), 1.46 (d, $J = 18.8$ Hz, 1 H), 1.43 (t, $J = 4.4$ Hz, 1 H), 1.29 (ddd, $J = 13.9, 9.2, 5.0$ Hz, 1 H), 1.22 (s, 3 H), 0.80 (ddd, $J = 12.8, 9.0, 4.1$ Hz, 1 H), 0.77 (s, 3 H). $^{13}\text{C}\{^1\text{H}\}$ NMR (125 MHz, C_6D_6) δ : 216.8, 168.5, 135.1, 115.2, 49.9, 43.6, 43.2, 41.3, 28.7, 27.8, 21.1, 20.3. GCMS (EI) $t_r = 8.63$ min m/z : 56, 69, 81, 95, 109, 123, 137, 152, 165, 178, 193, 206, 221.



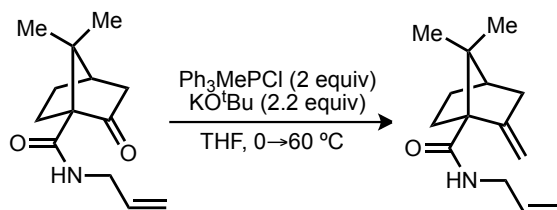
5.7:²¹⁴ Synthesized via Procedure F. Yield: 389 mg, 20% conversion. $^1\text{H NMR}$ (500 MHz, C_6D_6) δ : 9.36 (br. s, 1 H), 6.78 (br. s., 1 H), 6.20 (d, $J = 2.4$ Hz, 1 H), 6.07 (br. s., 1 H), 2.55 (dd, $J = 18.1, 3.4$ Hz, 1 H), 2.25–2.36 (m, 1 H), 2.20 (t, $J = 4.2$ Hz, 1 H), 2.14 (ddd, $J = 11.8, 7.9, 3.7$ Hz, 1 H), 2.03 (d, $J = 18.6$ Hz, 1 H), 1.83 (ddd, $J = 13.8, 9.2, 4.4$ Hz, 1 H), 1.40–1.53 (m, 1 H), 1.11 (s, 3 H), 0.86 (s, 3 H). $^{13}\text{C}\{^1\text{H}\}$ NMR (125 MHz, C_6D_6) δ : 218.4, 127.1, 116.9, 107.7, 106.1,

221. Carboxylic acid was generated from DL-10-camphorsulfonyl chloride according to the following procedure: Bartlett, P. D.; Knox, L. H. *Org. Synth.* **1965**, 45, 55.

60.7, 49.5, 43.6, 43.0, 30.7, 27.2, 20.2, 20.0. **HRMS** (ESI⁺) *m/z* Calc. 204.1388 [C₁₃H₁₈NO+H]⁺, Found 204.1413 [M+H]⁺.

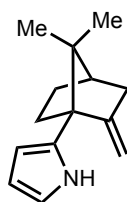


(^{CMPH_KETONE}**L**)**H**: Synthesized via Procedure G. Yield: 59% (over 2 steps). ¹H NMR (500 MHz, CDCl₃) δ/ppm: 7.40 (d, *J* = 8.3 Hz, 2 H), 7.30 (t, *J* = 7.8 Hz, 1 H), 6.29 (br. s., 4 H), 2.81 – 2.66 (m, 2 H), 2.59 (td, *J* = 3.8, 18.2 Hz, 2 H), 2.29 – 2.12 (m, 4 H), 2.11 – 2.01 (m, 2 H), 1.88 (ddd, *J* = 4.6, 9.3, 13.9 Hz, 2 H), 1.54 (ddd, *J* = 3.7, 8.9, 12.3 Hz, 2 H), 1.08 – 1.03 (m, 6 H), 1.01 (s, 6 H). ¹³C{¹H} NMR (125 MHz, CDCl₃) δ: 215.2, 153.1, 139.4, 135.9, 129.8, 127.7, 125.9, 117.9, 63.5, 50.7, 44.0, 28.2, 27.3, 20.8, 20.0. **HRMS** (ESI⁺) *m/z* Calc. 561.2076 [C₃₃H₃₄Cl₂N₂O₂ +H]⁺, Found 561.2074 [M+H]⁺.

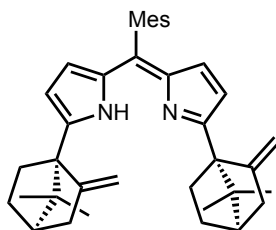


5.9:²²³ To a suspension of methyltriphenylphosphonium chloride (705 mg, 2.26 mmol, 2.0 equiv) in THF (1.75 mL, 0.6 M) was added solid KO^t-Bu (278 mg, 2.49 mmol, 2.2 equiv) in portions at 0 °C. The resulting bright yellow mixture was stirred for 45 minutes followed by slow addition of ketone **5.6** (250 mg, 1.36 mmol, 1.0 equiv) at 0 °C. After warming to room temperature, the orange mixture was refluxed for 4 hours. The reaction was quenched with sat'd NH₄Cl solution (4 mL) was added and the layers were separated. The remaining aqueous layer was extracted

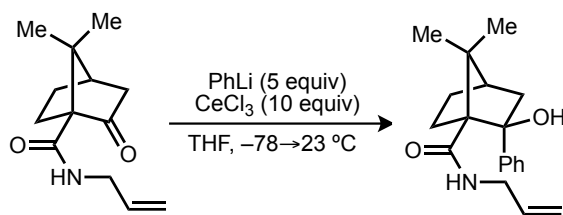
with ethyl acetate (2 x 4 mL). The combined organic layers were dried over MgSO₄, filtered, and concentrated. The residue was purified by flash chromatography (10:1 hexanes:ethyl acetate) to isolate **5.9** as a colorless oil (170 mg, 69%). **¹H NMR** (500 MHz, C₆D₆) δ: 5.92–5.65 (m, 2 H), 5.14 (dd, *J* = 1.0, 17.1 Hz, 1 H), 5.07 (td, *J* = 1.2, 10.3 Hz, 1 H), 4.89 (br. s., 1 H), 4.81 (s, 1 H), 4.01–3.81 (m, 2 H), 2.60 - 2.39 (m, 2 H), 2.00–1.92 (m, 1 H), 1.83 (dtd, *J* = 3.9, 8.1, 16.0 Hz, 1 H), 1.75 (t, *J* = 4.4 Hz, 1 H), 1.52–1.42 (m, 1 H), 1.24 - 1.17 (m, 1 H), 1.00 (s, 3 H), 0.95 (s, 3 H). **¹³C{¹H} NMR** (125 MHz, C₆D₆) δ: 171.4, 155.2, 134.5, 116.2, 105.3, 63.1, 50.1, 46.1, 41.7, 37.7, 31.6, 27.2, 21.4, 19.2. **HRMS** (ESI⁺) *m/z* Calc. 220.1701 [C₁₄H₂₁NO +H]⁺, Found 220.1719 [M+H]⁺.



5.10: Synthesized via Procedure F. Yield: 137 mg, 88%. **¹H NMR** (600 MHz, C₆D₆) δ: 8.03 (br. s, 1 H), 6.76 (dt, *J* = 1.2, 2.6 Hz, 1 H), 6.19 (q, *J* = 2.9 Hz, 1 H), 6.09–6.05 (m, 1 H), 4.80 (s, 1 H), 4.70 (s, 1 H), 2.60 (d, *J* = 16.4 Hz, 2 H), 2.34 (dt, *J* = 4.7, 12.0 Hz, 1 H), 1.98–1.88 (m, 1 H), 1.86 (t, *J* = 4.4 Hz, 1 H), 1.61 (ddd, *J* = 4.1, 9.4, 12.3 Hz, 1 H), 1.34 (ddd, *J* = 4.7, 9.4, 12.3 Hz, 1 H), 0.97 (s, 3 H), 0.80 (s, 3 H). **¹³C{¹H} NMR** (125 MHz, C₆D₆) δ: 157.9, 130.8, 116.7, 107.5, 107.2, 104.6, 57.0, 49.8, 45.3, 37.4, 33.2, 27.7, 21.0, 19.1. **GCMS** (EI) *t_R* = 8.14 min *m/z*: 53, 65, 80, 91, 104, 117, 132, 144, 158, 172, 186, 201.

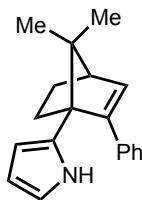


(^{C^{MPH}-ALKENE^L})**H**: Synthesized via Procedure G. Yield: 46% (over 2 steps). ¹H NMR (600 MHz, C₆D₆): δ/ppm 12.67 (br. s, 1H), 6.91 (s, 2H), 6.28 (t, *J* = 3.5 Hz, 2H), 6.20–6.25 (m, 2H), 4.86 (br. s, 4H), 2.58–2.71 (m, 4H), 2.33–2.39 (m, 3H), 2.13 (s, 6H), 1.93–2.03 (m, 2H), 1.87–1.92 (m, 2H), 1.65–1.74 (m, 2H), 1.35–1.43 (m, 2H), 1.05 (s, 6H), 0.88 (s, 6H). ¹³C{¹H} NMR (125 MHz, CD₂Cl₂): δ/ppm 156.5, 156.0, 139.9, 137.0, 130.5, 125.8, 117.4, 105.5, 59.0, 50.9, 46.1, 37.7, 32.8, 29.7, 27.8, 21.5, 21.2, 21.1, 20.5. HRMS (ESI⁺) *m/z* Calc. 531.3739 [C₃₈H₄₆N₂+H]⁺, Found 531.3850 [M+H]⁺.



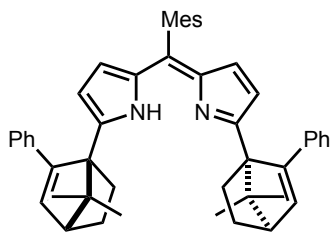
In an inert atmosphere, a 250-mL round-bottomed flask was charged with anhydrous cerium(III) chloride (4.00 g, 16.2 mmol, 10.0 equiv) and diluted with THF (160 mL, 0.1 M). After 12 hours, the reaction mixture was cooled in a liquid N₂ cooled cold well for 15 minutes before a solution of phenyl lithium (682 mg, 8.11 mmol, 5.0 equiv) in THF (10 mL) was added dropwise via pipette over 10 minutes. The resultant slurry was removed from box and placed in -78 °C ice bath under N₂ and stirred for 3 hours. A solution of ketone **5.6** (325 mg, 1.47 mmol, 1.0 equiv) in THF (3 mL) was then transferred dropwise via syringe to the stirred, cooled reaction mixture. The transfer was completed with two additional portions of THF (2 mL). The resultant mixture was warmed to room temperature over 3 hours. Saturated aqueous ammonium chloride solution

(50 mL) was then cautiously added to the reaction mixture. The resultant heterogeneous mixture was filtered through a pad of Celite and rinsed with water (20 mL) and EtOAc (150 mL). The layers of the filtrate were separated and the aqueous layer was extracted with EtOAc (3 x 100 mL). The combined organic layers were washed with saturated aqueous sodium bicarbonate solution (200 mL) and brine (200 mL), dried over MgSO₄, filtered, and concentrated. The resultant yellow oil was purified by hexanes trituration over night. The off-white solid (298 mg, 68%) was collected on a M porosity frit and used without any further purification. **¹H NMR** (500 MHz, CDCl₃) δ: 7.41 (d, *J* = 7.8 Hz, 2 H), 7.30 (t, *J* = 7.8 Hz, 2 H), 7.21–7.26 (m, 1 H), 6.20 (br. s., 1 H), 6.02 (s, 1 H), 5.84 (ddt, *J* = 16.7, 10.9, 5.5, 5.5 Hz, 1 H), 5.11–5.20 (m, 2 H), 3.89–4.02 (m, 2 H), 2.37–2.48 (m, 2 H), 1.95–2.03 (m, 1 H), 1.79–1.92 (m, 2 H), 1.64 (br. s, 1 H), 1.55 (s, 3 H), 1.23–1.32 (m, 1 H), 1.13 (t, *J* = 9.5 Hz, 1 H), 1.03 (s, 3 H). **¹³C{¹H} NMR** (125 MHz, CDCl₃) δ: 174.2, 145.6, 134.0, 128.0, 127.0, 126.4, 116.6, 84.5, 61.5, 53.6, 46.3, 44.7, 41.8, 27.0, 26.3, 22.5, 21.9. **HRMS** (ESI⁺) *m/z* Calc. 282.1858 [C₁₉H₂₃NO+H]⁺, Found 282.1909 [M+H]⁺.
(dehydration product)



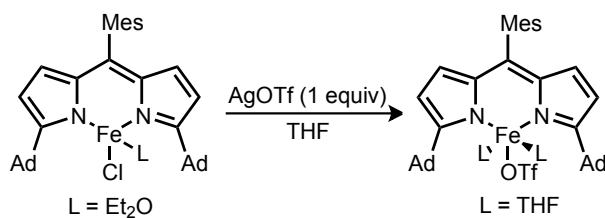
5.12: Synthesized via Procedure F. Yield: 202 mg, 77%. **¹H NMR** (600 MHz, C₆D₆) δ: 7.10–7.14 (m, 2 H), 7.00–7.05 (m, 2 H), 6.95–6.99 (m, 1 H), 6.93 (br. s, 1 H), 6.30–6.33 (m, 1 H), 6.24–6.27 (m, 1 H), 6.21–6.23 (m, 1 H), 6.16 (d, *J* = 3.5 Hz, 1 H), 2.34 (t, *J* = 3.2 Hz, 1 H), 2.29 (ddd, *J* = 11.9, 8.4, 3.8 Hz, 1 H), 1.90–1.97 (m, 1 H), 1.50 (ddd, *J* = 12.0, 9.1, 3.5 Hz, 1 H), 1.07 (ddd, *J* = 12.0, 9.1, 3.5 Hz, 1 H), 0.91 (s, 3 H), 0.70 (s, 3 H). **¹³C{¹H} NMR** (125 MHz, C₆D₆) δ:

147.2, 137.0, 133.0, 129.9, 128.4, 126.6, 125.9, 117.4, 108.1, 107.3, 59.4, 59.0, 52.4, 29.1, 26.3, 20.5, 19.8. **HRMS** (ESI⁺) *m/z* Calc. 264.1752 [C₁₉H₂₁N+H]⁺, Found 264.1788 [M+H]⁺.



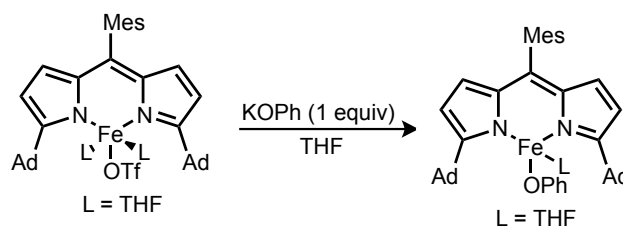
(^{CMPH_PHENYL}L)**H**: Synthesized via Procedure G. Yield: 177 mg, 70%. **¹H NMR** (600 MHz, C₆D₆) δ: 12.82 (br. s, 1 H), 7.11-7.14 (m, 4 H), 7.00–7.07 (m, 6 H), 6.80 (s, 2 H), 6.36 (d, *J* = 4.1 Hz, 2 H), 6.17 (d, *J* = 2.9 Hz, 2 H), 6.06 (d, *J* = 4.1 Hz, 2 H), 2.75 (m, *J* = 8.5, 8.5 Hz, 2 H), 2.42 (t, *J* = 3.2 Hz, 2 H), 2.19 (s, 3 H), 2.15 (s, 6 H), 2.07–2.13 (m, 2 H), 1.64–1.74 (m, 2 H), 1.18–1.31 (m, 6 H), 0.85–0.92 (m, 8 H). **¹³C{¹H} NMR** (125 MHz, C₆D₆) δ: 148.5, 137.2, 137.0, 134.5, 132.5, 127.8, 126.7, 119.0, 61.6, 60.3, 53.3, 34.9, 31.9, 28.9, 26.2, 25.6, 23.0, 21.0, 20.3, 20.0, 14.3. **HRMS** (ESI⁺) *m/z* Calc. 655.4052 [C₄₈H₅₀N₂+H]⁺, Found 655.3987 [M+H]⁺.

5.5.5 Synthesis of Metal Complexes

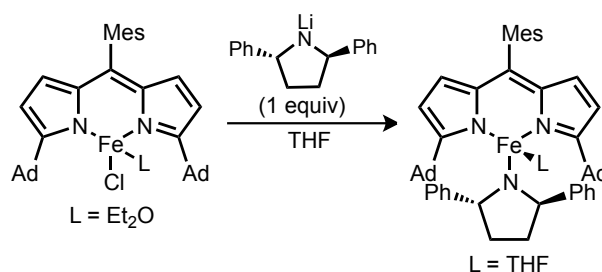


5.2: An oven-dried scintillation vial was charged with (^{Ad}L_{Mes})FeCl(OEt₂) (1.00 mg, 1.68 mmol) and 8 mL of THF. Silver triflate (474 mg, 1.85 mmol, 1.1 equiv.) was added portionwise to the reaction mixture at room temperature. After stirring for 2 hours, the dark brown reaction mixture is concentrated. The solid residue is redissolved in benzene and was filtered through a medium porosity glass frit with Celite to remove AgCl generated in the reaction. Sublimation of the benzene filtrate *in vacuo* yields (^{Ad}L_{Mes})FeOTf(THF)₂ (**5.2**) as a red brown powdery solid. Yield:

1.40 g, 94%. $^1\text{H NMR}$ (500 MHz, C_6D_6): δ 52.89 (br. s), 21.19 (br. s), 9.65 (s), 9.67 (br.s.), 6.61 (br. s.), 5.40 (br. s.), 4.19 (br. s.), 2.19 (s), 2.11(s), 1.70 (br. s.), 1.37 (br. s.), 0.93 (br. s.), 0.65 (br. s.), -2.67 (br. s.), -6.73 (br. s.).

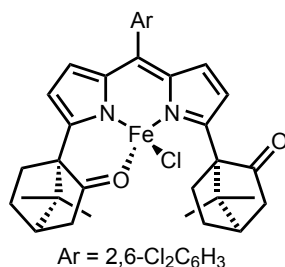


5.3: An oven-dried scintillation vial was charged with $(^{\text{Ad}}\text{L}_{\text{Mes}})\text{FeOTf}(\text{THF})_2$ (1.00 g, 1.14 mmol) and 8 mL of THF. Potassium phenoxide (166 mg, 1.25 mmol, 1.10 equiv.) was added portionwise to the reaction mixture at room temperature. After stirring for 2 hours, the dark brown reaction mixture is concentrated. The solid residue is redissolved in benzene and was filtered through a medium porosity glass frit with Celite to remove KOTf generated in the reaction. Sublimation of the benzene filtrate *in vacuo* yields $(^{\text{Ad}}\text{L}_{\text{Mes}})\text{FeOPh}(\text{THF})$ (**5.3**) as a red brown powdery solid. Yield: 752 mg, 88%. $^1\text{H NMR}$ (500 MHz, C_6D_6): δ 55.93 (s), 51.29 (s), 28.70 (s), 11.84 (s), 11.29 (s), 9.93 (br.s.), 6.06 (s), 5.51 (s), 5.34 (s), 3.43 (s), 1.71 (br. s.), -15.67 (br.s.), -30.46 (br.s.) .

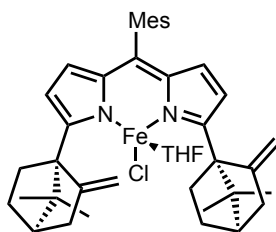


5.5: An oven-dried scintillation vial was charged with $(^{\text{Ad}}\text{L}_{\text{Mes}})\text{FeCl}(\text{OEt}_2)$ (124 mg, 0.179 mmol) and 4 mL of THF. Lithium (2*R*, 2*R*)-diphenylpyrrolidinide (229 mg, 0.179 mmol, 1.0 equiv.) was added portionwise to the reaction mixture at room temperature. After stirring for 2 hours, the dark brown reaction mixture is concentrated. The solid residue is redissolved in benzene and was

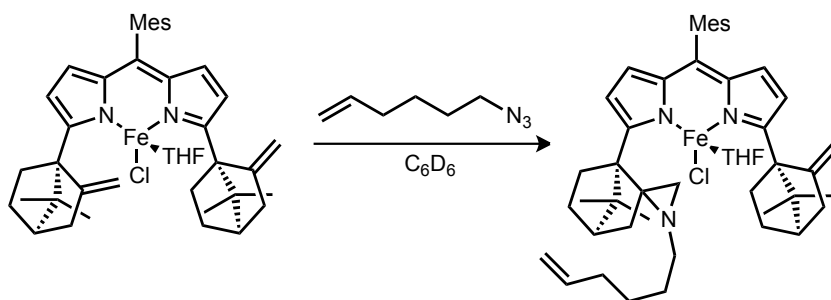
filtered through a medium porosity glass frit with Celite to remove LiCl generated in the reaction. Sublimation of the benzene filtrate *in vacuo* yields **5.5** as a red brown powdery solid. Yield: 100 mg, 64% $^1\text{H NMR}$ (400 MHz, C_6D_6) δ : 112.44, 68.63, 55.42, 49.12, 24.16, 13.88, 5.10, 2.11, 1.72, -1.07, -2.58, -11.18, -16.34, -35.07.



5.8: Prepared via Procedure I from the corresponding lithium salt of ligand. Yield: 526 mg, 91%. $^1\text{H NMR}$ (500 MHz, C_6D_6) δ : 73.80, 58.84, 55.10, 53.30, 35.62, 29.67, 15.06, 12.97, 10.20, 6.35, 5.32, -15.68.

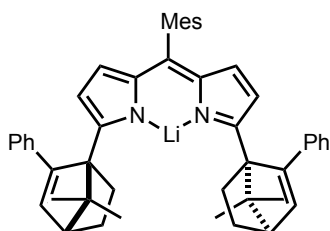


5.11: Prepared via Procedure I from the corresponding lithium salt of ligand. Yield: 445 mg, 70%. $^1\text{H NMR}$ (600 MHz, C_6D_6) δ : 112.75, 85.92, 53.90, 49.70, 36.13, 28.52, 25.46, 22.10, 19.40, 14.30, 10.04, 4.70, 1.96, -1.45, -3.45, -6.52, -9.30, -16.86, -25.50, -27.12, -90.70, -135.52.

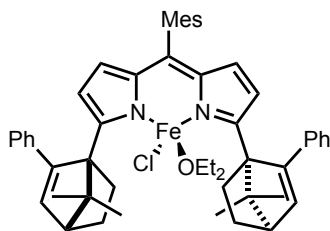


A 5 mL vial was charged with a stir-bar, **5.11** (20.0 mg), and 1 mL benzene- d_6 . One drop of 1-Azido-hex-5-ene (excess) was added to the stirring reaction mixture. The mixture was then

transferred to a J. Young tube. The tube was heated to 80 °C in an oil bath for 15 min. Consumption of **5.11** was confirmed by ^1H NMR, and formation of the ligand insertion product was confirmed by HRMS: (ESI⁺) m/z Calc. $[\text{C}_{44}\text{H}_{57}\text{N}_3+\text{H}]^+$ 628.4631, Found 628.4732 $[\text{M}+\text{H}]^+$. ^1H NMR (600 MHz, C_6D_6) δ : 160.79, 88.09, 77.10, 48.06, 28.32, 23.17, 18.45, 17.13, 15.95, 13.68, 13.20, 10.23, 8.53, 8.25, 6.81, 6.73, 6.56, 6.37, 5.62, 5.42, 5.27, 5.11, 4.93, 3.94, 3.80, 3.62, 3.20, 2.65, 2.46, 2.18, 2.10, 1.77, 1.45, 1.16, 1.10, 0.89, 0.31, -0.37, -0.97, -1.13, -2.09, -3.72, -7.72, -9.20, -12.72, -16.58, -19.21, -23.23, -33.14, -42.82, -58.08.



Prepared via Procedure H. ^1H NMR (600 MHz, C_6D_6) δ : 7.14 (d, $J = 7.6$ Hz, 4 H), 6.99 (t, $J = 7.6$ Hz, 4 H), 6.88–6.94 (m, 2 H), 6.86 (s, 2 H), 6.72 (d, $J = 4.1$ Hz, 2 H), 6.34 (d, $J = 3.5$ Hz, 2 H), 6.19 (d, $J = 3.5$ Hz, 2 H), 2.40 (t, $J = 2.9$ Hz, 2 H), 2.28 (s, 6 H), 2.21–2.26 (m, 5 H), 1.97–2.08 (m, 2 H), 1.39–1.49 (m, 2 H), 1.10–1.20 (m, 2 H), 0.92 (s, 6 H), 0.76 (s, 6 H). $^{13}\text{C}\{^1\text{H}\}$ NMR (125 MHz, C_6D_6) δ : 159.2, 147.8, 146.3, 140.9, 138.5, 137.0, 136.2, 134.0, 130.6, 128.7, 128.5, 127.4, 126.3, 116.9, 62.4, 59.4, 52.8, 29.2, 26.7, 21.2, 20.8, 20.2.



5.13: Prepared via Procedure I. Yield: 176 mg (over 2 steps), 88%. ^1H NMR (600 MHz, C_6D_6) δ : 74.34, 53.03, 36.08, 32.03, 18.29, 13.59, 11.03, 3.51, 2.15, -0.69, -3.34, -9.95, -19.10, -23.85, -36.18, -64.34, -114.86.

5.5.6 X-Ray Diffraction Techniques

Equipment and software details can be found in Section 2.6.6.

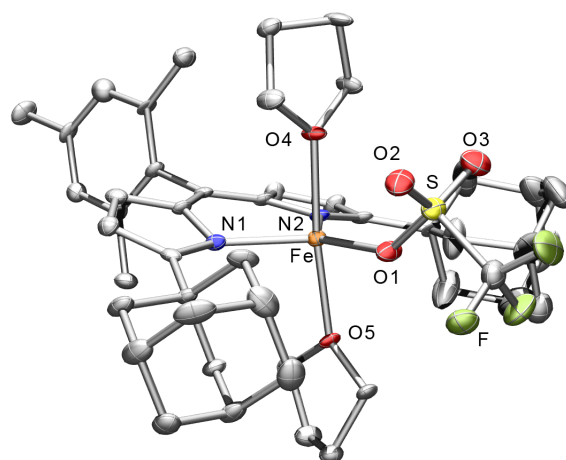


Figure 5.6. X-ray structure of **5.3**. Thermal ellipsoids set at the 50% probability level (Fe, orange; C, gray; H, white; N, blue; S, yellow; F, yellow-green; O, red). Bond lengths (Å): Fe-N1, 2.066(3); Fe-N2, 2.086(3); Fe-O1, 2.035(3); Fe-O4, 2.188(3); Fe-O5, 2.192(3); S-O1, 1.482(3); S-O2, 1.429(3), S-O3, 1.436(3).

(^{Ad}L_{Mes})FeOTf(THF)₂ (5.3): The structure was solved in the triclinic space group $P\bar{1}$ with 2 molecules per unit cell.

(^{Ad}L_{Mes})FeOPh(THF) (5.4): The structure was solved in the orthorhombic space group $Pbca$ with 8 molecules per unit cell.

(^{Ad}L_{Mes})Fe(2*R*,5*R*-diphenylpyrrolidinide) (5.5): The structure was solved in the orthorhombic space group $P2_12_12_1$ with 8 molecules per unit cell. The hexane fragment exhibited positional disorder and was refined in 2 parts using similarity restraints.

Table 5.2. X-ray crystallographic experimental properties.

	(5.3)	(5.4)	(5.5)
Moiety Formula	C ₄₇ H ₆₂ F ₃ FeN ₂ O ₅ S	C ₄₈ H ₅₈ FeN ₂ O ₂ ;	C ₄₂ H ₅₅ ClFeN ₂ O; C ₆ H ₁₄
FW	879.90	750.81	759.00
Crystal System	triclinic	orthorhombic	orthorhombic
Space Group (Z)	$P\bar{1}$ (2)	<i>Pbca</i> (8)	<i>P2₁2₁2₁</i> (8)
a (Å)	9.6368(10)	15.9524(17)	10.3377(7)
b (Å)	11.5976(12)	17.9261(19)	20.0699(13)
c (Å)	20.0334(19)	27.481(3)	25.3692(17)
α (°)	102.238(2)	90	90
β (°)	95.040(2)	90	90
γ (°)	98.195(2)	90	90
Volume (Å ³)	2149.6(4)	7858.7(14)	5269.1(6)
Calc. ρ (mg/m ³)	1.359	1.269	1.211
μ (mm ⁻¹)	0.461	0.426	0.589
Crystal Size (mm)	0.2×0.22 ×0.12	0.42×0.31 ×0.22	0.5×0.3 ×0.3
Reflections	6389	6952	10032
Completeness (to 2θ)	98.9% 28.79°	99.8% 25.05°	99.9% 25.71°
GOF on F ²	0.973	1.013	0.754
R1, wR2 ^c	0.0789,	0.1039,	0.0380,
[I>2σ(I)]	0.1407	0.1250	0.1094